UNIVERSITAT DE BARCELONA

Fluxos d'aigua subterrània i concentració de metalls en dipòsits marins costaners contaminats: aproximació metodològica i casos d'estudi a la costa mediterrània de la Península Ibèrica

Submarine groundwater discharge and metal concentration in polluted coastal marine deposits: methodological approach and case studies on the Mediterranean coast of the Iberian Peninsula

Marc Cerdà i Domènech

Aquesta tesi doctoral està subjecta a la llicència **Reconeixement – NoComercial – SenseObraDerivada 3.0. Espanya de Creative Commons.**

Esta tesis doctoral está sujeta a la licencia **Reconocimiento – NoComercial – SinObraDerivada3.0. España de Creative Commons.**

This doctoral thesis is licensed under the **Creative Commons Attribution – NonCommercial-NoDerivs 3.0. Spain License.**

Fluxos d'aigua subterrània i concentració de metalls en dipòsits marins costaners contaminats: aproximació metodològica i casos d'estudi a la costa mediterrània de la Península Ibèrica

Submarine groundwater discharge and metal concentration in polluted coastal marine deposits: methodological approach and case studies on the Mediterranean coast of the Iberian Peninsula

Marc Cerdà i Domènech

Memòria de Tesi Doctoral

Programa de Doctorat en Ciències del Mar

UNIVERSITAT DE BARCELONA

Fluxos d'aigua subterrània i concentració de metalls en dipòsits marins costaners contaminats: aproximació metodològica i casos d'estudi a la costa mediterrània de la Península Ibèrica

Submarine groundwater discharge and metal concentration in polluted coastal marine deposits: methodological approach and case studies on the Mediterranean coast of the Iberian Peninsula

Memòria de Tesi Doctoral presentada per

Marc Cerdà i Domènech

sota la direcció de

Dr. Miquel Canals i **Dr. Jaime Frigola**

al Departament de Dinàmica de la Terra i de l'Oceà de la Universitat de Barcelona, dins del programa de doctorat de Ciències del Mar, per optar al grau de Doctor per la Universitat de Barcelona.

Barcelona, 18 de juny de 2020

Doctorand | El Director | El Director

Aquesta Tesi ha estat realitzada al Departament de Dinàmica de la Terra i de l'Oceà de la Universitat de Barcelona, dins el Grup de Recerca en Geociències Marines amb reconeixement de la Generalitat de Catalunya com a Grup de Recerca Consolidat (ref. 2017 SGR 315). Durant el període d'elaboració de la Tesi el doctorand ha gaudit d'una beca predoctoral de Formación de Personal Investigador (FPI) del Ministerio de Ciencia, Innovación y Universidades (ref. A-2014-9185). L'estada que el doctorand realitzà al Centre Renard de Geologia Marina (Gant, Bèlgica) foren finançades pel Ministerio de Ciencia, Innovación y Universidades. Altres beques que el doctorand ha rebut per assistir a congressos i cursos han estat concedides per la Facultat de Ciències de la Terra de la Universitat de Barcelona a través del programa d'Ajuts a la Recerca de la Comissió de Recerca de la Facultat. A més dels projectes esmentats anteriorment, la recerca que es presenta en aquesta Tesi ha estat finançada pel projectes MIDAS (ref. 603418) i els projectes nacionals NUREIEV (ref. CTM2013-44598-R) i NUREIEVA (ref. CTM2016-75953-C2-1-R).

A la meva mare i pare,
per no deixar-nos caure mai.

"La vida és una unió simbiòtica i cooperativa que permet triomfar als que s'associen."

Lynn Margulis

"El més revolucionari que una persona pot fer és dir sempre en veu alta el que realment està passant."

Rosa Luxemburg

Portada: adaptació d'un fragment de "Model-driven design of self-observing products" de Mathias Funk

Acte d'agraïment

Són moltes les situacions i circumstàncies que passen al llarg de cinc anys de Tesi. I darrere d'aquestes coses que se succeeixen hi ha moltes persones que han fet que aquest període, a voltes llarg, a voltes sinuós, fos més fàcil de recórrer. I, òbviament, aquesta Tesi no hauria estat possible sense tres persones a qui estic profundament agraït. A en Miquel per donar-me l'oportunitat de ser un membre més del grup de recerca, per confiar en mi per fer aquest doctorat i per guiar-me en el camí. A l'Anna per ensenyar-me tant en tants sentits diferents, per comptar amb mi en tantes campanyes i per seguir estant al meu costat tot aquest temps. I finalment, a en Jaime per estar disponible sempre que ho he necessitat i per ajudar-me a avançar. A totes tres, gràcies per les hores dedicades i per la motivació i les ganes de seguir millorant.

Avui no estaria aquí si no fos perquè un migdia a la Universitat Autònoma de Barcelona en Jordi Garcia-Orellana va decidir que era una bona idea proposar-me un treball de recerca amb ell. A ell i a en Valentí Rodellas i a l'Albert Folch, un agraïment etern per acompanyar-me en els meus primers passos en aquest món i fer possible també aquesta Tesi.

També hi ha altres persones a les quals estic profundament agraït. Persones amb qui he compartit tants moments sobretot bons, però alguns també de dolents, tot s'ha de dir. No sabria per on començar, però potser començaria per l'Aitor, en Xavi i en David, per les hores de cafès, de torns de nit, de cerveses, de suport mutu i de confidències. I continuaria amb una persona que va aparèixer un estiu de campanya i de la qual ja no m'he desprès: gràcies Emma per ser una porta d'emergència en tants moments crítics però també per tants instants de riures i alegries. I òbviament, no puc oblidar una persona amb qui he fet el mateix camí, companya de Tesi, de preocupacions, de lluites, de converses que alliberen, de paraules que reconforten. Gràcies Judit per ser-hi sempre que ho he necessitat. A totes vosaltres, coneixeu-vos ha estat una de les millors coses que m'han passat aquests cinc anys.

I en aquest camí, no podria oblidar-me de totes les companyes que han omplert de vida, ciència i alegria les sales 336 i 337: Albert, Mercè, Ester, Olaia, Jose Noel, Anna Aymà, Marta, Liam, Andreu, Patricia, Andrea, Queralt, Nil, Helena, Eduardo, Maria, Xavi, Andreu, Maria i Rut. Però també totes les companyes del departament i de la facultat: Toni, Galderic, Isa, Leo, Patrícia, Jose Luís, Josep, Montserrat i Magda.

En aquest entramat de persones que fan que la ciència avanci, a la universitat tenim companyes que són pedra angular. Un agraïment profund i sentit a la Montserrat Guart, per voler sempre ajudar-me en el Laboratori de Sedimentologia i fer també que aquesta Tesi hagi estat

possible. I a les companyes dels Serveis Científics i Tecnològics de la UB, especialment a la Maite i a la Bàrbara que van ser-hi sempre que ho he necessitat per avançar en l'objectiu que em vaig proposar. Gràcies a totes, de tot cor.

Obviously, I can't forget at Maarteen Van Daele and Marjn Boone from the University of Gent. But also Karen, my roommate in Gent. Thank you a lot. Dank u!

Probablement tampoc no seria aquí sense un professorat d'educació primària i secundària que des de la precarietat i l'amor etern per l'ensenyament, van obrir-me nous camins, paisatges i horitzons. No sé si llegiran aquestes línies però gràcies Xavier Gual, Lídia Gil, Ferran Gadea i Carme Arenas.

I amb una generositat inabastable i controlant cada paraula i estructura gramatical d'aquesta Tesi, vull agrair profundament a en Carles l'esforç de corregir-la. Però també, per ser-hi sempre que he necessitat la seva ajuda i el seu savi consell. Gràcies de tot cor.

Fora i dins de la Universitat però més a prop que mai, hi ha persones que han viscut amb mi aquesta Tesi. Gràcies Mireia, Salva i Elisenda per donar-me suport durant aquests cinc anys. Gràcies per ser inspiració i ajut i per tots els aprenentatges compartits. I gràcies a la Yolanda, la Montse i l'Adrià, i a l'Ivan, el Jordi, el Pau i el Carles i a la Cristina i aviat la Queralt però també a la Neus, la Xènia l'Aina, per ser aquella part de la meva vida que un dia arriba i, tot i la meva personalitat, arrela per quedar-se i florir.

He de confessar, i he necessitat anys per fer-ho, que viure al meu costat no és cosa fàcil. Però hi ha una persona que hi ha estat més de vuit anys. Al meu costat sabent-se un far per a mi en aquestes aigües remogudes. Sense tu, Sandra, no hauria pogut arribar aquí. Has estat al meu costat quan més ho necessitava. Persistentment i amb tot l'amor del món em vas fer de pilar i, avui, aquesta Tesi és també teva.

A les acaballes d'aquest acte d'agraïment em reservo l'espai per a la meva família. Per a la meva mare i el meu pare, per ser tossudament generoses. Per deixar-se vida i salut en jornades laborals inacabables per fer de la nostra vida la millor possible. Res no és fàcil per a les filles dels barris obrers, però gràcies mare i pare per fer-nos creure que a la vida s'ha de lluitar. I gràcies també a les meves germanes, Cristina, Laura i Eduard, per aprendre ensenyant el que vol dir la paraula cuidem-nos. Us estimo.

18 de juny de 2020
Barcelona, Països Catalans

Sumari

Resum

L'estudi de la concentració i la distribució de metalls i metal·loides en ambients costaners ha guanyat rellevància durant els darrers quaranta anys, principalment a conseqüència de la creixent preocupació per llurs efectes nocius sobre els ecosistemes i la salut pública. Els cicles dels metalls i metal·loides, amb una gran quantitat de variables físiques, químiques, biològiques i també antropogèniques que hi influeixen, són extremadament complexos, la qual cosa en dificulta la comprensió. Per aquest motiu, la millora de les metodologies i l'aplicació de noves tècniques d'estudi són fonamentals per poder aprofundir en el coneixement dels processos associats a la contaminació i la pol·lució de l'oceà per metalls i metal·loides.

En aquest context, aquesta Tesi representa una contribució al desenvolupament i a la integració de les metodologies disponibles per a l'estudi dels fluxos de metalls i metal·loides d'origen antropogènic cap al medi marí. Per atènyer aquest objectiu, la Tesi s'ha centrat en l'estudi de dues vies d'entrada de metalls i metal·loides cap a la mar costanera: les descàrregues d'aigua subterrània (DAS) i l'abocament directe de residus en dues àrees de la costa mediterrània, la costa central de Catalunya i la badia de Portmán, a Múrcia.

En primer terme, s'han abordat les metodologies de quantificació de les DAS mitjançant isòtops de Ra i ^{222}Rn. L'anàlisi i monitoratge dels isòtops de Ra a l'aqüífer al·luvial de la riera d'Argentona al llarg de dos anys ha demostrat que la variabilitat observada en llurs concentracions, de més d'un ordre de magnitud, està governada pel desplaçament de la posició de la interfase salina durant períodes de precipitacions abundants. La variabilitat enregistrada en les concentracions dels isòtops dificulta la determinació d'un valor representatiu de Ra a l'aqüífer, la qual cosa és un requeriment necessari per quantificar els fluxos de les DAS. Puix que els fluxos de metalls i metal·loides derivats de las DAS s'incrementen significativament durant els episodis de precipitacions, l'elevada dinàmica dels aqüífers costaners en règims micromareals fa necessari un millor coneixement dels processos hidrogeològics locals o regionals per poder reduir les incerteses associades a la quantificació dels fluxos de metalls i metal·loides als sistemes costaners.

En segon terme, la Tesi situa el focus sobre els fluxos de metalls i metal·loides derivats de l'abocament massiu de residus, sia d'origen industrial i urbà, com al prodelta del riu Besòs, o d'origen miner, com a la badia de Portmán. A més, amb l'objectiu de millorar la resolució de l'estudi i poder descriure en detall l'evolució temporal del flux de metalls i metal·loides, s'ha dut a terme l'anàlisi dels sediments a molt alta resolució mitjançant un escàner de fluorescència de raigs X (*XRF core scanner*). Aquest equipament permet obtenir una gran quantitat d'informació en molt poc temps, de manera no destructiva i amb resolucions impossibles d'aconseguir amb mètodes tradicionals de caràcter destructiu. Així doncs, s'ha desenvolupat un procediment de calibratge per transformar les mesures semiquantitatives de l'*XRF core scanner* a concentracions totals per diversos metalls i metal·loides (Ti, Mn, Fe, Zn,

As i Pb). Els resultats demostren que els procediments analítics i estadístics desenvolupats en aquest treball milloren la qualitat de les regressions lineals, amb coeficients de correlació (r^2) superiors a 0,94 i amb una reducció de les desviacions estàndards de les funcions obtingudes, especialment pel mètode de regressió ponderat de mínims quadrats (WLS). Això es tradueix en una minoració significativa dels errors associats a les concentracions calibrades de metalls i metal·loides, la qual cosa ha permès quantificar els llindars de concentració establerts en diverses guies de qualitat del sediment (*Sediment Quality Guidelines*, SQGs) amb un rang d'error de 0,4% a 2% pel Fe, 1% a 7% pel Zn, 3 a 14% pel Pb, i 5% a 16% pel Mn.

Finalment, aquest procediment de calibratge ha estat aplicat a la caracterització física i geoquímica d'un dipòsit submarí altament contaminat generat per l'abocament de residus miners resultants de l'explotació de jaciments de sulfurs a la badia de Portmán. Mitjançant una metodologia que integra múltiples tècniques analítiques fisicoquímiques, sedimentològiques i de datació per ^{210}Pb de testimonis de sediment, hom ha identificat sis fàcies sedimentàries: quatre pertanyents als residus miners *sensu strictu* (fàcies 2, 3, 4 i 5) i dues corresponents a sediments marins amb un cert grau de contaminació que predaten i postdaten el dipòsit de residus (fàcies 1 i 6). Els resultats obtinguts han permès explicar acuradament l'evolució del dipòsit de residus miners, el qual es concentra principalment al nord-oest de l'àrea d'estudi com a resultat no només de la ubicació del punt de descàrrega sinó també de la dinàmica sedimentària governada per l'efecte dominant de l'onatge de component est i sud-oest i els corrents litorals associats. De l'anàlisi geoquímica se'n desprèn que les concentracions de metalls i metal·loides al dipòsit de residus miners són molt superiors a les reportades en altres llocs de la mar Mediterrània. En els sediments superficials acumulats després de la finalització dels abocaments les concentracions de metalls i metal·loides són encara significativament superiors als valors naturals previs a l'activitat minera. Això, conjuntament amb la modelització numèrica de les concentracions i les distribucions de metalls i metal·loides en el sediment marí superficial (14 cm superiors), ha evidenciat l'existència d'un flux persistent cap als sediments més recents i cap al fons marí després de vint-i-cinc anys de la clausura de l'abocament de residus miners.

Per tot plegat, aquesta Tesi contribueix, volem pensar que de manera significativa, a la millora de les metodologies d'estudi dels fluxos de metalls i metal·loides, i de determinació i quantificació de llurs concentracions i distribucions al medi marí costaner. L'esforç d'integració metodològica desenvolupat en aquesta Tesi ha permès assolir una millor comprensió dels processos de contaminació i de pol·lució, i demostra que l'ús integrat de diverses metodologies és clau per a la millora dels programes i actuacions de gestió ambiental que permetin reduir els fluxos de metalls i metal·loides d'origen antropogènic cap a l'oceà i els seus efectes sobre l'ecosistema costaner.

Resumen

El estudio de la concentración y la distribución de metales y metaloides en ambientes costeros, ha adquirido relevancia en los último cuarenta años, principalmente como consecuencia de la creciente preocupación por sus efectos nocivos sobre los ecosistemas y la salud pública. Los ciclos de los metales y metaloides, con una gran cantidad de variables físicas, químicas, biológicas y también antropogénicas que influyen, son extremadamente complejos, circunstancia que dificulta su comprensión. Por este motivo, la mejora de las metodologías y la aplicación de nuevas técnicas de estudio es fundamental para poder profundizar en el conocimiento de los procesos asociados a la contaminación y la polución del océano por metales y metaloides.

En este contexto, esta Tesis representa una contribución al desarrollo y a la integración de las metodologías disponibles para el estudio de los flujos de metales y metaloides de origen antropogénico hacia el medio marino. Para alcanzar este objetivo, la Tesis se ha centrado en el estudio de dos vías de entrada de metales y metaloides hacia el mar costero: las descargas de agua subterránea (DAS) y el vertido directo de residuos en dos áreas de la costa mediterránea, la costa central de Cataluña y la bahía de Portmán, en Murcia.

En primer lugar, se han abordado las metodologías de cuantificación de las DAS mediante isótopos de Ra y ^{222}Rn. El análisis y el monitoreo de los isótopos de Ra en el acuífero aluvial de la riera de Argentona, durante dos años ha demostrado que la variabilidad observada en sus concentraciones, de más de un orden de magnitud, está gobernada por el desplazamiento de la posición de la interfase salina durante períodos de precipitaciones abundantes. La variabilidad registrada en las concentraciones de los isótopos dificulta la determinación de un valor representativo de Ra en el acuífero, lo cual es un requisito necesario para cuantificar los flujos de DAS. Puesto que los flujos de metales y metaloides derivados de las DAS aumentan significativamente durante los episodios de precipitaciones, la elevada dinámica de los acuíferos costeros en regímenes micromareales hace necesario un mejor conocimiento de los procesos hidrogeológicos locales o regionales para poder reducir las incertidumbres asociadas a la cuantificación de los flujos de metales y metaloides hacia los sistemas costeros.

En segundo lugar, la Tesis sitúa el foco sobre los flujos de metales y metaloides derivados del vertido masivo de residuos, sean estos de origen industrial y urbano, como en el prodelta del río Besós, o de origen minero, como en la Bahía de Portmán. Además, con el objetivo de mejorar la resolución del estudio y poder describir en detalle la evolución temporal del flujo de metales y metaloides, se ha llevado a cabo el análisis de los sedimentos a muy alta resolución mediante un escáner de fluorescencia de rayos X (*XRF core scanner*). Este instrumento permite obtener una gran cantidad de información en muy poco tiempo, de modo no destructivo y con una resolución imposibles de conseguir con métodos tradicionales de carácter destructivo. Así pues, se ha desarrollado un procedimiento de calibración para transformar las medidas semicuantitativas del *XRF core scanner* en concentraciones totales para diversos metales y

metaloides (Ti, Mn, Fe, Zn, As y Pb). Los resultados demuestran que los procedimientos analíticos y estadísticos desarrollados en este trabajo mejoran la calidad de las regresiones lineales, con coeficientes de correlación (r^2) superiores a 0,94 y con una reducción de las desviaciones estándares de las funciones obtenidas, especialmente por el método de regresión ponderado de mínimos cuadrados (WLS). Esto se traduce en una minoración significativa de los errores asociados a las concentraciones calibradas de metales y metaloides, lo cual ha permitido cuantificar los umbrales de concentración establecidos en diversas guías de calidad del sedimento (*Sediment Quality Guidelines*, SQGs) con un rango de error de 0,4% a 2% para el Fe, 1% a 7% para el Zn, 3 a 14% para el Pb, y 5% a 16% para el Mn.

Finalmente, se ha aplicado este procedimiento de calibración a la caracterización física y geoquímica de un depósito submarino altamente contaminado generado por el vertido de residuos mineros resultantes de la explotación de yacimientos de sulfuros en la bahía de Portmán. Mediante una metodología que integra múltiples técnicas analíticas fisicoquímicas, sedimentológicas y de datación por ^{210}Pb de testigos de sedimento, se han identificado seis facies sedimentarias: cuatro pertenecientes a los residuos mineros *sensu strictu* (facies 2, 3, 4 y 5) y dos correspondientes a sedimentos marinos con un cierto grado de contaminación que pre-datan y post-datan el depósito de residuos (facies 1 y 6). Los resultados obtenidos han permitido explicar la evolución del depósito de residuos mineros, el cual se concentra principalmente al noroeste del área de estudio debido no sólo a la ubicación del punto de vertido si no también a la dinámica sedimentaria gobernada por el efecto dominante del oleaje de componente este y sudoeste y por las corrientes litorales asociadas. Del análisis geoquímico se desprende que las concentraciones de metales y metaloides en el depósito de residuos mineros son muy superiores a las reportadas para otros lugares del Mar Mediterráneo. En los sedimentos superficiales acumulados posteriormente al cese de los vertidos las concentraciones de metales y metaloides son aún significativamente superiores a los valores naturales previos a la actividad minera. Esto, junto con la modelización numérica de las concentraciones y las distribuciones de metales y metaloides en el sedimento marino superficial (14 cm superiores), ha puesto de manifiesto la existencia de un flujo persistente hacia los sedimentos más recientes y hacia el lecho marino después de veinticinco años de la clausura de los vertidos de residuos mineros.

Per todo lo expuesto, esta Tesis contribuye, queremos pensar que de manera significativa, a la mejora de las metodologías de estudio de los flujos de metales y metaloides, y de determinación y cuantificación de sus concentraciones y distribuciones en el medio marino costero. El esfuerzo de integración metodológica desarrollado en esta Tesis ha permitido alcanzar una mejor comprensión de los procesos de contaminación y de polución, y demuestra que el uso integrado de diversas metodologías es clave para la mejora de los programas y actuaciones de gestión ambiental que permitan reducir los flujos de metales y metaloides de origen antropogénico hacia el océano, así como sus efectos sobre el ecosistema costero.

Abstract

The study of the concentration and distribution of metals and metalloids in coastal environments has gained interest in the last forty years, mainly due to the growing concern about their harmful effects on the ecosystems and public health. Even so, the elevated complexity of the metals and metalloids cycles, which are influenced by numerous physical, chemical, biological and anthropogenic variables, makes their understanding difficult. Because of this, improving the state of the art methodologies and applying new techniques is essential to achieve a better knowledge of the processes associated with marine pollution by metals and metalloids.

In this context, this PhD Thesis represents a contribution to the development and integration of methodologies for the study of anthropogenic-sourced fluxes of metals and metalloids into the sea. To achieve this objective, the Thesis is focused in the study of two type of pathways of metals and metalloids fluxes to the coastal sea: submarine groundwater discharges (SGD) and direct waste disposal in two areas of the Iberian Mediterranean coast, which are the central coast of Catalonia and Portmán Bay, in Murcia.

Firstly, the Thesis addresses the methodologies for quantifying SGD using Ra and ^{222}Rn isotopes. The analysis and monitoring of Ra isotopes in the alluvial aquifer of the Argentona torrent during two years has shown that the variability of their concentrations, which is more than one order of magnitude, is mainly governed by the displacement of the saline interface during heavy rain periods. The recorded variability of the isotopic concentrations makes difficult determining a representative value of Ra in the aquifer, which is a requirement to quantify SGD. Given the significant increase of SGD metals and metalloids fluxes derived during heavy rain events, the high dynamics of coastal aquifers in microtidal regimes imposes a better knowledge of the hydrogeological processes at local or regional scales in order to reduce the uncertainties associated with the quantification of such fluxes in coastal systems.

Secondly, this PhD Thesis focuses in metals and metalloids fluxes from massive coastal waste accumulations, whether they result from mining activities, as in Portmán Bay, or from industrial and urban sources, as in the Besòs River prodelta off Barcelona city. To improve the fineness of analysis needed to carefully describe the temporal evolution of metal and metalloids fluxes, we have carried out high-resolution measurements of the sediments by means of a XRF core scanner. This equipment produces huge amounts of data within a reduced time of analysis, in a non-destructive way and with resolutions that are unachievable by traditional, sample destructive methods. A calibration procedure has been developed to transform the semi-quantitative measurements from the XRF core scanner into total concentrations of various metals and metalloids (Ti, Mn, Fe, Zn, As and Pb). The results demonstrate that the analytical and statistical procedures developed in this study improve the quality of linear regressions, with correlation coefficients (r^2)

above 0.94 and a reduction of standard deviations, especially when applying the weighted least squares regression method (WLS). This translates into a reduction of errors associated with the calibrated concentrations of metals and metalloids, which allows quantifying the concentration thresholds defined by various sediment quality guides (SQG) with an error range of 0.4% to 2% for Fe, 1% to 7% for Zn, 3% to 14% for Pb and 5% to 16% for Mn.

The same calibration procedure has been applied to the physical and geochemical characterization of a highly polluted marine deposit originated by the dumping of mining wastes in Portmán Bay. The application of multiple analytical physicochemical, sedimentological and ^{210}Pb dating techniques to a large set of short sediment cores allowed identifying six main sedimentary facies, four of which correspond to the mine tailings *sensu strictu* (facies 2, 3, 4 and 5) and two to contaminated marine sediments that predate (facies 1) and postdate (facies 6) the mine tailings deposit. The results allow explaining the evolution of the mine tailings deposit, which mainly concentrate into the northwest corner of the study area as a consequence not only of the location of the discharge point but also of the sedimentary dynamics governed by the dominant effect of an easterly and southwesterly wave pattern and associated littoral currents. The analyses show that the metals and metalloids concentrations in the main tailings facies are significantly higher than those commonly found in other regions of the Mediterranean Sea. Within the top layer of sediments, which formed following the cessation of waste disposal, the concentration of metals and metalloids is less but still is significantly higher than background natural values prior to mining activities. This data, together with the numerical modeling of the concentrations and distribution of metals and metalloids in the uppermost layer of marine sediments (top 14 cm), evidences a persistent flow to the most recent sediments and the seafloor twenty-five years after the closure of mine waste discharge.

Finally, the outcomes of this Thesis involve a significant improvement of the methodologies applied to the study of metal and metalloid fluxes to the marine coastal environment, and also on the determination and quantification of their concentrations and distributions. The major effort for methodological integration carried out in this Thesis has led to a better understanding of the processes controlling those fluxes and the ensuing contamination and pollution effects. We think that we have also proven that the integrated used of complementary methodologies is critical for improving environmental management programs and actions aimed at reducing the fluxes of anthropogenic metals and metalloids to the ocean and their deleterious effects on marine coastal ecosystems.

Presentació de la Tesi

"Cap cosa torna al no-res,
ans totes, per la disgregació,
tornen als elements
de la pròpia matèria."
Lucreci
De rerum natura (50 aC)

La gènesi dels metalls i metal·loides és la història dialèctica entre el naixement i la mort de les estrelles en els cúmuls galàctics. És en el cor d'aquests sistemes, a elevades temperatures i pressions, on es desencadenen les reaccions de fusió nuclear que permetran la formació dels elements més pesants de la taula periòdica. Alguns d'ells, com el ferro o el níquel, es formaran en el nucli; altres, com la sílice, en capes més exteriors, i els més pesants, com l'or o el mercuri, es generaran durant la formació de les estrelles de neutrons. És al final de la vida de les estrelles, amb el seu col·lapse i posterior explosió, quan els metalls i metal·loides seran disseminats arreu de la galàxia i de les runes còsmiques generades naixeran nous sistemes estel·lars i planetes.

Del polsim metàl·lic que emana de les estrelles al floriment de la vida a la Terra, doncs, alguns metalls, com el ferro, el coure o el cobalt, són essencials per al desenvolupament cel·lular i la síntesi de vitamines, i alhora controlen la productivitat primària als oceans. No entendríem la vida sense aquests elements. Com tampoc el desenvolupament de les societats humanes que s'han valgut d'ells per fabricar eines, productes i instruments molt diversos. Tant és així que, en els dos darrers segles, la gran demanda de metalls i metal·loides necessaris per al desenvolupament agroindustrial capitalista ha incrementat significativament la seva extracció de l'escorça terrestre. Aquest fet s'ha traduït en un increment dels fluxos de metalls i metal·loides des dels continents cap als oceans així com de llurs concentracions a les aigües i els

sediments costaners. Sense cap mena de dubte, aquest enriquiment és actualment un dels principals impactes antropogènics sobre els ecosistemes marins.

Els cicles dels metalls i dels metal·loides presenten una complexitat elevada. L'esforç científic de les darreres dècades ha permès entendre el comportament fisicoquímic dels metalls i els metal·loides i els processos de partionament en els oceans, identificar i quantificar els principals fluxos i determinar la seva distribució a la columna d'aigua i al sediment. Aquests avenços, però, no haurien estat possibles sense el progrés i el perfeccionament metodològic i tècnic. Puix que l'increment de metalls i metal·loides als ambients costaners és una tendència a l'alça causada per l'activitat antropogènica, la present Tesi Doctoral té l'objectiu general de contribuir al desenvolupament de les metodologies d'anàlisi i quantificació dels fluxos de metalls i metal·loides d'origen antropogènic cap al mar costaner, així com llur caracterització fisicoquímica i la seva distribució en el sediment marí.

Conceptualment, la Tesi Doctoral se situa en l'encreuament entre l'oceanografia, la sedimentologia, la hidrogeologia i la geoquímica. Així, en els successius capítols s'emfatitzarà l'estudi de dos tipus de fluxos de metalls i metal·loides cap al medi marí: la descàrregues d'aigua subterrània (DAS) i l'abocament directe de residus al mar costaner. Els resultats d'aquest treball els podríem resumir fent referència, primer, a la revisió de les metodologies emprades en la quantificació dels fluxos de metalls i metal·loides per DAS mitjançant traçadors com el radi i el radó i, segon, al desenvolupament de noves metodologies de quantificació de les concentracions de metalls i metal·loides, així com la integració de múltiples tècniques i modelitzacions numèriques per a la caracterització del sediment marí afectat per l'abocament de residus amb alts continguts de metalls i metal·loides.

Aquesta Tesi doctoral s'emmarca en el projecte europeu MIDAS (*Managing Impacts Of Deep Sea Resource Exploitation*, ref. GA 603418, 2013-16) i en els projectes estatals NUREIEV (*NUevos REtos en la investigación de cañones submarinos: Indicadores del Estado ambiental y Variabilidad espacio-temporal − El papel de los temporales*, ref. CTM2013-44598-R) i NUREIEVA (*NUevos REtos de Investigación en el ambiente Extremo de los Vertidos mineros de la Bahía de Portmán: aplicación de tecnologías Avanzadas*, ref. CTM2013-44598-R), centrats en l'avaluació dels impactes de l'explotació de recursos minerals al medi marí i, especialment, en l'avenç de la caracterització geofísica i fisicoquímica dels dipòsits costaners de residus miners, amb la badia de Portmán (Múrcia) com a cas d'estudi paradigmàtic.

Concretament, en el marc d'aquesta Tesi Doctoral s'han establert els següents objectius específics:

- Investigar el paper de les dinàmiques hidrogeològiques en el comportament dels isòtops de Ra i ^{222}Rn en un aqüífer al·luvial mediterrani i discutir l'ús d'aquests com a traçadors de DAS i dels fluxos de metalls i metal·loides associats.

- Desenvolupar un mètode de calibratge que permeti transformar les mesures semiquantitatives d'elevada resolució obtingudes mitjançant un escàner de fluorescència de raigs X a concentracions totals de metalls i metal·loides.

- Quantificar els errors analítics i estadístics associats a aquest calibratge i avaluar el seu potencial per a determinar les concentracions de diversos metalls i metal·loides segons les guies de qualitat del sediment (*sediment quality guidelines*, SQG).

- Analitzar la dispersió de metalls i metal·loides en sediments marins afectats per l'abocament de residus miners mitjançant la combinació de diverses tècniques fisicoquímiques d'anàlisi no destructiva, en continu i d'alta resolució.

- Integrar mitjançant models numèrics les dades fisicoquímiques obtingudes de l'anàlisi de l'extensió submergida del dipòsit de residus miners de la badia de Portmán i quantificar el flux total de metalls i metal·loides un cop finalitzà l'abocament.

Així doncs, en aquesta Tesi Doctoral defensem la necessitat d'avançar en la integració de múltiples tècniques sedimentològiques, hidrogeològiques i geoquímiques amb la modelització numèrica per a l'anàlisi i la quantificació de metalls i metal·loides en el medi marí. Els resultats obtinguts es poden traduir en una millora de les metodologies emprades i demostren que la utilització de tècniques complementàries aporta una nova perspectiva, redueix l'esforç analític i incrementa el volum de dades tractades, la qual cosa permet un major enteniment dels processos de distribució de metalls i metal·loides a la columna d'aigua i als sediments marins.

Estructura de la Tesi Doctoral

Aquesta Tesi doctoral es presenta com a compendi de tres publicacions, dues de les quals estan publicades ja en revistes indexades als Journal Citation Reports de la Web of Science, mentre que la tercera, també inclosa en format article, és a punt per a ésser sotmesa a una revista indexada. La Tesi s'estructura en cinc capítols i segueix la normativa establerta en el text consolidat del 23 de juliol del 2019 de la Norma Reguladora del Doctorat de la Universitat de Barcelona, així com la norma específica del Programa de Doctorat de Ciències del Mar d'aquesta universitat.

El **Capítol 1** consisteix en una introducció general que té per objectiu centrar el lector en el marc conceptual i metodològic del treball realitzat. S'inicia amb la definició fisicoquímica de metall i metal·loide i amb les diverses classificacions emprades per ordenar aquests elements. Aquest primer capítol inclou una descripció de les principals fonts i fluxos de metalls i metal·loides cap als oceans i, especialment, els ambients costaners, alhora que també s'introdueixen els conceptes de contaminació i pol·lució. Més endavant, en aquest mateix capítol, es descriuen l'àrea d'estudi, les mostres analitzades i les tècniques emprades.

El **Capítol 2** presenta els resultats obtinguts, recollits en els tres articles científics esmentats adés. Els dos primers han estat reproduïts de manera fidedigna tal i com van ser publicats. Seguidament, incloem un breu resum de cadascun d'ells.

Capítol 2.1 Cerdà-Domènech, M., Rodellas, V., Folch, A., Garcia-Orellana, J., 2017. *Constraining the temporal variations of Ra isotopes and Rn in the groundwater end-member: Implications for derived SGD estimates.* Science of the Total Environment, 595, 849-857. Doi: 10.1016/j.scitotenv.2017.03.005.

En aquest article s'avalua durant dos anys la influència dels paràmetres hidrogeològics i la posició de la interfase salina sobre la variabilitat temporal de les concentracions dels isòtops de Ra i ^{222}Rn a l'aqüífer al·luvial de la riera d'Argentona (Barcelona). L'estudi emfatitza la necessitat d'entendre la hidrogeologia dels aqüífers costaners a l'hora d'emprar els isòtops de Ra i ^{222}Rn com a traçadors de DAS i per la quantificació dels fluxos d'elements que se'n deriven (p. ex. micronutrients, metalls o contaminants orgànics). La metodologia i les recomanacions que s'hi proposen han estat aplicades en treballs posteriors de quantificació del flux de metalls i metal·loides, en els quals el doctorand també és coautor (p. ex. Alorda et al., 2019).

Capítol 2.2 Cerdà-Domènech, M., Frigola, J., Sanchez-Vidal, A., Canals, M., 2020. *Calibrating high resolution XRF core scanner data to obtain absolute metal concentrations in highly polluted marine deposits after two case studies off Portmán Bay and Barcelona, Spain*. Science of the Total Environment, 717, 134778. Doi: 10.1016/j.scitotenv.2019.134778.

En aquest article es presenta un procediment inèdit de calibratge per transformar les mesures semiquantitatives obtingudes mitjançant un escàner de fluorescència de raig X a concentracions totals de diversos metalls i metal·loides en dos dipòsits submarins altament contaminats, el de residus miners de la badia de Portmán i el de fangs de depuradora del Besòs, a Barcelona. Alhora, s'examinen les regressions lineals i la propagació d'errors analítics i estadístics mitjançant tres mètodes de mínims quadrats. La robustesa del procediment de calibratge obtingut permet discutir l'ús d'aquesta metodologia en la determinació precisa i acurada de la concentració de metalls i metal·loides en sediments marins atenent a les restriccions imposades per les SQGs.

Capítol 2.3 Cerdà-Domènech, M., Frigola, J., Canals, M., Sanchez-Vidal, A., Rodes, N., Van Daele, M., Boone, M., Baza, A., Amblas, D., Soldevila, E., Garcia-Orellana, J., Roqué, J., 2020. *Physical and geochemical characterization of a submarine sulfide mine tailings deposit, Portmán Bay, SE Spain* (pendent de submissió).

En aquest treball s'analitzen per primera vegada les característiques físiques i químiques de la part més superficial de l'extensió submergida del dipòsit de residus miners de la badia de Portmán i de la capa de sediments formada al llarg dels vint-i-cinc anys posteriors a la clausura dels abocaments. Aportem una explicació acurada de l'evolució de l'abocament des d'una perspectiva integradora, partint de la combinació de tècniques d'anàlisi no destructiva i d'alta resolució de testimonis de sediment, amb mesures de mida de gra i l'aplicació del calibratge desenvolupat en el subcapítol 2.2 per a l'obtenció de la concentració absoluta de diversos metalls i metal·loides. La integració de les dades fisicoquímiques del sediment permet, mitjançant una modelització numèrica per interpolació tridimensional, obtenir la distribució de les concentracions de metalls i metal·loides a la làmina més superficial de sediment (0 − 1 cm). Alhora, mitjançant aquesta modelització s'obté per primera vegada la massa total dels elements d'interès en el paquet de sediment acumulat a partir del cessament dels abocaments.

El **Capítol 3** és dedicat a la síntesi i la discussió integrada dels principals resultats obtinguts en els capítols anteriors, tot enriquint la discussió amb altres publicacions de les quals el doctorand és coautor (p. ex. Alorda et al., 2019) i que són també d'interès científic en el context de la present Tesi Doctoral.

El **Capítol 4** inclou les conclusions més rellevants i les possibles línies futures de recerca, mentre que al **Capítol 5** s'hi recull la bibliografia de la resta de capítols de la Tesi. Finalment, les darreres pàgines corresponen a l'**Annex** en què es reprodueixen els articles tal i com foren publicats, per cloure amb un Índex terminològic i els llistats d'abreviatures, símbols i sigles emprats, amb la finalitat de facilitar la lectura i la compressió del text.

Capítol 1

"Fer és una lluita tenaç
contra un mateix.
Fer és contradir-se."

Anna Gual

Introducció

L'estudi dels metalls i els metal·loides a l'oceà

Definició fisicoquímica de metall i metal·loide
Fonts de metalls i metal·loides a l'oceà
Distribució i concentració de metalls i metal·loides a l'oceà
Fluxos de metalls i metal·loides cap a l'oceà
Contaminació i pol·lució per metalls i metal·loides en el medi marí

Zones d'estudi

El prodelta del riu Besòs
L'aqüífer de la riera d'Argentona
La badia de Portmán

Metodologia

Tècniques de mostreig
Tècniques analítiques
Tractament i computació numèrica de les dades

1.1 L'estudi dels metalls i metal·loides a l'oceà

1.1.1 Definició fisicoquímica de metall i metal·loide

El concepte metall, que prové del grec μεαλλον o *métallon*, és emprat per definir els elements químics «que condueixen l'electricitat, tenen una brillantor metàl·lica, són mal·leables i dúctils, formen cations i tenen òxids bàsics» (Atkins i Jones, 1997). Aquests elements poden presentar altres característiques com ara una elevada conductivitat i densitat. Tanmateix, certs elements com B, el Si, el Ge, el As o el Te presenten una conductivitat elèctrica baixa que augmenta amb la temperatura, motiu pel qual són categoritzats com a metal·loides o semimetalls. A escala atòmica, els metalls i els metal·loides es caracteritzen per una estructura cristal·lina, en la qual els àtoms s'uneixen per mitjà d'enllaços metàl·lics, és a dir, per enllaços químics fonamentats en la força d'atracció electrostàtica entre el núvol d'electrons deslocalitzats de l'àtom i els ions metàl·lics carregats positivament (cations). Aquesta configuració genera estructures cristal·lines compactes que confereixen als metalls i metal·loides les característiques fisicoquímiques anteriorment descrites (Figura 1.1).

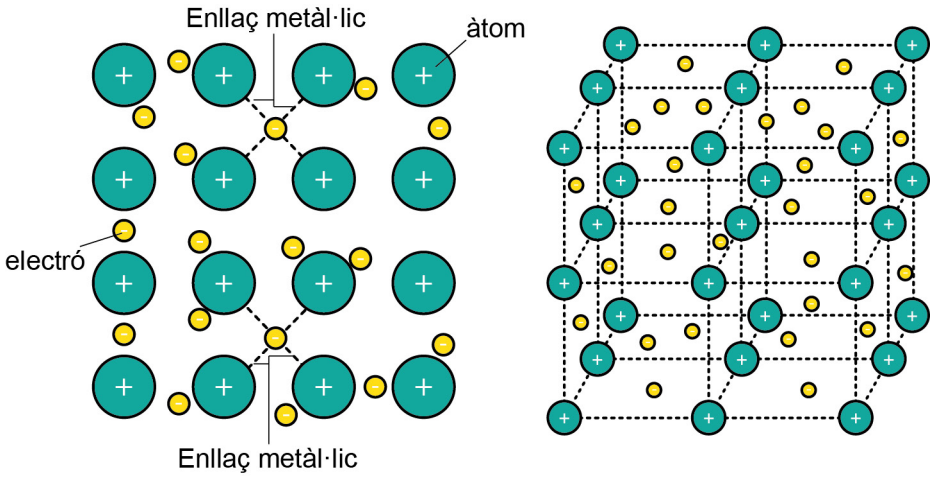

Figura 1.1 Esquema simplificat en dos i tres dimensions de l'estructura atòmica de metalls i metal·loides amb els enllaços metàl·lics que la conformen.

El grup dels metalls i els metal·loides és notablement extens i el seu comportament a l'ambient dels elements que el conformen pot diferir apreciablement. Així, seixanta-nou elements de la taula periòdica, excloent la sèrie dels transurànids, són considerats metalls i metal·loides (Figura 1.2). Concretament, les dues primeres columnes de la taula, amb l'excepció del H, corresponen als metalls alcalins i alcalinoterris, respectivament, que són elements de densitat baixa i que reaccionen amb facilitat

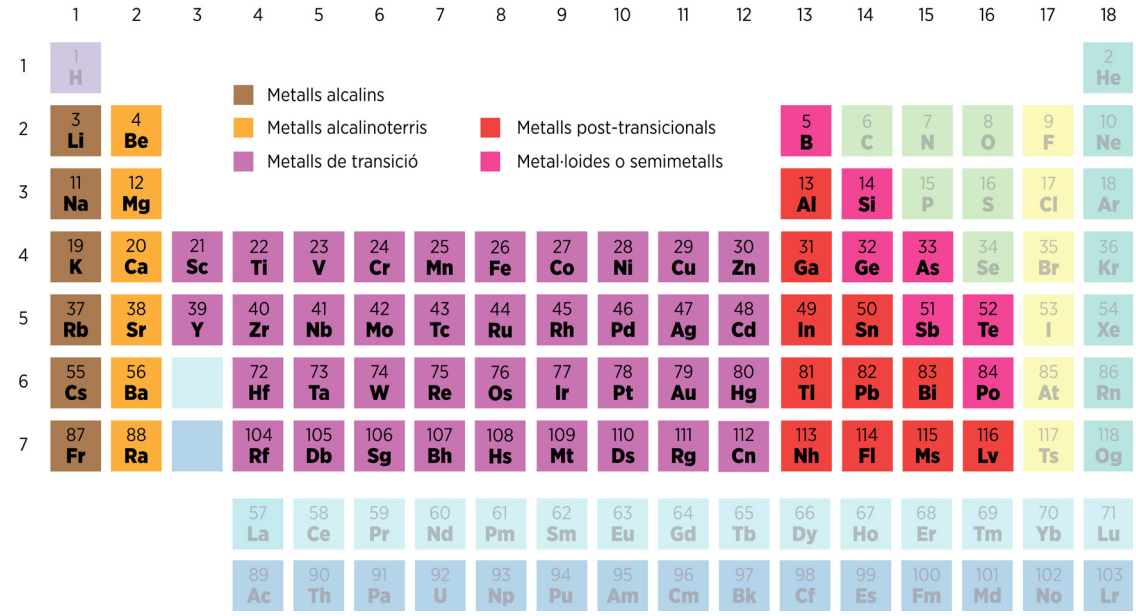

Figura 1.2 Taula periòdica dels elements en què es destaquen els metalls alcalins, alcalinoterris, de transició i posttransicionals, i els metal·loides.

amb els halògens (columna disset) per formar sals iòniques i hidròxids bàsics. A continuació, les columnes tres i dotze corresponen a l'extens grup dels metalls de transició. Aquests són els metalls més convencionals i més utilitzats en aplicacions industrials. Tenen una aparença metàl·lica i són molt durs, llevat del Hg, el qual té un comportament similar a la resta de metalls de transició a temperatures molt baixes. Finalment, a les columnes tretze, catorze i quinze, hi ha els metalls posttransicionals, és a dir, els elements situats entre els metalls de transició com el Al, el Sn o el Pb i els metal·loides esmentats anteriorment.

Així i tot, convé assenyalar que hi ha altres classificacions dels metalls i els metal·loides, per exemple segons les seves propietats o la seva concentració i efectes en el medi (p. ex. metall essencial, metall traça, micronutrient o metall tòxic). D'aquestes classificacions, la que agrupa els elements metàl·lics segons les seves propietats físiques i toxicològiques és la més emprada, especialment en publicacions científiques i legislacions ambientals, tot diferenciant metalls lleugers i metalls pesants (Duffus, 2002). El primer grup, el dels metalls lleugers, comprèn els elements metàl·lics amb una densitat inferior a 4,1 g cm^{-3}, els quals generalment presenten una toxicitat baixa com, per exemple, el Al, el Mg, el Ti i el Be. El segon grup, el dels metalls pesants, concentra els elements amb densitats superiors a 6 g cm^{-3} i amb un potencial tòxic més alt. Inclou metalls de transició com el Mn, el Fe, el Co, el Ni, el Cu, el Cr i el Zn, metalls posttransicionals com el Sn i el Pb i metal·loides com el As i el Po.

Tot i l'ús tan estès d'aquesta classificació, un informe de la Unió Internacional de Química Pura i Aplicada considerà que el concepte «metall pesant» no disposa d'una base científica consistent (Duffus, 2002). Atès que no hi ha una relació generalitzada entre les propietats físiques i químiques, com la densitat i la toxicitat, Duffus (2002) recomana l'ús d'una classificació fonamentada en l'especiació química, la selectivitat de l'absorció biològica, la funcionalitat i la toxicitat. En conseqüència, i amb la voluntat d'emprar sempre la mateixa nomenclatura i així evitar equívocs, en aquesta Tesi s'empra la terminologia «metall i metal·loide» en la seva estricta definició fisicoquímica donada per Atkins i Jones (1997).

1.1.2 Fonts de metalls i metal·loides a l'oceà

La presència de metalls i metal·loides a l'oceà és el resultat dels processos de meteorització física, química i biològica de les roques continentals i el seu transport posterior en forma dissolta o particulada. Quantitativament, els metalls més abundants a l'escorça terrestre són el Al (7,5% m/m), el Fe (4,7%), el Na (3,4%), el K (2,6%), el Mg (2,4%) i el Ti (0,6%) (Giddings, 1973). Aquests metalls, especialment el Fe i el Al, i també el Si, són els constituents majoritaris dels minerals primaris de les roques ígnies i metamòrfiques originades a partir de la cristal·lització del magma i la modificació en estat sòlid de les roques ígnies i sedimentàries preexistents. És precisament durant aquests processos quan els metalls i metal·loides menys abundants, com el Cd, el Co, el Cu, el Zn, el As, i el Hg, s'incorporen a la xarxa cristal·lina dels minerals mitjançant la substitució isomorfa dels elements majoritaris (Taula 1.1). En general, els minerals ferromagnèsics com l'olivina ($(Mg,Fe)_2SiO_4$) i l'augita ($(Ca,Mg,Fe)_2(Si,Al)_2O_6$) presenten una concentració i una diversitat d'elements metàl·lics i de metal·loides més altes que els minerals amb més contingut de Si, els quals són més resistents a la meteorització i a la substitució isomorfa. Entre els minerals primaris destaquen els hidròxids com la gibbsita ($Al(OH)_3$) i els aluminosilicats com els feldespats ($(K,Na,Ca,Ba,NH_4)(Si,Al)_4O_8$), però també sulfurs com la pirita (FeS_2), la galena (PbS), l'esfalerita (ZnS), l'arsenopirita (FeAsS), l'orpiment (As_2S_3) i la cobaltita (CoAsS).

La fragmentació mecànica d'aquests minerals i de les roques que els contenen facilita el seu transport i acumulació en ambients sedimentaris. Tot seguit, els processos de la diagènesi i la litificació conduiran a la formació de roques sedimentàries (Figura 1.3). La concentració de metalls i metal·loides en sediments i roques sedimentàries és variable (Taula 1.1) i, naturalment, està condicionat per la mineralogia de la roca mare,

	Escorça terrestre	Roques ígnies			Roques sedimentàries		
		Ultramàfiques	Màfiques	Granítiques	Calcàries	Gres	Esquistos
Ag	0,07	0,06	0,1	0,04	0,12	0,25	0,07
As	1,5	1	1,5	4,5	1	1	13
Au	0,004	0,003	0,003	0,002	0,002	0,003	0,0025
Cd	0,1	0,14	0,13	0,09	0,025	0,05	0,22
Co	20	110	35	1	0,1	0,3	19
Cr	100	2,980	200	4	11	35	90
Cu	50	42	90	13	5,5	30	39
Hg	0,05	0,004	0,01	0,08	0,16	0,29	0,18
Mo	1,5	0,3	1	2	0,16	0,2	2,6
Ni	80	500	150	0,5	7	9	68
Pb	14	14	3	24	5,7	10	23
Sb	0,2	0,1	0,2	0,2	0,3	0,005	1,5
Se	0,05	0,13	0,05	0,05	0,03	0,01	0,5
Sn	2,2	0,5	1,5	3,5	0,5	0,5	6
Tl	0,6	5	0,08	1,1	0,14	0,36	1,2
U	2,4	0,03	0,43	4,4	2,2	0,45	3,7
V	160	40	250	72	45	20	130
W	1	0,1	0,36	1,5	0,56	1,6	1,9
Zn	75	58	100	52	20	30	120

Taula 1.1 Concentració de diversos metalls i metal·loides a l'escorça terrestre i a les roques ígnies i sedimentàries en mg kg^{-1} (adaptat d'Alloway, 1990).

la capacitat d'adsorció dels materials sedimentaris i el contingut de metalls de la massa d'aigua on eventualment s'hagin format (Alloway, 1990). L'exposició dels sediments i roques sedimentàries a condicions oxidants, per exemple per contacte amb l'atmosfera o aigües continentals i/o marines, pot afavorir la desestabilització química i determinar l'inici de reaccions d'oxidació dels minerals. Hi ha diversos factors que poden influir en aquests processos: la mida del cristall, fragment o partícula; la seva porositat i àrea superficial; l'estructura cristal·lina del mineral; la presència d'elements de substitució, és a dir, inclusions i impuritats; la temperatura ambiental; la presència d'aigua i/o aire; el pH de la solució en contacte amb el mineral; o l'activitat microbiològica (Lottermoser, 2010). La combinació d'aquests factors pot provocar la dissolució i la hidròlisi dels metalls i metal·loides, i l'alliberament de cations (p. ex. Fe^{2+}, Fe^{3+}, Al^{3+}, Cu^{2+}, Cd^{2+} i Zn^{2+}) o compostos clorats (p. ex. $CdCl_2$ i $ZnCl_2$); la seva precipitació en forma d'hidròxids (p. ex. $Fe(OH)_3$ o $Al(OH)_3$); la formació de minerals secundaris fàcilment solubles com ara sulfats i hidrosulfats; i l'alliberament en estat gasós a l'atmosfera dels elements més volàtils com el Hg, el Se i el As. En apartats posteriors s'aprofundirà en els processos químics que intervenen en el procés d'alliberament de metalls i metal·loides al medi.

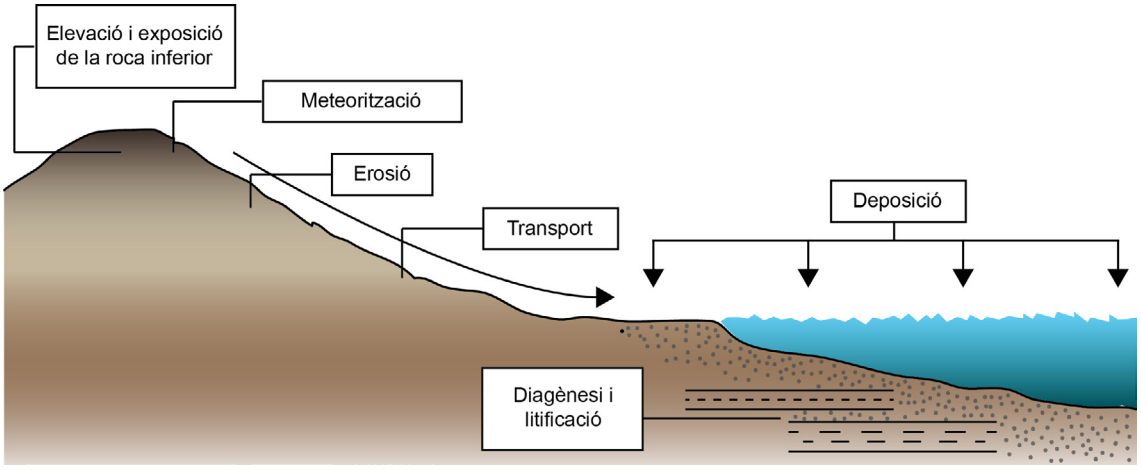

Figura 1.3 Principals processos que intervenen en la formació de roques sedimentàries (adaptat de Nichols, 2009).

Tot i que la meteorització de les roques continentals és la principal font de metalls a l'oceà, en el darrer segle les fonts antropogèniques han guanyat rellevància com a resultat del desenvolupament agroindustrial i urbà, especialment a les zones costaneres i a les conques fluvials que hi aboquen (Ridgway i Shimmield, 2002). Una proporció significativa dels metalls i els metal·loides d'origen antropogènic prové del transport rodat, especialment en zones urbanes, com a resultat de les emissions de gasos i partícules dels motors de combustió i del desgast de pneumàtics i discs de frens (Schauer et al., 2006, Querol et al., 2007, Keulen et al., 2013). Un dels metalls més freqüents és el Pb, utilitzat en els combustibles com a additiu antidetonant en forma de tetraetilè de plom ($(CH_3CH_2)_4Pb$) (Boyle et al., 2014). La seva emissió a l'atmosfera durant la combustió de les benzines arribà al seu màxim durant les darreres dècades del segle XX, fet que en va incrementar en dos ordres de magnitud les concentracions als rius i oceans (Patterson, 1965). Alhora, altres metalls com el Cd i el Zn són utilitzats en la fabricació de pneumàtics, per exemple en forma de ditiofosfat de zinc ($Zn[S_2P(OR)_2]_2$) o òxid de zinc (ZnO) i conjuntament amb el Pb i el Cr també s'usen preferentment en la fabricació de pigments i pintures sintètiques (p. ex. ZnO i $PbCrO_4$) i bateries (p. ex. PbO_2 i $ZnCl_2$)(Adachi i Tainosho, 2004). El Cu es un dels metalls més emprats en la fabricació dels discs de frens de vehicles, el desgast dels quals és una de les principals fonts de Cu en zones urbanes (Davis et al. 2001).

En el sector industrial, el Cd s'usa en forma d'organocadmi en la fabricació de PVC (p. ex. dimetillcadmi, CH_3-Cd-CH_3 o dietilcadmi, CH_3CH_2-Cd-CH_2CH_3), un dels materials de construcció més comuns, per estabilitzar el polímer i fer-lo resistent a la temperatura, la llum i la decoloració. Junt amb el Cu s'utilitza principalment

en la fabricació de cablejat elèctric i en la indústria automobilística i ferroviària, i també com additiu de pigments i en la fabricació de canalitzacions i monedes. Un altre metall d'origen antropogènic present als oceans és el Hg el qual és alliberat a l'atmosfera en forma de metil mercuri (CH_3Hg) i arriba als oceans per deposició atmosfèrica. Les principals fonts d'Hg estan relacionades amb la mineria de l'or, la crema de combustibles fòssils i la producció primària de metalls no fèrrics, a més de participar en el procés de fabricació de ciment.

Finalment, en l'agricultura, és molt comú l'ús del As en forma d'òxid d'arsènic (As_2O_3) − també present en les cendres de la combustió del carbó − per a la fabricació de pesticides, insecticides i herbicides, i també a la indústria com a pigment (As_2S_2), decolorant, conservant de la fusta i semiconductor. Cal destacar també l'ús del Cu en agricultura com a adob en forma de sulfat de coure ($CuSO_4$) i pesticida (p. ex. $Cu_2(OH)_3Cl$).

1.1.3 Distribució i concentració de metalls i metal·loides a l'oceà

La distribució de metalls i metal·loides a l'oceà està influenciada per les formes físiques i químiques en què hi són presents. Així, hom sol distingir tres fraccions: dissolta, col·loïdal i particulada (Figura 1.4.C). Per bé que aquesta classificació depèn significativament del coeficient de partició (K_D), és a dir, de la tendència d'un element a associar-se amb la fase particulada, experimentalment la diferenciació respon a l'ús de filtres que retenen les partícules de mida igual o superior 0,4 μm (Figura 1.4.C). Els metalls dissolts comprenen els cations lliures en diversos estats d'oxidació, ions hidratats, i complexos solubles orgànics i inorgànics, com els oxianions (p. ex. MoO_4^{2-} o el $Hg(Cl)_4^{2-}$), que són una potencial font de col·loides (Figura 1.4.A). La fracció col·loïdal, tant orgànica com inorgànica, presenta una mida de les partícules que oscil·la entre 0,02 i 0,4 μm. Aquesta fracció també inclou virus, bacteris i altres petits organismes. Les dificultats tècniques per separar els col·loides de les mostres fan que sovint hom els consideri dins de la fracció dissolta en la determinació dels coeficients de partició.

La fracció particulada, superior a 0,4 μm, inclou metalls i metal·loides adsorbits en partícules orgàniques i inorgàniques, incorporats a l'estructura cristal·lina de minerals com els aluminosilicats i els sulfurs, i coprecipitats en minerals autigènics que es formen in situ a la columna d'aigua o en el sediment. La fracció particulada a la qual estan fortament associats metalls i metal·loides és la predominant en el transport

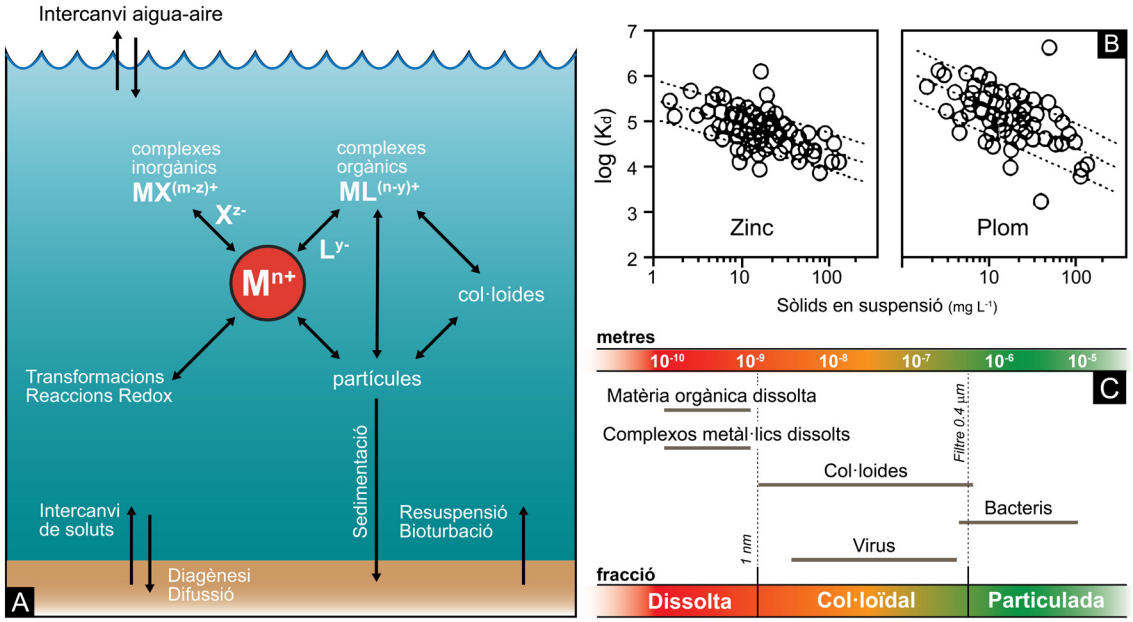

Figura 1.4 A) Esquema dels processos d'especiació o partició dels metalls i els metal·loides a la columna d'aigua i al sediment. Els símbols M, X i L fan referencia als cations metàl·lics i de metal·loides, als ions inorgànics i als ions orgànics, respectivament. B) Relació entre els coeficients de partició del Zn, el Pb i els sòlids en suspensió (adaptat de Mason, 2013 que partí del treball d'Honeyman i Santschi, 1988). C) Classificació de les fraccions (dissolta, col·loidal i particulada) presents a l'oceà amb indicació del seu rang de mides.

atmosfèric, i en ambients fluvials i costaners (vegeu apartat 1.1.4). Tanmateix, en alguns casos s'ha observat que aquesta associació entre metalls i metal·loides i la fracció particulada en suspensió presenta una correlació negativa (Figura 1.4.B). Aquest fet s'explica per un biaix metodològic degut a l'ús de filtres que no retenen la totalitat de partícules, per la qual cosa la concentració de metalls i metal·loides és imputada a la fracció dissolta (Honeyman i Santschi, 1988), error que s'intensifica quan el contingut de sòlids en suspensió és elevat.

A la columna d'aigua, els principals processos que determinen la partició de metalls i metal·loides són la complexació per mitjà de lligants forts tant amb la matèria orgànica com amb la fracció inorgànica; l'assimilació biològica cel·lular; i l'adsorció a la superfície de les partícules en suspensió, especialment dels elements més bioactius com ara el Fe, el Zn, el Cu, el Co i el Cd (Herlng i Morel, 1990). Aquests tres processos són particularment importants en les aigües amb més activitat biològica, com les superficials, les costaneres i les estuarines. L'alt contingut de sòlids en suspensió en aquestes aigües, així com els canvis químics que es produeixen a les zones de mescla de l'aigua dolça i la salada, faciliten el pas dels metalls i els metal·loides de la fase dissolta a les fases col·loïdal i particulada. El comportament d'aquestes partícules

portadores de metalls i el seu procés de sedimentació dependran de la mida de gra i de la seva densitat, i també de la velocitat dels corrents. Les partícules més grans i més denses requereixen fluxos més energètics per ser transportades alhora que sedimenten més ràpidament. Contràriament, les partícules més fines i menys denses, com les de mida argila i llim, són remobilitzades i transportades amb més facilitat, cosa que incrementa llur dispersió.

En el sediment, la distribució de metalls i metal·loides depèn principalment de la seva capacitat de fixació, sovint correlacionada positivament amb el contingut de matèria orgànica, i la presència de sulfits reduïts i també de sulfurs volàtils àcids, AVS en anglès (Jones et al., 2009). Els AVS estan compostos principalment per formes amorfes de la pirita (FeS), principalment mackinawita i greigita. Els metalls associats als AVS són inestables i tendeixen a ser adsorbits a la superfície dels minerals o a incorporar-se a l'estructura cristal·lina de la pirita per coprecipitació. Diversos autors han assenyalat que la toxicitat del sediment i per tant, la biodisponibilitat de metalls com el Hg, la Ag, el Cu, el Co, el Pb i el Cd, està relacionada amb la presència d'AVS (p. ex. Ankley, 1996; Simonsen et al., 2019). Així i tot, aquests metalls també poden presentar comportaments diferenciats. Per exemple, el Hg i el Cu mostren una forta afinitat amb la matèria orgànica i els AVS, mentre que el Cd té afinitat pels sulfurs i el Zn per a la matèria orgànica.

Finalment, convé esmentar també que els processos de formació de roques sedimentàries (p. ex. compactació, cementació, cristal·lització o litificació) a partir de sediments marins comporten la fixació dels metalls i els metal·loides a les estructures cristal·lines dels minerals que formen la roca. Inversament, els metalls i metal·loides poden tornar a ser alliberats a la columna d'aigua o a l'aigua de porositat del sediment mitjançant processos de degradació, oxidació i remineralització.

La concentració de metalls i metal·loides a l'oceà, sia a l'aigua o al sediment, és condicionada pels processos de partició i d'especiació química a la columna d'aigua però també per la magnitud de les fonts. Tanmateix, convé ressaltar que globalment, llur concentració és molt baixa − valors inferiors a 10 μmol kg^{-1} − motiu pel qual molt sovint s'utilitza el concepte de «metall traça» (p. ex. Tovar-Sánchez et al., 2019; Wagner i Hendy, 2017).

Els metalls més abundants a la columna d'aigua són els alcalins i alcalinoterris, com el Na (~470 mmol kg^{-1}), el Ba (~60 nmol kg^{-1}) i el Mg (~50 nmol kg^{-1}). Per la seva part, els metalls de transició de la primera fila de la taula periòdica com el Al, el Fe,

el Mn i el Zn presenten concentracions lleugerament inferiors, les quals rarament ultrapassen el centenar de nmol kg^{-1} (Figura 1.5) (Rijkenberg et al., 2014). En canvi, les concentracions dels metalls posttransicionals i de metal·loides com el Cd, el Zr, el Pb i el Hg són significativament menors, de ~pmol kg^{-1} (Bruland et al., 2013 i referències allà citades). Aquestes concentracions varien significativament, tant en profunditat (Figura 1.5) com entre la costa i l'oceà obert. Tueros et al. (2008) determinaren que les concentracions a les zones costaneres no contaminades eren superiors a les de mar obert per uns factors de 3, 20, 30 i 30 per al Mn, el Cu, el Zn i el Pb, respectivament. L'elevada variabilitat observada resulta principalment de la influència de les fonts continentals sobre els fluxos de metalls i metal·loides cap a les zones costaneres.

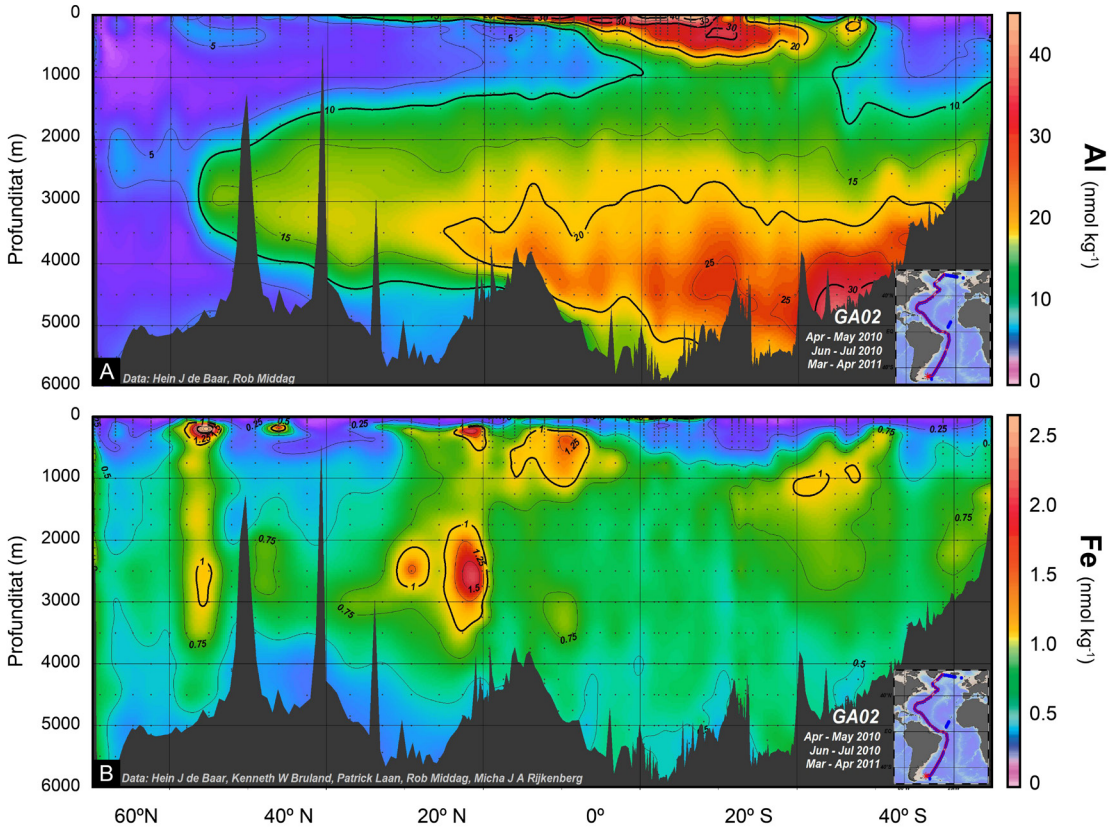

Figura 1.5 Concentracions d'alumini dissolt (A) i de ferro dissolt (B) en nmol kg^{-1} a la columna d'aigua del transsecte GA02 del projecte GEOTRACES a l'oceà Atlàntic (modificat de Bruland et al., 2014, i Rijkenberg et al., 2014).

En el sediment, les concentracions de metalls i metal·loides són significativament més elevades que a la columna d'aigua. Per exemple, el rang de concentració del Fe és de l'~1 al 2% (m/m) mentre que altres elements presenten valors inferiors, com ho

il·lustren el Co (~12 mg kg^{-1}), el Zn (~3 mg kg^{-1}), el Pb (~62 mg kg^{-1}) i el As (~0,2 mg kg^{-1}) (Mason, 2013). Tanmateix, la concentració de metalls i metal·loides tant a l'aigua com en el sediment marí és influenciada pels fluxos antropogènics, especialment a les zones costaneres sotmeses a una forta pressió industrial, agrícola i/o urbana. Aquesta concentració pot ser diversos ordres de magnitud superior a l'existent en indrets no contaminats (Taula 1.2).

Diversos estudis han mostrat factors d'enriquiment de metalls com el Hg, el Cd, el Pb, el Co i el Zn, amb concentracions un ordre de magnitud superiors als valors de referència (Palanques et al., 2017, 2008; Lao et al., 2019). L'enriquiment en aquests metalls com a resultat de l'activitat antropogènica suposa un risc potencial per als organismes i els ecosistemes marins (Burger et al., 2002; Martínez-Sánchez et al., 2008; Paytan et al., 2009: Bosch et al., 2016) i un repte per a la gestió ambiental de materials com ara els productes de dragatge dels ports (Garcia-Orellana et al., 2011).

Entorn	**Mn**	**Fe**	**Zn**	**As**	**Pb**	**Cr**	**Cd**
	mg kg^{-1}	% (m/m)	mg kg^{-1}	mg kg^{-1}	mg kg^{-1}	mg kg^{-1}	mg kg^{-1}
Àrees costaneres							
Plataforma Cont. Barcelona [1]	-	-	100 - 990	-	50 - 760	40 - 830	0,10 - 5,3
Golf de Taranto [2]	550 - 2.830	0,3 - 0,4	90 - 130	-	50 - 80	75 - 103	-
Torrent de Gromolo [3]	300 - 1.210	1,8 - 8,8	80 - 260	10 - 20	10 - 40	270 - 300	-
Badia de Tòquio [4]	350 - 1.540	3 - 4,1	110 - 410	-	30 - 60	30 - 126	0,5 - 1,4
Badia de Bengal [5]	260 - 460	1,7 - 3,7	40 - 200	-	30 - 40	150 - 240	5 - 8
Estuari de Huelva [6]	180 - 580	1,6 - 3,5	140 - 650	-	20 - 200	10 -50	-
Ria Vigo [7]	263 - 310	5 - 7	90 - 140	-	40 - 80	50 - 80	-
Ports							
Port de Nàpols [8]	100 - 420	-	40 - 1.200	8 - 21	40 - 300	10 - 160	0,2 - 2,5
Port de Barcelona [9]	260 - 430	2,2 - 3	180 - 1.130	-	90 - 590	-	-
Port de Quebec [10]	-	-	70 - 560	5 - 18	10 - 210	30 - 100	0,1 - 1,3
Gold de Puzzouli [11]	-	1,3 - 8,9	50 - 6.300	10 - 840	20 - 2810	-	-

Taula 1.2 Rangs de concentració de Mn, Fe, Zn, As, Pb, Cr i Cd reportades en diversos estudis de zones costaneres, estuarines i de ports. Les concentracions són en mg kg^{-1} amb l'excepció del Fe que està en % (m/m). [1] Palanques et al. (2017), [2] Buccolieri et al. (2006), [3] Capello et al. (2016), [4] Fukushima et al. (1992), [5] Raj i Jayaprakash (2007), [6] Morillo et al. (2004), [7] Rubio et al. (2010), [8] Adamon et al. (2005), [9] Guevara-Riba et al. (2004), [10] Pourabadehei i Mulligan (2016), i [11] Romano et al. (2016).

1.1.4 Fluxos de metalls i metal·loides cap a l'oceà

Les principals aportacions de metalls cap a l'oceà es produeixen a través de les zones de transició entre el continent i el mar, és a dir, en els ambients costaneres situats entre la zona intermareal i la submareal, ja damunt la plataforma continental (Burke et al., 2001). És rellevant destacar que a les regions costaneres hi viu aproximadament el 45% de la població encara que només ocupa el 20% de la superfície terrestre (Crossland et al., 2005). Conseqüentment, els fluxos de metalls en aquestes regions estan fortament influenciats per l'activitat antropogènica especialment per la generació de residus municipals, els efluents industrials i de depuradores i la fertilització agrícola. En aquest context, els fluxos de metalls i metal·loides cap als sistemes costaners tenen com a vectors principals les descàrregues fluvials i d'aigües subterrànies, la deposició atmosfèrica i l'abocament directe de residus a la línia de costa o a curta distància (Figura 1.6).

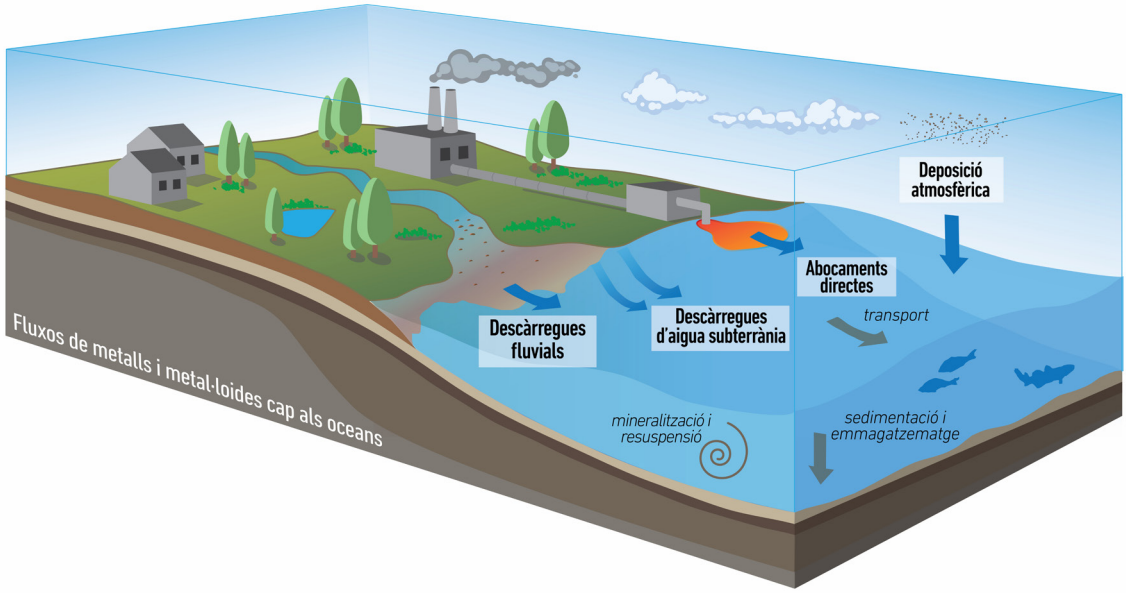

Figura 1.6 Representació esquemàtica dels principals fluxos de metalls als oceans. Concretament, rius, descàrregues d'aigua subterrània, deposició atmosfèrica i abocaments directes.

1.1.4.1 Descàrregues fluvials

Els rius són el principal mecanisme de transport d'elements dissolts i particulats, inclosos els metalls i metal·loides, des dels continents cap a l'oceà. La concentració de metalls i metal·loides als rius depèn principalment de la tipologia i les característiques fisicoquímiques de les partícules sedimentàries en suspensió. Hom calcula que

aproximadament el 95% del flux global de sediments que arriba a l'oceà (25 Gt any^{-1}) és degut al transport fluvial (Syvitski, 2003).

Els paràmetres climàtics i meteorològics, l'extensió, la geologia i el relleu de la conca hidrogràfica, i la tipologia dels residus que hom hi aboca directament o indirecta, juguen un paper determinant en les quantitats de metalls i metal·loides transportats pels sistemes fluvials (Walling, 2009). Part d'aquests metalls i metal·loides serà retinguda a les desembocadures i estuaris mercès a l'elevada afinitat que alguns metalls, com el Fe i el Mn, tenen amb la matèria orgànica i, en general, les partícules sedimentàries. L'alta terbolesa i les fortes taxes de sedimentació pròpies d'aquests ambients afavoreixen la precipitació i/o l'adsorció a les partícules en suspensió dels metalls i metal·loides més insolubles (vegeu l'apartat 1.1.3).

Es calcula que aproximadament el 90% dels metalls transportats pels rius són sostrets de la columna d'aigua als estuaris, cosa que impedeix llur exportació des de la costa cap a mar oberta (Taula 1.2) (Yeats i Bewers, 1982). Això és especialment rellevant en els casos del Fe i del Ni, els quals presenten una retenció en ambients costaners del 99% i del 92%, respectivament. En canvi, metalls més solubles com el Zn i el Cu presenten un percentatge de retenció sensiblement menor (54% i 66%, respectivament) i, conseqüentment són transportats en major mesura cap a l'oceà obert en fase dissolta (Taula 1.3).

Paràmetre/ metall	**Flux fluvial**	**Flux de sortida net de la zona costanera**	**Retenció**	**Concentració en el sediment**
	10^7 mol yr^{-1}	10^7 mol yr^{-1}		mol kg^{-1}
Fe	1.650	100	99,8	5,3*
Mn	40	14	69	5.600
Co	0,51	0,13	79	60
Ni	2,6	0,39	92	180
Cu	3,9	0,91	66	410
Zn	8,3	4,3	54	1.900
Cd	0,03	0,01	69	8,5
	10^{13} kg yr^{-1}	10^{13} kg yr^{-1}	**%**	
TSS	1,8	0,1	-	-

Taula 1.3 Estimacions de la descàrrega global de sediments i metalls pels rius i dels corresponents fluxos de sortida des de la zona costanera. TSS: sòlids totals en suspensió (de l'anglès *total suspended solids*). La concentració en el sediment en el cas del Fe s'expressa en % (m/m) (adaptat de Yeats i Bewers, 1982).

1.1.4.2 Deposició atmosfèrica

La deposició atmosfèrica és una de les principals fonts de metalls cap a la superfície de l'oceà, especialment de compostos tant marcadament estables com volàtils, com els hidrurs i metilats (Maher et al., 2010). És per això que a moltes regions oceàniques la deposició atmosfèrica és la font dominant de micronutrients i un factor de control de la productivitat biològica (Falkowski et al., 1998; Mahowald et al., 2005; Ussher et al., 2013). La presència de metalls i metal·loides a l'atmosfera tant en forma particulada com en estat gasós és producte de l'erosió continental i del transport de partícules per l'acció del vent. Aquesta erosió i el transport eòlic de partícules són predominants en regions àrides i semiàrides on la manca de recobriment vegetal incrementa l'efecte d'embornal de partícules i dels metalls associats, com el Fe i el Al, que resten així disponibles per a ésser transportats. Així mateix, com ja s'ha assenyalat a l'apartat 1.1.3, la crema de combustibles fòssils com el petroli i el carbó (Dore et al., 2014; Li et al., 2017), la producció de certs materials industrials com el ciment (Abril et al., 2014), les activitats mineres (Blondet et al., 2019) i l'ús i el desgast de pneumàtics (Zhao et al., 2016) han fet augmentar l'emissió de metalls en fase particulada cap a l'atmosfera (p. ex. Cr, Mn i Pb), però també d'elements metàl·lics en estat gasós, com és el cas del Hg (Figura 1.7).

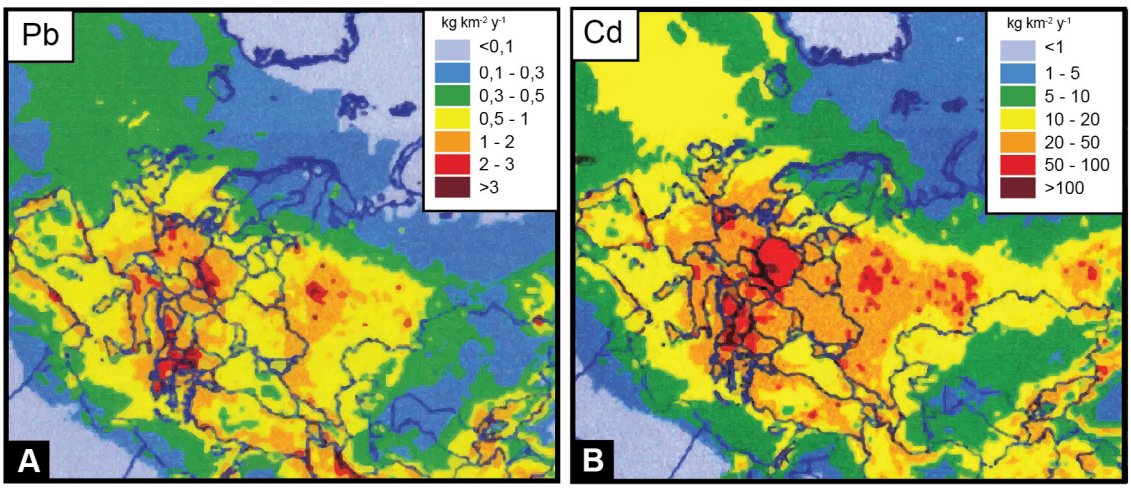

Figura 1.7 Modelització de la deposició de Pb (A) i Cd (B) l'any 1990 a Europa en g km^{-2} a^{-1} i kg km^{-2} a^{-1}, respectivament (adaptat de Mason, 2013).

Des de l'atmosfera, els metalls i els metal·loides poden ser transferits a l'oceà per mitjà de processos de deposició seca i humida. En el primer cas, la deposició seca, l'intercanvi de substàncies i elements entre l'atmosfera i la superfície del mar es produeix per l'acció del vent, les turbulències atmosfèriques i per l'intercanvi de gasos

a la interfase atmosfera-oceà. La distància de transport i la velocitat de deposició de les partícules depèn de la seva mida, densitat i forma (Finlayson-Pitts i Pitts Jr, 1986). Generalment, les partícules més fines i, per tant, més lleugeres són transportades a grans distàncies des de les àrees font continentals cap a l'oceà mentre que les més grolleres es dipositen a les regions costaneres.

En el cas de la deposició humida, els metalls i els metal·loides són arrossegats cap a la superfície de l'oceà per la precipitació atmosfèrica de pluja o neu, i també per formes intermèdies com l'aiguaneu i la calamarsa. Aquest tipus de deposició també comporta l'escombrat de gasos i de material particulat, així com reaccions i formació de compostos implicats en el desenvolupament dels núvols. Tot i que molts metalls i metal·loides estan associats amb la fase particulada atmosfèrica, algunes reaccions químiques poden incrementar la seva solubilitat com, per exemple, ocorre amb el Fe, que té un catió soluble (Fe^{2+}) l'oxidació del quan en genera un altre de molt insoluble (Fe^{3+}), o el Hg amb una forma en estat gasós (Hg) i una altra de molt soluble (Hg^{2+}) (Mason i Sheu, 2002; Selin et al., 2007).

1.1.4.3 Abocaments directes

L'expansió de l'activitat industrial i el creixement de les àrees urbanes durant el darrer segle han incrementant els abocaments directes de deixalles, sediments i aigües amb concentracions elevades de metalls i metal·loides als ambients costaners (Di Leonardo et al., 2008; Palanques et al., 2008; Pan i Wang, 2012; Oyarzun et al., 2013; Hanebuth et al., 2018). En gran part es tracta d'efluents industrials i domèstics, tractats o no, abocats mitjançant emissaris submarins. La presència de partícules en suspensió i de matèria orgànica en aquests efluents facilita els processos de complexació i adsorció de metalls i metal·loides (vegeu apartat 1.1.2) i la seva posterior acumulació ulterior en els ambients costaners (Bay et al., 2003; Kruge et al., 2010).

En les darreres dècades, les millores dels sistemes de tractament de les aigües i l'aplicació de regulacions ambientals més restrictives (p. ex. European Union Directive, 1991), si més no en els països industrialitzats, ha conduit a una reducció significativa dels fluxos de metalls i metal·loides des de les zones urbanes i industrials cap a les regions costaneres (Figura 1.8) (Cearreta et al., 2000; Kress et al., 2016; Lopes-Rocha et al., 2017; Palanques et al., 2017; Hatje et al., 2019). Tot i això, la presència de metalls d'origen antropogènic no s'ha eliminat per complet, com ho il·lustra el fet que l'any 2017, només als estats membres de la Unió Europea, les plantes de tractament

d'aigües residuals urbanes abocaren ~900, ~45, ~25 i ~8 tones de Zn, Pb, As i Cd als rius i aigües marines costaneres (European Environment Agency, 2018). Convé assenyalar també que part dels abocaments directes tenen el seu origen en els vaixells i en la resta d'activitats humanes realitzades en el medi marí. Així, hom calcula que cada any s'aboquen a l'oceà 1,3 milions de tones de petroli i derivats, com el gasoil i les benzines, substàncies que com s'ha assenyalat en apartats anteriors contenen altes concentracions de metalls i metal·loides com ara el Pb i el As (GESAMP, 2007).

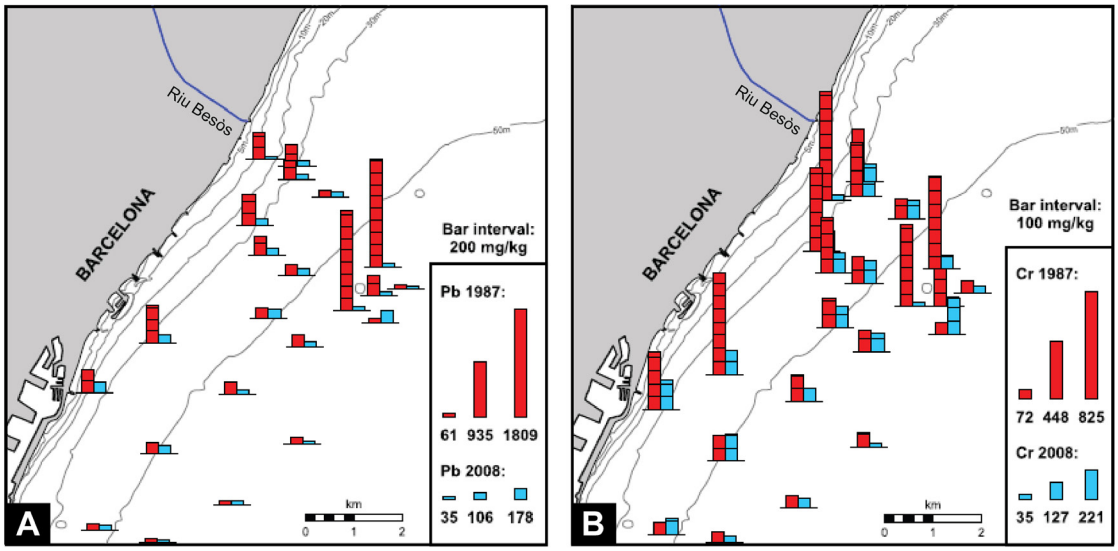

Figura 1.8 Distribució de concentracions de (A) Pb i (B) Cr en el sediment superficial del prodelta del riu Besòs l'any 1987 (vermell) i 2008 (blau). Adaptat de Palanques et al. (2017).

Altrament, els residus miners, en anglès *mine tailings*, abocats a la costa o prop d'ella la mateixa també són una font potencial de metalls i metal·loides, en fase dissolta o particulada, cap als ambients marins costaners (GESAMP, 2016). La baixa eficiència dels processos de separació del mineral genera elevats volums de residus miners, la gestió i el tractament dels quals constitueixen un repte ambiental major. Hom calcula que anualment es produeixen entre 15.000 i 20.000 milions de tones de residus miners a tot el món cada any, la qual cosa indueix un flux de metalls i de metal·loides cap als rius, les aigües subterrànies i els oceans de milions de tones anuals (Smith i Huyck, 1999). Una part significativa d'aquests residus és abocada directament al mar.

En aquest context, s'acostuma a distingir tres tipologies d'abocaments de residu miner: (i) a la costa, en anglès *coastal tailing disposal*, és a dir, en indrets poc profunds dins la zona eufòtica (Castilla i Nealler, 1978; Lancellotti i Stotz, 2004; Lottermoser, 2010; Oyarzun et al., 2013); (ii) en ambients submarins, en anglès *submarine tailing disposal*,

és a dir a fondàries situades per sota de la capa fòtica (>100 m), sovint en canyons submarins (Ellis et al., 1995); i (iii) a gran profunditat, en anglès *deep-sea tailing disposal*, generalment per sota dels 1.000 m de profunditat en el talús continental o més avall (Cervantes-Guerra et al., 2019; Hughes et al., 2015). L'exposició dels residus miners (generalment minerals de sulfur; vegeu l'apartat 1.1.2) a condicions oxidants facilita l'alliberament al medi marí de quantitats considerables de metalls i metal·loides, com el Cu, el Ni, el Zn, el Pb, el Hg i el As, i també de productes químics utilitzats en el processament del mineral, amb efectes tòxics potencials per als ecosistemes i els organismes marins (Martínez-Sánchez et al., 2008; Simonsen et al., 2019).

1.1.4.4 Descàrregues d'aigua subterrània

Les descàrregues d'aigua subterrània (DAS) o el seu terme en anglès *submarine groundwater discharge* (SGD) han estat identificades com una font important de nutrients, metalls i contaminants orgànics i inorgànics als oceans (Johannes, 1980; Kim et al., 2003; Gonneea et al., 2014). Aquesta descàrrega d'aigua formada per aigües subterrànies dolces i marines recirculades, es produeix en la zona de mescla dels aqüífers costaners també anomenats estuaris submarins (Moore, 1999), els quals juguen un paper rellevant com a font de nutrients i d'altres elements en les zones costaneres (Tovar-Sánchez et al., 2014). En mars oligotròfics com la Mediterrània, la descàrrega d'aigua subterrània és la principal font de nutrients inorgànics dissolts (nitrogen, fòsfor i silici) per sobre de les descàrregues fluvials (Rodellas et al., 2015a), i també una font important de metalls i metal·loides (p. ex. Cd, Co, Cu, Fe, Ni, Pb i Zn), especialment en les zones costaneres (Beck et al., 2007; Trezzi et al., 2017).

Puix que la càrrega de metalls i metal·loides associada a la DAS depèn de la seva concentració en els estuaris submarins, els abocaments d'aigües contaminades d'origen urbà o industrials als rius o l'ús de pesticides, herbicides o fertilitzants en zones agrícoles intensifica el flux als ambients costaners. Diversos estudis han evidenciat un increment dels fluxos de metalls i metal·loides dissolts per descàrregues d'aigua subterrània als oceans en zones urbanes (Beck et al., 2009) i industrials (Burnett et al., 2019; Wang et al., 2019), especialment de Mn, Zn, Cr i Cd (Figura 1.9). Alhora, en àrees costaneres amb activitat minera, la composició i la concentració de metalls en les DAS es pot veure influenciada significativament per la presència de residus miners i d'aigües àcides de mineria (Lee et al., 2002; Trezzi et al., 2016b; Alorda-Kleinglass et al., 2019).

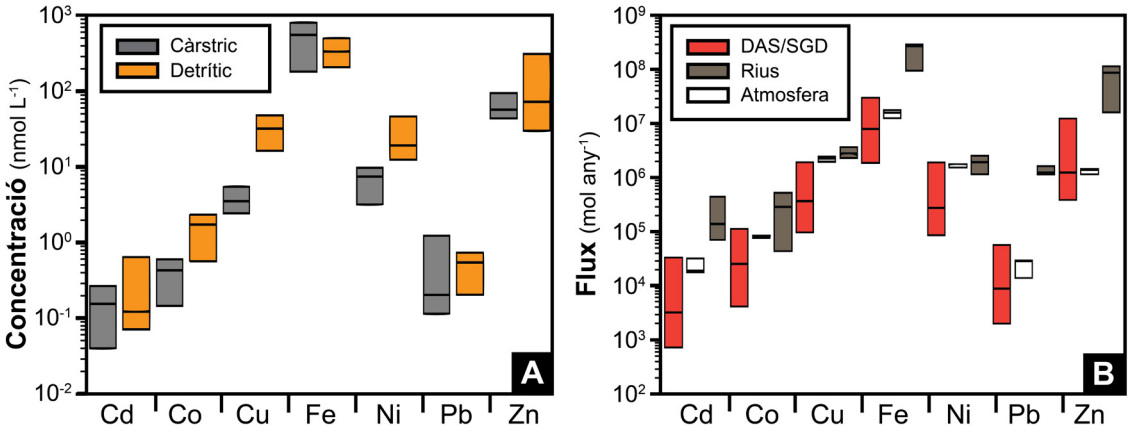

Figura 1.9 A) concentració de diversos metalls en les aigües subterrànies d'aqüífers càrstrics i detrítics en nmol L^{-1} de la Mediterrània Occidental i B) flux de diversos metalls per mitjà de DAS, rius i atmosfera a la Mediterrània Occidental en mol any^{-1}. Modificat de Trezzi et al. (2017).

1.1.5 Contaminació i pol·lució per metalls i metal·loides en el medi marí

Alguns metalls, com el Fe, el Co i el Cu, juguen un paper cabdal per al desenvolupament de la vida i la productivitat primària als oceans (Bruland et al., 1991; Morel i Price, 2003; Sunda, 2012). Per aquest motiu són considerats micronutrients, és a dir, elements essencials per al desenvolupament de l'activitat biològica (Otero et al., 2013). Entre ells destaca el Fe, necessari per a molts processos cel·lulars com, per exemple, la fixació de C i N o la síntesi de la clorofil·la (Falkowski et al., 1998; Boyd et al., 1999; Boyd i Ellwood, 2010; Twining i Baines, 2013). Per la seva banda, el Cu i el Co són essencials per al transport d'electrons en la respiració i la fotosíntesi, i per a la síntesi de la vitamina B12, respectivament (Peers i Price, 2006; Panzeca et al., 2008; Dulaquais et al., 2014).

Tot i això, un increment excessiu de les concentracions de metalls i metal·loides en els ambients marins com a resultat de l'activitat antropogènica pot produir efectes negatius sobre els ecosistemes (Jordi et al., 2012). Concretament, hi ha dotze metalls i metal·loides (As, Be, Cr, Cu, Cd, Pb, Hg, Ni, Se, Ag, Ti, i Zn) inclosos entre els principals elements ecotòxics per a la vida marina (Protano et al., 2014; Li et al., 2015). Aquests metalls i metal·loides presenten un seguit de característiques que poden generar alteracions crítiques de les funcions biològiques i cel·lulars dels organismes, com ara la no biodegradació, la persistència en l'ambient, i la bioacumulació i la biomagnificació, és a dir, l'acumulació creixent al llarg de la xarxa tròfica (Hedge et al., 2009; Ribeiro et al., 2013; Bastami et al., 2015). L'acumulació de metalls i

metal·loides com el Hg o el Cr en espècies marines comercials a través de la xarxa tròfica pot arribar a afectar, generalment a llarg termini, la salut de les persones (Llull et al., 2017; Junqué et al., 2018). Per aquests motius, l'estudi dels processos de contaminació i de pol·lució dels oceans per metalls i metal·loides ha anat adquirint rellevància científica els darrers quaranta anys, en paral·lel amb l'aprovació de noves legislacions i d'estàndards de qualitat més restrictius (Johnson et al., 2020).

En aquest punt, convé abordar la diferència entre els conceptes de "contaminació" i de "pol·lució" inclosos en el títol d'aquest apartat. En català, hom empra aquests dos termes, contaminació i pol·lució (en anglès *contamination* i *pollution*), com a sinònims per descriure «la introducció, generalment deguda a l'acció directa o indirecta de l'home, de pertorbacions, materials o radiacions en un medi, alterant-ne les propietats i modificant l'estructura i la funció dels ecosistemes afectats» (Sallas Campmany, 2011). Per altra banda, no es pot negar que a la literatura científica i tècnica hi ha una certa confusió i desavinença pel que fa a l'ús d'aquests termes (Clark, 1992). En aquest context, el Grup d'Experts en Aspectes Científics de la Pol·lució Marina (GESAMP) de les Nacions Unides recomana diferenciar els conceptes de contaminació i pol·lució per referir-se a la presència i als impactes de determinades substàncies i elements sobre els ecosistemes marins, diferenciació que també fem nostra en aquesta Tesi.

Així, la contaminació es defineix com l'entrada de substàncies a l'oceà a causa de l'activitat humana, fet que incrementa per damunt dels nivells de fons la seva concentració a l'aigua, els sediments i/o els organismes. Per la seva part, el GESAMP defineix pol·lució com «la introducció per l'home, de manera directa o indirecta, de substàncies o energia en el medi marí (incloent els estuaris), tot causant efectes perjudicials com ara el deteriorament de la qualitat de les aigües marines, danys als éssers vius, impediments per a les activitats a mar inclosa la pesca, disminució dels béns i serveis, i riscos per a la salut humana».

El grau de pol·lució i la toxicitat dels metalls i metal·loides en el medi marí està íntimament relacionat amb la biodisponibilitat dels que estan associats principalment amb la fracció AVS del sediment i amb la matèria orgànica (vegeu l'apartat 1.1.3). Donat que l'impacte potencial de l'enriquiment en aquests metalls i metal·loides (contaminació) depèn dels efectes adversos sobre els organismes (pol·lució), és necessari establir pautes interpretatives que permetin relacionar llur enriquimient amb els efectes biològics adversos que provoca (Long et al., 1995; Wenning, 2005). Per aquest motiu, hom avalua l'impacte toxicològic dels metalls i metal·loides mitjançant

estàndards de qualitat de l'aigua i del sediment, els quals defineixen els rangs de concentració a partir dels quals es podrien produir efectes biològics (Figura 1.10) (Long et al., 1995). Tot i que hi ha cert debat al voltant de l'estratègia metodològica emprada per definir aquestes rangs o llindars (Birch, 2018), també és cert que són una eina de gestió ambiental molt útil i àmpliament utilitzada per analitzar els riscos ecotoxicològics en els sediments dels ports (Fatoki i Mathabatha, 2001; Adamo et al., 2005; Casado-Martínez et al., 2006; Garcia-Orellana et al., 2011; Pourabadehei i Mulligan, 2016), dels ambients costaners (Fukushima et al., 1992; Morillo et al., 2004; Buccolieri et al., 2006; Palanques et al., 2008; Rubio et al., 2010) i d'indrets afectats per l'abocament de residus miners (Sternal et al., 2017).

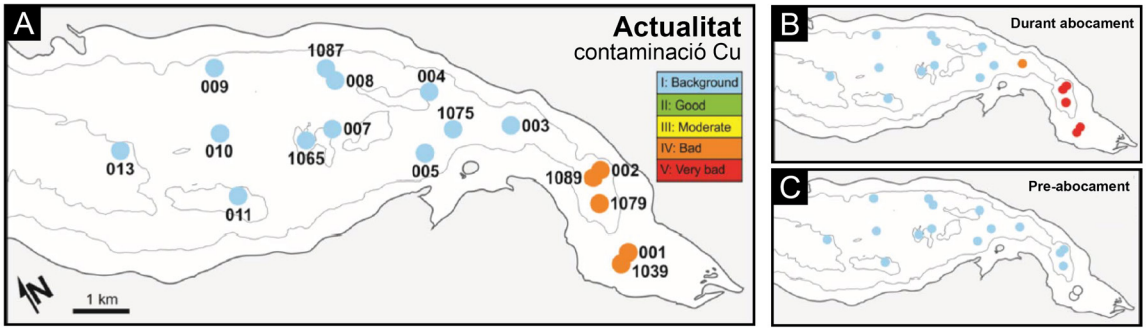

	I Background	II Good	III Moderate	IV Bad	V Very Bad
	Nivell de fons	Semse efectes tòxics	Efectes tòxics per exposició crònica	Efectes tòxics per exposició curta	Efectes tòxics severs
As (mg kg^{-1})	<20	20 - 52	72 - 76	76 - 580	>580
Cd (mg kg^{-1})	<0,25	0,25 - 2,6	2,6 - 15	15 - 140	>140
Cr (mg kg^{-1})	<70	70 - 560	560 - 5.900	5.900 - 59.000	>59.000
Cu (mg kg^{-1})	<35	35 - 51	51 - 55	55 - 220	>220
Hg (mg kg^{-1})	<0,15	0,15 - 0,63	0,63 - 0,86	0,86 - 2	>2
Ni (mg kg^{-1})	<30	30 - 46	46 - 120	120 - 840	>840
Pb (mg kg^{-1})	<30	30 - 83	83 - 100	100 - 720	>720
Zn (mg kg^{-1})	<150	150 - 360	360 - 590	590 - 4.500	>4.500

Figura 1.10 Afectació de la qualitat del sediment per l'abocament de residus miners al fiord Repparfjorden, al nord de Noruega. A), B) i C) Qualitat del sediment actualment, durant el període d'abocament i abans de l'abocament del residus, respectivament. A la taula s'especifiquen el valors establerts a la classificació de qualitat del sediment de Noruega (modificat d'Sternal et al., 2017).

L'interès creixent de la comunitat científica en relació amb les distribucions i les concentracions de metalls i metal·loides, i l'ús d'estàndards de qualitat, especialment en els ambients costaners, estan relacionats indefectiblement amb l'increment de la preocupació pels seus efectes sobre els ecosistemes i la salut pública (Borg i Jonsson,

1996; Hornberger et al., 1999; Garcia-Orellana et al., 2011; Capello et al., 2016; Martínez-Soto et al., 2016; Zhang et al., 2019). És una bona mostra de l'interès que suscita el tema el fet que el nombre de publicacions sobre contaminació marina per metalls i metal·loides, moltes de les quals referides al sud-est asiàtic, no ha parat de créixer (Rahman et al., 2015; Lao et al., 2019; Mathew i Gopinath, 2019; Schlosser et al., 2019). A aquesta explosió hi han contribuït en gran manera els avenços tecnològics i metodològics de les darreres dècades pel que fa a la quantificació de les concentracions de metalls i metal·loides. La popularització de tècniques com l'espectrometria i la fluorescència de raig X per a la determinació de la composició elemental ha estat clau per aprofundir en la mesura i el coneixement de les concentracions de metalls i metal·loides a l'oceà. I també hi ha ajudat molt l'ús d'isòtops metàl·lics estables, com el δ^{56}Fe i el δ^{65}Cu (Bergquist i Boyle, 2006; Vance et al., 2008), i de radionúclids metàl·lics, com el Ra (^{223}Ra, ^{224}Ra, ^{226}Ra i ^{228}Ra), emprats com a traçadors de processos i de fluxos de metalls des de rius i aqüífers, a la columna d'aigua i fins els sediments marins. Així i tot, els cicles dels metalls i metal·loides en el medi ambient, així com la multiplicitat de variables físiques, químiques i biològiques però també antropogèniques que els influeixen, són extremadament complexos, situació que en dificulta l'estudi des d'una perspectiva holística.

1.2 Zones d'estudi

Les zones d'estudi se situen a la mar Mediterrània occidental, concretament a les províncies de Barcelona i de Múrcia de l'Estat espanyol. La Mediterrània és considerada una de les conques marines més complexes del planeta atenent a la seva història geològica i les seves característiques físiques i ambientals. La seva formació es remunta a 150 milions d'anys enrere aproximadament, a conseqüència de la convergència i la col·lisió de les plaques Eurasiàtica i Africana durant el Mesozoic, que culminaren amb el tancament de l'estret de Gibraltar fa uns 5,66 milions d'anys (Picotti et al., 2014). L'aïllament resultant de la conca alterà brutalment el balanç hídric de la Mediterrània. Tallada la connexió amb l'oceà Atlàntic, el volum d'aigua que entrava a la conca per via fluvial i per precipitació directa era inferior al volum d'aigua evaporada, circumstància que conduí al seu dessecament i a la formació d'extensos dipòsits d'evaporites. Aquest episodi es coneix com la "crisi de salinitat messiniana". Arran de la reobertura de l'estret de Gibraltar fa uns 5,33 milions d'anys les aigües atlàntiques tornaren a inundar la Mediterrània en el decurs de l'anomenada "inundació zancliana" (Garcia-Castellanos et al., 2009).

La Mediterrània moderna és el fruit d'aital evolució geològica. Es tracta d'una mar semitancada envoltada per sistemes muntanyosos que configuren unes conques de drenatge fluvials generalment petites. Amb una profunditat mitjana que no arriba per poc als 1.500 m, la Mediterrània és formada per dues subconques principals: l'oriental i l'occidental amb unes profunditats màximes de 5.267 m i 3.785 m (a la mar Tirrena), respectivament, connectades per l'estret de Sicília (Tomczak i Godfrey, 2013). La condició de mar semitancada i d'extensió limitada configura un sistema micromareal amb un rang d'oscil·lació de menys de 20 cm. La Mediterrània és, per altra banda, una conca de concentració on l'evaporació superficial supera el flux d'aigua entrant des de rius, aqüífers subterranis i per precipitació directa. Tanmateix, a diferència de la crisi de salinitat messiniana, el dèficit hídric actual és compensat per l'entrada per l'estret de Gibraltar d'aigües superficials menys denses i salades de l'Atlàntic. Aquest flux atlàntic superficial entrant és compensat per un flux profund de sortida d'aigües denses i salades formades a la Mediterrània per efecte de l'evaporació (Tsimplis i Bryden, 2000).

El flux mediterrani ixent determina l'exportació de nutrients des de la Mediterrània cap a l'Atlàntic, essent aquest fet una de les raons que expliquen que aquesta conca sigui una de les més oligotròfiques del planeta (Béthoux et al., 1998). És en aquest tipus de sistemes amb baixos continguts de nutrients on les entrades d'aigües fluvials (Ludwig et al., 2009) i subterrànies (Rodellas et al., 2015a), i la precipitació i deposició de partícules atmosfèriques (Herut et al., 1999; Bonnet i Guieu, 2006) juguen un paper clau afavorint la productivitat primària.

Des d'una perspectiva climàtica, la mar Mediterrània, localitzada entre 30°N i 45°N, està fortament influenciada per les condicions climàtiques subtropicals nord-africanes i temperades de l'Europa central. Això configura un clima de transició en què es combinen períodes molt càlids a l'estiu a conseqüència del moviment de masses d'aire subtropicals cap al nord, i uns hiverns moderadament freds i humits mercès al desplaçament cap al sud de masses d'aire humides des de l'Atlàntic (Folch, 1993). Per consegüent, el règim de precipitacions presenta una variabilitat anual significativa, que oscil·la entre 100 i 2.500 mm i unes temperatures mitjanes entre 5 i 18 °C. Tot l'anterior i la llarga història humana de la regió mediterrània han determinat que sigui una de les més poblades i industrialitzades del planeta i, en conseqüència, una de les àrees amb una major pressió antròpica sobre l'entorn natural i particularment sobre els seus ecosistemes marins (UNEP, 2017).

Per tot el que s'ha exposat fins ara, en aquesta Tesi hem considerat dues vies d'entrada de metalls i metal·loides al medi marí: les DAS i els abocaments a la costa a les dues zones d'estudi indicades a l'inici d'aquest apartat situades a Barcelona i a Múrcia (Figura 1.11). Totes dues són representatives d'indrets del litoral mediterrani sotmesos a fortes pressions industrials i mineres (cas de la badia de Portmán, Múrcia) a prop de Cartagena (Banos-González i Páez, 2013), agrícoles (cas de la riera d'Argentona, a

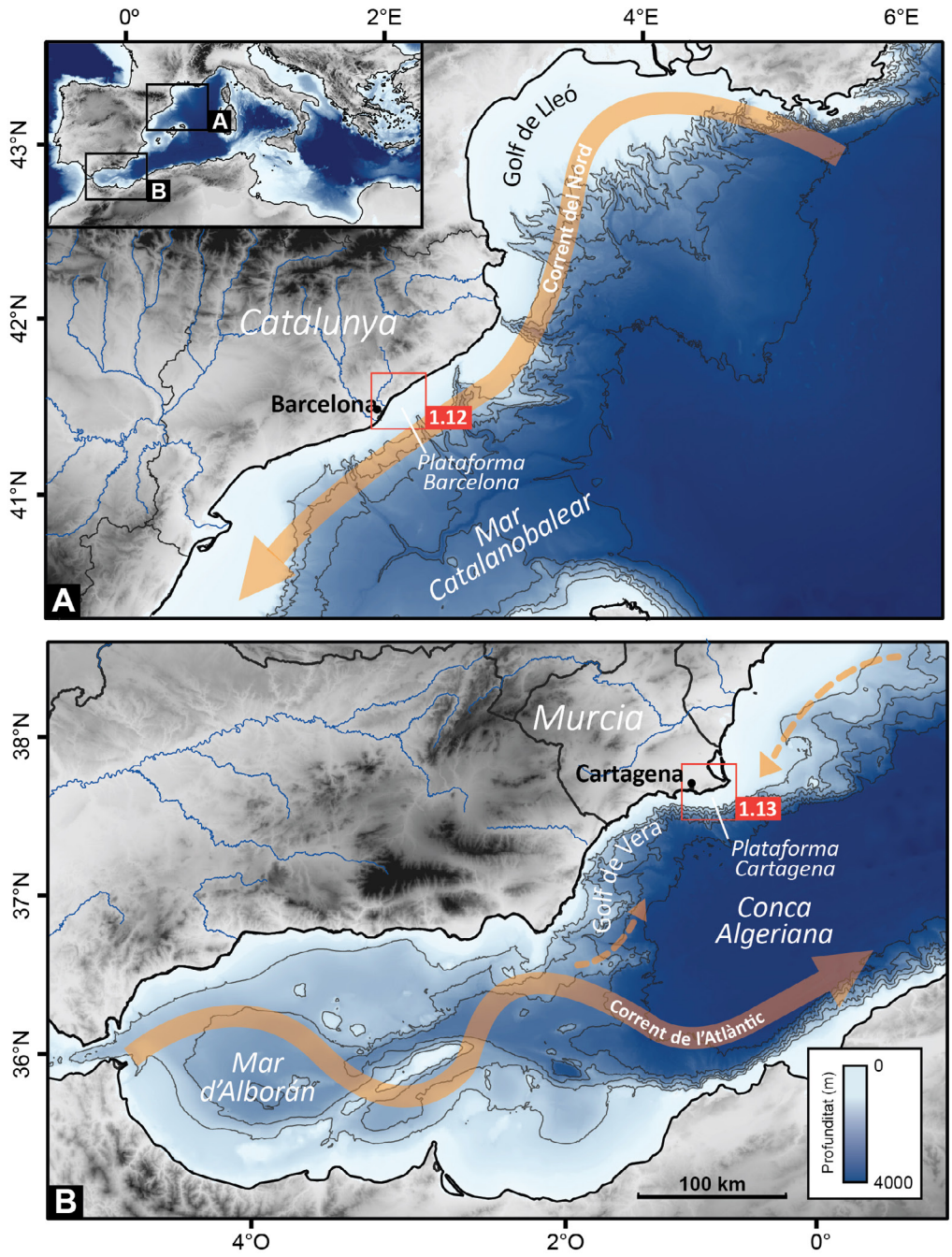

Figura 1.11 Mapes batimètrics i circulació general en les àrees d'estudi. A) Mar Catalanobalear. B) Mar d'Alborán i conca Algeriana. S'indiquen també els rius principals a les regions emergides circumdants.

Barcelona) (Cerdà-Domènech et al., 2017) o urbanes (cas de la conca i el prodelta del riu Besòs, a Barcelona) (Palanques et al., 1998, 1991). És en aquesta mena d'indrets on la presència de metalls i metal·loides, tant als rius, aqüífers i «estuaris submarins» com en el medi marí, s'ha intensificat al llarg de les darreres dècades a conseqüència de l'activitat antròpica (Garcia-Orellana et al., 2011; Trezzi et al., 2016b; Palanques et al., 2017; Alorda-Kleinglass et al., 2019). Aquesta bateria de casos és idònia per poder testar metodologies i aprofundir en l'estudi dels fluxos de metalls i de metal·loides cap als ambients marins costaners, així com en la quantificació de llurs concentracions i distribució en els sediments marins. Incidirem, doncs, en la quantificació dels fluxos de DAS com a mecanisme de transport des dels aqüífers costaners cap a la columna d'aigua, i en l'esdevenidor d'aquests elements un cop incorporats als sediments.

1.2.1 El prodelta del riu Besòs

El prodelta del riu Besòs se situa a la plataforma continental interna de Barcelona. Aquesta plataforma té una llargada de 91 km, una amplada mitjana de 15 km i una superfície total de 1.317 km^2 (Figura 1.12). La profunditat màxima se situa entre 110 i 120 m i presenta un pendent mitjà de 0,6° (Durán et al., 2014). Liquete et al. (2008) la subdividiren en plataforma interna, mitja i externa, separades per les isòbates de 30 − 40 m i 80 m, respectivament.

La circulació costanera és dominada per un corrent principal de direcció sud-est (Grifoll et al., 2012). Diversos forçaments regulen les variacions d'aquest corrent. Sota condicions de temporal, la força del vent i el nivell del mar dominen el balanç mentre que en condicions de vents suaus i moderats, el balanç és controlat pel gradient de pressió (Grifoll et al., 2012). El rang de marea a la plataforma continental de Barcelona és de <20 cm. Des del punt de vista sedimentari, i de nord a sud, la plataforma continental interna de Barcelona és dominada per tres dipòsits principals alimentats pels rius Tordera, Besós i Llobregat, i s'hi desenvolupen també altres cossos més petits com els que formen algunes rieres del Maresme, entre les quals la riera d'Argentona.

La dinàmica sedimentària de la zona d'estudi (Figura 1.12) està fortament influenciada, com és natural, per les descàrregues d'aigua del riu Besòs, amb un cabal mitjà de 5 m^3 s^{-1} i màxim de <2.000 m^3 s^{-1}. El flux anual de sediments del riu Besòs és d'unes 15.000 tones que en gran mesura s'incorporen a un prodelta que s'estén en direcció sud-oest damunt la plataforma continental interna i mitja (Liquete et al., 2007). La conca de drenatge del riu Besòs ocupa uns 1.000 km^2 i travessa àrees urbanes densament

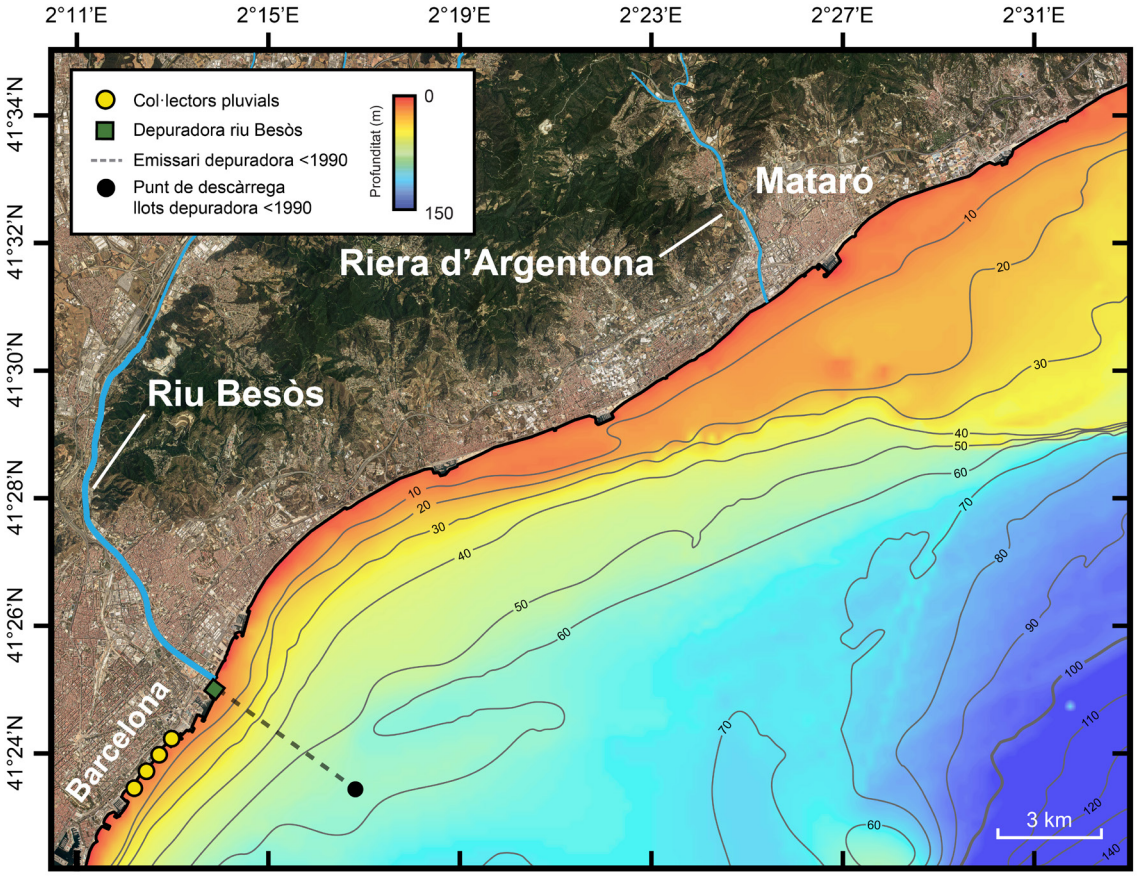

Figura 1.12 Ortofotomapa i mapa batimètric de la Plataforma continental de Barcelona a la desembocadura del riu Besòs i de la riera d'Argentona en el qual s'indica la localització de l'emissari marí abans del 1990, la depuradora i els col·lectors pluvials de la ciutat de Barcelona que desemboquen a la costa.

poblades així com àrees industrials i agrícoles, la qual cosa permet explicar els alts nivells de contaminació observats durant molt de temps en el riu, especialment de metalls i metal·loides (Navarro i Carbonell, 2007). Així, estudis realitzats a la dècada de 1980 reportaren elevades concentracions de metalls en els sediments del prodelta del Besòs (171 mg kg^{-1} de Cu, 290 mg kg^{-1} de Cr i 1.458 mg kg^{-1} de Pb), així com a la capçalera del canyó del Foix, situat més al sud, en el límit oriental de la plataforma de Barcelona (Palanques et al., 1998; Puig et al., 1999).

L'increment de la població i de l'activitat econòmica i industrial a l'Àrea Metropolitana de Barcelona i l'aplicació d'estàndards ambientals més restrictius forçaren la construcció, l'any 1979, d'una planta de tractament d'aigües residuals prop de la desembocadura del riu Besòs. El tractament generava elevats volums de llots altament contaminats que eren abocats a 56 m de profunditat per mitjà d'un emissari submarí de 4 km de llarg (Figura 1.12). La descàrrega continuada de llots, aproximadament $1{,}4{\cdot}10^{6}$ m^{3} a^{-1} entre 1979 i 1984, combinada amb l'acció de processos de remobilització i transport

acabaren estenent els residus en una extensa àrea al voltant de l'emissari (Palanques et al., 1991). A la dècada dels anys 90 del segle passat, l'emissari del 1979 (emissari antic) va ser clausurat i substituït per un de nou, tot i coincidint amb la construcció d'una nova estació depuradora d'aigües residuals, l'EDAR del Besòs. Mercès a aquesta actuació, les concentracions de metalls en els sediments superficials del prodelta del Besòs van reduir-se a menys de la meitat, un comportament que també té una relació directa amb l'augment del nombre de depuradores d'aigües a la conca del riu Besòs entre els anys 1979 i 2008 (Palanques et al., 2008).

1.2.2 L'aqüífer de la riera d'Argentona

La conca de la riera d'Argentona, de 35 km^2, se situa a la comarca del Maresme, al nord-est de la ciutat de Barcelona. S'emplaça i drena la Serralada Litoral Catalana, la qual està estructuralment associada a una tectònica de fracturació i enfonsament de blocs, en direcció nord-oest sud-est, vinculada a una fracturació transversal sobre la qual es desenvolupen diverses valls com la de la riera d'Argentona (Agència Catalana de l'Aigua, 2010) (Figura 1.12). Els dipòsits al·luvials costaners quaternaris són formats per materials detrítics resultants de la meteorització i el transport del basament granític (Montoto, 1967). El ventall al·luvial del peu de la serralada és constituït per capes no consolidades de graves, arenes i argiles, tot i que a l'alçada de la línia de costa l'aqüífer se situa principalment en sediments marins (Agència Catalana de l'Aigua, 2010).

L'aqüífer al·luvial de la riera d'Argentona és, doncs, un aqüífer som amb materials sedimentaris granulars i no confinat. El nivell freàtic oscil·la entre 6 i 7 m a la zona al·luvial i entre 10 i 15 m al sector intermedi de l'aqüífer. A més, el gruix saturat augmenta com més a prop de la línia de costa mar, i és aproximadament de 45 m a 300 m de la costa mateixa (Agència Catalana de l'Aigua, 2010). L'escorrentia superficial té lloc principalment durant els períodes de pluges intenses de tardor i primavera amb un rang anual d'entre 500 a 800 mm. El model de flux numèric de l'aqüífer de la riera d'Argentona realitzat per l'Agència Catalana de l'Aigua (2010) durant el període 2006 − 2009, estimà una recàrrega de l'aqüífer de $3{,}6 \cdot 10^6$ a $5{,}4 \cdot 10^6$ m^3 a^{-1}. Les principals sortides de l'aqüífer corresponen a l'extracció urbana, agrícola i industrial ($1{,}4 - 1{,}9 \cdot 10^6$ m^3 a^{-1}), mentre que la descàrrega subterrània d'aigua dolça al mar és d'1,2 a $2{,}4 \cdot 10^6$ m^3 a^{-1}.

Des del punt de vista sedimentari, l'onatge és l'agent dominant de la dinàmica

sedimentària en el sistema litoral del Maresme. L'onatge més característic és de component sud-est i sud-oest amb l'alçada d'ona més probable de 0,5 m i el període de 3 s (Calafat, 1986). Els corrents tenen una influència en el transport general cap al sud-oest de materials en suspensió i l'acció de les marees, les quals presenten valors mínims, és negligible. La deriva litoral genera un transport net de sorra direcció sud-oest quantificat en 45.000 $m^3 a^{-1}$ (Dir. Gral. de Ports i Costes, 1983). El dipòsit litoral submergit presenta prismes sedimentaris amb una morfologia externa força homogènia que semblen progradar mar en dins. Aquest sediments estan constituïts fonamentalment per sorres quars- feldespàtiques amb petites proporcions de miques i fragments de roques metamòrfiques i minerals pesants (Serra i Sorribas, 1995).

1.2.3 La badia de Portmán

La badia de Portmán és situada a prop de la ciutat de Cartagena, en el terme municipal de La Unión, de gran tradició minera, a la província de Múrcia, i s'obre a la plataforma continental de Cartagena, al nord-est del golf de Vera. Aquesta plataforma està orientada en direcció NE-SW, té entre 3 i 9 km d'ample i una profunditat màxima de 150 m. Està constituïda per dues unitats principals, la plataforma continental interna i l'externa amb un pendent mitjà de 0,5 i 1,5°, respectivament (Acosta et al., 2013). La vora de plataforma vestà determinada per la presència d'un seguit de promontoris entre els quals s'obren les capçaleres d'un alt nombre de canyons submarins, com el canyó d'Escombreras, situat al sud de la badia de Portmán. El talús continental és molt rost, amb pendents entre 14° i 31° (Acosta et al., 2013). La circulació marina en aquesta àrea de transició entre el mar d'Alboran i la conca Algeriana està dominada per la confluència de dues masses d'aigua superficials diferenciades: el doll, en anglès *jet*, d'Aigua Atlàntica Superficial i l'Aigua Mediterrània Superficial (Millot, 1999). La primera massa d'aigua, amb unes salinitats inferiors a les 36,5 ups (unitats pràctiques de salinitat), prové de l'Atlàntic i flueix des de l'estret de Gibraltar cap a l'est. La segona massa d'aigua, molt més salada (més de 37,5 ups) i força càlida prové del canal d'Eivissa i circula de nord a sud damunt la plataforma i el talús continentals (Millot, 1999).

La badia de Portmán està encaixada a la Sierra de Cartagena, de 450 m d'altura, originada arran de la convergència entre les plaques Ibèrica i Africana a finals del Mesozoic i durant el Cenozoic (Figura 1.13)(Sanz de Galdeano, 1990). La localització i la configuració de la badia estan controlades estructuralment per un grup de falles

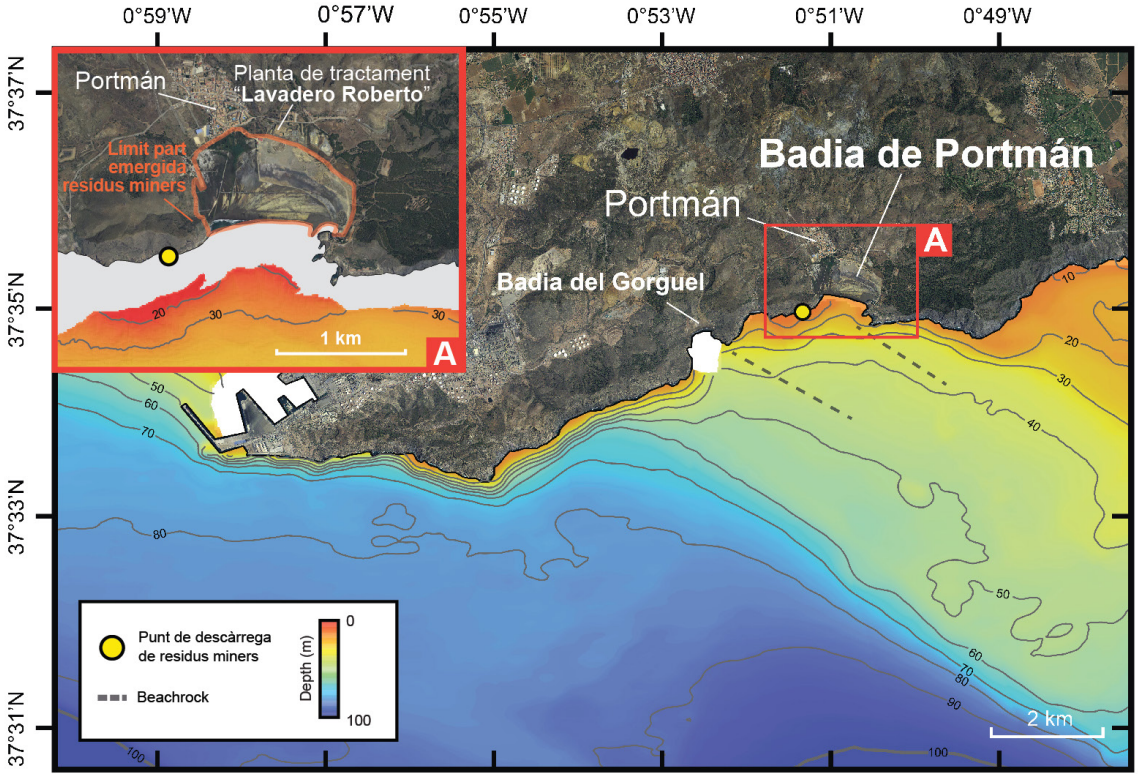

Figura 1.13 Ortofotomapa i mapa batimètric de la plataforma continental davant la badia de Portmán. S'indica la localització del punt de descàrrega dels residus miners al mar des de 1953 fins 1990, i els límits de la part emergida del dipòsit de residus causant del rebliment de la badia. També s'assenyala la situació d'un parell de platges fòssils cimentades o "beachrocks".

normals de direcció NW-SE que provocaren l'aixecament i el desplaçament cap al sud del sector oriental de la serra. Una forta acció erosiva sobreposada acabà de determinar la formació de la badia de Portmán (Manteca, 1992).

Des d'una perspectiva històrica, els usos i les transformacions de la badia de Portmán han estat lligats a l'aprofitament dels rics jaciments metal·lífers de la Sierra de Cartagena, explotats des de l'època preromana i més intensament durant l'ocupació romana i cartaginesa de la regió, principalment per l'obtenció de galena argentífera, blenda i minerals de ferro (Manteca, 1992). La badia, amb la seva forma original de mitja lluna gairebé perfecta, era un port natural excel·lent, com ho palesen el seus noms en llatí i àrab, Portus Magnus i Burtuman Al-Kabir, és a dir "port gran" (Hernández, 1978). Durant la Baixa Edat Mitjana i els segles posteriors, l'activitat minera fou de baixa intensitat i no va revifar fins l'aprovació de Ley de Minas de 1825, mercès a la proliferació de petites concessions que conduïren a un increment molt remarcable de la producció (Manteca, 1992).

El període d'or de la mineria murciana finalitzà l'any 1912 per una caiguda significativa

de la producció, situació que conduí a un procés de concentració de les concessions i a la creació de l'empresa Sociedad Minero−Metalúrgica Zapata Portmán, S.A. Posteriorment, l'any 1930 la Sociedad Minero−Metalúrgica de Peñarroya España S.A., una multinacional francesa coneguda a la zona senzillament com "Peñarroya" adquirí el 50% de l'anterior. L'entrada de l'empresa francesa, vinculada a la família banquera Rothschild, comportà la remodelació de les explotacions i el desenvolupament de noves tècniques que milloraren els processos de concentració de mineral. Aquests canvis es materialitzaren en la construcció, l'any 1935, de la primera instal·lació de flotació diferencial, una tècnica que aprofita les propietats adhesives dels minerals metàl·lics per separar-los més eficientment de la matriu. Però la rebel·lió militar contra la Segona República i l'inici de la Guerra d'Espanya endarreriren la seva posada en funcionament fins l'any 1940.

Finalitzada la guerra, l'explotació minera a gran escala i a cel obert, a fi d'aconseguir una major rendibilitat, reactivà la construcció de noves plantes de flotació diferencial al districte miner de la Sierra de Cartagena, entre les quals destaca la planta anomenada "Lavadero Roberto", bastida a la badia de Portmán i que entrà en servei l'any 1953. Molt poc temps després, el 1954, Peñarroya adquirí el 50% restant de Zapata Portmán, reforçant així encara més la concentració de concessions mineres sota el seu control (Manteca, 1992).

La nova tècnica de la flotació diferencial, juntament amb millores ulteriors de les infraestructures, permeteren incrementar el volum de mineral processat en aquesta planta des de 1.000 tones diàries l'any 1953 fins 10.000 tones l'any 1990 (Oyarzun et al., 2013). L'elevat volum de material tractat a la planta, aproximadament 60 milions de tones de mineral en tot el període, principalment pirita (FeS2), galena (PbS) i esfalerita (ZnS), i la baixa eficiència del procés de flotació diferencial generaren 57 milions de tones de residus miners rics en metalls i metal·loides (Oyarzun et al., 2013). La qüestió de què fer amb aquest enorme volum de residus trobà una aparent solució quan, a la dècada dels 50, s'iniciaren els abocaments directes al mar per mitjà d'un emissari emergit que desguassava en els penya-segats situats a tocar de l'extrem occidental de la badia (Figura 1.14).

A mesura que s'anaven abocant al mar, els residus miners s'anaren escampant per la plataforma continental i cap a l'interior de la badia de Portmán per l'acció de les onades i els corrents litorals, que per altra banda els anaven seleccionant granulomètricament, si més no en certa mesura. La circulació a la badia de Portmán original, abans del seu

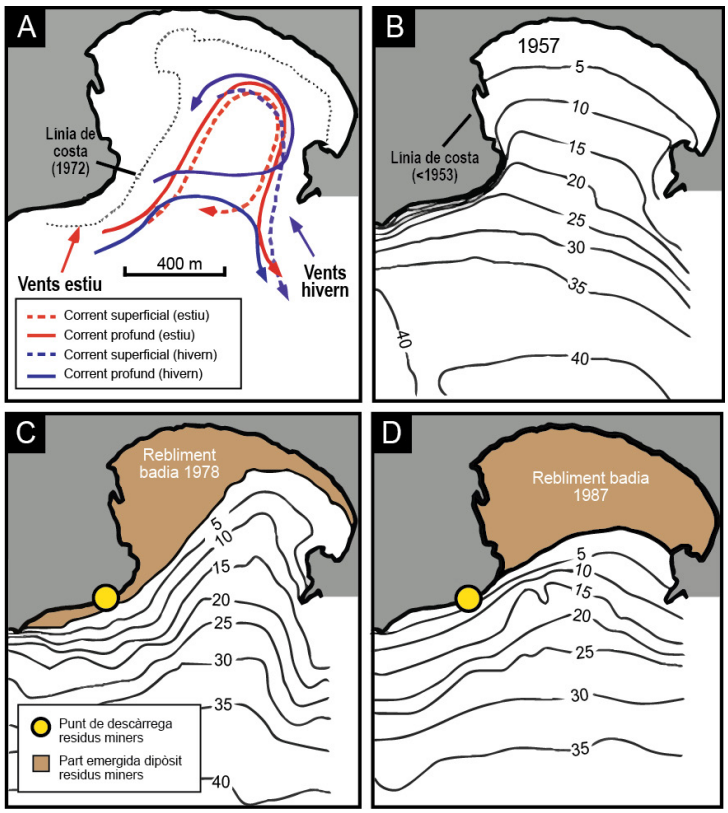

Figura 1.14 A) Circulació superficial i de fons, a l'estiu i a l'hivern, a la badia de Portmán a l'hivern amb la línia de costa de l'any 1972 (adaptat de Pauc i Thibault, 1976). B), C) i D) Progressió del rebliment de la badia per acumulació de residus miners i evolució de la batimetria entre 1957 i 1987 segons Martínez et al. (1993) (adaptat de Manteca et al., 2014).

rebliment, era condicionada per la batimetria local (Pauc i Thibault, 1976) (Figura 1.14.A). Durant l'estiu predominaria una circulació horària, amb un flux d'entrada cap al nord-est pel sud-oest de la badia i un d'eixida cap al sud per l'extrem oriental de la badia. La circulació hivernal seria més complexa amb dos corrents diferenciats. El primer descriuria un gir antihorari a l'interior de la badia mentre que el segon es desplaçaria d'oest a est, paral·lelament a la costa, sense acabar d'entrar a la badia. Conseqüentment, el rebliment de la badia per l'acumulació dels residus miners abocats a ponent seu es va produir d'oest a est, tal i com mostren les imatges aèries històriques (Figura 1.14.B,D) i els mapes de gradients magnètics del mateix rebliment (Peña et al., 2013).

Aproximadament 14 Mt de residus contaminats es van acabar acumulant dins la badia de Portmán, tot causant un avenç de la línia de costa d'uns 500 metres. Uns altres 43 Mt de residus van dipositar-se a la plataforma interna als encontorns de la badia (Manteca et al., 2014). Se sap que els residus emergits acumulats dins de la badia

presenten elevades concentracions d'elements metàl·lics, com ara Fe, Zn i Pb, i de metal·loides, com el As, amb concentracions màximes de 10.510, 4.590 i 1.910 mg kg^{-1} de Zn, Pb i As, respectivament (Figura 1.15) (Gómez-García et al., 2015).

Figura 1.15 Imatges dels abocaments a la badia de Portmán i els seus efectes. A) Ortofotomapa actual de la badia on es mostren un seguit d'elements rellevants i la situació de les imatges B,C i D. B) Fotografia de la boca de la canonada que abocava els residus miners a la costa. C) "Lavadero Roberto", planta de processament del mineral per flotació diferencial. D) Superfície de la part emergida dels dipòsits de rebliment de la badia. Les fotografies B i D i 3 són de Banos-González i Páez (2013).

L'any 1990, després d'una intensa campanya de la societat civil i el moviment ecologista, l'emissari fou clausurat, i l'any 1991 l'empresa posava punt i final a l'explotació minera i a gairebé quaranta anys d'abocament de residus al mar. Tanmateix, trenta anys després de l'aturada dels abocaments, les concentracions de metalls com el Zn o el Pb en els sediments superficials de la plataforma continental interna de Portmán encara ultrapassen per un factor de deu les d'altres indrets de la Mediterrània occidental qualificats de *priority pollution*, com els fons marins de la plataforma interna davant el delta de l'Ebre i l'albufera de València (Martínez-Gómez et al., 2012).

1.3 Metodologia

Amb l'objectiu de contribuir a la caracterització i la quantificació de fluxos d'aigua i de metalls cap al medi marí, en aquesta Tesi hom ha avaluat i aplicat diverses tècniques hidrogeològiques, sedimentològiques i geoquímiques, tant en aigües subterrànies com en sediments marins (Figura 1.16). Així, l'estudi de la metodologia de quantificació de les DAS mitjançant els isòtops de radi (^{223}Ra, ^{224}Ra, ^{226}Ra i ^{228}Ra) i radó (^{222}Rn) en aqüífers costaners com a mecanisme de transport de metalls i metal·loides des del continent cap al mar costaner es dugué a terme a la riera d'Argentona (vegeu apartat 1.2.2) entre el mesos de gener de 2013 a juliol de 2014 en el marc del projecte MEDISTRAES (*Mezcla y dispersión en el transporte de energía y solutos*) finançat pel MINECO.

Per altra banda, les metodologies per quantificar la concentració i avaluar la distribució de metalls en sediments marins superficials s'aplicaren a la plataforma continental interna de Cartagena, enfront la badia de Portmán (vegeu apartat 1.2.3), durant un seguit de campanyes oceanogràfiques des de l'agost de 2014 fins al setembre de 2017 en el marc del projecte europeu MIDAS (*Managing Impacts of Deep seA reSource exploitation*) i dels projectes estatals NUREIEV (*NUevos REtos en la investigación de cañones submarinos: Indicadores del Estado ambiental y Variabilidad espacio-temporal − El papel de los temporales*) i NUREIEVA (*NUevos REtos de Investigación en el ambiente Extremo de los Vertidos mineros de la Bahía de Portmán: aplicación de tecnologías Avanzadas*), finançats pel MINECO. A més, s'aplicaren en mostres de sediments del prodelta del riu Besòs (vegeu apartat 1.2.1), en el marc de les campanyes oceanogràfiques de pràctiques del grau de Ciències del Mar de la Universitat de Barcelona.

1.3.1 Tècniques de mostreig

1.3.1.1 Mostreig d'aigües subterrànies

Les mostres d'aigua de l'aqüífer de la riera d'Argentona s'obtingueren per mitjà de dos piezòmetres: el primer, PZ1, de 50 m de profunditat, 60 mm de diàmetre i ranurat a totes les profunditats, fou instal·lat a uns 300 m de la línia de costa (Figura 1.17.A). El segon, PZ0, de 3 m de profunditat, 60 mm de diàmetre i ranurat els 0,5 m inferiors, s'instal·là a uns 8 m de la línia de costa. Hom recobrí aquest piezòmetre amb un filtre de grava per reduir la presència de partícules en suspensió a l'aigua del seu interior.

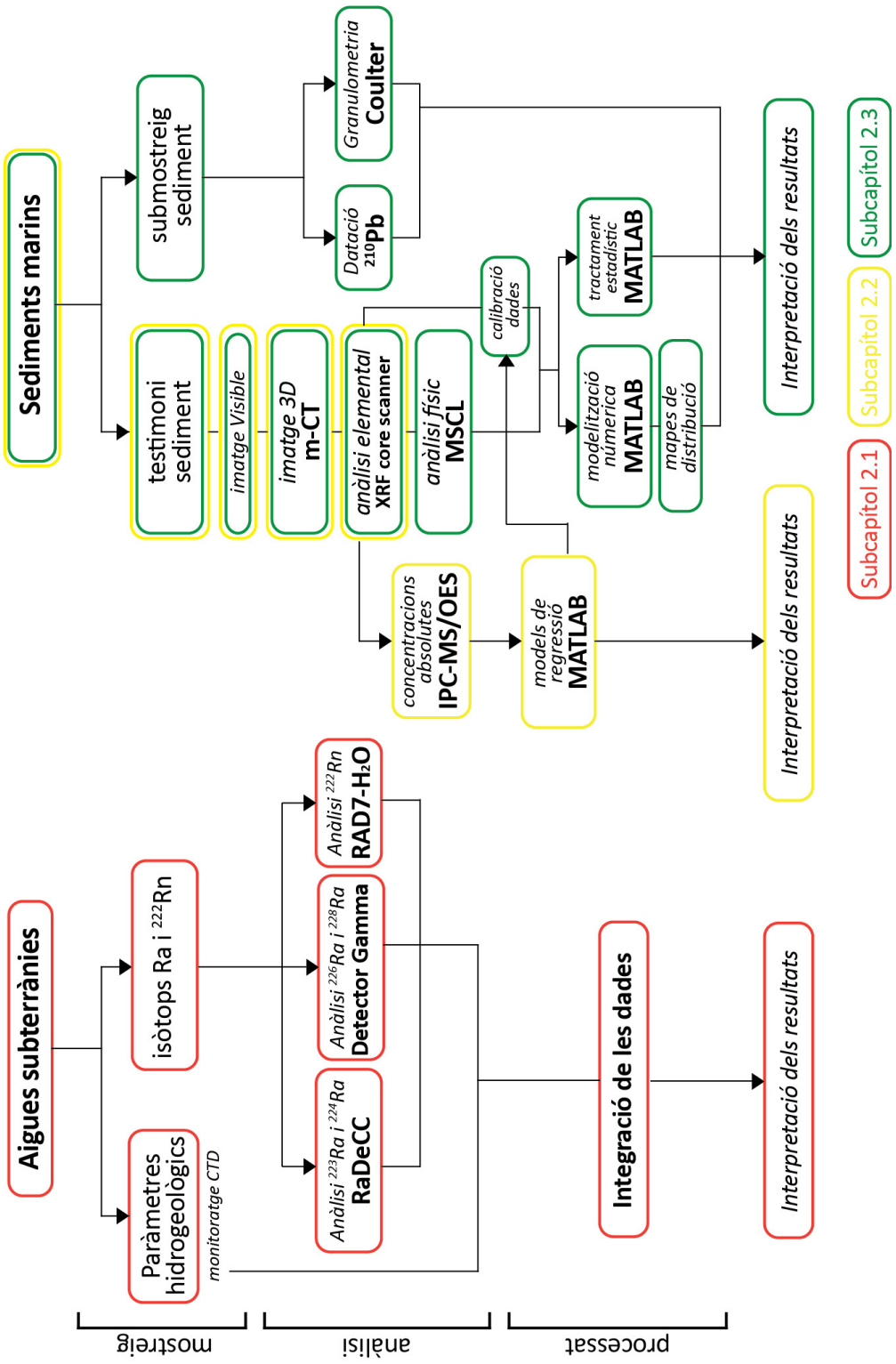

Figura 1.16 Flux de treball que hom ha seguit en el mostreig, anàlisi i processament de les mostres d'aigües subterrànies i dels sediments marins en aquesta Tesi. Els colors dels requadres indiquen el subcapítol de la Tesi en què es realitzà el procés concret: blau, subcapítol 2.1, groc, subcapítol 2.2 i verd subcapítol 2.3.

La mesura dels paràmetres hidrogeològics de l'aqüífer de la riera d'Argentona s'efectuà amb tres mesuradors de conductivitat, temperatura i profunditat, CTD-Diver®, instal·lats entre tots dos piezòmetres, PZ1 i PZ0 (Figura 1.17). El primer instrument s'instal·là en el PZ1 a 10 m sota la superfície (3 − 4 m sota el nivell freàtic) per avaluar les condicions de l'aigua dolça (d'ara endavant, PZ1-S). El segon instrument s'instal·là en el PZ1 a 34 m de profunditat amb l'objectiu de monitorar la zona de mescla entre l'aigua dolça i l'aigua salada (d'ara endavant, PZ1-B). Finalment, el tercer instrument fou emplaçat en el PZ0 a una profunditat de 1,8 m de la superfície (0,2 m sota el nivell freàtic) per avaluar les condicions de l'aigua subterrània prop de la zona on es produeix la descàrrega d'aigua des de l'aqüífer cap al mar. Les dades del nivell freàtic obtingudes pels instruments CTD-Diver® foren compensades amb la pressió atmosfèrica mesurada simultàniament amb un instrument Baro-Diver® també instal·lat al PZ1.

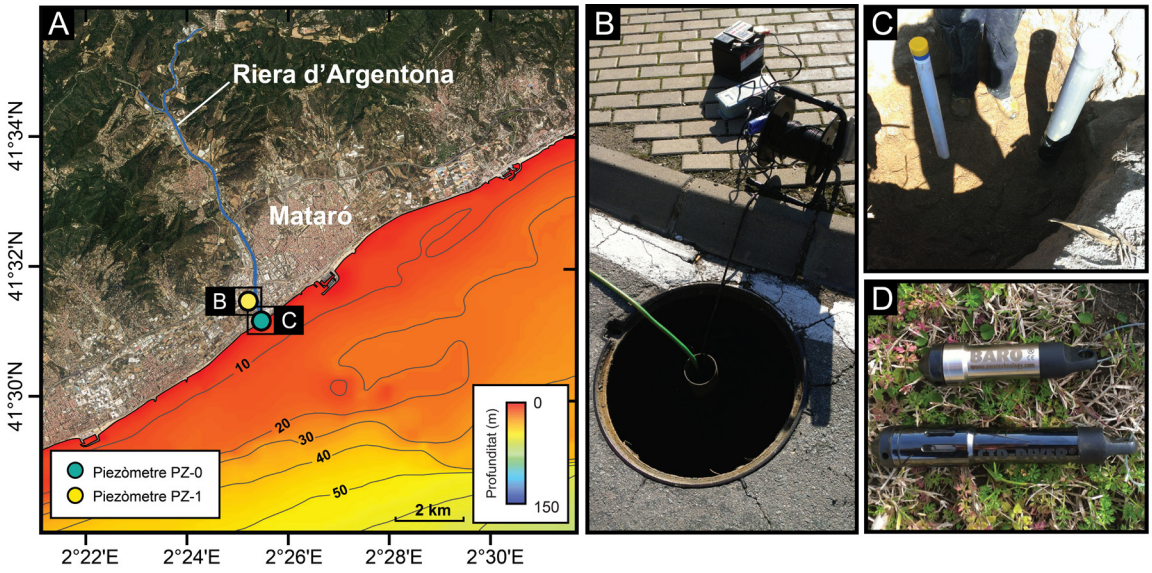

Figura 1.17 A) Sector proper a la riera d'Argentona. S'indica la localització dels piezòmetres utilitzats per aquesta Tesi. Profunditats en metres. B) Piezòmetre PZ1 de 50 m de profunditat, totalment ranurat, instal·lat per l'Agència Catalana de l'Aigua. C) Piezòmetre PZ0 de 3 m de profunditat, ranurat a la part inferior, instal·lat en el marc d'aquesta Tesi. D) Mesuradors de conductivitat, temperatura i profunditat CTD-Diver® i CTD-Baro®.

Les mostres d'aigua subterrània foren recollides a les mateixes profunditats dels instruments CTD-Diver®. Les mostres del PZ1-S (n = 15), del PZ1-B (n = 15) i del PZ0 (n = 8) s'obtingueren, per tant, a 10 m, 34 m i 1,8 m de la superfície. Per obtenir les mostres d'aigua, hom emprà una bomba submergible en ambdós piezòmetres. Les mostres d'aigua per analitzar els isòtops de Ra s'emmagatzemaren en contenidors

de 60 L (PZ1-S), 25 L (PZ1-B) i 10 L (PZ0) de capacitat mentre que les mostres per analitzar ^{222}Rn del PZ1-S i del PZ1-B s'emmagatzemaren en ampolles de vidre de 250 mL. Al PZ0 no es pogué analitzar el ^{222}Rn degut al baix nivell d'aigua en el piezòmetre (<20 cm), circumstància que fa augmentar l'intercanvi de ^{222}Rn amb l'aire, impedint així l'obtenció de mostres representatives. Durant el mostreig, la salinitat i la temperatura foren mesurades in situ utilitzant una sonda de mà YSI-556.

1.3.1.2 Mostreig de sediments marins

Els sediments marins de la plataforma continental interna davant la badia de Portmán s'obtingueren mitjançant un testificador múltiple (multicorer) que permet recuperar sis testimonis de sediment de cop de fins a 60 cm de llargada sense pertorbar la mostra (Figura 1.18.A). Per acotar les possibles heterogeneïtats i complexitats dels sediments superficials de l'àrea d'estudi hom mostrejà 52 estacions entre 10 i 60 m de profunditat. Al prodelta del Besòs el mostratge de sediment es realitzà amb un testificador de gravetat (gravity corer), que proporciona un únic testimoni de fins 3 m de llargada (Figura 1,18.B). El testimoni, de 5 cm de diàmetre, del prodelta del Besòs analitzat en aquesta Tesi mesurà 137 cm de llarg (Figura 1.19.D).

Els testimonis de sediment obtinguts amb testificador múltiple foren descrits visualment a bord del vaixell, i per cada estació de mostratge es guardà com a mínim un testimoni íntegre que fou emmagatzemat en cambra frigorífica a 4 °C tant a bord com després del seu trasllat amb camió refrigerat a la Universitat de Barcelona. A bord mateix, es procedí a submostrejar un dels testimonis de cada estació, en llesques de 0,5 cm de gruix per als primers 5 cm i d'1 cm des d'aquesta cota fins la base del testimoni. Aquestes submostres foren preservades en bosses de plàstic segellades i emmagatzemades a 4 °C. Un cop al laboratori, cadascuna de les mostres embossades fou pesada i assecada per avaluar el contingut d'aigua, i seguidament congelada i liofilitzada per analitzar la mida de gra.

1.3.2 Tècniques analítiques

1.3.2.1 Isòtops de radi i radó en mostres d'aigua

Els isòtops de Ra (^{223}Ra, ^{224}Ra, ^{226}Ra i ^{228}Ra) i de Rn (^{222}Rn) són molt estesos a la natura, especialment en sòls, roques, aigües subterrànies i superficials, a conseqüència de la desintegració dels isòtops de Th. Aquests isòtops han estat emprats com a traçadors

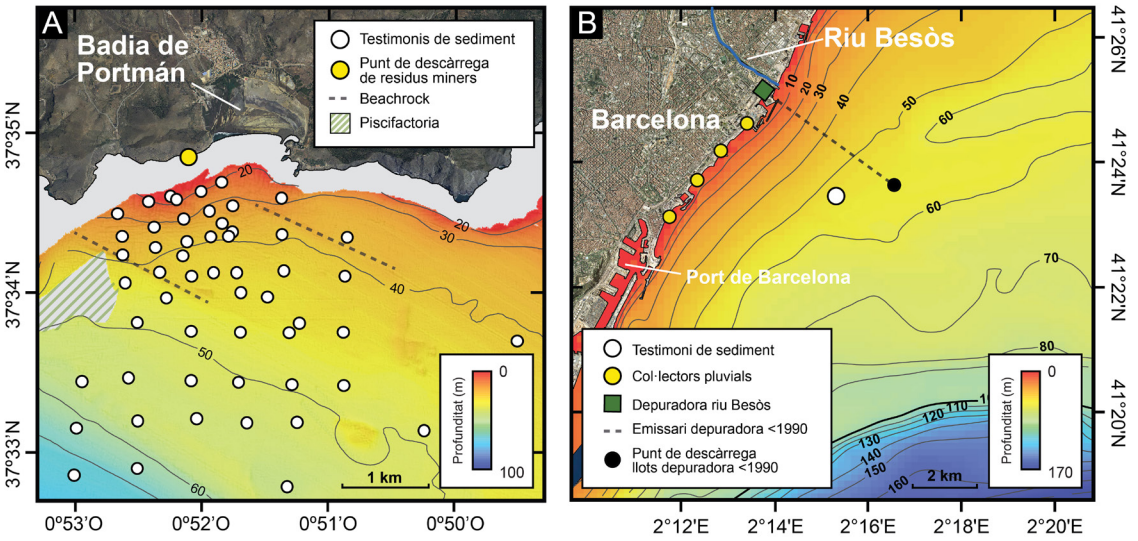

Figura 1.18 Ortofotomapes i mapes batimètrics de la plataforma continental de Cartagena i Barcelona. A) Sector de la badia de Portmán. S'indica la localització dels testimonis de sediment analitzats, del punt de descàrrega de residus miners, de la piscifactoria i de les *beachrocks*. B) Sector proper a la gola del riu Besòs. S'indica la localització del testimoni de sediment analitzat així com de la depuradora del Besòs, dels col·lectors pluvials de la ciutat de Barcelona que desguassen a la costa, i de l'emissari submarí de la depuradora abans de l'any 1979 (emissari antic). Profunditats en metres.

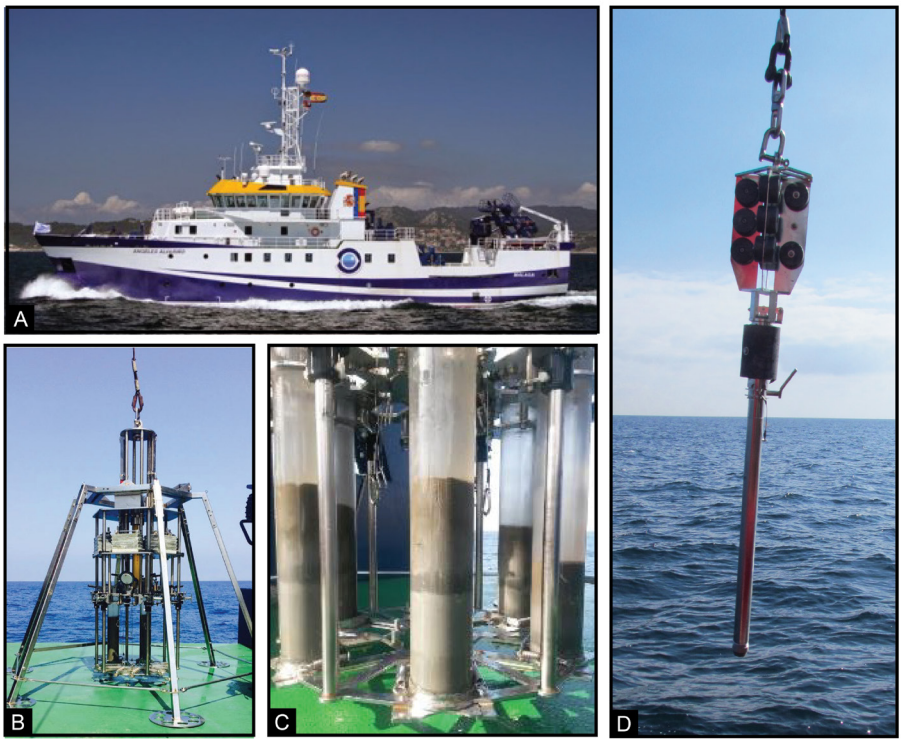

Figura 1.19 A) Vaixell oceanogràfic "Ángeles Alvariño" de l'Instituto Español de Oceanografía (IEO) des del qual s'obtingueren els testimonis de sediment de la zona d'estudi de la badia de Portmán. B) i C) Testificador múltiple i detall d'uns testimonis de sediment recuperats amb aquest mostrejador. D) Testificador de gravetat, emprat en el mostreig de sediments al prodelta del Besòs a bord del B/O García del Cid del CSIC..

de DAS en badies i estuaris (Dulaiova i Burnett, 2008; Gonneea et al., 2013; Rodellas et al., 2015b), llacunes costaneres (Garcia-Solsona et al., 2010; Rapaglia et al., 2012) i en àrees costaneres extenses (Windom et al., 2006; Ollivier et al., 2007; Moore, 2010; Rodellas et al., 2015b; Trezzi et al., 2016a).

La baixa concentració de Ra a les aigües naturals, especialment l'aigua marina, fa necessari un procés de preconcentració de la mostra. Això s'aconsegueix filtrant volums elevats d'aigua (5 − 60 L per aigües subterrànies i 50 − 350 L per aigua de mar) amb un flux constant de <1 L min^{-1} a través d'una columna cilíndrica de PVC (4,5 cm de diàmetre i 23 cm de llarg) reomplerta amb 25 g en sec de fibra de manganès (MnO_2) que prèviament ha estat estirada per incrementar-ne la superfície activa (Charette et al., 2012) (Figura 1.20.A). Per filtrar les possibles partícules en suspensió a les mostres d'aigua, es col·loca un filtre de fibra acrílica a la part superior del tub de PVC (Moore, 2008).

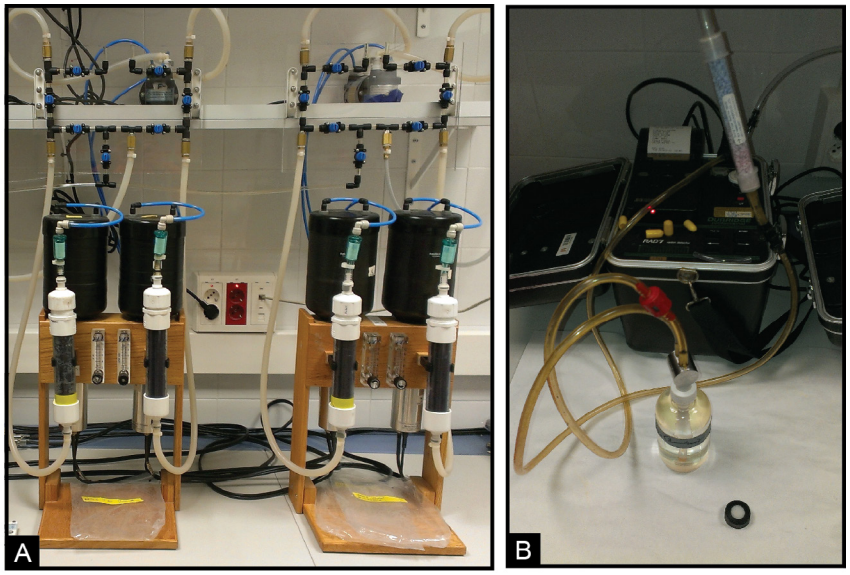

Figura 1.20 Equips de quantificació d'activitat d'isòtops de (A) ^{223}Ra i ^{224}Ra Radium Delayed Coincidence Counter (RaDeCC) i (B) ^{222}Rn RAD_7 amb l'accessori RAD-H_2O.

Un cop al laboratori, les fibres MnO_2 foren esbandides amb aigua lliure de Ra (Sun i Torgersen, 1998), assecades parcialment i mesurades amb un equip *Radium Delayed Coincidence Counter* (RaDeCC) del Laboratori de Radioactivitat Ambiental de la Universitat Autònoma de Barcelona per quantificar els isòtops de Ra de vida curta, ^{223}Ra i ^{224}Ra, i llurs incerteses (Moore i Arnold, 1996; Garcia-Solsona et al., 2008). A continuació, les fibres de MnO_2 foren incinerades (820 °C, 16 h), mòltes i emmagatzemades en vials durant tres setmanes per determinar l'activitat dels isòtops

Ra de vida llarga, ^{228}Ra i ^{226}Ra, mitjançant un equip d'espectrometria gamma amb un detector de tipus HPGe. Els isòtops ^{226}Ra i ^{228}Ra s'analitzaren a partir dels fotopics del ^{214}Pb a 351,9 keV i ^{228}Ac a 911 keV, respectivament.

Les activitats del ^{222}Rn a les mostres d'aigua subterrània es mesuraren amb un espectròmetre alfa ^{222}Rn en aire RAD7 (Durridge Inc.) (Burnett et al., 2001) adaptat a un sistema RAD-H2O (Durrigde Inc.) per a la determinació directa de ^{222}Rn a partir d'ampolles de 250 mL (Figura 1.20.B).

1.3.2.2 Tomografia computeritzada

Les darreres dècades, l'ús d'escàners de tomografia computada (TC) en l'àmbit de les ciències naturals ha revolucionat, entre moltes altres, l'anàlisi dels registres sedimentaris (Fortin et al., 2013; Van Daele et al., 2016), de l'estructura mineralògica de les roques (De Boever et al., 2015) i de la morfologia i estructura d'organismes vius (Dierick et al., 2014). La rapidesa de l'anàlisi així com el seu caràcter no destructiu (no cal destruir la mostra i aquesta, un cop analitzada, resta íntegra) han contribuït a estendre extraordinàriament el seu ús en el món de la recerca (Kak i Slaney, 1988). La TC proporciona imatges tridimensionals dels objectes analitzats, depenent del seu coeficient d'atenuació dels raigs X, el qual al seu torn és funció de la seva composició (nombre atòmic efectiu) i densitat (Cnudde et al., 2006). Per obtenir visualitzacions 3D cal reconstruir les diverses projeccions analitzades, és a dir el conjunt d'imatges enregistrades segons direccions específiques en funció de diferents angles d'adquisició.

La solució matemàtica al problema de com reconstruir les projeccions per obtenir una imatge final fou desenvolupada, teòricament, per Allan MacLeod a la dècada de 1950 i, des del punt de vista pràctic, per Godfrey Newbold Hounsfield la dècada següent, una investigació per la qual rebé el premi Nobel de Medicina l'any 1979. Els algoritmes desenvolupats van demostrar que era possible computar les imatges d'alta resolució de seccions transversals d'un objecte amb una elevada precisió. La millora posterior dels algoritmes inicials permeté reduir el temps de reconstrucció i obtenir imatges molt més acurades numèricament, aspectes determinants en l'aparició dels primers escàners de tomografia computada per raigs X adreçats al sector mèdic.

La generació de feixos de raigs X és l'element bàsic de la tomografia computada (Figura 1.21). Amb aquest nom es fa referència a una radiació electromagnètica, situada en

un rang de longitud d'ona entre 10^{-12} i 10^{-8} m (0,01 a 100 Å), que es genera a escala atòmica a partir de dos processos: la transició dels electrons entre dos nivells atòmics i la desacceleració, a causa dels camps electromagnètics, de partícules carregades. El primer procés es caracteritza per la transició d'un electró entre dos nivells energètics diferents, la qual va acompanyada per l'emissió d'un quàntum de radiació amb una energia equivalent a la diferència energètica entre ambdós nivells. Aquesta energia és característica de cada element i nivell i, per tant, l'emissió electromagnètica només pot ser discreta.

El segon procés, la desacceleració de partícules carregades com els electrons, protons o partícules alfa, provoca la pèrdua d'energia, que és emesa com a quàntum de raigs X amb un valor únic per damunt dels 20 MeV. Aquesta radiació és contínua i és coneguda amb el nom de "radiació de frenada" o "raigs X de Bremsstrahlung".

L'emissió de raigs X en els escàners de tomografia computada es produeix mitjançant un tub de raigs X. Normalment es tracta d'un tub metàl·lic a baixa pressió (entre 10^{-3} i 10^{-5} Pa) que conté un ànode (anticàtode) i un càtode. Els electrons emesos al càtode són accelerats i xoquen contra l'ànode, generant així feixos de raigs X que es focalitzen cap a la mostra. El material de què estigui fet l'ànode (habitualment Mb, Cu o Zr) definirà l'espectre d'emissió de raigs X (Figura 1.21).

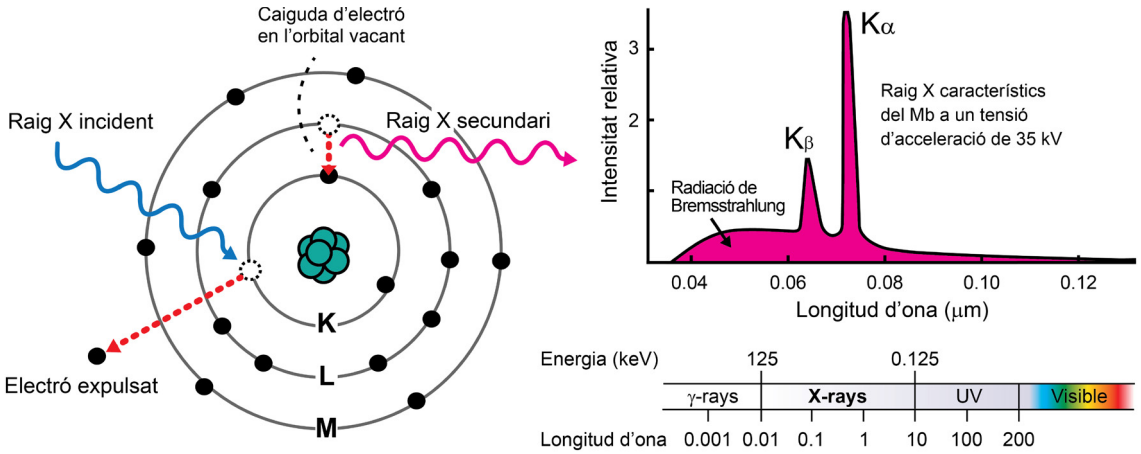

Figura 1.21 Esquemes de la generació de raigs X secundaris, característics de cada element, de l'espectre d'emissió típic d'una font de raigs X de Mb i de les longituds d'ona de diverses ones electromagnètiques inclosos els raigs X.

Un cop el feix de raigs X ha travessat la mostra o objecte, uns detectors instal·lats dins de l'equip de tomografia computada permeten quantificar la radiació electromagnètica incident. Els detectors, especialment els de cambres proporcionals de xenó i els de

centelleig, són molt semblants als utilitzats als aparells de radiografia de raigs X. Els resultats es visualitzen mitjançant imatges en escala de grisos, on el blanc i el negre representen les atenuacions màxima i mínima dels raigs X, respectivament, les quals s'interpreten en termes de major i menor densitat del material.

Els testimonis de sediment utilitzats per aquesta Tesi van ser escanejats amb l'equip *X-ray micro-CT MultiTom* del Laboratori CORELAB de la Universitat de Barcelona (Figura 1.22.A). Aquest instrument permet escanejar testimonis de sediment de fins 1,5 m de llarg, i també mostres molt més petites (p. ex. un foraminífer o un gra d'arena) amb resolucions compreses entre 0,1 i 1 mm. L'anàlisi dels testimonis es realitzà després de l'excitació del tub de raigs X de 120 kV i 80 W del *MultiTom*, amb un temps d'exposició de 120 s, tot i emprant un filtre de Cu de 0,5 mm. S'obtingueren així un seguit de talls de 0,254 mm de gruix en 1.001 projeccions i una resolució del vòxel de 0,125 x 0,125 x 0,125 mm, el qual es defineix com la unitat mínima d'informació d'una imatge tridimensional. Dit d'una altra manera, és la unitat volumètrica del píxel utilitzada per a representar objectes en tres dimensions (Duliu, 1999).

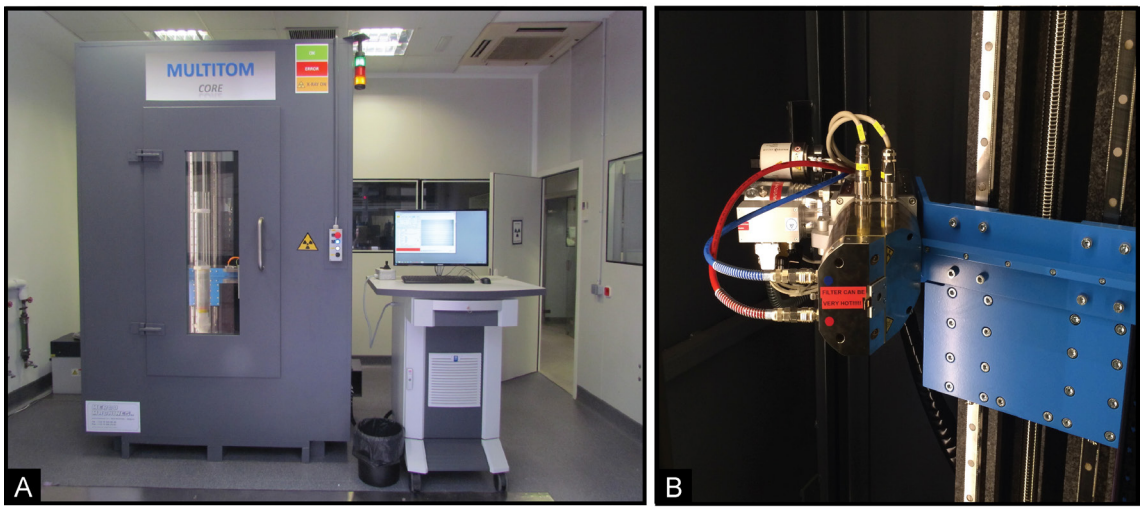

Figura 1.22 A) Equip de microtomografia computada *X-ray micro-CT MultiTom* del Laboratori CORELAB de la Universitat de Barcelona. B) Detall de la font de raigs X d'aquest 'equip.

En total s'obtingueren ~140.000 imatges en format Tiff, que ocuparen 1,30 Tb, amb més d'1,1 x 10^{12} bytes de dades. Posteriorment, les imatges foren processades amb el programari especialitzat de l'equip MultiTom i visualitzades i analitzades amb el programari de processament d'imatges digital de domini públic ImageJ i amb el programari de visualització i anàlisi d'imatges en tres dimensions Avizo®.

1.3.2.3 Anàlisi de la composició elemental

La composició elemental dels testimonis de sediment s'ha obtingut amb un escàner de fluorescència de raigs X, o escàner de FRX (en anglès *XRF core scanner*), que permet l'escaneig en continu, amb caràcter no destructiu i en alta resolució. Aquesta tècnica, amb la qual hom pot analitzar fins a 80 elements amb una gran sensibilitat, és actualment una de les més utilitzades per a la determinació de la composició química dels materials (Jansen et al., 1998). Les darreres dècades aquesta tècnica ha estat emprada amb molt d'èxit en l'estudi de sediments tous; de roques, inclosos espeleotemes; de dipòsits orgànics com la torba; de fusta i de molts altres materials amb finalitats diverses (Rothwell i Croudace, 2015; Hanebuth et al., 2015; Guo i Yang, 2016). Així, i a títol il·lustratiu, hom se n'ha servit per mesurar canvis relatius en la composició química de sediments marins i lacustres (Rothwell i Rack, 2006), en paleoclimatologia i paleooceanografia (Calvert i Pedersen, 2007), en sedimentologia (Croudace et al., 2012; Croudace i Rothwell, 2015), i en litoestratigrafia i estudis de la diagènesi (Löwemark et al., 2011; Croudace et al., 2019).

La mesura de la composició elemental per fluorescència de raigs X es basa en l'expulsió dels electrons de la capa exterior de l'àtom a conseqüència de la irradiació d'un feix de raigs X. L'espai buit deixat per l'electró expulsat és ocupat per altres electrons de nivells energètics superiors i la diferència d'energia entre ambdós nivells és emesa en forma de radiació de raigs X (Figura 1.23). Aquesta diferència d'energia d'emissió és característica de cada element, fet que en permet la identificació (Richter et al., 2006).

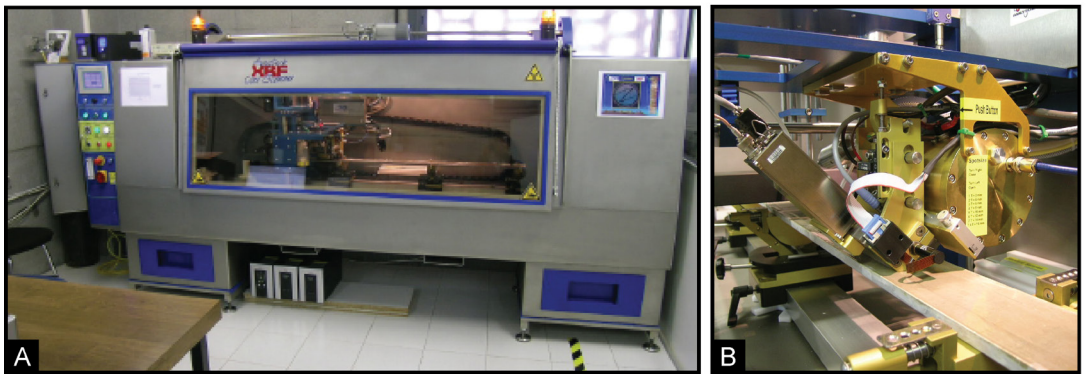

Figura 1.23 A) Escàner de fluorescència de raigs X del Laboratori CORELAB de la Universitat de Barcelona. B) Detall de la font i el detector de raigs X d'aquest aparell.

En el marc d'aquesta Tesi, l'anàlisi de la composició elemental dels elements majoritaris en els testimonis de sediment objecte d'estudi s'ha fet amb un escàner de FRX de

l'empresa Avaatech instal·lat al Laboratori CORELAB de la Universitat de Barcelona. Aquest escàner està equipat amb una font de raigs X model *Oxford Rhodium* (4–50 kV), un detector *Canberra X − Pips 1500 − 1,5* amb una finestra de Be de 125 μm i un analitzador multicanal *Canberra DSA 1000* (MCA). Amb aquesta configuració hom pot analitzar l'espectre d'emissió d'un alt nombre d'elements, concretament els de pes atòmic comprès entre el Al i el U.

Abans de fer l'escaneig, els testimonis foren partits longitudinalment, de manera que de cada secció s'obtingueren dues mitges canyes plenes de sediment, una de les quals s'emprà per a l'escaneig. En cas de ser necessari, hom allisà curosament amb una espàtula la superfície del sediment de la mitja canya destinada a l'escaneig, a fi d'obtenir una superfície perfectament horitzontal i llisa. La mateixa mitja canya es deixà assecar durant 16 hores a temperatura ambient per facilitar l'evaporació d'una part de l'aigua continguda en el sediment, a fi i efecte de reduir l'absorció de la radiació per l'aigua, aconseguint així augmentar la intensitat del senyal mesurat (Böning et al., 2007; Tjallingii et al., 2008). A continuació, hom recobrí la superfície del sediment de la mitja canya amb film *Ultralene X-ray transmission* de 4 μm, un film especial que no interactua amb la radiació X i que alhora permet evitar la dessecació i la contaminació potencial del sediment.

Les mesures s'efectuaren a 2 mm de resolució amb unes condicions d'excitació de 10 kV i 1,2 mA amb un temps d'exposició de 10 s per als elements de pes atòmic entre el Al i el Fe, i 30 kV i 1,6 mA amb un temps d'exposició de 50 s i un filtre de Pd per als elements de pes atòmic entre el Ni i el Pb. Amb l'objectiu d'obtenir la màxima intensitat de cada element, per al Ti, el Ca, el S, el Mn, el Fe, el Zn i el As es va analitzar la línia d'emissió Kα mentre que per al Pb es va analitzar la línia d'emissió L$_\beta$ amb la finalitat de reduir l'efecte de superposició amb l'emissió del As. Per determinar l'àrea de l'espectre d'emissió de cada element, expressada en comptes totals, i la intensitat, en comptes per segon (en anglès *counts per second*, cps), es va emprar el programari d'anàlisi espectral bAxil (BrightSpec NV/SA).

1.3.2.4 Anàlisi de la susceptibilitat magnètica i densitat del sediment

L'anàlisi de la susceptibilitat magnètica i de la densitat gamma s'efectuà amb un perfilador de testimonis multisensorial (en anglès *Multi-sensor Core Logger*, MSCL) de l'empresa *Geotek* instal·lat al Laboratori CORELAB de la Universitat de Barcelona (Figura 1.24). El MSCL permet l'anàlisi en continu, d'alta resolució i no destructiu de

diversos paràmetres físics en testimonis de sediment i roca. Entre aquests paràmetres destaquen la susceptibilitat magnètica, la densitat, la velocitat de transmissió de les ones P i la resistivitat elèctrica. El MSCL està adaptat per a l'anàlisi de testimonis de sediment, tant tancats com oberts en mitja canya, de 50 a 150 mm de diàmetre amb resolucions màximes 5 mm.

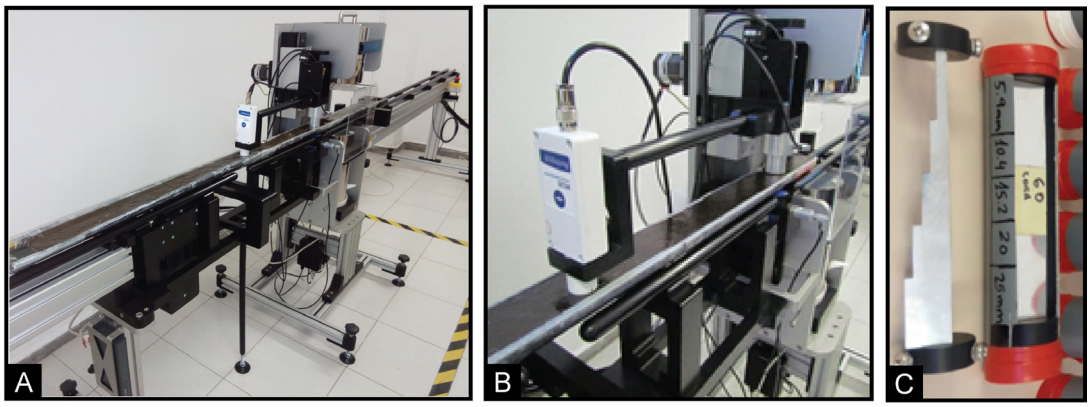

Figura 1.24 A) Perfilador de testimonis multisensorial (MSCL) del Laboratori CORELAB de la Universitat de Barcelona en configuració per testimonis de sediment oberts. B) Detall del sensor de susceptibilitat magnètica. C) Peça d'alumini per al calibratge de la densitat gamma.

La densitat s'obtingué mitjançant la mesura de l'atenuació de la radiació gamma en travessar el sediment. Amb aquesta finalitat, el MSCL incorpora una font de ^{137}Ce i un detector de centelleig de NAI (Tl). Atès que la llei de l'atenuació de la radiació electromagnètica estableix que la variació de la intensitat de la radiació en travessar un material és proporcional al gruix màssic o la densitat del material, hom la pot quantificar per mitjà d'una calibració amb estàndards de densitat coneguda (Figura 1.24.C). Normalment, s'utilitzen tubs estandarditzats amb dues fases diferenciades, representades per una peça d'alumini de diferents diàmetres i aigua destil·lada. Fent una regressió lineal entre l'atenuació de radiació gamma i la densitat dels estàndards, s'obté una funció que permet determinar la densitat del sediment a partir del valor d'atenuació.

El MSCL també compta amb un sensor per analitzar la susceptibilitat magnètica del sediment, és a dir, la quantitat de material que pot ser magnetitzat per unitat de volum si se li aplica un camp electromagnètic exterior. Aquesta mesura és adimensional i, per tant, per obtenir la susceptibilitat màssica (m^3 kg^{-1}) és necessari analitzar la densitat del sediment (Blum, 1997). L'anàlisi de la susceptibilitat magnètica permet una primera estimació de l'abundància de mineral ferromagnètic en el sediment, la

qual està directament relacionada amb la presència de minerals com la magnetita.

El MSCL incorpora dos sistemes de mesura de la susceptibilitat magnètica. El primer permet la mesura de testimonis tancats mercès a un sensor circular Bartington (MSC2C), adaptable a diversos diàmetres de testimoni. Aquest sistema té una resolució limitada, ja que integra els valors de tot el sediment del testimoni, els quals poden variar en funció del diàmetre del tub i també del mateix sensor. El segon sistema usa un sensor Bartington (MS2E) aplicat a testimonis oberts, amb la qual cosa s'aconsegueix una resolució més gran en l'anàlisi de la susceptibilitat magnètica. Aquest sensor se situa en contacte amb la superfície del sediment, i cobreix una àrea de 3,8 x 10,5 mm (Figura 1.24.B).

1.3.2.5 Anàlisi de la concentració elemental

L'anàlisi de la concentració elemental en mostres de sediment es determinà per espectrometria de masses de plasma acoblat inductivament (en anglès *inductively coupled plasma mass spectrometry*, ICP-MS) i espectrometria d'emissió òptica de plasma acoblat inductivament (en anglès *inductively coupled plasma optical emission spectroscopy*, ICP-OES). En totes dues tècniques, la mostra és vaporitzada i ionitzada a temperatures elevades mitjançant el dispositiu de plasma acoblat inductivament, el qual forma un plasma, generalment a partir del gas noble argó.

En ICP-MS l'anàlisi química de la mostra s'efectua per mitjà de la caracterització de la massa i la càrrega dels elements. Per fer-ho possible, el plasma ionitzat és transportat fins l'analitzador de masses on un filtre quadrupolar en una interfase de buit permet separar els elements segons la relació de càrrega i massa de cada isòtop. Finalment, el detector analitza la quantitat i l'abundància d'ions a la mostra. En ICP-OES el plasma ionitzat és transportat fins l'espectròmetre òptic que analitza la longitud d'ona i la freqüència de la radiació electromagnètica emesa, la qual en ésser característica de cada element permet la seva identificació química. Per bé que el nombre total d'ions i de fotons de cada element és directament proporcional a la concentració original de l'element, ambdues tècniques permeten determinar la concentració química de cada element a la mostra analitzada per calibratge amb estàndards de concentració coneguda.

Per procedir a l'anàlisi química elemental, les mostres de sediment foren congelades, liofilitzades, moltes i homogeneïtzades amb un morter d'àgata i introduïdes en un

reactor de Teflon amb 2,5 mL de HNO_3 (65%) a 100°C durant 18 hores. A continuació, s'introduí l'extracte en un tub de polietilè que se sotmeté a centrifugació a 3.000 rpm durant 3 minuts per separar la fase sòlida. El sobrenedant fou decantat i diluït amb HNO_3 a l'1% fins assolir 50 mL per a la seva anàlisi directa. El residu s'introduí un altre cop dins el reactor de Teflon amb 1 mL d'HNO_3 (65%), 7 mL d'HF i 1 mL d'H_2O_2 i s'escalfà durant 18 hores a 100°C. Posteriorment, s'afegiren 2 mL de $HClO_4$ a la mescla i es procedí a escalfar el reactor de Teflon en un bany de sorra a 270°C fins l'evaporació total de l'àcid. El residu calent fou tractat amb 2 mL d'HNO_3 (65%), 2 mL d'H_2O_2 i tot seguit es decantà dins un matràs volumètric on es diluí amb HNO_3 a l'1% fins assolir 50 mL.

Les dues solucions obtingudes per cada mostra foren analitzades amb un ICP-OES *Perkin-Elmer Optima 8300* per als elements en concentracions baixes (Ti, Zn, As i Pb) i amb un ICP-MS *Perkin-Elmer Elan-6000* per als elements en concentracions altes (Mn i Fe), tots dos instruments dels Centres Científics i Tecnològics de la Universitat de Barcelona.

1.3.2.6 Anàlisi granulomètrica

Les anàlisis granulomètriques es realitzaren per mitjà d'un difractòmetre de raig làser LS230 de *Beckman Coulter* del Laboratori de Sedimentologia del Departament de Dinàmica de la Terra i de l'Oceà de la Universitat de Barcelona. El *Coulter LS230* disposa d'un mòdul òptic amb una font de feix de llum monocromàtica, una lent per intensificar el feix, una cel·la per on circula la mostra en suspensió en aigua destil·lada, les lents que concentren el feix de llum difractat i l'anella detectora que disposa de 126 detectors.

Aquest equip permet mesurar la mida de les partícules d'una mostra a partir de la quantificació de l'angle de difracció d'un feix llum monocromàtica (750 nm) quan aquest travessa una matriu aquosa i impacta contra la partícula. El feix difractat és concentrat per les lents fins al detector que mesura en interval de temps la distribució angular de la llum difractada obtenint així la mida de la partícula aplicant la teoria de la difracció de Fraunhofer. Així, com més gran és l'angle de difracció observat més petit és el diàmetre de les partícules.

L'equip *Coulter LS230* permet la mesura del percentatge en volum dels diàmetres de les partícules d'entre 0,04 i 2.000 μm (Figura 1.25). Els principals avantatges d'aquesta

metodologia són la rapidesa i la bona reproductibilitat de les anàlisis d'un elevat rang de diàmetres de partícula així com la petita quantitat de mostra necessària.

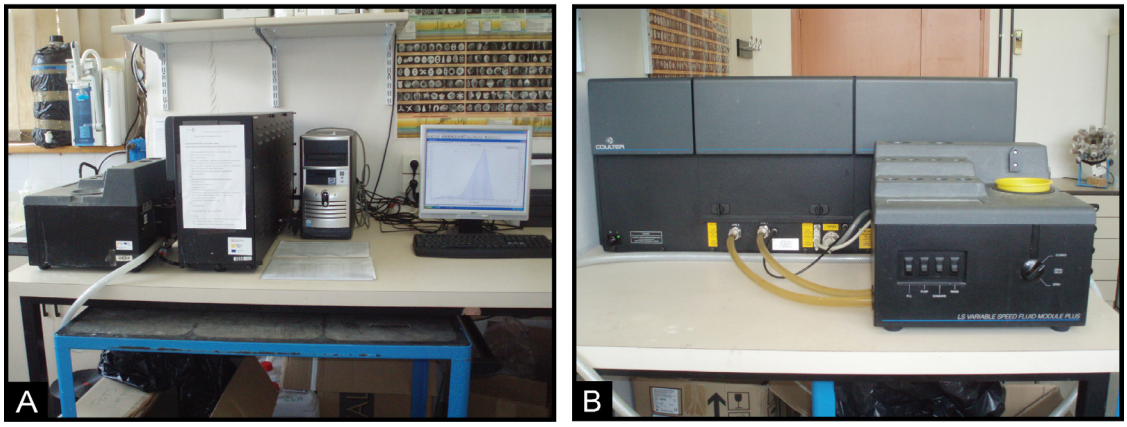

Figura 1.25 A) i B) Analitzador de mida de partícules per difractometria de raigs làser Coulter LS230 de Beckman Coulter del Laboratori de Sedimentologia del Departament de Dinàmica de la Terra i de l'Oceà de la Universitat de Barcelona.

Per realitzar les anàlisis de granulometria, en la present Tesi s'empraren 0,5 grams per cada mostra de sediment per assegurar l'obturació òptica del feix làser necessària per fer les mesures. En primer lloc, la mostra fou atacada amb peròxid d'hidrogen (10%) per eliminar la matèria orgànica que poden formar agregats amb les partícules. Posteriorment, s'afegí una solució de 2,7% d'àcid acètic – 0,34 M acetat de sodi (pH=4) per eliminar la fracció carbonatada sense afectar la resta de la mostra i provocar canvis en la mineralogia del material. A continuació, l'àcid fou retirat per centrifugació, rentat amb aigua destil·lada i finalment, se li afegí una solució de polifosfat de sodi per prevenir la floculació de les argiles. Prèviament a l'anàlisi de mida de partícula, es procedí a sacsejar la mostra amb un agitador mecànic durant dues hores. Finalment, la mostra fou introduïda al Coulter utilitzant un tamís de 2 mm per tal de retenir qualsevol partícula d'un diàmetre superior que pugui obstruir el circuit de l'equip.

1.3.2.7 Taxes de sedimentació i datació dels sediments

Les taxes de sedimentació de l'àrea d'estudi foren obtingudes mitjançant l'anàlisi del ^{210}Pb en dos testimonis de sediment submostrejats prèviament (secció 1.3.2). Les mostres guardades en les bosses estanques foren congelades, liofilitzades i finalment triturades abans de l'anàlisi, la qual es dugué a terme en el Laboratori de Radioactivitat Ambiental de la Universitat Autònoma de Barcelona. La determinació de les activitats totals de ^{210}Pb fou realitzada mitjançant la mesura del seu radioisòtop fill i emissió

gamma, el ^{210}Po (Sanchez-Cabeza et al., 1998).

Per realitzar les anàlisis es prengueren entre 0,2 − 0,3 g de mostra a la qual se li afegí un traçador intern de ^{209}Po subministrat per l'IAEA (0,7031 ± 0,050 Bq mL^{-1}) i es digeriren totalment en medis àcids mitjançant un forn de microones analític en discos de plata amb HCl 1M a 70 °C mentre s'agitaven durant 8 hores. Les activitats de ^{210}Po es determinaren mitjançant espectròmetres α amb detectors de silici (SSB) de baix fons (EG&G Ortec) durant 1 − 4·10^5 s. Les mostres foren emmagatzemades durant tres setmanes permetent així arribar a l'equilibri secular entre el ^{226}Ra i llurs fills de curta vida. L'activitat ^{226}Ra fou determinada partir del ^{214}Pb a través de la línia d'emissió gamma de 351 keV per espectrometria en un detector de Ge coaxial d'alta puresa. L'excés de ^{210}Pb (^{210}Pb$_{xs}$) es va determinar restant l'activitat ^{226}Ra assumint que representa l'activitat ^{210}Pb de l'activitat ^{210}Pb total. La qualitat de les mesures s'avaluaren mitjançant el test de competència de l'AIEA i l'anàlisi contínua de materials i rèpliques dels certificats.

1.3.4 Tractament i computació numèrica de les dades

El gran volum de dades obtingudes amb les múltiples tècniques analítiques emprades en la present Tesi fa necessari l'ús d'entorns de computació numèrica per al seu processament. Aquests entorns permeten la integració de grans bases de dades i el seu posterior tractament analític. En la present Tesi, l'entorn de computació emprat ha estat el programari MATLAB (abreviatura de *MATrix LABoratory*) desenvolupat per l'empresa *The MathWorks Inc.* Com indica el seu nom, aquest programari està fonamentat en la manipulació de matrius en un entorn de desenvolupament integrat, és a dir, programaris que ofereixen serveis integrals per al desenvolupament del mateix programa i que inclouen un editor de codi font, eines de construcció automàtiques i un depurador del codi. Concretament, MATLAB disposa d'un llenguatge de programació propi (llenguatge M). Aquest programari fou dissenyat per realitzar càlculs matemàtics tant simples com complexos: analitzar i visualitzar dades, la creació i aplicació d'algoritmes o el desenvolupament del codi font de nous programaris (Trauth et al., 2006).

Un dels aspectes rellevants de MATLAB és l'extensa llibreria de funcions, aplicacions i rutines de què disposa, els anomenats Toolbox, que permeten a l'usuari resoldre múltiples problemes computacionals. Consegüentment, en les darreres dècades, MATLAB ha esdevingut una eina popular en el camp de les ciències de la terra (Wu

et al., 2015; Zekollari, 2017) i específicament, en l'oceanografia (Gerber et al., 2009; Iglesias et al., 2012; Rumín-Caparrós et al., 2016). El seus usos s'estenen des de la modelització numèrica aplicada als estudis de morfodinàmica, el processament de dades sísmiques i per satèl·lit fins a la generació de models digitals del terreny.

L'ús de MATLAB en aquesta Tesi s'ha centrat principalment en:

1. La implantació dels mètodes de regressió lineal que es recullen en el subcapítol 2.2 i la seva aplicació en el calibratge de les mesures obtingudes mitjançant l'equip *XRF core scanner* i la concentració absoluta de metalls i metal·loides.

2. La propagació i quantificació dels errors associats a les concentracions calibrades de metalls i metal·loides dels testimonis de sediment (subcapítol 2.2).

3. La integració de les mesures físiques i químiques dels testimonis de sediment, llur representació gràfica i tractament estadístic (subcapítol 2.3).

4. La modelització numèrica per interpolació tridimensional de les mesures físiques i químiques i la quantificació de la massa total de cada metall i metal·loides dels primers 14 centímetres de sediment marí en l'àrea d'estudi (subcapítol 2.3).

Capítol 2

"Als teus ulls he descobert
que teníem la mirada per fer estiu."

Mireia Calafell

Resultats

Constraining the temporal variation of Ra isotopes and Rn in the groundwater end-member: implications for derived SGD

Calibrating high resolution XRF core scanner data to obtain absolute metal concentrations in highly polluted marine deposits after two case studies off Portmán Bay and Barcelona, Spain

Physical and geochemical characterization of a submarine sulfide mine tailings deposit, Portmán Bay, SE Spain

2.1 Constraining the temporal variations of Ra isotopes and Rn in the groundwater end-member: implications for derived SGD estimates

Marc Cerdà-Domènech[a], Valentí Rodellas[b,c], Albert Folch[d,e], Jordi Garcia-Orellana[b,f]

[(a)] GRC Geociències Marines, Dep. de Dinàmica de la Terra i de l'Oceà, Universitat de Barcelona, 08028 Barcelona, Spain.
[(b)] Institut de Ciència i Tecnologia Ambientals (ICTA), Universitat Autònoma de Barcelona, 08193 Bellaterra, Spain.
[(c)] Center de Recherche et d'Enseignement de Géosciences de l'Environment (CEREGE), Aix-Marseille Université, 13545 Aix-en-Provence, France.
[(d)] Department of Civil and Environmental Engineering, Universitat Politècnica de Catalunya (UPC), c/Jordi Girona 1-3, Barcelona, Spain
[(e)] Associated Unit: Hydrogeology Group (UPC-CSIC), Spain
[(f)] Departament de Física, Universitat Autònoma de Barcelona, 08193 Bellaterra, Spain.

Science of the Total Environment 595 (2017) 849–857
https://doi.org/10.1016/j.scitotenv.2017.03.005

Keywords: Submarine groundwater discharge, radium, radon, salinity interface, end-member

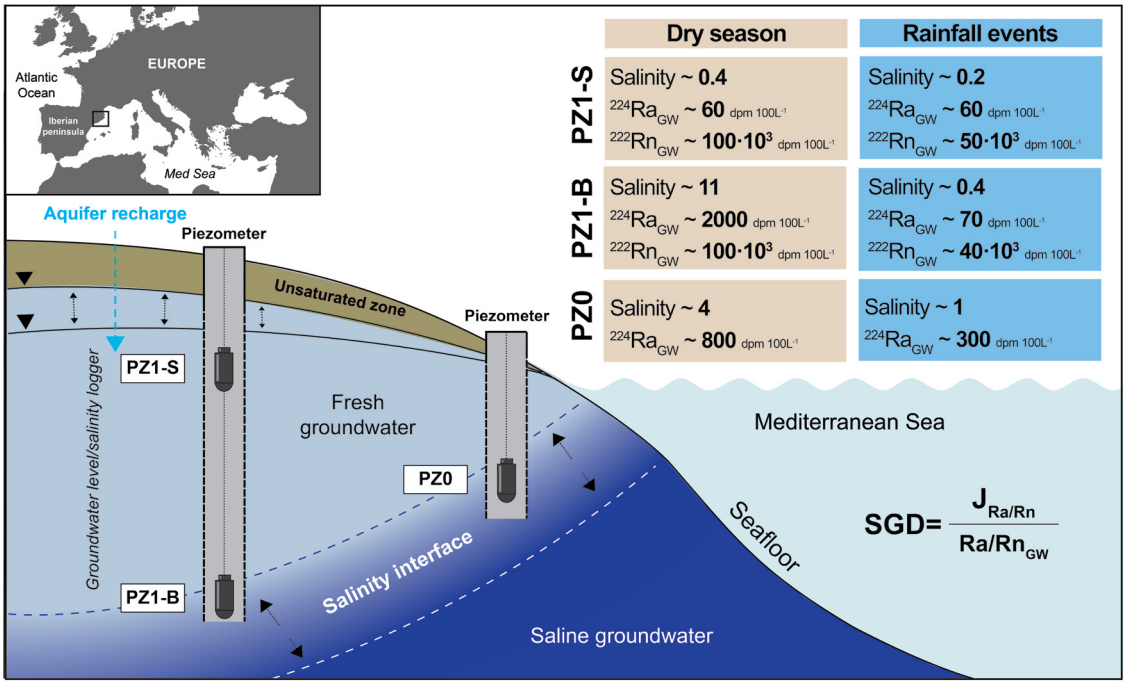

Figure 2.1 Graphical Abstract.

Abstract Submarine groundwater discharge (SGD) has been recognized as an important supplier of chemical compounds to the ocean that may influence coastal geochemical cycles.

Radium isotopes (^{223}Ra, ^{224}Ra, ^{226}Ra, ^{228}Ra) and radon (^{222}Rn) have been widely applied as tracers of SGD. Their application requires the appropriate characterization of both the concentrations of tracers in the discharging groundwater and their distribution in the coastal water column. This study evaluates the temporal evolution of Ra isotopes and ^{222}Rn concentrations in a dynamic subterranean estuary of a microtidal Mediterranean coastal aquifer that experiences large displacements of the fresh-saltwater interface as a necessary initial step in evaluating the influence of SGD in coastal waters. We show that changes in groundwater salinities due to the seaward displacement of the fresh-saltwater interface produced large variations in Ra activities in groundwater (by a factor of ~19, ~14, ~6, and ~11 for ^{223}Ra, ^{224}Ra, ^{226}Ra and ^{228}Ra, respectively), most importantly during rainfall events. In contrast, the ^{222}Rn activities in groundwater oscillated by a factor of 3 during these rainy periods. The large temporal variability in Ra activities hampers characterization of the SGD end-member when using Ra isotopes as tracers, and thus presents a challenge for obtaining accurate SGD estimates. This study emphasizes the need to understand the hydrodynamics of coastal aquifers to appropriately constrain the Ra isotopes and ^{222}Rn concentrations in groundwater and when applying both tracers in dynamic microtidal coastal systems.

2.1.1 Introduction

Submarine Groundwater Discharge (SGD) includes both meteoric fresh groundwater flowing into the sea and seawater recirculation through coastal aquifers (Burnett et al., 2003). Both flows mix in coastal aquifers, so-called subterranean estuaries (STEs), where biogeochemical reactions occur as a consequence of interactions between terrestrially derived groundwater, recirculated seawater and the geological matrix (Moore, 1999). This dynamic mixing zone influences the transfer of several chemical constituents to the coastal ocean (Tovar-Sánchez et al., 2014; Sadat-Noori et al., 2016). SGD is now recognized as a relevant source of nutrients, trace metals and other compounds and contaminants to the coastal sea (Kim et al., 2003; Johnson et al., 2008; Gonneea et al., 2014; Pavlidou et al., 2014; Rodellas et al., 2015b; Trezzi et al., 2016)

Radium (Ra) isotopes (^{223}Ra, ^{224}Ra, ^{226}Ra, ^{228}Ra) and radon (^{222}Rn) have been widely used as tracers to quantify SGD (e.g., Charette et al., 2001; Moore, 2003; Burnett et al., 2006, Burnett et al., 2008; Lee et al., 2012). Ra isotopes and ^{222}Rn, which are continuously produced in geological materials by the decay of their uranium and thorium parents, are appropriate SGD tracers, mainly because they behave conservatively once released to the sea and because they are significantly enriched in SGD fluids relative to seawater (Burnett et al., 2006). The approach used to estimate

SGD flows using Ra isotopes or ^{222}Rn is based on characterizing the flux of Ra/Rn supplied by SGD (J_{Ra} or J_{Rn}) using the Ra/Rn distribution in coastal waters and the Ra/Rn concentration in groundwater inflowing to the sea, the so-called SGD end-member (Ra_{GW} or Rn_{GW}) (Burnett and Dulaiova, 2003; Moore, 1996a).

Most SGD studies have been devoted primarily to estimating the fluxes of Ra and Rn (J_{Ra} or J_{Rn}) (e.g., Kim et al., 2005; Beck et al., 2008; Smoak et al., 2012), whereas the Ra and Rn concentrations in the groundwater end-member have been largely overlooked, even though they are a critical component of the tracer-derived estimates (Cho and Kim, 2016; Burnett et al., 2007; Gonneea et al., 2013, 2008). Ra activities in subterranean estuaries can vary significantly (one or two orders of magnitude) over space and time at a given study site (Ollivier et al., 2007; Beck et al., 2008). Thus, the lack of constraint on this term remains a significant source of uncertainty in Ra-derived SGD estimates (Charette, 2007; Gonneea et al., 2013).

Several factors influence Ra activities in SGD, including the presence of Mn-Fe oxides (Gonneea et al., 2008), the pH of the subterranean estuary (Beck and Cochran, 2013), the ionic strength (Elsinger and Moore, 1980; Webster et al., 1995), the properties of the geological matrix (Swarzenski, 2007) and the residence time within the STE (Rodellas et al., 2017). Among them, the ionic strength of the solution (i.e., its salinity) has long been recognized as the main factor influencing the Ra activities in the SGD end-member, and Ra desorption increases significantly with salinity (Cho and Kim, 2016; Elsinger and Moore, 1980; Webster et al., 1995). As a consequence, Ra activities in SGD may vary substantially depending on the position of the freshwater-saltwater interface within the subterranean estuary. The position of this interface may oscillate, due to variations in the hydraulic gradient of the fresh groundwater (caused by, e.g., recharge and abstraction) and marine driving forces (e.g., tides, wave and storms) (Gonneea et al., 2013; Heiss and Michael, 2014). These temporal oscillations of Ra activity in STEs, along with the spatial heterogeneity of coastal aquifers, make it difficult to characterize the Ra_{GW} end-member, which is needed to provide accurate estimates of SGD (Michael et al., 2011).

Unlike Ra, Rn is an inert gas. Thus, its chemical behavior is not influenced by the physicochemical characteristics of the coastal aquifer (e.g., groundwater salinity, temperature or redox conditions). Radon activities in coastal aquifers are thus primarily controlled by the content of ^{226}Ra in the aquifer solids and dissolved in groundwater (Dulaiova et al., 2008). However, the physical and geochemical processes

occurring in coastal aquifers (e.g., manganese cycling or ionic exchange) can affect the ^{226}Ra distribution, thus driving changes in the ^{222}Rn concentration of groundwater (Dulaiova et al., 2008).

In contrast to many coastal areas of the world, the Mediterranean Sea is characterized by a microtidal regime, with tidal amplitudes commonly lower than 0.2 m. Therefore, tidal forces do not exert a significant water pumping influence in the coastal aquifers there. As a consequence, the location and movement of the salinity interface in subterranean estuaries in the Mediterranean region, as well as in other microtidal sea regions (e.g., the Caribbean Sea or the Baltic Sea), are mainly regulated by hydrogeological factors, such as aquifer properties and the aquifer water budget. Thus, understanding the hydrogeological characteristics (i.e. recharge, discharge, etc.) of coastal aquifers in microtidal regions and their impacts on the Ra and Rn concentrations in groundwater is particularly important for improving tracer-derived estimates of SGD.

This study evaluates the temporal evolution of Ra isotopes and ^{222}Rn concentrations in a Mediterranean microtidal coastal aquifer (Argentona, Catalonia, Eastern Iberian Peninsula) over almost 2 years. During this period, two piezometers (PZ) were continuously monitored to measure variations in groundwater levels, salinity and the Ra and ^{222}Rn concentrations in the groundwater. The aim of this study is to assess hydrogeological dynamics affecting the variability in the concentrations of Ra isotopes and ^{222}Rn in groundwater from this coastal microtidal aquifer. This variability may have critical implications for the quantification of Ra/Rn-derived SGD fluxes and therefore their implications for coastal biogeochemical cycles.

2.1.2 Study area and methods

2.1.2.1 Study area: The Argentona alluvial aquifer and the oceanographic setting

The Argentona alluvial aquifer is located between the Catalan Littoral Mountain Range and the Mediterranean Sea (Barcelona, NW Mediterranean) and extends in the SW-NE direction (Figure 2.2). It has an area of approximately 35 km^2 that is mainly devoted to agricultural uses. The climatology of this region is characterized by Western Mediterranean conditions, and the region experiences high temperatures in summer (mean ~23 °C) and mild temperatures in winter (mean ~10 °C). The annual precipitation of the area ranges from 500 to 800 mm, and is mainly related to

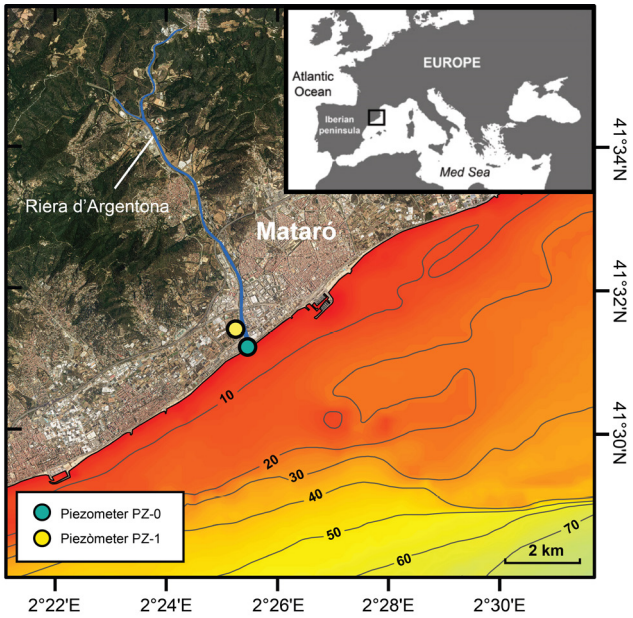

Figure 2.2 Location of the Argentona stream in the NW Mediterranean Sea, including the location of the two monitored piezometers (PZ).

intense and short storms during the fall and spring season. Surface water flows in the Argentona main stream are restricted to the rainy seasons, particularly during major rainfall events (e.g., > 50 mm in a few hours).

The Argentona aquifer is associated with a tectonic fault and sinking blocks where stream valleys have developed. The geology of the alluvial aquifer, which is unconfined, is dominated by detrital Quaternary sediments that are the product of chemical weathering of the granitic basement along fissures (Montoto, 1967). These sediments constitute layers of unconsolidated sands, gravels and clays deposited in an alluvial fan system during basin formation. In the nearshore area, the aquifer is mainly composed of marine sands (Catalan Water Agency, 2010).

A water budget for the aquifer conducted by the Catalan Water Agency (ACA), which used a numerical flow model of the aquifer system and covered the period 2006 – 2009, estimated an aquifer recharge rate between $3.6 \cdot 10^6$ to $5.4 \cdot 10^6$ m^3 y^{-1}. Major outputs from the aquifer include urban, agricultural and industrial extraction ($(1.4 - 1.9) \cdot 10^6$ m^3 y^{-1}) and fresh groundwater discharge to the sea ($(1.2 - 2.4) \cdot 10^6$ m^3 y^{-1}).

2.1.2.2 Groundwater monitoring and sample collection

During a period of 2 years (from January 2013 to December 2014), hydrogeological conditions (groundwater level and salinity), Ra isotopes and ^{222}Rn activities were

monitored in the Argentona coastal aquifer using two entirely screened piezometers. The first piezometer, PZ1, was drilled to a depth of 35 m by the Catalan Water Agency in 2007. It is located 380 m from the shoreline and has a groundwater level approximately 6 − 7 m below the ground surface. The second piezometer, PZ0, which was only monitored for 7 months (May 2014 to December 2014), was drilled approximately 8 m from the shoreline to a depth of 2 m. Three CTD-Diver® data loggers were installed in the piezometers to measure temporal salinity, temperature and groundwater table variations. The first instrument was installed in PZ1 10 m below the ground surface (3 − 4 m below the water level) to evaluate the freshwater conditions (hereinafter referred to as PZ1-S). The second instrument was installed in PZ1 at a depth of 34 m to monitor variations in the mixing zone between the freshwater and saltwater (hereinafter referred to as PZ1-B) (Figure 2.2). The third instrument was installed in PZ0 at a depth of 1.8 m below the ground surface to evaluate conditions in the groundwater close to the coastal seepage face. Variations in air pressure were compensated for using air pressure measurements that were made simultaneously using a Baro-Diver® that was also installed at the top of the PZ1 piezometer.

Groundwater samples were collected at the same depths where the CTDs were installed, samples from PZ1-S (n=15) were collected 10 m below the ground surface, samples from PZ1-B (n=15) were collected 34 m below the ground surface, and samples from PZ0 (n=8) were collected 1.5 m below the ground surface). A submersible pump was used to collect samples with volumes of 60 L (PZ1-S), 25 L (PZ1-B) and 10 L (PZ0) for Ra isotopes. Samples with volumes of 250-mL were collected for ^{222}Rn analyses from PZ1-S and PZ1-B. Radon-222 was not analyzed in PZ0 due to the low water level (less than 20 cm), which increased the exchange of ^{222}Rn with the air and did not permit us to obtain a representative sample. During each sampling survey, salinity and temperature were measured in situ using a YSI-556 handheld probe.

Water samples for Ra isotopes were filtered through MnO_2 impregnated acrylic fibers (hereinafter referred to as Mn fibers) at flow rates < 1 L min^{-1} to quantitatively sorb Ra onto the Mn fibers (Moore and Reid, 1973). For the ^{222}Rn samples, groundwater was pumped directly through a tube that reached to the bottom of each 250-mL bottle. The groundwater was allowed to overflow for several volumes of the sample bottle to reduce Rn losses to the atmosphere.

2.1.2.3 Analytical methods

Once in the laboratory, the Mn fibers containing the Ra isotopes were rinsed with Ra-free water (Sun and Torgersen, 1998), partially dried and placed in a Radium Delayed Coincidence Counter (RaDeCC) to quantify the short-lived Ra isotopes, ^{223}Ra and ^{224}Ra (Garcia-Solsona et al., 2008; Moore and Arnold, 1996). After these measurements, the Mn fibers were ashed (820°C, 16 hours), ground and aged for 3 weeks in counting vials to allow ^{222}Rn to come into secular equilibrium with ^{226}Ra. Samples were measured using a well-type HPGe gamma detector. ^{226}Ra and ^{228}Ra were measured via ^{214}Pb at the 351.9 keV photopeak and ^{228}Ac at the 911 keV photopeak, respectively. ^{222}Rn activities in groundwater samples were determined using a portable ^{222}Rn-in-air alpha spectrometer RAD7 (Durridge Inc.) coupled with a RAD-H_2O attachment that allows the direct determination of ^{222}Rn from 250-mL bottles (Burnett et al., 2001).

2.1.3 Results

2.1.3.1 Hydrogeological features and dynamics

Results of the continuous monitoring of the groundwater table and salinity at PZ1 are shown in Figure 2.3. The fresh groundwater part of the coastal aquifer (PZ1-S) showed relatively constant salinities (~ 0.4) with minimum values of 0.05 occurring during some rainfall events (Figure 2.3.b). In contrast, salinities at the bottom level (PZ1-B) varied significantly during the studied period and ranged from 0.3 to 17 (Figure 2.3.c). Two general patterns in salinity can be identified at the bottom. Salinities were stable during dry periods (sometimes showing minor and constant salinity increases due to reductions in recharge), with maximum values of 15 − 17 (e.g., January − February 2013 and July − September 2013). On the other hand, large fluctuations occur during rainfall events, and sudden decreases in groundwater salinity were followed by gradual increases after rain/recharge episodes. This behavior is exemplified by a particular rainfall event (RFE-8; Figure 2.3.d,e). After the precipitation fell, the groundwater table increased by 60 cm and the salinity at the bottom of PZ1 decreased sharply (over 23 hours) from 13 to 0.2. This fast piezometric response to precipitation can be attributed to the hydrogeological features of the alluvial aquifer, which has a high hydraulic conductivity and a small non-saturated zone in the lower part of the basin (Catalan Water Agency, 2010), but it is also accentuated due to the use of a fully screened piezometer (Shalev et al.,

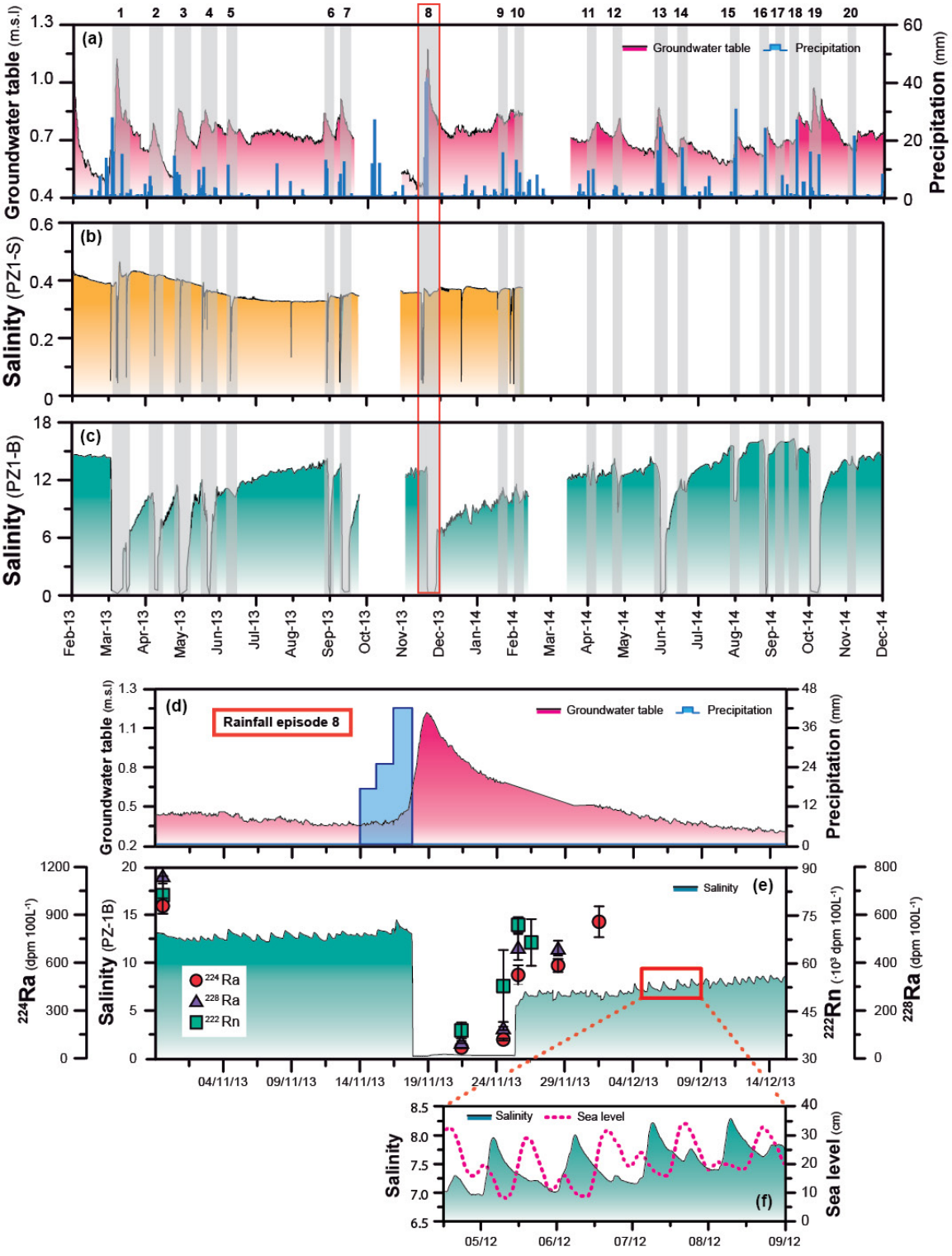

Figure 2.3 Temporal evolution of the hydrogeological conditions and the Ra and Rn activities in the coastal aquifer: (a) Daily cumulative precipitation in the area and measured groundwater table elevations in the coastal aquifer; (b) and (c) groundwater salinities in the shallow (PZ1-S) and bottom (PZ1-B) parts, respectively, of piezometer PZ1; (d) groundwater table elevation and precipitation records from rainfall episode 8 (RFE-8); (e) Variations in Rn and Ra activities and salinity in PZ1-B during RFE-8; (f) Sea level and salinity oscillations in PZ1-B. Vertical gray lines indicate rainfall events (RFEs) that significantly affected groundwater table elevation.

2009). Under stable conditions, an equilibrium exists between the aquifer, which is governed by the laws of groundwater motion, and the entire screened piezometer, which is governed by the hydrostatic law (Rushton, 1980). However, under changing conditions, this equilibrium is broken, and the position of the salinity interface in the piezometer may not correspond to its actual position in the aquifer (Rushton, 1980; Tellam et al., 1986; Carrera et al., 2010). For instance, during heavy rainfall events, the higher hydraulic level of fresh groundwater occurring in the upper part of the entirely screened piezometer pushes the saltwater downward faster than it occurs in the aquifer. As a result, after these episodes, salinity decreased faster in the piezometer than in the aquifer itself.

Rainfall-derived aquifer recharge produced an increase in the hydraulic gradient between the coastal aquifer and the sea, leading to seaward displacement of the salinity interface and a significant decrease in groundwater salinity in the bottom section of the piezometer (Figure 2.3.c,e). Once the infiltration of rainfall water had finished, the hydraulic gradient decreased gradually, resulting in landward displacement of the salinity interface and a consequent increase in groundwater salinity in the bottom section of the piezometer (Figure 2.3.c,e). While the seaward displacement of the salinity interface occurred shortly (a few hours to days) after the precipitation episode, several weeks or even months were needed to recover the salinity values observed prior to the rain event(s). For instance, salinity at PZ1-B decreased from 13 to 0.3 in less than a day (~23 hours) associated with RFE-8, whereas several months (~6 months) were needed to recover the initial salinity of 13 − 15 (Figure 2.3.e).

Unlike aquifers dominated by tidal cycles, the impact of microtides on the hydraulic gradient, and consequently the position of the salinity interface, can be negligible in PZ1. As shown in Figure 2.3.f, the tidal range in the area was on the order of ~20 cm (data compiled from the Barcelona mareograph and obtained from the State Ports Authority; www.puertos.es), a pattern commonly observed in the NW Mediterranean Sea. These small tidal oscillations induced only small variations in the groundwater table and in the groundwater salinities at the bottom of the piezometer (tidally derived groundwater salinity variations of ~1).

Regarding PZ0, the piezometer closest to the shoreline but located in the same aquifer unit, the recorded data on groundwater table and salinity followed a similar pattern as those observed in PZ1 (Figure 2.4). Namely, stable salinities were observed during dry periods, with maximum values of 3 (e.g., May 2014 and August − November

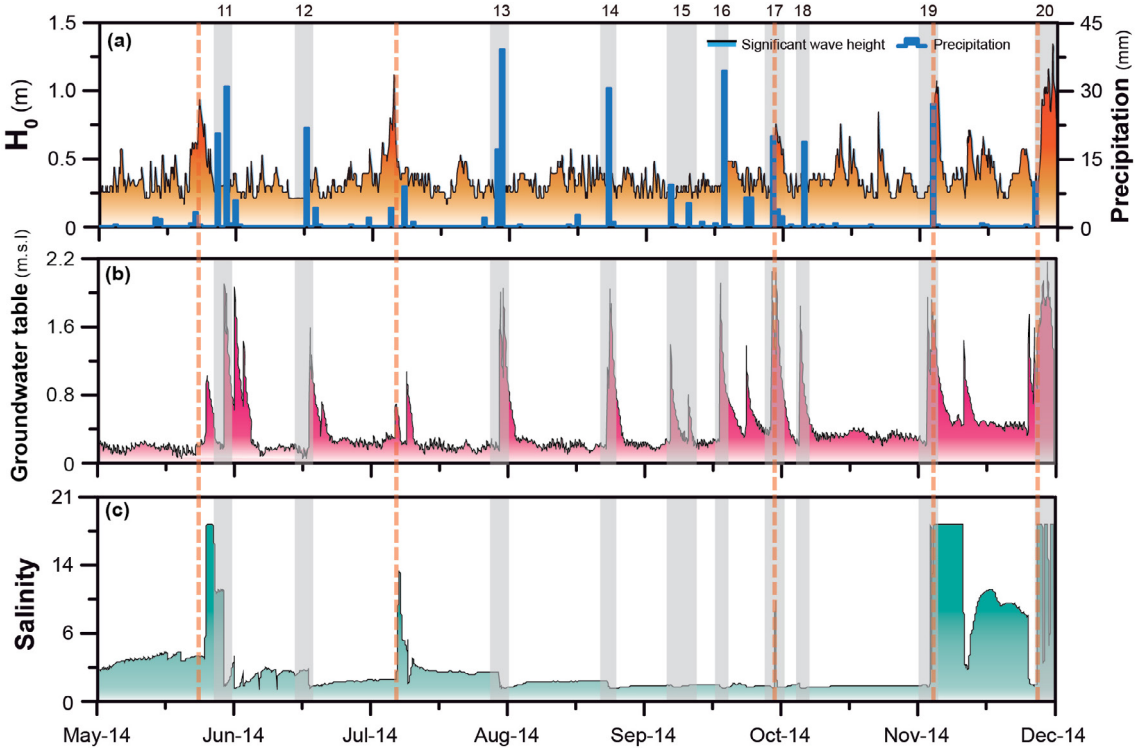

Figure 2.4 Temporal evolution of hydrogeological conditions in PZ0: (a) Significant wave heights of coastal seawater (H_0) derived from the SIMAR dataset (2115138) oceanographic model (State Ports Authority; www.puertos.es); (b) daily cumulative precipitation in the area and measured groundwater table elevations in the coastal aquifer; (c) groundwater salinities in PZ0. Vertical gray lines and orange dotted lines indicate the major rainfall events (RFEs) and eastern storm events, respectively, that significantly affected groundwater table elevation or salinity in PZ0.

2014), and fluctuations of salinity were observed during rainfall events, with salinity decreasing to reach minimum values of 0.1. Although the piezometers, PZ1 and PZ0, are located 380 and 8 m from the shoreline, respectively, CTDs installed in both piezometers registered almost the same variations in the groundwater table and salinity (e.g., RFE-12, 13, 14 and 16), indicating similar responses to recharge/rain events, as expected. However, various significant increases in groundwater salinities in PZ0 (up to salinities higher than 18) that did not correspond with the fluctuations recorded in PZ1 were also observed. These salinity increases in PZ0 coincided with increases in the significant wave height (H_0) in the coastal sea, mainly related to the eastern storms characteristic of the spring and autumn seasons in the northwestern Mediterranean Sea. The increase in the frequency and height of waves at the shoreline modifies the equilibrium of the hydraulic gradient, moving the salinity interface landward and increasing the salinity in PZ0 (Moore and Wilson, 2005). The influence of these storms on PZ0 lasted for short periods (less than 6 days), and PZ0 rapidly recovered the groundwater salinities observed before storm events, due

to the contrary effect of the downward groundwater flow of the aquifer. Given the limited influence of these kind of storm events, the groundwater recharge-discharge cycle appears to be the main driver controlling the position of the salinity interface in the studied NW Mediterranean coastal aquifer.

2.1.3.2 Ra isotopes and ^{222}Rn characterization in groundwater

The activities of Ra isotopes and ^{222}Rn measured in groundwater samples from PZ1-S, PZ1-B and PZ0, together with their corresponding salinities, are presented in Table 2.1. The activities of Ra isotopes in shallow groundwater (PZ1-S) samples showed relatively constant values that ranged from 0.4 to 3.8 dpm 100 L^{-1} for ^{223}Ra, 40 to 90 dpm 100 L^{-1} for ^{224}Ra, 9 to 20 dpm 100 L^{-1} for ^{226}Ra and 60 to 90 dpm 100 L^{-1} for ^{228}Ra. The activity of Ra in PZ1-B presented a larger variability, and these values ranged from 2 to 80 dpm 100 L^{-1} for ^{223}Ra, 70 to 2100 dpm 100 L^{-1} for ^{224}Ra, 30 to 440 dpm 100 L^{-1} for ^{226}Ra and 70 to 1700 dpm 100 L^{-1} for ^{228}Ra. The activities of Ra isotopes were particularly low during rainfall events, when groundwater salinities in the piezometer were minimal, whereas the largest activities were measured during dry periods that corresponded to the highest groundwater salinities. On the other hand, Ra activities in PZ0 showed a similar variability as those seen in PZ1-B, and they ranged from 3 to 10 dpm 100 L^{-1} for ^{223}Ra, 260 to 830 dpm 100 L^{-1} for ^{224}Ra, 40 to 70 dpm 100 L^{-1} for ^{226}Ra and from 200 to 760 dpm 100 L^{-1} for ^{228}Ra. Ra activities in groundwater samples were higher than values commonly found in NW Mediterranean coastal aquifers (e.g., Rodellas et al., 2015a), most likely due to the high radium content of the granitic basement (which are rich in ^{232}Th decay chain radionuclides) and the relatively high salinities of the groundwater in the aquifer that favor radium desorption. The activities of Ra isotopes measured in the two piezometers showed strong positive correlations with salinity (r^2=0.91, 0.97, 0.87 and 0.95 for ^{223}Ra, ^{224}Ra, ^{226}Ra and ^{228}Ra, respectively; $p<0.001$), suggesting that the groundwater sampled in PZ0, which is near the discharge area, has similar characteristics as the groundwater in PZ1 (Figure 2.5.a). Unlike Ra isotopes activities, the activities of ^{222}Rn in groundwater samples reflected relatively constant concentrations in the water samples from PZ1-S and PZ1-B throughout the studied period, with values ranged from $40{\cdot}10^3$ to $120{\cdot}10^3$ dpm 100 L^{-1} (Figure 2.5.b).

A detailed analysis of the rainfall event RFE-8 suggested that Ra activities in groundwater from PZ1-B followed a pattern linked to groundwater recharge cycles

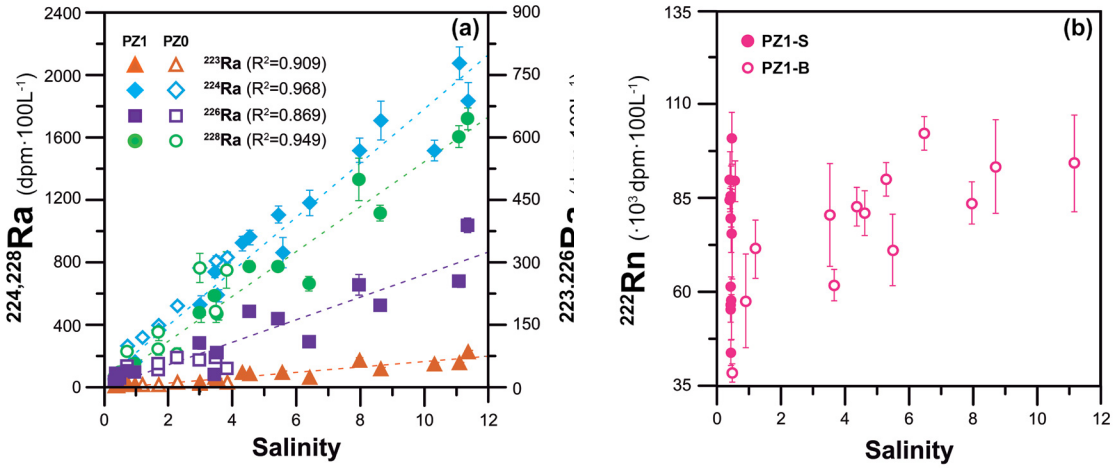

Figure 2.5 Ra isotopes and ^{222}Rn activities vs salinity in groundwater from the Argentona aquifer (PZ1-S, PZ1-B and PZ0). Dashed lines represent the best linear fits to the data.

(Figure 2.3; Table 2.1). Thus, just after the precipitation event, Ra activities diminished by a factor of ~19, ~14, ~6, and ~11 for ^{223}Ra, ^{224}Ra, ^{226}Ra and ^{228}Ra, respectively, in a short period of time (Table 2.1). A few days after the event, and coupled with an increase of groundwater salinity, Ra activities gradually increased toward the activities measured before the rainfall event. The activity of ^{222}Rn followed a similar pattern to those of the Ra isotopes, although it only decreased by a factor of ~2 (from $81{\cdot}10^3$ to $39{\cdot}10^3$ dpm 100 L^{-1}) after the precipitation event.

2.1.4 Discussion

2.1.4.1 Variability in the activity of ^{222}Rn and the activities of Ra isotopes

The activities of Ra isotopes measured in groundwater from PZ1 and PZ0 spanned a wide range. In particular, ^{224}Ra in PZ1-B varied by a factor of 31 during the two monitored years, whereas ^{222}Rn activities were relatively constant throughout the sampling period and varied by less than a factor of 3. This contrasting pattern between Ra isotopes and ^{222}Rn is likely a consequence of differences in their geochemical behavior in the subterranean estuary. Radium desorption is an exchange process that is highly dependent on the ionic strength (salinity) of the solution; it commonly represents the main factor determining the activities of Ra isotopes dissolved in groundwater (Cho and Kim, 2016; Gonneea et al., 2008). Consequently, the activities of Ra isotopes in fresh groundwater from the shallow depths of the subterranean estuary are considerably lower than those in brackish groundwater from greater depths. Ra activities at the salinity interface are likely explained by binary mixing between

	Date	Sal	^{222}Rn	^{223}Ra	^{224}Ra	^{226}Ra	^{228}Ra	^{224}Ra/^{228}Ra AR	^{226}Ra/^{228}Ra AR
			10^3 dpm 100L^{-1}			dpm 100 L^{-1}			
PZ-1S (shallow)									
ARG3-PZ-S	20/12/2012	0.51	90 ± 5	2.0 ± 0.3	85 ± 5	18 ± 1	85 ± 4	43 ± 7	0.21 ± 0.01
ARG4-PZ-S	29/1/2013	0.42	101 ± 7	0.8 ± 0.2	53.± 3	9 ± 1	70 ± 3	70 ± 20	0.13 ± 0.02
ARG6-PZ-S	24/4/2013	0.39	86 ± 8	0.8 ± 0.2	56 ± 4	14 ± 1	65 ± 4	37 ± 20	0.22 ± 0.02
ARG7-PZ-S	28/5/2013	0.36	90 ± 8	0.9 ± 0.1	50 ± 3	10 ± 1	56 ± 1	474 ± 300	0.18 ± 0.02
ARG8-PZ-S	28/6/2013	0.35	85 ± 3	0.4 ± 0.2	44 ± 3	n.a	n.a	222 ± 112	n.a
ARG10-PZ-S	23/9/2013	0.39	80 ± 9	1.5 ± 0.2	66 ± 3	n.a	n.a	47 ± 7	n.a
ARG11-PZ-S	30/10/2013	0.40	76 ± 12	1.2 ± 0.2	68 ± 3	13 ± 1	65 ± 5	56 ± 8	0.20 ± 0.02
ARG12-PZ-S	21/11/2013	0.37	45 ± 3	0.8 ± 0.2	59 ± 3	12 ± 1	62 ± 5	74 ± 20	0.19 ± 0.02
ARG13-PZ-S	24/11/2013	0.37	57 ± 6	0.9 ± 0.2	56 ± 3	n.a	n.a	63 ± 13	n.a
ARG15-PZ-S	26/11/2013	0.39	62 ± 3	0.6 ± 0.2	61 ± 3	n.a	n.a	3 ± 1	n.a
ARG16-PZ-S	28/11/2013	0.39	n.a	0.5 ± 0.2	60 ± 3	13 ± 1	68 ± 5	114 ± 40	n.a
ARG17-PZ-S	1/12/2013	0.39	n.a	0.8 ± 0.2	59 ± 3	n.a	n.a	73 ± 20	0.19 ± 0.02
ARG18-PZ-S	9/12/2013	0.38	n.a	0.4 ± 0.2	56 ± 3	n.a	n.a	139 ± 70	n.a
ARG19-PZ-S	9/2/2014	0.36	n.a	0.5 ± 0.2	43 ± 2	n.a	n.a	85 ± 30	n.a
ARG20-PZ-S	13/4/2014	0.39	n.a	3.8 ± 0.5	62 ± 3	12 ± 1	60 ± 5	16 ± 2	0.20 ± 0.02
PZ-1B (bottom)									
ARG3-PZ-B	20/12/2012	8.68	94 ± 12	42 ± 5	1,704 ± 123	193 ± 11	1,108 ± 50	1.54 ± 0.13	0.17 ± 0.01
ARG4-PZ-B	29/1/2013	6.43	103 ± 5	21 ± 2	1,179 ± 90	106 ± 8	658 ± 47	1.79 ± 0.18	0.16 ± 0.02
ARG6-PZ-B	24/4/2013	11.14	95 ± 13	55 ± 4	2,074 ± 108	251 ± 11	1,596 ± 68	1.30 ± 0.09	0.16 ± 0.01
ARG7-PZ-B	28/5/2013	3.47	81 ± 14	20 ± 2	737 ± 40	26 ± 2	574 ± 27	1.28 ± 0.09	0.05 ± 0.01
ARG8-PZ-B	28/6/2013	5.46	92 ± 4	22 ± 1	1,102 ± 50	161 ± 7	762 ± 30	1.45 ± 0.09	0.21 ± 0.01
ARG10-PZ-B	23/9/2013	4.32	83 ± 5	33 ± 2	917 ± 50	n.a	n.a	n.a	n.a
ARG11-PZ-B	30/10/2013	4.55	81 ± 6	30 ± 2	956 ± 50	178 ± 8	764 ± 30	1.25 ± 0.08	0.23 ± 0.01
ARG12-PZ-B	21/11/2013	0.39	39 ± 2	1.6 ± 0.5	67 ± 4	29 ± 6	68 ± 5	0.99 ± 0.08	0.42 ± 0.09
ARG13-PZ-B	24/11/2013	0.74	53 ± 11	3.6 ± 0.5	118 ± 7	34 ± 2	125 ± 7	0.94 ± 0.08	0.28 ± 0.02
ARG15-PZ-B	26/11/2013	0.98	72 ± 2	3 ± 1	160 ± 8	33 ± 2	139 ± 7	1.15 ± 0.08	0.24 ± 0.02
ARG16-PZ-B	28/11/2013	3.57	72 ± 2	17 ± 2	582 ± 40	79 ± 6	461 ± 30	1.26 ±- 0.12	0.17 ± 0.02
ARG17-PZ-B	1/12/2013	5.60	66 ± 7	33 ± 4	856 ± 100	n.a	n.a	n.a	n.a
ARG18-PZ-B	9/12/2013	8.00	n.a	61 ± 7	1,516 ± 80	244 ± 30	1,344 ± 137	1.14 ± 0.13	0.18 ± 0.03
ARG19-PZ-B	9/2/2014	10.36	n.a	23 ± 2	1,513 ± 70	n.a	n.a	n.a	n.a
ARG20-PZ-B	13/4/2014	11.42	n.a	82 ± 6	1,834 ± 121	440 ± 18	1,715 ± 70	1.07 ± 0.08	0.22 ± 0.01
PZ-0									
ARG21-PM0	24/4/2014	0.75	n.a	5 ± 0.4	257 ± 11	47 ± 4	222 ± 12	1.16 ± 0.08	0.21 ± 0.02
ARG22-PM0	30/4/2014	2.99	n.a	9 ± 2	762 ± 33	62 ± 7	755 ± 95	1.01 ± 0.13	0.08 ± 0.01
ARG23-PM0	13/5/2014	3.85	n.a	9 ± 2	828 ± 35	40 ± 7	741 ± 117	1.12 ± 0.18	0.05 ± 0.01
ARG24-PM0	16/5/2014	3.51	n.a	12 ± 2	802 ± 37	67 ± 4	480 ± 67	1.67 ± 0.25	0.14 ± 0.02
ARG25-PM0	3/6/2014	1.20	n.a	3 ± 1	313 ± 15	n.a	n.a	n.a	n.a
ARG26-PM0	7/6/2014	1.70	n.a	4 ± 1	392 ± 19	38 ± 6	232 ± 34	1.69 ± 0.26	0.16 ± 0.04
ARG27-PM0	11/6/2014	1.70	n.a	4 ± 1	357 ± 16	55 ± 11	343 ± 51	1.04 ± 0.16	0.15 ± 0.04
ARG28-PM0	26/6/2014	2.30	n.a	8 ± 2	517 ± 23	67 ± 12	200 ± 44	2.59 ± 0.58	0.34 ± 0,10

n.a: not analyzed

Table 2.1 Salinity, Ra isotopes and ^{222}Rn activities and Activity Ratios (ARs) in the shallow and bottom parts of piezometer PZ1 (n.a: not analyzed).

low-Ra, low-salinity groundwater and high-Ra, high-salinity groundwater. Indeed, this behavior explains the strong linear correlations between the concentrations of Ra isotopes and groundwater salinities observed over the entire period of the study (Figure 2.5.a). Unlike Ra isotopes, groundwater salinity has little influence on the behavior of ^{222}Rn in the aquifer because it is a noble gas. Moreover, ^{222}Rn supported by ^{226}Ra dissolved in groundwater usually represents a minor fraction of the total ^{222}Rn activity in groundwater. Therefore, similar ^{222}Rn activities are expected in fresh, brackish and salty groundwater, thus explaining the lack of significant correlations between ^{222}Rn activities and salinity in groundwater from the studied site (Figure 2.5.b). However, it should be noted that, after rainfall events, ^{222}Rn activities decreased considerably, together with salinity. This coupled ^{222}Rn-salinity decrease is attributed to dilution that is due to the vertical infiltration of rainwater into the highly permeable coastal aquifer, since rainwater has a salinity close to 0 and contains negligible amounts of ^{222}Rn. After the rainwater had interacted with the geological matrix, the activity of ^{222}Rn in the meteoric fresh water started to increase, due to its production within the aquifer solids. Concentrations in equilibrium with the aquifer matrix were achieved within 15 − 20 days after rainwater infiltration into the aquifer.

2.1.4.2 Temporal variability of the salinity interface: Implications for Ra- and Rn-derived SGD estimates

The position and dynamics of the salinity interface are influenced to a large degree by multiple forcing mechanisms, which include marine (e.g., wave setup and swash infiltration, as well as tidal pumping) and terrestrial drivers (e.g., recharge patterns) (Li et al., 2008; Henderson et al., 2010; Santos et al., 2012; Abarca et al., 2013). Whereas tides are physical forces that are relevant for determining freshwater-seawater mixing in most coastal areas (Kim and Hwang, 2002; Michael et al., 2003; Charette, 2007; Bokuniewicz et al., 2015), they play a minor role in microtidal environments such as the Mediterranean Sea, the Baltic Sea and the Caribbean Sea (Szymczycha et al., 2012; Gonneea et al., 2014; Rodellas et al., 2014;). In such systems, the dynamics of the salinity interface are mainly governed by the inland hydraulic gradient, which mainly reflects the terrestrial groundwater recharge rate (Dausman and Langevin, 2005). Microtidal coastal aquifers are thus highly influenced by precipitation regimes, and they become highly dynamic systems when precipitation events are temporally variable. This pattern is commonly observed in the Mediterranean basin, where 4 − 6 short (lasting hours to a few days) and intense (a maximum precipitation rate

of 40 mm day^{-1} occurred during the studied period, but it can be much higher) rainfall events represent more than 70% of the annual precipitation (e.g., RFE-1, 8, 13 and 15, Figure 2.3) (Gasith and Resh, 1999). According to the change in hydraulic gradient observed in PZ0 (the closest to the sea) over a period of nearly 8 months, it can be estimated that 50% of the discharge is produced during and/or within a few days after rain events. Thus, short and intense rainfall events are likely to produce the highest rates of fresh SGD to the coastal sea, which would account for a significant proportion of the freshwater that seeps into the sea yearly. For the rest of the year, fresh SGD flows are expected to be significantly lower and more constant. Thus, estimating SGD fluxes in microtidal systems during periods of intense precipitation are particularly relevant from both a hydrogeological and a biogeochemical perspective.

The quantification of SGD flows to the coastal sea using Ra isotopes and ^{222}Rn requires accurately characterizing their activities in groundwater discharging to the coastal sea (i.e., the SGD end-member). Indeed, Ra- and ^{222}Rn-derived SGD fluxes can only be resolved at levels where the tracer concentration in the end-member is well constrained. Thus, the selection of an appropriate end-member is commonly the main source of uncertainty in final SGD estimates (Cho and Kim, 2016; Burnett et al., 2007; Dulaiova et al., 2008; Garcia-Orellana et al., 2010; Gonneea et al., 2013). Given that Ra isotopes are highly influenced by the ionic strength of the dissolved phase, the process of freshwater-seawater mixing dynamics are key processes in understanding the distribution of Ra in a coastal aquifer and constraining the Ra concentration in the SGD end-member (Charette et al., 2001; Gonneea et al., 2013; Michael et al., 2011). Indeed, several studies have reported that the activities of Ra isotopes in the SGD end-member vary over a wide range (up to orders of magnitude) both in space and time, and are often linked to changes in the ionic strength of the dissolved phase (Cho and Kim, 2016). Thus, accurately evaluating the complex and dynamic mixing of fresh groundwater with seawater (i.e., the position of the salinity interface) becomes critical for obtaining reliable Ra-derived SGD estimates.

In highly dynamic microtidal systems, achieving an appropriate understanding of the hydrodynamics of coastal aquifers requires significant monitoring and characterization efforts that are often unavailable when SGD studies are conducted. To overcome this limited hydrogeological understanding, studies that use Ra isotopes to quantify SGD commonly rely on collecting a relatively large number of samples, as well as using

different approaches to characterize the SGD end-member (potential approaches include, e.g., averaging the Ra activities from all the samples collected (Gonneea et al., 2014), taking the maximum measured Ra activities to obtain conservative estimates (Moore, 1996b), or using ranges of Ra activities covering the samples collected (Kim et al., 2005). Whereas these approaches may work in many of the tidal systems studied, using them in coastal aquifers characterized by highly dynamic freshwater-seawater mixing zones (with large salinity and thus large Ra variations) may introduce large uncertainties into the final SGD quantification. Constraining Ra activities in the SGD end-member during (or just after) intense rainfall events may be particularly challenging, given the large temporal variations in salinity and Ra in coastal groundwater, making it difficult to obtain reliable SGD estimates. As detailed above, it should be noted that inputs of fresh groundwater to coastal seas are expected to be much higher during these rainfall periods, and thus, the SGD evaluations during these periods have a major hydrological and biogeochemical interest. Conversely, Ra activities in the SGD end-member can be more easily constrained during dry periods because they are associated with reduced variability in coastal groundwater, thus allowing appropriate estimates of Ra-derived SGD fluxes to be made for the rest of the year.

Unlike Ra isotopes, the activity of ^{222}Rn in coastal groundwater appears to be relatively constant throughout the year due to the relatively small influence of groundwater salinity on ^{222}Rn behavior, even during intense rainy events (^{222}Rn activities only varied by a factor 2 during these events). These small variations allow us to better constraint the activity of ^{222}Rn in the SGD end-member and, thus, better estimate SGD flows during rainy periods. This observed pattern suggests that ^{222}Rn may be a more appropriate SGD tracer than Ra isotopes in systems with highly dynamic salinity interfaces, particularly during the wet season, when groundwater salinities (and thus Ra activities) may change significantly over short temporal scales. However, whereas the Rn end-member can be relatively well constrained, Rn-derived SGD estimates are highly sensitive to Rn mixing losses and especially the loss of Rn to the atmosphere by degassing. These two loss terms are difficult to determine, particularly under conditions with strong winds and high waves, which often occur concurrently with eastern storm events.

2.1.5 Conclusions

Understanding the behavior of tracers used to determine submarine groundwater discharge (SGD) fluxes is crucial for accurately quantifying groundwater- and chemical-driven fluxes to the ocean in order to better understand coastal biogeochemical cycles. The results obtained in this work reveal that activities of Ra isotopes, which are commonly used tracers to quantify SGD, show a large variability in microtidal coastal groundwater systems throughout the year and particularly during intense rainfall events (e.g., activity changes by a factor of ~19, ~14, ~6, and ~11 for ^{223}Ra, ^{224}Ra, ^{226}Ra and ^{228}Ra during a particular rainfall event, RFE-8). This large variability, which is linked to the displacement of the salinity interface seawards, complicates the accurate estimation of the Ra-SGD end-member, resulting in Ra-derived SGD estimates with large uncertainties. In contrast, ^{222}Rn activities present only minor variations (by a factor of 3), as a consequence of the relatively small influence of groundwater salinity on ^{222}Rn activities. In microtidal systems, high SGD-driven fluxes to the sea of both freshwater and dissolved chemical compounds are expected to occur during the rainy season and/or intense rainfall events. Thus, scientific efforts should be particularly directed toward understanding SGD fluxes during this season, when the influence of SGD on hydrological budgets is expected to be significant. The observed differences between the rainy season and the dry period indicate that appropriate SGD quantification over longer (monthly or yearly) time scales cannot be carried out properly without considering the temporal variability in Ra activities.

In addition to the difficulties in estimating SGD flows during rainfall events (which are mainly due to the difficulty of characterizing the SGD end-member), the extreme variability in the concentrations of chemical compounds (e.g., nutrients, trace metals, contaminants, and other species) in the groundwater poses an additional challenge in constraining a representative groundwater end-member. The fluxes of dissolved compounds transported by SGD have usually been calculated by multiplying the SGD flux derived using Ra isotopes or Rn by the concentration of the chemical compounds in the inflowing SGD. As in the case of the Ra end-member, it is particularly critical to identify a representative concentration of the studied dissolved chemical compound in the discharging groundwater during intense rainfall events. A poor understanding of the behavior of dissolved chemicals in the coastal aquifer during rainfall events may lead to large uncertainties in SGD-driven chemical fluxes. Since the SGD-driven fluxes during the wet periods may account for a significant

fraction of the chemical fluxes to the coastal areas, it is expected that the impact of SGD on coastal biogeochemical cycles is particularly relevant during these events. Characterizing the behavior of Ra/Rn and dissolved chemical compounds within subterranean estuaries during rainfall events in microtidal systems remains a challenge, which must be considered in future studies of SGD-driven nutrient fluxes to coastal areas in order to understand the relative impact of SGD on coastal biogeochemical cycles.

Acknowledgments This work was funded by projects CGL2013-48869-C2-1 and CGL2013-48869-C2-2-R of the Spanish Government. M.C.D acknowledges financial support from the Ministerio de Economía y Competitividad (PhD fellowship, A-2014-9185) through the NUREIEV project (CTM2013-44598-R) coordinated by GRC Geociències Marines of the Departament de Dinàmica de la Terra i de l'Oceà (Universitat de Barcelona). The authors wish to thank the Generalitat de Catalunya for its support of MERS (2014 SGR-1356) and Agència Catalana de l'Aigua (ACA). V.R. also acknowledges financial support from the European Union's FP7 program (Marie Curie Actions PCOFUND-GA-2013-609102) through the PRESTIGE program coordinated by Campus France. This study is a contribution to the ANR @RAction chair (ANR-14-ACHN-0007-01) and Labex OT-Med (ANR-11-LABEX-0061), which was funded by the "Investissements d'Avenir" program through the A*MIDEX project (ANR-11-IDEX-0001-02) of the French National Research Agency (ANR).

2.1.6 References

Abarca, E., Karam, H., Hemond, H.F., Harvey, C.F., 2013. Transient groundwater dynamics in a coastal aquifer: The effects of tides, the lunar cycle, and the beach profile. Water Resour. Res. 49, 2473–2488. https://doi.org/10.1002/wrcr.20075

Beck, A.J., Cochran, M.A., 2013. Controls on solid-solution partitioning of radium in saturated marine sands. Mar. Chem. 156, 38–48. https://doi.org/10.1016/j.marchem.2013.01.008

Beck, A.J., Rapaglia, J.P., Cochran, J.K., Bokuniewicz, H.J., Yang, S., 2008. Submarine groundwater discharge to Great South Bay, NY, estimated using Ra isotopes. Mar. Chem. 109, 279–291. https://doi.org/10.1016/j.marchem.2007.07.011

Bokuniewicz, H., Cochran, J.K., Garcia-Orellana, J., Rodellas, V., Daniel, J.W., Heilbrun, C., 2015. Intertidal percolation through beach sands as a source of ^{224,223}Ra to Long Island Sound, New York, and Connecticut, United States. J. Mar. Res. 73, 123–140. https://doi.org/10.1357/002224015816665570

Burnett, W.C., Bokuniewicz, H., Huettel, M., Moore, W., Taniguchi, M., 2003. Groundwater and pore water inpunts to the coastal zone. Biogeochemistry 66, 3–33. https://doi.org/10.1023/B:BIOG.0000006066.21240.53

Burnett, W.C., Dulaiova, H., 2003. Estimating the dynamics of groundwater input into the coastal zone via continuous radon-222 measurements. J. Environ. Radioact. 69, 21–35. https://doi.org/10.1016/S0265-931X(03)00084-5

Burnett, W.C., Peterson, R., Moore, W.S., de Oliveira, J., 2008. Radon and radium isotopes as tracers of submarine groundwater discharge – Results from the Ubatuba, Brazil SGD assessment intercomparison. Estuar. Coast. Shelf Sci. 76, 501–511. https://doi.org/10.1016/j.ecss.2007.07.027

Burnett, W.C., Taniguchi, M., Oberdorfer, J., 2001. Measurement and significance of the direct discharge of groundwater into the coastal zone. J. Sea Res. 46, 109–116. https://doi.org/10.1016/S1385-1101(01)00075-2

Burnett, W.C., Wattayakorn, G., Taniguchi, M., Dulaiova, H., Sojisuporn, P., Rungsupa, S., Ishitobi, T., 2007. Groundwater-derived nutrient inputs to the Upper Gulf of Thailand. Cont. Shelf Res. 27, 176–190. https://doi.org/10.1016/j.csr.2006.09.006

Burnett, W.C., Aggarwal, P.K., Aureli, A., Bokuniewicz, H., Cable, J.E., Charette, M.A. a, Kontar, E., Krupa, S., Kulkarni, K.M., Loveless, A., Moore, W.S., Oberdorfer, J.A. a, Oliveira, J., Ozyurt, N., Povinec, P., Privitera, A.M.G., Rajar, R., Ramessur, R.T., Scholten, J., Stieglitz, T., Taniguchi, M., Turner, J.V., 2006. Quantifying submarine groundwater discharge in the coastal zone via multiple methods. Sci. Total Environ. 367, 498–543. https://doi.org/10.1016/j.scitotenv.2006.05.009

Carrera, J., Hidalgo, J.J., Slooten, L.J., Vazquez-Sune, E., 2010. Computational and conceptual issues in the calibration of seawater intrusion models. Hydrogeol. J. 18, 131–145. https://doi.org/10.1007/s10040-009-0524-1

Catalan Water Agency, 2010. Model numèric de l'aqüífer al·luvial de la riera d'argentona.

Charette, M. a., Buesseler, K.O., Andrews, J.E., 2001. Utility of radium isotopes for evaluating the input and transport of groundwater-derived nitrogen to a Cape Cod estuary. Limnol. Oceanogr. 46, 465–470. https://doi.org/10.4319/lo.2001.46.2.0465

Charette, M.A., 2007. Hydrologic forcing of submarine groundwater discharge: Insight from a seasonal study of radium isotopes in a groundwater-dominated

salt marsh estuary. Limnol. Oceanogr. 52, 230–239. https://doi.org/10.4319/lo.2007.52.1.0230

Cho, H.-M., Kim, G., 2016. Determining groundwater Ra end-member values for the estimation of the magnitude of submarine groundwater discharge using Ra isotope tracers. Geophys. Res. Lett. 43, 3865–3871. https://doi.org/10.1002/2016GL068805

Dausman, A., Langevin, C.D., 2005. Movement of the saltwater interface in the surficial aquifer system in response to hydrologic stresses and water-management practices, Broward County, Florida. US Department of the Interior, US Geological Survey, 2005.

Dulaiova, H., Gonneea, M.E., Henderson, P.B., Charette, M. a., 2008. Geochemical and physical sources of radon variation in a subterranean estuary - Implications for groundwater radon activities in submarine groundwater discharge studies. Mar. Chem. 110, 120–127. https://doi.org/10.1016/j.marchem.2008.02.011

Elsinger, R.J., Moore, W.S., 1980. ^{226}Ra behavior in the Pee Dee River-Winyah Bay estuary. Earth Planet. Sci. Lett. 48, 239–249. https://doi.org/10.1016/0012-821X(80)90187-9

Garcia-Orellana, J., Cochran, J.K., Bokuniewicz, H., Yang, S., Beck, a J., 2010. Time-series sampling of ^{223}Ra and ^{224}Ra at the inlet to Great South Bay (New York): A strategy for characterizing the dominant terms in the Ra budget of the bay. J. Environ. Radioact. 101, 582–588. https://doi.org/10.1016/j.jenvrad.2009.12.005

Garcia-Solsona, E., Garcia-Orellana, J., Masqué, P., Dulaiova, H., 2008. Uncertainties associated with ^{223}Ra and ^{224}Ra measurements in water via a Delayed Coincidence Counter (RaDeCC). Mar. Chem. 109, 198–219. https://doi.org/10.1016/j.marchem.2007.11.006

Gasith, A., Resh, V.H., 1999. Stream in Mediterranean climate regions: Abiotic Influences and Biotic Responses to Predictable Seasonal Events. Annu. Rev. Ecol. Syst. 30, 51–81. https://doi.org/10.1146/annurev.ecolsys.30.1.51

Gonneea, M.E., Charette, M.A., Liu, Q., Herrera-Silveira, J.A., Morales-Ojeda, S.M., 2014. Trace element geochemistry of groundwater in a karst subterranean estuary (Yucatan Peninsula, Mexico). Geochim. Cosmochim. Acta 132, 31–49. https://doi.org/10.1016/j.gca.2014.01.037

Gonneea, M.E., Morris, P.J., Dulaiova, H., Charette, M. a., 2008. New perspectives on radium behavior within a subterranean estuary. Mar. Chem. 109, 250–267. https://doi.org/10.1016/j.marchem.2007.12.002

Gonneea, M.E., Mulligan, A.E., Charette, M.A., 2013. Seasonal cycles in radium and barium within a subterranean estuary: Implications for groundwater derived chemical fluxes to surface waters. Geochim. Cosmochim. Acta 119, 164–177. https://doi.org/10.1016/j.gca.2013.05.034

Heiss, J.W., Michael, H.A., 2014. Saltwater-freshwater mixing dynamics in a sandy beach aquifer over tidal, spring-neap, and seasonal cycles. Water Resour. Res. 50, 6747-6766. https://doi.org/10.1002/2014WR015574

Henderson, R.D., Day-Lewis, F.D., Abarca, E., Harvey, C.F., Karam, H.N., Liu, L., Lane, J.W.J., 2010. Marine electrical resistivity imaging of submarine groundwater discharge: sensitivity analysis and application in Waquoit Bay, Massachusetts, USA. Hydrogeol. J. 18, 173–185. https://doi.org/10.1007/s10040-009-0498-z

Johnson, A.G., Glenn, C.R., Burnett, W.C., Peterson, R.N., Lucey, P.G., 2008. Aerial infrared imaging reveals large nutrient-rich groundwater inputs to the ocean. Geophys. Res. Lett. 35, L15606. https://doi.org/10.1029/2008GL034574

Kim, G., Hwang, D.-W., 2002. Tidal pumping of groundwater into the coastal ocean revealed from submarine ^{222}Rn and CH_4 monitoring. Geophys. Res. Lett. 29, 23-1-23–4. https://doi.org/10.1029/2002GL015093

Kim, G., Lee, K.-K., Park, K.-S., Hwang, D.-W., Yang, Han-Soeb, Y., 2003. Large submarine groundwater discharge (SGD) from a volcanic island. Geophys. Res. Lett. 30, 2098. https://doi.org/10.1029/2003GL018378

Kim, G., Yun, S.T., Yang, H.-S., Ryu, J.-W., Burnett, W.C., Dulaiova, H., Sholkovitz, E., Moore, W.S., Charette, M. a., Bokuniewicz, H.J., Chanton, J.P., Yun, S.T., Yang, H., Ryu, J.W., 2005. Submarine groundwater discharge (SGD) into the Yellow Sea revealed by ^{228}Ra and ^{226}Ra isotopes: Implications for global silicate fluxes. Earth Planet. Sci. Lett. 237, 156–166. https://doi.org/10.1016/j.epsl.2005.06.011

Lee, C.M., Jiao, J.J., Luo, X., Moore, W.S., 2012. Estimation of submarine groundwater discharge and associated nutrient fluxes in Tolo Harbour, Hong Kong. Sci. Total Environ. 433, 427–433. https://doi.org/10.1016/j.scitotenv.2012.06.073

Li, H., Boufadel, M.C., Weaver, J.W., 2008. Tide-induced seawater-groundwater circulation in shallow beach aquifers. J. Hydrol. 352, 211–224. https://doi.org/10.1016/j.jhydrol.2008.01.013

Michael, H.A., Charette, M.A., Harvey, C.F., 2011. Patterns and variability of groundwater flow and radium activity at the coast: A case study from Waquoit

Bay, Massachusetts. Mar. Chem. 127, 100–114. https://doi.org/10.1016/j.marchem.2011.08.001

Michael, H.A., Lubetsky, J.S., Harvey, C.F., 2003. Characterizing submarine groundwater discharge: A seepage meter study in Waquoit Bay, Massachusetts. Geophys. Res. Lett. 30. https://doi.org/10.1029/2002GL016000

Montoto, M., 1967. Estudio petrológico y petrogenético de las rocas graníticas de la Cadena Litoral Catalana. 800.

Moore, W.S., 2003. Sources and fluxes of submarine groundwater discharge delineated by radium isotopes. Biogeochemistry 66, 75–93. https://doi.org/10.1023/B:BIOG.0000006065.77764.a0

Moore, W.S., 1999. The subterranean estuary: a reaction zone of ground water and sea water. Mar. Chem. 65, 111–125. https://doi.org/10.1016/S0304-4203(99)00014-6

Moore, W.S., 1996a. Using the radium quartet for evaluating groundwater input and water exchange in salt marshes. Geochim. Cosmochim. Acta 60, 4645–4652. https://doi.org/10.1016/S0016-7037(96)00289-X

Moore, W.S., 1996b. Large groundwater inputs to coastal waters revealed by 226Ra enrichments. Nature 380, 612–614. https://doi.org/10.1038/380612a0

Moore, W.S., Arnold, R., 1996. Measurement of ^{223}Ra and ^{224}Ra in coastal waters using a delayed coincidence counter. J. Geophys. Res. 101, 1321–1329. https://doi.org/10.1029/95jc03139

Moore, W.S., Reid, D.F., 1973. Extraction of radium from natural waters using manganese-impregnated acrylic fibers. J. Geophys. Res. 78, 8880. https://doi.org/10.1029/JC078i036p08880

Moore, W.S., Wilson, A.M., 2005. Advective flow through the upper continental shelf driven by storms, buoyancy, and submarine groundwater discharge. Earth Planet. Sci. Lett. 235, 564–576. https://doi.org/10.1016/j.epsl.2005.04.043

Ollivier, P., Claude, C., Radakovitch, O., Hamelin, B., 2007. TIMS measurements of ^{226}Ra and ^{228}Ra in the Gulf of Lion, an attempt to quantify submarine groundwater discharge. Mar. Chem. 109, 337–354. https://doi.org/10.1016/j.marchem.2007.08.006

Pavlidou, A., Papadopoulos, V.P., Hatzianestis, I., Simboura, N., Patiris, D., Tsabaris, C., 2014. Chemical inputs from a karstic submarine groundwater discharge (SGD) into an oligotrophic Mediterranean coastal area. Sci. Total Environ. 488, 1–13. https://doi.org/10.1016/j.scitotenv.2014.04.056

Rodellas, V., Garcia-Orellana, J., Masqué, P., Font-Muñoz, J.S.J.S., 2015. The influence of sediment sources on radium-derived estimates of Submarine Groundwater Discharge. Mar. Chem. 171, 107–117. https://doi.org/10.1016/j.marchem.2015.02.010

Rodellas, V., Garcia-Orellana, J., Tovar-Sánchez, A., Basterretxea, G., López-Garcia, J.M.J.M., Sánchez-Quiles, D., Garcia-Solsona, E., Masqué, P., 2014. Submarine groundwater discharge as a source of nutrients and trace metals in a Mediterranean bay (Palma Beach, Balearic Islands). Mar. Chem. 160, 56–66. https://doi.org/10.1016/j.marchem.2014.01.007

Rodellas, V., Garcia-Orellana, J., Trezzi, G., Masqué, P., Stieglitz, T.C., Bokuniewicz, H., Cochran, J.K., Berdalet, E., 2017. Using the radium quartet to quantify submarine groundwater discharge and porewater exchange. Geochim. Cosmochim. Acta 196, 58–73. https://doi.org/http://dx.doi.org/10.1016/j.gca.2016.09.016

Rushton, K.R., 1980. Differing positions of saline interfaces in aquifers and observation boreholes. J. Hydrol. 48, 185–189. https://doi.org/10.1016/0022-1694(80)90074-8

Sadat-Noori, M., Santos, I.R., Tait, D.R., Maher, D.T., 2016. Fresh meteoric versus recirculated saline groundwater nutrient inputs into a subtropical estuary. Sci. Total Environ. 566, 1440–1453. https://doi.org/10.1016/j.scitotenv.2016.06.008

Santos, I.R., Eyre, B.D., Huettel, M., 2012. The driving forces of porewater and groundwater flow in permeable coastal sediments: A review. Estuar. Coast. Shelf Sci. 98, 1–15. https://doi.org/10.1016/j.ecss.2011.10.024

Shalev, E., Lazar, A., Wollman, S., Kington, S., Yechieli, Y., Gvirtzman, H., 2009. Biased monitoring of fresh water-salt water mixing zone in coastal aquifers. Ground Water 47, 49–56. https://doi.org/10.1111/j.1745-6584.2008.00502.x

Smoak, J.M., Sanders, C.J., Patchineelam, S.R., Moore, W.S., 2012. Radium mass balance and submarine groundwater discharge in Sepetiba Bay, Rio de Janeiro State, Brazil. J. South Am. Earth Sci. 39, 44–51. https://doi.org/10.1016/j.jsames.2012.07.004

Sun, Y., Torgersen, T., 1998. The effects of water content and Mn-fiber surface conditions on ^{224}Ra measurement by ^{220}Rn emanation. Mar. Chem. 62, 299–306. https://doi.org/10.1016/S0304-4203(98)00019-X

Swarzenski, P.W., 2007. U/Th Series Radionuclides as Coastal Groundwater Tracers. Chem. Rev. 107, 663–674. https://doi.org/10.1021/cr0503761

Szymczycha, B., Vogler, S., Pempkowiak, J., 2012. Nutrient fluxes via submarine groundwater discharge to the Bay of Puck, southern Baltic Sea. Sci. Total Environ. 438, 86–93. https://doi.org/10.1016/j.scitotenv.2012.08.058

Tellam, J.H., Lloyd, J.W., Walters, M., 1986. The morphology of a saline groundwater body: Its investigation, description and possible explanation. J. Hydrol. 83, 1–21. https://doi.org/10.1016/0022-1694(86)90179-4

Tovar-Sánchez, A., Basterretxea, G., Rodellas, V., Sánchez-Quiles, D., García-Orellana, J., Masqué, P., Jordi, A., López, J.M., Garcia-Solsona, E., 2014. Contribution of Groundwater Discharge to the Coastal Dissolved Nutrients and Trace Metal Concentrations in Majorca Island: Karstic vs Detrital Systems. Environ. Sci. Technol. 48, 11819–11827. https://doi.org/10.1021/es502958t

Trezzi, G., Garcia-Orellana, J., Rodellas, V., Santos-Echeandia, J., Tovar-Sánchez, A., Garcia-Solsona, E., Masqué, P., 2016. Submarine groundwater discharge: A significant source of dissolved trace metals to the North Western Mediterranean Sea. Mar. Chem. 186, 90–100. https://doi.org/10.1016/j.marchem.2016.08.004

Webster, I.T., Hancock, G.J., Murray, A.S., 1995. Modelling the effect of salinity on radium desorption from sediments. Geochim. Cosmochim. Acta 59, 2469–2476. https://doi.org/10.1016/0016-7037(95)00141-7

2.2 Calibrating high resolution XRF core scanner data to obtain absolute metal concentrations in highly polluted marine deposits after two case studies off Portmán Bay and Barcelona, Spain

Marc Cerdà-Domènech[a], Jaime Frigola[a], Anna Sanchez-Vidal[a], Miquel Canals[a]

[(a)] GRC Geociències Marines, Departament de Dinàmica de la Terra i de l'Oceà, Universitat de Barcelona, 08028 Barcelona, Spain.

Science of the Total Environment 717 (2020) 134778
https://doi.org/10.1016/j.scitotenv.2019.134778

Keywords: XRF core scanner, calibration, trace metals, contaminated sediment, sediment quality guidelines

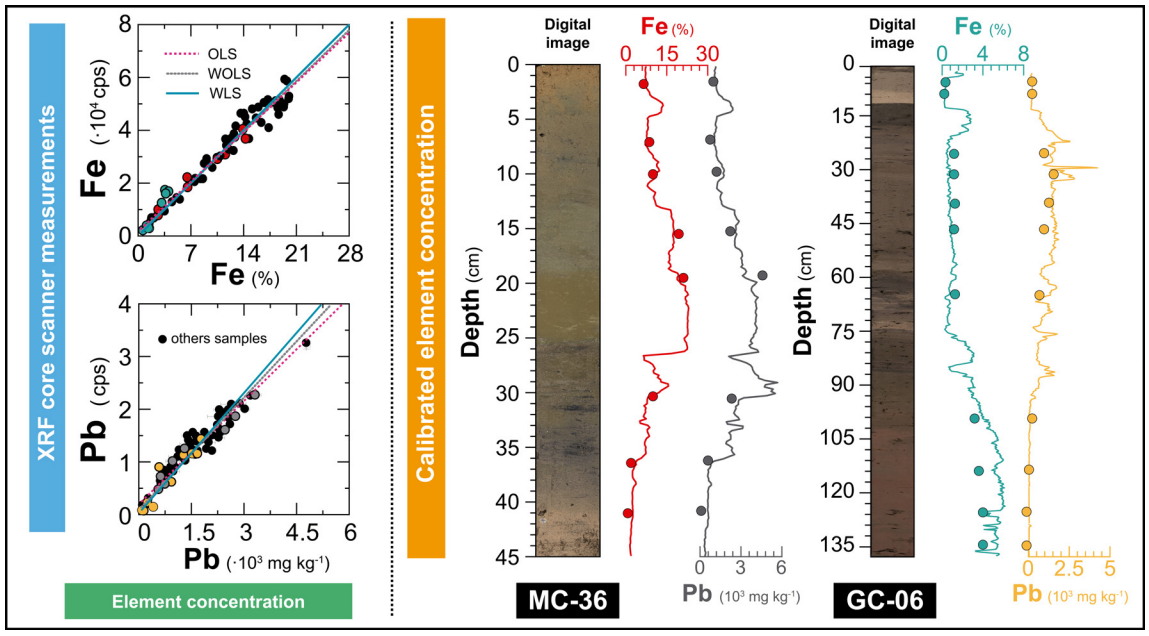

Figure 2.6 Graphical Abstract.

Abstract X-ray fluorescence core scanners (XRF-CS) allow rapid, non-destructive, continuous and high-resolution analyses of the elemental composition of sediment cores, providing large sets of semi-quantitative data. These data can be converted to quantitative data through the linear regression approach using a relatively small number of discrete samples analyzed by techniques providing absolute concentrations. However, a precise characterization of the errors associated with the linear function is required to evaluate the quality of the calibrated element concentrations. Here we present a calibration of high-resolution XRF-CS for six metals (Ti, Mn, Fe, Zn, Pb and As) measured in heavily contaminated marine deposits so

that absolute concentrations are obtained. In order to determine the best linear function for conversion of XRF data, we have tested three regression methods: the ordinary least-squares (OLS), which does not consider the standard error in any variable (x and y), the weighted ordinary least-squares (WOLS), which considers the weighted standard error of the vertical variable (y), and the weighted least-squares (WLS), which incorporates the standard error in both x and y variables. We demonstrate that the calibration method presented in this study significantly increases the correlation coefficient, higher than r^2=0.94, and reduces both the data deviation and the errors of the linear function for the three regression methods. Nonetheless, the WLS appears as the best regression method to minimize errors in the calibrated element concentrations. Our results open the door to use calibrated XRF-CS data to evaluate marine sediment pollution according to the levels of the strictest sediment quality guidelines (SQG) with errors lower than 0.4% to 2% for Fe, 1% to 7% for Zn, 3 to 14% for Pb and 5% to 16% for Mn. They highlight the robustness of the calibration procedure here presented for accurate and precise quantification of element concentrations from XRF-CS semi-quantitative data.

2.2.1 Introduction

X-ray fluorescence core scanners (XRF-CS) allow rapid and non-destructive acquisition of high resolution, continuous elemental composition data from sediments on split cores. XRF-CS have been widely used in the last decades to estimate relative changes of the chemical composition of marine and lacustrine sediments in a variety of geosciences research topics (Rothwell and Rack, 2006) such as paleoclimatology and paleoceanography (Calvert and Pedersen, 2007), sedimentology (Croudace et al., 2012; Croudace and Rothwell, 2015), lithostratigraphy or diagenesis studies (Löwemark et al., 2011; Croudace et al., 2019). Furthermore, XRF-CS have further been used in the analysis of cores made of hard rock, loess, peat bogs, river deposits and polluted materials, and also on speleothems and wood samples for a variety of purposes (Rothwell and Croudace, 2015; Hanebuth et al., 2015; Guo and Yang, 2016).

Elemental intensities obtained by means of XRF-CS are expressed in counts (cts) or counts per second (cps), which depend on the excitation conditions and the X-ray exposure time in every analysis. Since XRF-CS analyses are performed in fresh untreated materials, changes in elemental intensities can be affected by pore water content (Böning et al., 2007), grain size variations (Richter et al., 2006), sediment roughness and matrix modifications (Tjallingii et al., 2007; Weltje and Tjallingii, 2008; Hennekam and De Rick, 2012; Hennekam et al., 2018). Because of these

reasons, the records of the measured down-core elemental intensity cannot be considered quantitative, although they are assumed to reflect proportional changes in element concentrations. Normalization with a conservative element, e.g. Al (Din, 1992), is a common practice to overcome some of these problems, especially those affecting the dilution of heavier elements, i.e. the closed-sum effect (Rollinson, 1993; Löwemark et al., 2011), to finally achieve a better assessment of relative changes. Nonetheless, normalization with conservative elements can be problematic in coarse-grained industrial wastes such as mine tailings or foundry slags. For some studies it may be not necessary converting XRF-CS data into absolute concentrations, and both element intensities and ratios are frequently used for identifying relative changes in the intensity of the processes controlling the accumulation of each element. Using the logarithm of elemental ratios, i.e. log-ratios, has also become common practice to better represent changes in element concentrations, as log-ratios preserve a lineal relation between XRF-CS data and element concentrations, thus allowing sound statistical modelling of compositional data (Weltje and Tjallingii, 2008).

Determining absolute concentrations of elements is, however, crucial in many studies, such as those addressing environmental pollution issues. On the other side, performing large amounts of analyses to get absolute concentrations by means of conventional methods (e.g. Inductively Coupled Plasma-Mass or Optical Emission Spectrometry, ICP-MS or ICP-OES, or off-line X-ray fluorescence, XRF) involving the treatment and final destruction of the samples is very time consuming and costly. Conversely, non-destructive XRF-CS analyses quickly and cheaply supply high-resolution, practically continuous along core data. But this implies one step further to get absolute concentration data from measured XRF-CS elemental intensities (Jansen et al., 1998; Kido et al., 2006; Spofforth et al., 2008; Lyle and Backman, 2013; MacLachlan et al., 2015; Hunt et al., 2015). Such conversion provides a powerful tool to determine pollution levels in sediments from contaminated areas at very high resolution, thus rendering unnecessary to perform chemical analyses of plenty of discrete samples along the whole core (Rodríguez-Germade et al., 2015a). The benefits of such an approach in terms of cost and time saving are obvious. Despite this, errors associated with such conversion have not been addressed so often, thus leaving a lack of information regarding range errors in the transformation estimates, which can be of the utmost importance for evaluating contamination levels.

The most common practice for the conversion of the XRF-CS data to absolute

concentrations is the ordinary least-squares (OLS) regression method for stablishing a linear function between pairs of values obtained by means of two different analytical techniques (Tjallingii et al., 2007; Böning et al., 2007; Weltje and Tjallingii, 2008; Chen et al., 2016; Mejía-Piña et al., 2016). This classic method, widely implemented in spreadsheet software, does not consider the standard error associated with both abscissas (x) and ordered (y) variables, i.e. element concentration and element intensity, respectively. Few solutions have been proposed for introducing x and y standard error in the least-squares procedure. One option is to include the weighting of the standard error only in the ordered axis (y), called weighted ordinary least-squares (WOLS). However, the most accepted method is the unified solution proposed by York et al. (2004) that incorporates standard error in both x and y, called weighted least-squares (WLS).

In this study, we present a novel calibration procedure to convert high-resolution XRF-CS from highly polluted submarine deposits collected offshore Portmán Bay and Barcelona, in Spain, into absolute concentrations for five metals, namely Ti, Mn, Fe, Zn, and Pb and one metalloid, namely As. The above-mentioned three linear least-squares methods, i.e. OLS, WOLS, and WLS, have been tested to assess the quality of the linear regressions thus obtained together with the influence of the standard deviation of both element concentration and element intensity measurements. Our results highlight that establishing a detailed calibration procedure is critical to obtain high quality records for calibrated concentrations derived from XRF-CS semi-quantitative measurements. In turn, we also demonstrate the potential of XRF-CS data calibration to precisely establish metal contents in highly polluted marine deposits according to sediment quality guidelines (SQGs).

2.2.2 Methods

2.2.2.1 Study area and sample collection

Core samples considered in this study were obtained from two heavily polluted inner continental shelves offshore Portmán Bay (Murcia, SW Spain) and Barcelona (Catalonia, NE Spain), in the western Mediterranean Sea. From 1957 to 1990 about 60 Mt of metal bearing mine tailings were dumped into Portmán Bay from a froth flotation plant on the coast (Oyarzun et al., 2013). Such sustained discharge resulted in a mean advance of the shoreline of 650 m and in the complete infill of the original horseshoe-shaped Portmán Bay (Manteca et al., 2014). The dumped tailings form

today a prograding coastal prism with its thickest and more extensive lays submerged over the inner continental shelf (Canals and shipboard party, 2015). Our target metals (Mnm Fe, (Zn and Pb) and the metalloid (As) have been selected because of the compositional characteristics of the mine tailing deposit off Portmán Bay, which is rich in galena (PbS), sphalerite (ZnS) and pyrite (FeS) derivatives, also containing significant amounts of Mn and As (Manteca et al., 2014; Gómez-García et al., 2015).

Up to 50 cm long high-quality sediment cores from the submerged mine tailings deposit were collected with a multicorer system in August 2014 and March 2015 within the framework of EC and Spanish funded research projects MIDAS and NUREIEV, respectively. Eleven of these cores distributed from the proximal to the distal part of the submarine deposit down to 55 m of water depth) were selected for detailed scanning with XRF-CS (Figure 2.7.a and Table 2.2). The cored materials consisted mostly of silts with abundant fine sands, especially at some levels. Visual inspection showed two distinct units in most cores: (i) a lower unit made of dark greenish grey materials, with no bioturbation and occasional highly laminated intervals, and (ii) a ~20 cm thick, quite homogeneous and dark top unit with abundant bioturbation. According to Cerdà-Domènech et al. 2016, this depositional change is most likely related with the end of the mine tailings dump into the sea and its re-accommodation in the posterior years until present together with the re-establishment of natural-like sedimentation conditions. The second study area offshore Barcelona is in front of

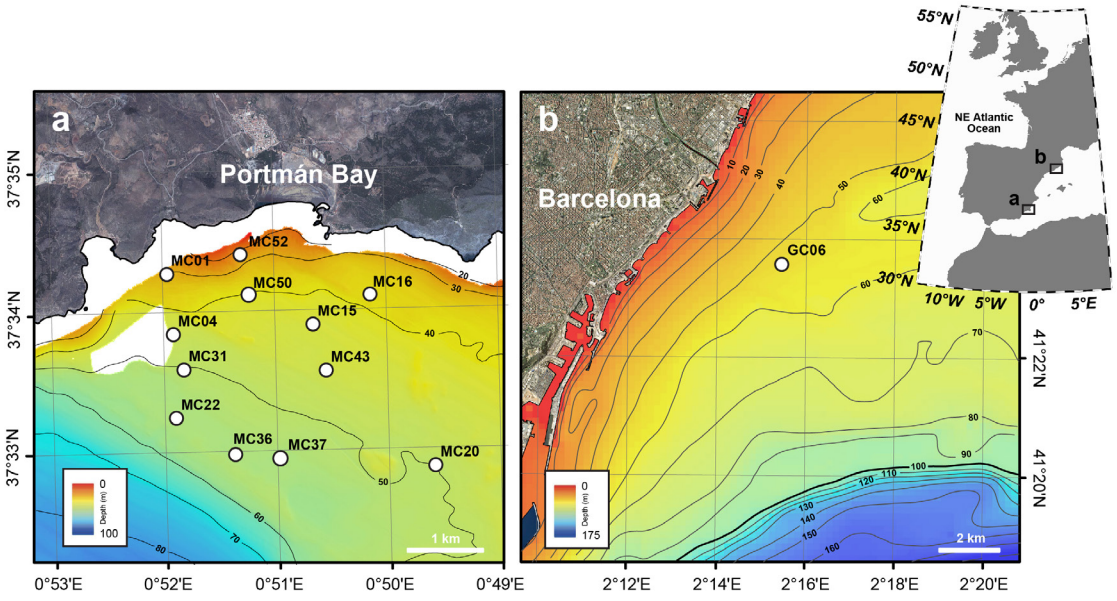

Figure 2.7 General bathymetric maps of the inner continental shelf off (a) Portmán Bay and (b) Barcelona showing the location of the sediment cores analyzed in this study. Contours every 10 m.

Station ID	Depth (m)	Latitude	Longitude	Device	Lenght (cm)
MC-01	29.7	37°34.449'N	0° 51.961'W	Multicorer	37.0
MC-04	46.0	37°34.016'N	0° 51.928'W	Multicorer	29.5
MC-15	43.4	37°34.070'N	0°50.659'W	Multicorer	40.0
MC-20	49.5	37°33.047'N	0°49.586'W	Multicorer	25.3
MC-22	53.9	37°33.420'N	0°51.902'W	Multicorer	55.5
MC-31	50.0	37°33.765'N	0°51.826'W	Multicorer	15.0
MC-36	53.7	37°33.155'N	0°51.377'W	Multicorer	45.3
MC-37	53.3	37°33.122'N	0°50.978'W	Multicorer	29.5
MC-43	44.9	37°33.740'N	0°50.548'W	Multicorer	24.6
MC-50	39.8	37°34.291'N	0°51.230'W	Multicorer	33.4
MC-52	23.1	37°34.577'N	0°51.298'W	Multicorer	28.0
GC-06	53.0	41°23.856'N	2°15.953'E	Gravity corer	137.0

Table 2.2 Sediment core depth, latitude, longitude, sampling device and length.

the Besòs River mouth where sewage sludge from a single primary treatment plant of wastewater accumulated for an unknown period of time. Sludge was discharged through a 3 km long pipe lying on the seafloor. Previous studies have shown that the resulting deposit is rich in metals (including those found in the mine tailings deposit off Portmán Bay) and organic matter (Palanques et al., 1998, 2017; Kruge et al., 2010). In the current study we analyzed a sediment core collected from this sludge deposit in February 2017 with a gravity corer (Figure 2.7.b) during the UNIBARNA 2017 cruise organized by the University of Barcelona. The materials consisted mainly of organic matter-rich clays.

The above-mentioned background information on the nature of the pollution in both sites led to the selection of the previously referred five metals (Ti, Mn, Fe, Zn and Pb) and one metalloid (As) to carry out the calibration of XRF-CS data for obtaining fine-tuned absolute concentrations. These elements are thus considered to be highly significant and have a diagnostic value for the studied reference deposits.

We are aware most studies on marine sediment pollution are focused on metals (and metalloids), especially As, Pb, Cd, Cu or Co (e.g. Buccolieri et al., 2006; Palanques et al., 2017). However, trace metals like Cd, Cu or Co appear in concentrations that according to the manufacturer are close to the detection limits of the Avaatech XRF core scanner, which may hinder highly accurate and precise calibrations for them. Also, for these reason Ti, Mn, Fe, Zn, As and Pb are the target elements selected in our study.

2.2.2.2 XRF core scanner analysis

All sediment cores have been scanned with an Avaatech XRF core scanner at the CORELAB facility of the University of Barcelona. The core scanner is equipped with an Oxford Rhodium X-ray source (4 − 50 kV) and a Canberra X - Pips 1500-1.5 Detector with a 125-µm beryllium window and a multichannel analyzer Canberra DSA 1000 (MCA). This configuration allows detecting a wide range of emission spectra for elements with atomic weight from Al to U.

Prior to scanning, the split cores were left for 16 hours at room temperature to evaporate water, thus reducing the water effect on the radiation absorption and increasing the measured signal intensity (Böning et al., 2007; Tjallingii et al., 2008). Then, the cores were covered with Ultralene X-ray transmission foil (4µm thick) to avoid desiccation and potential contamination and scanned at 2 mm resolution. The excitation configuration parameters were set at 10 kV and 1.2 mA during 10 s for elements with atomic weights between Al and Fe, and 30 kV and 1.6 mA during 50 s, with a Pd-thick filter, for elements with atomic weights between Ni and Pb. Each element presents various energy emissions in the X-ray spectrum that correspond to the different electron states of the atom. Ti, Mn, Fe, Zn and As intensities, expressed as counts (cts) were obtained by integration of their Kα X-ray emission line. Lead intensity was obtained by integration of the Lβ emission line in order to reduce the effect on the integration produced by the overlap of Pb (Lα) and As (Kα). The bAxil spectrum analysis software (BrightSpec) was used to obtain the integration of the elemental peaks and the estimation of their intensity areas, expressed as counts per seconds (cps).

2.2.2.3 Geochemical analysis of discrete samples

77 subsamples from core tops were analyzed for quantitative metal concentrations by means of ICP-OES and ICP-MS. In order to obtain the best representative calibration function between XRF intensities and the absolute concentrations of each metal, subsamples were selected considering the widest range of intensities from all target elements. As XRF core scanner analyses were carried out at 2 mm resolution, subsamples were extracted from 1 cm-width intervals with essentially constant intensities to avoid interferences eventually coming out from layers with different responses. To further reduce eventual multi-layer interferences, subsamples

were obtained from the area irradiated during XRF core scanning (2 x 12 mm^2) and from a maximum depth of 2 mm in the split sediment core, which corresponds approximately to the maximum penetration of X-rays in soft sediment. Obviously, the minimum mass of sample (~1 g dry) needed for ICP analyses was also taken into account while subsampling the split cores.

Each subsample was lyophilized, grounded and homogenized with an agate mortar, and placed in a Teflon reactor with 2.5 mL of HNO_3 (65%) at 100°C for 18h. The extract was poured into a polyethylene tube and centrifuged 3 minutes at 3,000 rpm to separate the solid phase. The supernatant was decanted and diluted with HNO_3 at 1% until 50-mL ready to be analyzed were obtained. The residue was placed again into a Teflon reactor, leached with 1 mL HNO_3 (65%), 7 mL of HF and 1 mL H_2O_2, and heated for 18h at 100°C. Then, 2 mL $HClO_4$ were added to the Teflon reactor and heated in a sand bath at 270°C until all acid volume evaporated. The hot residue was further treated with 2 mL $HClO_4$ and heated again in the sand bath at 270°C until the acid evaporated. The resultant residue was leached with 2 mL HNO_3 (65%) and 2 mL H_2O_2, and decanted into a volumetric flask where it was diluted with HNO_3 at 1% until 50-mL.

Two solutions per sample were analyzed using a Perkin-Elmer Elan-6000 ICP-MS for metals in lower concentrations (Ti, Zn, As and Pb) and a Perkin Elmer Optima 8300 ICP-OES for metals in higher concentrations (Mn and Fe).

2.2.2.4 Standard deviation of XRF-CS and ICP-MS/OES measurements

The error associated with the XRF-CS and the ICP-MS/OES measurements, hereinafter referred to as standard deviation, has been examined to quantify its influence on the calibration function. The standard deviation of the XRF-CS measurements was obtained directly through the spectral analysis software (bAxil) that adjusts the regression function to the spectral emission of each element by a non-linear least-squares algorithm. This allows detecting the deviation of the spectral areas with regards to the regression model, which increases when the spectral peak is not well defined, as it is generally the case for low intensity peaks.

The standard deviation of the ICP-MS/OES analysis has been calculated as the mean standard deviation of the three measurements performed on each sample.

2.2.2.5 Calibration of element intensities to absolute concentrations

Defining the best regression line between two experimental data sets is a significant tool to predict the theoretical value of one variable from the other variable (Webster et al., 1995; Piippanen et al., 1997; Saylor et al., 2006; Hennekam and De Rick, 2012). Generally, the linear relationship between n number of (xi, yi) data pairs (i=0,...,n) can be described by the function:

(1) $$y(x) = \beta_0 + \beta_1 bx$$

where β_1 is the slope of the straight line and β_0 is the y-axis intersection.

The ordinary least-squares (OLS) method has been extensively used to provide a linear function between x (as the independent variable) and y (as the dependent variable). By definition, the OLS method minimizes the sum of the squares of the y residuals:

(2) $$\sum_{i=1}^{n} (y_i - Y_p)^2 = \sum_{i=1}^{n} (y_i - \beta_0 + \beta_1 x_i)^2$$

where Y_P is the y-prediction and y_i is each point lying on the regression.

Although OLS is a simple solution to obtain a linear function, if one or both variables have associated errors, the OLS regression can be biased. Considering only the effect of the y-errors in the regression, the x_i and y_{ii} data pairs can be weighted by a factor inversely proportional to the variance of the y-values:

(3) $$\sum_{i=1}^{n} w_i (y_i - y_p)^2 = \sum_{i=1}^{n} w_i (y_i - \beta_0 + \beta_1 x_i)^2$$

(4) $$w_i = \frac{1}{\sigma_1^2},$$

where w_i is the weight factor and σ^2_i is the standard error of y-values.

This derivation of the OLS method, named weighted ordinary least-squares (WOLS), considers that the dependent variable, y, contains a random error of measurement, while the independent variable, x, is error-free. However, the measured analytical data generally includes instrumental errors in both directions, which vary from point

to point with no fixed relation to each other. Deming (1943) proposed a solution with errors in both regressed variables that minimize the sum of squared residuals, as:

(5) $$S = \sum \left[\omega(X_i)(x_i - X_i)^2 + \omega(Y_i)(y_i - Y_i)^2\right]$$

(6) $$\omega(X_i) = \frac{1}{\sigma_{X_i}^2}, \ \omega(Y_i) = \frac{1}{\sigma_{Y_i}^2}$$

where (x_i, y_i) are the observed points, (X_i, Y_i) are predicted values and $(\sigma_{Xi}, \sigma_{Yi})$ correspond to the standard errors of each variable.

York et al. (2004) proposed a general solution to the sum of squared residuals (Equation 5) by unifying the problem of finding parameters β_1 and β_0 through an iterative numerical least-squares technique including the possibility of identifying a correlation factor between the errors of x and y. In this weighted least-squares (WLS) regression technique the unification of standard errors in both x and y observations is presented as:

(7) $$W_i = \frac{w(X_i)w(Y_i)}{w(X_i) + b^2 w(X_i) - 3br_i\sqrt{w(X_i)w(Y_i)}.}$$

where $w(X_i)$ and $w(Y_i)$ are the weights of X_i and Y_i, b is the slope of the best line and r_i is the correlation coefficient between errors in X_i and Y_i.

In order to compare and assess the impact of the standard deviation of the element intensity and concentration in both directions of the linear function, the three regression methods (OLS, WOLS, and WLS) have been implemented in MATLAB® version 2016a or higher. The XRF-CS outputs expressed in cps have been defined as the dependent variable (y_i) and the metal concentrations expressed in % (weight/weight) and mg kg^{-1} have been set as the independent variable (x_i). The quality of the linear function has been determined by two goodness-of-fit measures: the correlation coefficient (r^2) and the standard deviation of the estimate (S). The correlation coefficient (r^2), described as the degree of association between two variables, has been widely used as a quality index for regression models and is defined as:

(8) $$r^2 = \frac{cov\ (X,\ Y)}{\sqrt{var(X)var(Y)}} = \frac{\frac{1}{N}\sum_{i=1}^{n}(x_i - x^-)(y_i - y^-)}{\sqrt{\frac{1}{N}\sum_{i=1}^{n}(x_i - x^-)^2 \sum_{i=1}^{n}(y_i - y^-)^2}}$$

where y_i and x_i are the observational values, $\bar{x}$ and $\bar{y}$ are the mean values of y_i and x_i values, and W_i is the weight value expressed in equation (4). In the case of WLS, York's (2004) solution differs from the mean value of y_i, as defined by:

(9) $$\bar{y} = \frac{\sum W_i x_i}{\sum W_i}$$

Otherwise, the standard deviation of the estimate (S) is a measure of the accuracy of the predictions and provides the absolute measure of the data point distance from the linear function, which is expressed in the units of the dependent variable and is defined by:

(10) $$S^2\,(OLS) = \sum_{i=1}^{n} \frac{(y_i - y_p)^2}{n-2} = \sum_{i=1}^{n} \frac{(y_i - \beta_0 + \beta_1 x_i)^2}{n-2}$$

(11) $$S^2(WOLS/WLS) = \sum_{i=1}^{n} W_i \frac{(y_i - y_p)^2}{n-2} = \sum_{i=1}^{n} W_i \frac{(y_i - \beta_0 + \beta_1 x_i)^2}{n-2}$$

where y_p is the prediction value from the data point y_i, n the number of observations and W_i the weighted parameter defined in equations (4) and (6) for WOLS and WLS methods, respectively.

2.2.3 Results and discussion

2.2.3.1 Linear function estimated by OLS, WOLS and WLS methods

Element intensities and concentrations in marine sediments off Portmán Bay and Barcelona, and the linear functions estimated by OLS, WOLS and WLS methods are presented in Figure 2.8 and Table 2.3. The main parameters assessed to compare the three linear functions for each element are the statistical significance (P), the y-intercept value, the relative standard deviation of the slope (RSD) and the residual plot, as well as the goodness-of-fit measures: the correlation coefficient (r^2) and the standard deviation of the estimate (S). Contrary to previous researches (e.g. Mejía-Piña et al., 2016), the linear functions have not been adjusted to pass through the origin of coordinates, thus allowing to determine the influence of errors associated to the XRF-CS output in the linear function. Metal concentrations measured in

Portmán's Bay samples show a larger variability, with values of 1600 – 3400 mg kg^{-1} for Ti, 200 – 7000 mg kg^{-1} for Mn, 1 – 26% for Fe, 50 – 7300 mg kg^{-1} for Zn, 20 – 800 mg kg^{-1} for As and 40 – 5400 mg kg^{-1} for Pb. These concentrations are noticeably higher than those reported from other sites in the Mediterranean Sea (e.g. Buccolieri et al., 2006; Sprovieri et al., 2007; Palanques et al., 2008; Christophoridis et al., 2009; Martínez-Gómez et al., 2012), thus evidencing metal enrichment in Portmán's mine tailings deposit (Oyarzun et al., 2013). Metal concentrations are significantly lower in sediments from the Barcelona inner continental shelf, ranging from 540 – 4440 mg kg^{-1} for Ti, 220 – 430 mg kg^{-1} for Mn, 0.4 – 4.0% for Fe, 110 – 1150 mg kg^{-1} for Zn, 5 – 200 mg kg^{-1} for As and 30 – 1730 mg kg^{-1} for Pb.

The three regression methods (OLS, WOLS, and WLS) show correlation coefficients better than r^2=0.94 for all elements (Table 2.3), which are higher than those obtained

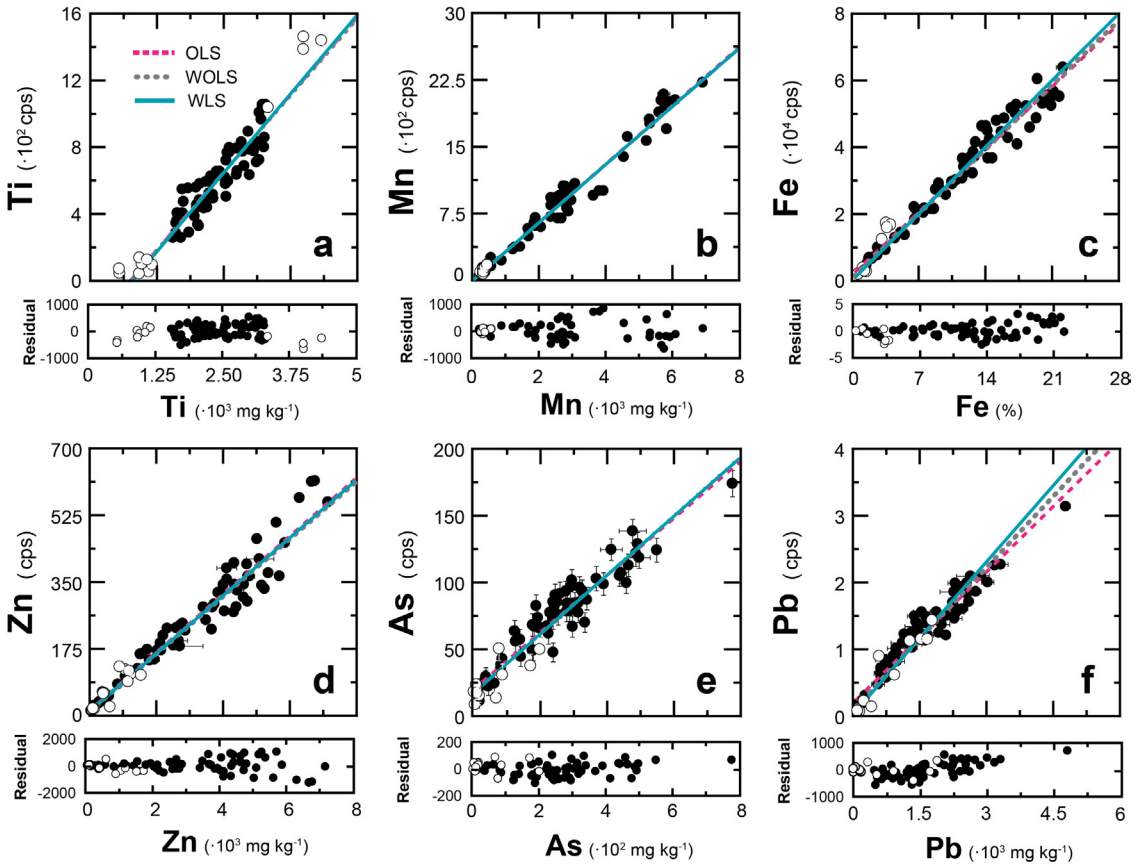

Figure 2.8 Scatterplots of element intensities in counts per second (cps) and chemical concentration expressed in % and mg kg-1 for (a) Ti, (b) Mn, (c) Fe, (d) Zn, (e) As and (f) Pb from Portmán Bay (black dots) and Barcelona (white open dots) inner shelf sediment samples. Continuous blue and dashed dark grey and pink lines indicate the regression equation line for each statistical model, namely WLS, WOLS and OLS (see legend in plot a). Residual values in cps for the correlation of each data pair is shown in the smaller plots below each main plot.

		Intercept		Slope		RSD	S	r^2	n
Ti	OLS	-276.07	34.74	0.3708	0.0142	3.82	95.8	0.949	77
	WOLS	-269.23	35.74	0.3678	0.0146	3.96	5.0	0.946	77
	WLS	-296.24	7.82	0.3776	0.0033	0.87	4.2	0.949	77
Mn	OLS	-1.51	19.58	0.3279	0.0064	1.96	101	0.988	66
	WOLS	2.20	19.07	0.3264	0.0063	1.92	4.8	0.988	66
	WLS	0.12	3.68	0.3262	0.0015	0.47	3.9	0.989	66
Fe	OLS	1,367.7	633.3	2,535.0	51.8	2.04	3096	0.985	77
	WOLS	439.4	420.8	2,626.2	34.4	1.31	55.3	0.994	77
	WLS	-197.0	9.3	2,695.8	2.2	0.08	23.3	0.993	77
Zn	OLS	9.31	7.29	0.0762	0.0021	2.77	37.0	0.972	77
	WOLS	7.56	3.57	0.0768	0.0010	1.35	16.6	0.993	77
	WLS	6.90	0.19	0.0758	0.0002	0.20	11.5	0.987	77
As	OLS	19.41	2.08	0.2133	0.0076	3.57	10.8	0.955	77
	WOLS	17.36	2.03	0.2226	0.0074	3.34	1.5	0.961	77
	WLS	16.71	1.27	0.2203	0.0055	2.48	1.4	0.958	77
Pb	OLS	21.56	3.26	0.0654	0.0020	3.01	16.3	0.967	77
	WOLS	11.98	2.82	0.0724	0.0017	2.35	8.6	0.980	77
	WLS	5.20	0.32	0.0761	0.0006	0.75	4.1	0.985	77

Table 2.3 Statistical parameters of OLS, WOLS and WLS regression models for each analyzed metal including: intercept value, slope, relative slope deviation (RSD), statistical significance (P), correlation coefficient (r^2) and number of observations (n). Statistical significance (p) for all regressions was $p<0.001$.

in previous studies (Böning et al., 2007; Tjallingii et al., 2007). However, the WLS method presents a significantly lower standard deviation of the estimate (S) compared to the OLS method, which shows the highest values. Since the correlation coefficient simply provides a relative quantification of the dependence variable variance that can be explained by the regression model, the standard deviation of the estimate is more adequate to quantitatively evaluate the precision of the linear function. Indeed, the standard deviation of the estimate decreases when the analytical standard deviations in both variables are weighted in the WOLS and WLS methods (Table 2.3).

Increasing the precision has a direct influence mainly on the relative standard deviation of the slope (RSD), which represents the main source of errors in the linear function. Accordingly, the results show that RSDs from OLS and WOLS methods are significantly higher than those obtained with the WLS method for all elements except As, which displays a relatively high RSD for the three methods (Table 2.3). The differences between OLS/WOLS and WLS regression methods are especially clear in the case of Ti, element which also presents a significant scattering.

As high RSD for the three regression methods is likely related to the large standard deviation of the As intensity values, which is in turn affected by the overlapping of the emission peaks of Pb and As given their close proximity (Pb Lα 10.551 KeV and As Kα 10.543 KeV, Figure 2.9). Indeed, the peak area of a characteristic XRF line could be partially overlapped by a contiguous peak, which may affect significantly the determination of the peak area (cts). Such overlapping has been noticed elsewhere in samples with high concentrations of sulfides (Baucells et al., 1988).

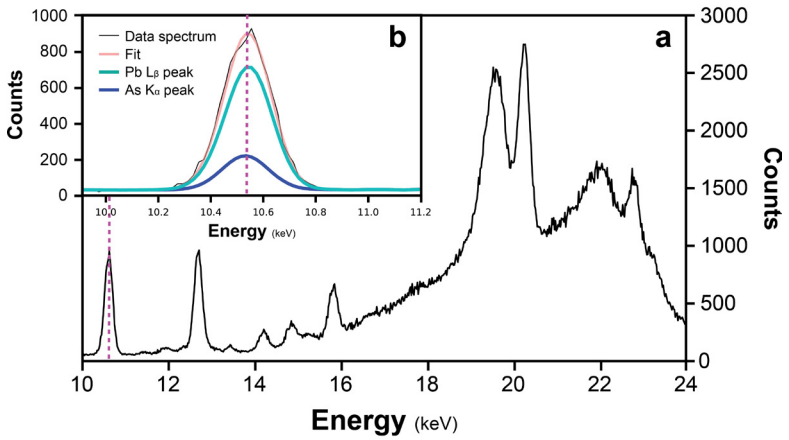

Figure 2.9 a) Example of the X-ray spectrum plot of one sample measured at 30kV and 1.6 mA during 50 s, with a Pd-thick filter. b) Detail of spectral overlap of As Kα and Pb Lβ.

To overcome the above limitation the spectral analysis software determines the peak area (e.g. As Kα) by a mathematical adjust considering the emission probability from another peak (e.g. As K*β*) that would increase the standard deviation of the element intensity (Scholze et al., 2006). The standard deviation can be slightly reduced by selecting a non-overlapping XRF peak for the element intensity estimation, like the secondary line emission of As K*β* (11.726 KeV) and Pb*β* (12.614 KeV). However, while the Pb L*β* peak that we have selected to determine the element intensity of Pb is relatively pronounced in our samples, the As K*β* peak area is significantly lower than the Kα peak (Figure 2.9). This implies that its integration would generate again rather high standard deviations. For a more accurate analysis and to reduce the standard deviation of the integrated As intensities, it would be necessary to use a predefined standard calibration to quantify the interference factor between Pb Lα and As Kα peaks (Baucells et al., 1988).

As shown in Figure 2.8, the y-intercept values for all models show minimum deviations from zero for Mn, Fe, Zn, As and Pb, which might be related to the wide

concentration range and the high accuracy of the linear regression. In contrast, the elevated negative y-intercept for Ti (Figure 2.8.a) is likely related to a matrix effect and to indirect excitation that are both more common in transition elements like Ti. This occurs when part of the Ti-emitted fluorescence is scattered or absorbed by Ca, thus enhancing its measured intensity and, consequently, leading to a negative intercept (e.g. Böning et al., 2007). The deviation of the y-intercept from zero is particularly relevant in calibration studies for obtaining element concentrations at lower values, and is directly related to the detection limit of the regression method. Indeed, a comparison between the y-intercept values after the three regression methods shows that, with the exception of Ti and As, the WLS method presents a minor y-intercept deviation from zero than OLS and WOLS (Table 2.3). Moreover, all regressions show a robust statistical significance (P), with a P-value lower than 0.001, and the residual values plots evidence a constant distribution of data for all concentrations range (Figure 2.8).

Overall, the regressions obtained for the six target metals show lower scattering and standard deviation of the slope, as well as higher correlation coefficients, than those from previous calibration studies (e.g. Böning et al., 2007; Tjallingii et al., 2007). These results can be attributed to the increased element intensities recorded due to the reduction of water content in the split core. Indeed, Tjallingii et al. (2007) found that the thin water film formed under the foil that covers the split core strongly reduces element intensities. Given that the analytical precision of the XRF core scanner varies with the element intensity (Ramsey et al., 1995), the drying step of 16 hours before performing XRF analyses contributed to reduce the scatter of the regression. This leads to an enhanced accuracy of the linear function by decreasing the deviation of the observed value from the fitted value provided by the linear function, thus improving the correlation coefficient. Nonetheless, the high-resolution sediment subsampling carried out in the same irradiated area and the avoidance of interferences between different sediment layers likely contributed to minimize the scattering effect. Additionally, even though the element intensities measured by XRF-CS are largely influenced by lithology and other sediment characteristics (Rodríguez-Germade et al., 2015b), our results present a very good overlay between intensity data from the two sampling locations (Figure 2.8).

Our results evidence that the calibration method used in our study to convert XRF-CS output data into fully quantitative data improves significantly the quality of the

linear regression for the three regression methods, as illustrated by high correlation coefficients, low errors and deviation to zero. Nevertheless, WLS appears to be the best method for highly accurate determinations of the linear function between element intensities and concentrations. This points out that analytical and statistical errors should be properly evaluated in calibration studies to convert XRF-CS output data into quantitative concentrations.

2.2.3.2 Errors of calibrated elemental concentrations

The most commonly applied approach to obtain quantitative elemental data from XRF-CS outputs is to replace the y variable of the linear functions by the element intensity value (Kelloway et al., 2014; Chen et al., 2016; Mejía-Piña et al., 2016). Given that these linear functions have errors associated to the slope and the intersect, and also to element intensities (Table 2.3), it is necessary to determine the errors of the calibrated element concentration in order to evaluate the quality and the limitations of the linear functions. Considering the three linear functions (OLS, WOLS and WLS) obtained for each element, 1850 element intensities have been converted into calibrated element concentrations. The errors of the calibrated element concentrations have been calculated according to the law of propagation of errors (Taylor and Kuyatt, 1994):

$$\begin{aligned} \Delta f &= \Delta f(x_1, x_2, \cdots, x_n; \Delta x_1, \Delta x_2, \cdots, \Delta x_n) \\ &= \left[\sum_{i=1}^{n} \left(\frac{\partial f}{\partial x_i} \Delta x_i \right)^2 \right]^{1/2} \end{aligned} \tag{12}$$

where f is the given function, n is the number of uncorrelated variables (x_1, x_2, ..., x_n) and their errors (Δx_1, Δx_2,..., Δx_n). The relative errors calculated as the ratio of the errors to the calibrated element concentration for each linear regression (OLS, WOLS and WLS) has been regressed by the least-squares method to evaluate their distribution (Figure 2.10).

As expected, the three regression methods are characterized by an exponential increase of the relative errors at low calibrated element concentrations. However, each element showed different trends. For Fe and Zn, errors of the calibrated concentrations by the WLS method were significantly lower than those obtained from OLS and WOLS, especially at low concentrations. Instead, Ti, Mn and Pb

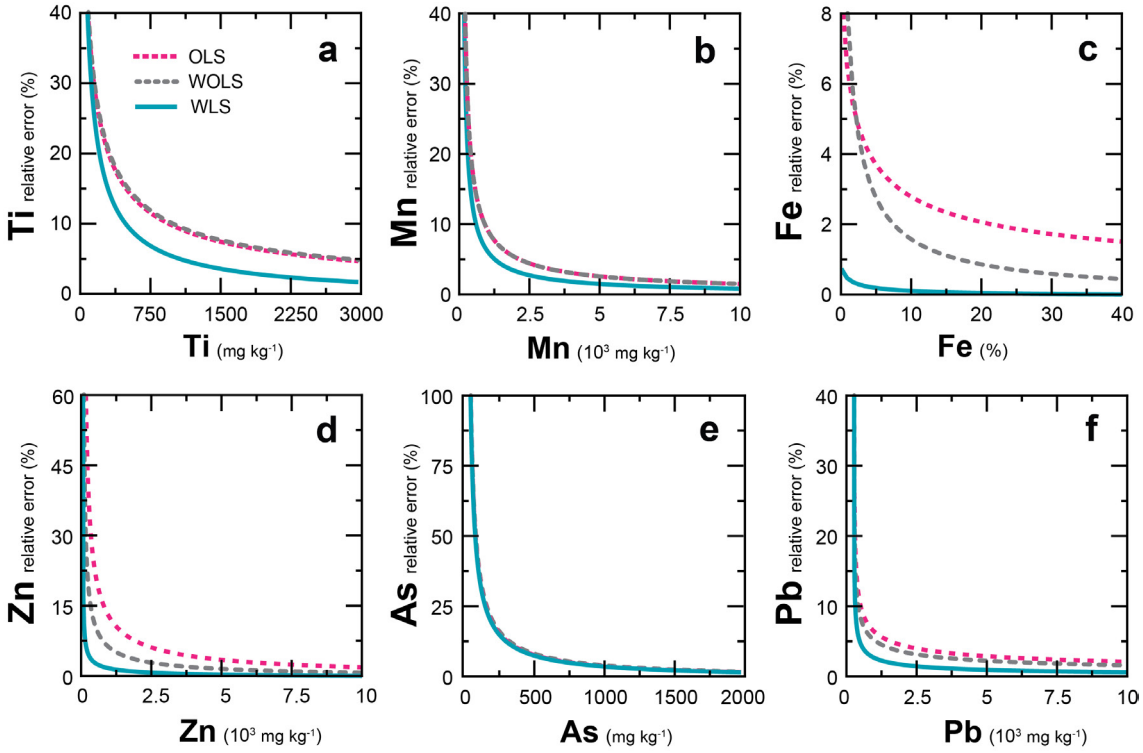

Figure 2.10 Relative errors of the calibrated concentrations as a function of the calibrated concentrations in % for (a)Ti, (b) Mn, (c) Fe, (d) Zn, (e) As and (f) Pb as a function of concentration prediction expressed in % and mg kg^{-1} for each regression model (see legend in plot a).

differences in errors after the three methods were minor. The contrasting patterns between the three regression methods (OLS, WOLS, and WLS) likely result from the differences in their slopes and intercept errors, which commonly represent the main error factor in the linear functions (cf. Section 2.2.3.1). Indeed, as shown in Table 2.3, relative standard deviations of the slope for the OLS method are higher than those from the WLS method by a factor ~4.4, ~4.2, ~25.8, ~14.0, ~1.5 and ~4.0 for Ti, Mn, Fe, Zn, As and Pb. In contrast, As shows the same trend independently of the regression model and a minimal standard deviation from OLS to WLS, which relates to the high standard deviation in As intensities due to the spectral overlap between Pb Lβ and As Kα peaks (section 2.2.3.1, Figure 2.9).

Nevertheless, obtaining the calibrated element concentrations requires an accurate methodology to avoid the influence of the effects of the physical properties so that the correlation coefficient is increased and the scattering is reduced (e.g. Tjallingii et al., 2007). An accurate estimation of the errors is also required to evaluate the quality of the regression method and the representativeness of the results (Weltje and Tjallingii, 2008). Beyond the high correlation and lower scattering achieved from

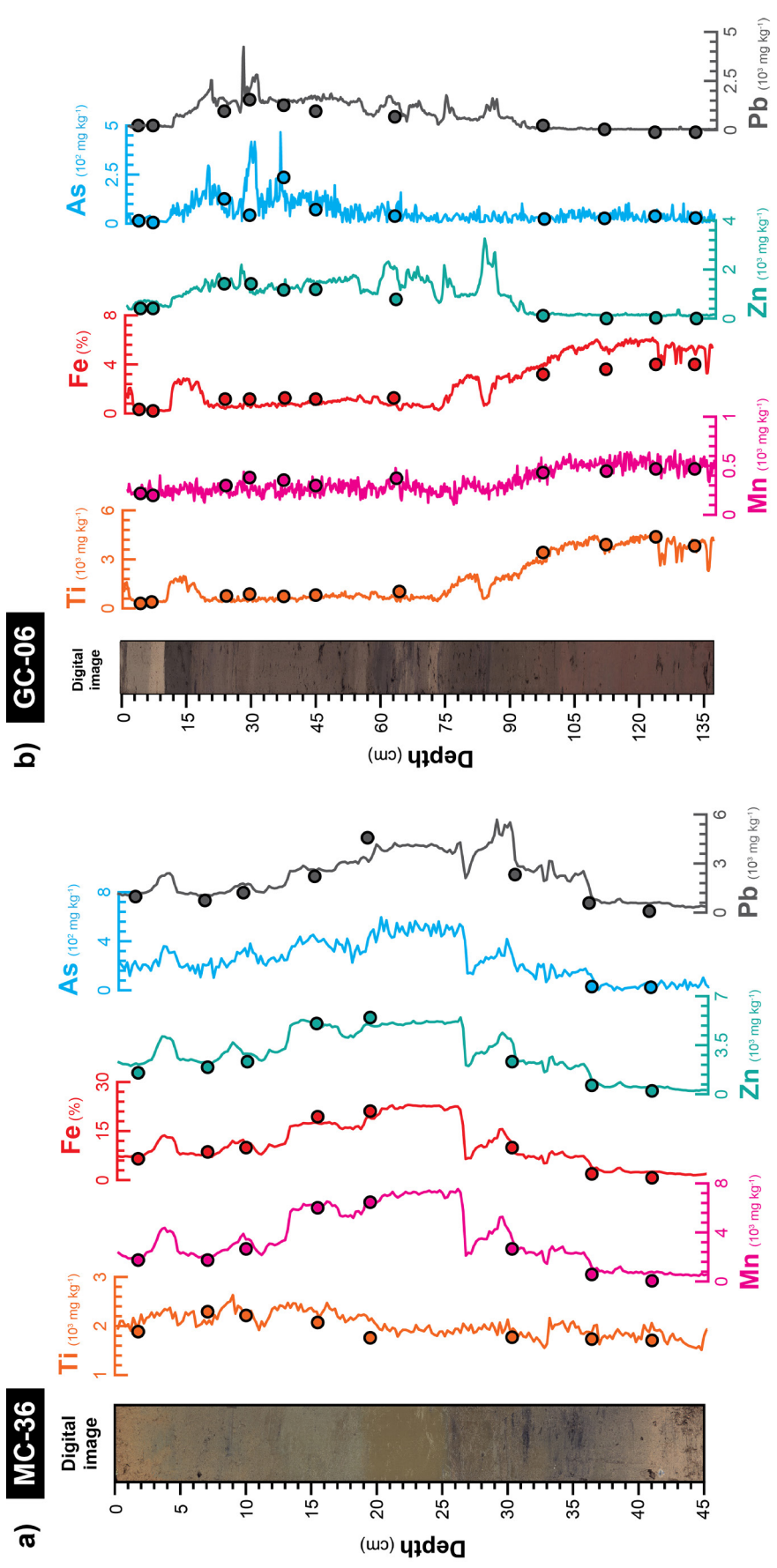

Figure 2.11 Calibrated element concentration of sediment cores (a) MC-36 in Figure 1a and (b) GC6 in Figure 1b from the inner continental shelf offshore Portmán Bay and Barcelona, respectively. Points show the location of discrete subsamples on which that were analyzed by IPC-MS/OES for absolute metal concentrations, subsequently used for calibrations (Figure 2). Note that core logs in the figure are at cm-scale whereas XRF scans were carried out at 2 mm resolution. Therefore, location of subsamples is merely indicative. All subsamples were extracted from 1 cm-width intervals with essentially constant intensities to avoid eventual multi-layer interferences (see main text for further explanation).

the three regression methods, likely due to the calibration methodology developed in this study, our results demonstrate that the regression method most commonly used (OLS) for XFR-CS calibrations is the one developing the highest errors for the calibrated element concentrations. This is mainly related to the non-weighted analytical errors. In contrast, the WLS method, which considers the analytical and statistical errors in the calibration of the XRF-CS output, provides more accurate calibrations, significantly reducing the errors of the calibrated element concentrations.

Our results also reveal that the exponential distribution of the errors observed in Figure 2.10 is mainly explained by the influence of the standard deviation of the element intensity. It is well known that the relative standard deviation of XRF-CS measurements increases exponentially as the concentration falls down to the detection limit (Ramsey et al., 1995). Depending on energy resolution and detection efficiency, the irregularities in the spectral signal are more significant at low peak areas (Scholze et al., 2006). Consequently, the nonlinear least-squares algorithm cannot adjust accurately the peak area, thus resulting in an increase of the standard deviation of the element intensity and hence in an increase of errors for the calibrated element at low concentrations. Some authors (e.g. Rodríguez-Germade et al., 2015b; Hennekam et al., 2018) have demonstrated that increasing exposure time should reduce the standard deviation of the element intensity. However, the increase of exposure time also implies an augmentation of the time required for analysis and of associated costs, which should be taken into account too.

2.2.3.3 Sediment quality guideline levels and XRF-CS calibration

In the last century, anthropogenic fluxes of metals to the marine environment has grown as a result of accelerated industrial, urban, agricultural and mining developments (Di Leonardo et al., 2008; Palanques et al., 2008; Pan and Wang, 2012; Hanebuth et al., 2018). Commonly, the pollution degree of marine sediments assessed by using sediment quality guidelines (SQGs), which are defined as the concentration range or limit of the chemical compounds (e.g. trace metals, PCBs, pesticides or PAH) that could produce potential biological effects (Long et al., 1995). SQGs have been widely applied to evaluate ecotoxicological risks and biological effects in harbors (Fatoki and Mathabatha, 2001; Adamo et al., 2005; Casado-Martínez et al., 2006; Garcia-Orellana et al., 2011; Pourabadehei and Mulligan, 2016) and also in estuarine and coastal environments (Fukushima et al., 1992; Morillo et al., 2004; Buccolieri et al., 2006;

	Spanish Harbor Authority				Ontario Ministry Environment				Environmental Protection Agency			
	Action level B		Action level C		Lowest level		Severe level		Mod polluted		Heavily polluted	
	Limit	%Error	Limit	%Error	Limit	%Error	Limit	%Error	Limit	%Error	Limit	%Error
Mn (mg kg^{-1})	-	-	-	-	460	11	1100	5	300	16	500	11
Fe (%)	-	-	-	-	2	1	4	0.4	2	0.6	2.5	0.5
Zn (mg kg^{-1})	410	3	1640	1	120	6	820	2	90	7	200	4
As (mg kg^{-1})	70	>40	280	14	6	>40	33	>40	3	>40	8	>40
Pb (mg kg^{-1})	218	5	600	3	31	14	250	5	40	12	60	10

Table 2.4 Metal concentration limits and associated relative errors quantified after the WLS regression method for three widely used sediment quality guidelines (SQGs) in mg kg^{-1}.

Palanques et al., 2008; Rubio et al., 2010). Classically, performing pollution studies of marine sediments relied on conventional analytical methods requiring discrete samples from whole sediment cores, involving significant laboratory effort and time, together with high costs, which generally led to a reduction in the total number of samples finally analyzed (Rodríguez-Germade et al., 2015b). The calibration of the XRF-CS output data appears as a major step forward to overcome these limitations, as it advantageously provides high-resolution metal concentration data in a fast, continuous and repeatable way (Figure 2.11). However, for a meaningful use of XRF-CS calibrated data it is mandatory to quantify and minimize the errors of the calibrated element concentrations. This becomes even more necessary to assess pollution levels through SQGs at low element concentrations.

We have considered the concentration limits defined in three widely used SQGs (see further down) to estimate the relative errors of the calibrated element concentration for such limits using the WLS method developed in this study for XRF-CS data calibration. Those SQGs address various potential biological effects of the chemicals, which are: (i) the lowest effect level and severe effect level developed by the Ontario Ministry of the Environment (Persaud et al., 1993): (ii) moderately polluted and heavily polluted levels developed by the Environmental Protection Agency (U.S. Environmental Protection Agency, 2005); and (iii) action level B and action level C developed by the Spanish Harbor Authority "Puertos del Estado" on the basis of the "Guidelines for the characterization of dredged material and its relocation in waters of the maritime-terrestrial public domain" (Comisión nacional de estrategias marinas, 2015). A summary of metal concentration limits and associated relative errors for each of the above SQGs, expressed in percentage, is shown in Table 2.4.

Reference papers	Environment	Ti		Mn		Fe		Zn		As		Pb	
		(mg kg^{-1})		(mg kg^{-1})		(%)		(mg kg^{-1})		(mg kg^{-1})		(mg kg^{-1})	
		Min	Max	Min	Max	Min	Max	Min	Max	Min	Max	Min	Max
This research	Portmán Bay	1,600	3,400	200	7,000	1	26	50	7,300	20	800	40	5,400
	Barcelona cont. shelf	540	4,400	220	430	0.4	4	110	1,150	2	200	30	1,730
Coastal areas													
Palanques et al. 2017	Barcelona cont. shelf	-	-	-	-	-	-	100	990	-	-	50	760
Buccolieri et al. 2006	Gulf of Taranto	2,340	3,880	550	2,830	0.3	0.4	90	130	-	-	50	80
Capello et al. 2016	Gromolo Torrent	-	-	299	1,207	1.8	8.8	78.7	262.7	9	23	14	43
Fukushima et al. 1992	Tokio Bay	2,520	3,700	350	1,540	3	4.1	106	405	-	-	25	58
Raj & Jayaprakash, 2007	Bay of Bengal	-	-	260	460	1.7	3.7	40	200	-	-	25	37
Morillo et al. 2004	Huelva estuary	-	-	180	576	1.6	3.5	141	649	-	-	20	197
Rubio et al. 2010	Ria Vigo	-	-	263	306	5	7	85	135	-	-	36	84
Harbour													
Adamon et al. 2005	Port of Naples	240	480	100	420	-	-	40	1,200	8	21	40	310
Guevara-Riba et al. 2004	Port of Barcelona	-	-	255	427	2.2	3	183	1,133	-	-	86	589
Pourabadehei & Mulligan, 2016	Quebec harbour	-	-	-	-	-	-	66	563	4.6	18.4	11	212
Romano et al. 2016	Puzzouli Gulf	-	-	-	-	1.3	8.9	50	6,300	10	837	21	2,811
Casado-Martínez et al. 2006	Port of Cartagena	-	-	-	-	-	-	900	8,660	62	101	487	1,397
He & Morrison, 2001	Port Kemblar harbour	-	-	-	-	7.3	10	1,209	2,220	14	46	151	484
Fatoki & Mathabatha, 2001	Elizabeth harbour	-	-	103	499	0.4	1.5	19	126	-	-	9	62
Müller-Karulis et al. 2003	Ventspils Harbor	-	-	162	1,120	0.6	3.8	17	254	-	-	3	44
Metal concentration average		1,700	2,687	252	939	2	5	208	1,549	18	174	69	478

Table 2.5 Minimum, maximum and averaged minimum and maximum (lower row) metal concentrations in this research and coastal and harbour sediments worldwide.

It is to be noted that SQGs are usually based on standardized analytical procedures, especially when results can constrain management actions. Also, as aptly pointed out by Böning et al. (2007), it is reasonable to expect some degree of data scattering rather than a perfect correlation between XRF and ICP data. In any case, these factors do not condition the calculated errors as assessing the errors of the regression functions by any method (OLS, WOLS and, WLS) as well as propagating the errors of the calibrated element concentrations allow constraining calibration procedure errors and evaluating the quality of the regression functions and the data themselves, thus significantly contributing to improve comparisons.

Even though the errors depend on each SQGs, the errors of the calibrated element concentration for each limit in the guidelines should be considered satisfactory for most metals under consideration (Mn, Fe, Zn and Pb) but As. Titanium is not included in the referred SQGs. Iron shows the lesser relative errors, from 0.4% to 2%, due to the high concentration limits considered in SQGs and also to the low errors of the linear function. For the rest of metals under consideration also included in SQGs, Zn ranges from 1% to 7%, Pb from 3 to 14%, and Mn from 5% to 16%. Errors for As are equal or higher than 14%, because of the large standard deviation of the linear function resulting from the Pb peak overlap effect (cf. Section 2.2.3.1). The range of metal concentration levels found in coastal and harbor sediments worldwide (Table 2.5) reinforces the potential applicability to many polluted settings of the calibration method presented in this paper.

2.2.4 Conclusions

Calibrating XRF-CS output data from polluted marine sediments is critical to obtain absolute concentrations at high resolution in a rapid, non-destructive and continuous way. Practical issues to take fully into account when converting XRF-CS semi-quantitative data into quantitative data are the physical properties of the sediment (e.g. pore water content, grain size, sediment irregularities and changes in matrix) and the selected excitation configuration parameters, as both have an influence on measurements. The resulting errors in the linear function of the calibration should be addressed so that the quality of the calibrated metal concentration data could be assessed. Our results, derived from the analysis of metal-polluted sediments from two locations off Portmán Bay and Barcelona, in the Mediterranean Sea off Spain, demonstrate that the applied calibration procedure improves the quality of the linear

regression for any of the three most widely applied regression methods (OLS, WOLS, and WLS), thus increasing correlation coefficients and reducing the data deviation from the linear function. Of the three regression methods, WLS appears as the best suited as it provides accurate calibrated element concentrations from XRF-CS output data. The WLS method considers the standard deviation of the element intensity and of concentrations in the regression significantly reducing the errors of the calibrated element concentration, which is particularly advantageous when compared with the most commonly used regression method (OLS). Reducing the errors is critical when using XRF-CS calibrations to assess metal pollution levels according to SQGs. Indeed, our results evidence that a fine-tuned calibration of XRF-CS output data using the WLS regression method allows quantifying the Mn, Fe, Zn and Pb concentration limits according three widely used SQGs with low levels of errors, namely 0.4% to 2% for Fe, 1% to 7% for Zn, 3 to 14% for Pb and 5% to 16% for Mn. The only drawback, which is unrelated to the calibration method itself, results from the Pb and As peaks overlap which affects the quantification of As absolute concentrations. Beyond the regression methods assessed to obtain the linear functions (OLS, WOLS, and WLS), this is the first study in incorporating and evaluating the analytical and statistical errors of the calibration of the XRF-CS data, and in evidencing that the errors of the calibrated element concentration must be properly evaluated in future calibration studies.

Acknowledgments We would like to thank the crew of RV Ángeles Alvariño and all scientific and technical staff involved in the NUREIEV and NUREIVA research cruises. We thank Maite Romero, Francisco Menéndez, and Bárbara Baena from the Scientific and Technical Centres of the University of Barcelona for technical assistance with the ICP-OES and ICP-MS. This research has been funded by the research projects NUREIEV (CTM2013-44598-R) and NUREIEVA (ref. CTM2016-75953-C2-1-R), and a Catalan Government Grups de Recerca Consolidats grant to GRC Geociències Marines (ref. 2017 SGR 315). J.F. acknowledges financial support from the Generalitat de Catalunya through a Serra Húnter Tenure-eligible Lecturer contract, and M.C.D from the Ministerio de Economía y Competitividad (PhD fellowship, A-2014-9185) through the NUREIEV project coordinated by GRC Geociències Marines of the Departament de Dinàmica de la Terra i de l'Oceà (Universitat de Barcelona).

2.2.5 References

Adamo, P., Arienzo, M., Imperato, M., Naimo, D., Nardi, G., Stanzione, D., 2005. Distribution and partition of heavy metals in surface and sub-surface sediments

of Naples city port. Chemosphere 61, 800–809. https://doi.org/10.1016/j.chemosphere.2005.04.001

Baucells, M., Lacort, G., Roura, M., de Gyves, J., 1988. Rapid determination of arsenic in the presence of lead in a zinc sulphide matrix by X-ray fluorescence spectrometry. Analyst 113, 1325–1328.

Böning, P., Bard, E., Rose, J., 2007. Toward direct, micron-scale XRF elemental maps and quantitative profiles of wet marine sediments. Geochemistry, Geophys. Geosystems 8. https://doi.org/10.1029/2006GC001480

Buccolieri, A., Buccolieri, G., Cardellicchio, N., Dell'Atti, A., Di Leo, A., Maci, A., 2006. Heavy metals in marine sediments of Taranto Gulf (Ionian Sea, Southern Italy). Mar. Chem. 99, 227–235. https://doi.org/10.1016/j.marchem.2005.09.009

Calvert, S.E., Pedersen, T.F., 2007. Chapter Fourteen Elemental Proxies for Palaeoclimatic and Palaeoceanographic Variability in Marine Sediments: Interpretation and Application. Dev. Mar. Geol. 1, 567–644. https://doi.org/10.1016/S1572-5480(07)01019-6

Canals, M., Party, S., 2015. The two-vessel cruise to Portman Bay, SE Spain: a breakthrough experience. MIDAS Newsl. 3, 1–6.

Casado-Martínez, M.C., Buceta, J.L., Belzunce, M.J., DelValls, T.A., 2006. Using sediment quality guidelines for dredged material management in commercial ports from Spain. Environ. Int. 32, 388–396. https://doi.org/10.1016/j.envint.2005.09.003

Cerdà-Domènech, M., Sanchez-Vidal, A., Frigola, J., Baraza, T., Andrade, L., Amblas, D., Canals, M., 2016. Multi-proxy characterization of the mine tailings deposit of Portmán Bay, SE Spain, in: Comission, M.S., Commission Internationale pour l'Exploration Scientifique de la mer Méditerranée (Eds.), .

Chen, Q., Kissel, C., Govin, A., Liu, Z., Xie, X., 2016. Correction of interstitial water changes in calibration methods applied to XRF core-scanning major elements in long sediment cores: Case study from the South China Sea. Geochemistry, Geophys. Geosystems 17, 1925–1934. https://doi.org/10.1002/2016GC006320

Christophoridis, C., Dedepsidis, D., Fytianos, K., 2009. Occurrence and distribution of selected heavy metals in the surface sediments of Thermaikos Gulf, N. Greece. Assessment using pollution indicators. J. Hazard. Mater. 168, 1082–1091. https://doi.org/10.1016/j.jhazmat.2009.02.154

Comisión nacional de estrategias de Marinas, 2015. Directrices para la caracterización del material dragado y su reubicación en aguas del dominio público marítimo-

terrestre, Ministerio de agricultura, alimentación y medio ambiente.

Croudace, I.W., Rothwell, R.G., 2015. Future developments and innovations in high-resolution core scanning, in: Micro-XRF Studies of Sediment Cores. Springer, pp. 627–647.

Croudace, I.W., Teasdale, P.A., Cundy, A.B., 2019. 200-year industrial archaeological record preserved in an Isle of Man saltmarsh sediment sequence: Geochemical and radiochronological evidence. Quat. Int. 514, 195–203. https://doi.org/10.1016/j.quaint.2018.09.045

Croudace, I.W., Warwick, P.E., Morris, J.E., 2012. Evidence for the preservation of technogenic tritiated organic compounds in an estuarine sedimentary environment. Environ. Sci. Technol. 46, 5704–5712. https://doi.org/10.1021/es204247f

Deming, W.E., 1943. Statistical adjustment of data., Dover Publications. Wiley.

Di Leonardo, R., Bellanca, A., Angelone, M., Leonardi, M., Neri, R., 2008. Impact of human activities on the central Mediterranean offshore: Evidence from Hg distribution in box-core sediments from the Ionian Sea. Appl. Geochemistry 23, 3756–3766. https://doi.org/10.1016/j.apgeochem.2008.09.010

Din, Z.B., 1992. Use of aluminium to normalize heavy-metal data from estuarine and coastal sediments of Straits of Melaka. Mar. Pollut. Bull. 24, 484-491 https://doi.org/10.1016/0025-326X(92)90472-I

Fatoki, O.S., Mathabatha, S., 2001. An assessment of heavy metal pollution in the East London and Port Elizabeth harbours. Water SA 27, 233–240. https://doi.org/10.4314/wsa.v27i2.4997

Fukushima, K., Saino, T., Kodama, Y., 1992. Trace metal contamination in Tokyo Bay, Japan. Sci. Total Environ. 125, 373–389. https://doi.org/10.1016/0048-9697(92)90402-E

Garcia-Orellana, J., Cañas, L., Masqué, P., Obrador, B., Olid, C., Pretus, J., 2011. Chronological reconstruction of metal contamination in the Port of Maó (Minorca, Spain). Mar. Pollut. Bull. 62, 1632–1640. https://doi.org/10.1016/j.marpolbul.2011.06.013

Gómez-García, C., Martin-Hernandez, F., López García, J.Á., Martínez-Pagón, P., Manteca, J.I., Carmona, 2015. Rock magnetic characterization of the mine tailings in Portman Bay (Murcia, Spain) and its contribution to the understanding of the bay infilling process. J. Appl. Geophys. 120, 48–59. https://doi.org/10.1016/j.jappgeo.2015.06.008

Guo, Y., Yang, S., 2016. Heavy metal enrichments in the Changjiang (Yangtze River) catchment and on the inner shelf of the East China Sea over the last 150 years. Sci. Total Environ. 543, 105–115. https://doi.org/10.1016/j.scitotenv.2015.11.012

Hanebuth, T.J.J., King, M.L., Mendes, I., Lebreiro, S., Lobo, F.J., Oberle, F.K., Antón, L., Ferreira, P.A., Reguera, M.I., 2018. Hazard potential of widespread but hidden historic offshore heavy metal (Pb, Zn) contamination (Gulf of Cadiz, Spain). Sci. Total Environ. 637–638, 561–576. https://doi.org/10.1016/j.scitotenv.2018.04.352

Hanebuth, T.J.J., Zhang, W., Hofmann, A.L., Löwemark, L.A., Schwenk, T., 2015. Oceanic density fronts steering bottom-current induced sedimentation deduced from a 50ka contourite-drift record and numerical modeling (off NW Spain). Quat. Sci. Rev. 112, 207–225. https://doi.org/10.1016/j.quascirev.2015.01.027

Hennekam, R., de Lange, G., De Rick, G., 2012. X-ray fluorescence core scanning of wet marine sediments: Methods to improve quality and reproducibility of highresolution paleoenvironmental records. Limnol. Oceanogr. Methods 10, 991–1003. https://doi.org/10.4319/lom.2012.10.991

Hennekam, R., De Rick, G., 2012. X-ray fluorescence core scanning of wet marine sediments: Methods to improve quality and reproducibility of highresolution paleoenvironmental records. Limnol. Oceanogr. Methods 10. https://doi.org/10.4319/lom.2012.10.991

Hennekam, R., Sweere, T., Tjallingii, R., de Lange, G.J., Reichart, G.J., 2018. Trace metal analysis of sediment cores using a novel X-ray fluorescence core scanning method. Quat. Int. 514, 55–67. https://doi.org/10.1016/j.quaint.2018.10.018

Hunt, J.E., Croudace, I.W., Maclachlan, S.E., 2015. Use of Calibrated Itrax-XRF data in determining turbidite Geochemistry and provenance in Agadir Basin, Northwest African Passive Margin, in: Micro-XRF Studies of Sediment Cores: Applications of a Non-Destructive Tool for Environmental Sciences. pp. 127–146. https://doi.org/10.1007/978

Jansen, J.H.. H.F., Van der Gaast, S.. J., Koster, B., Vaars, A.. J., 1998. CORTEX, a shipboard XRF-scanner for element analyses in split sediment cores. Mar. Geol. 151, 143–153. https://doi.org/10.1016/S0025-3227(98)00074-7

Kelloway, S.J., Ward, C.R., Marjo, C.E., Wainwright, I.E., Cohen, D.R., 2014. Quantitative chemical profiling of coal using core-scanning X-ray fluorescence techniques. Int. J. Coal Geol. 128, 55–67. https://doi.org/10.1016/j.coal.2014.04.006

Kido, Y., Koshikawa, T., Tada, R., 2006. Rapid and quantitative major element analysis method for wet fine-grained sediments using an XRF microscanner. Mar. Geol. 229, 209–225. https://doi.org/10.1016/j.margeo.2006.03.002

Kruge, M.A., Permanyer, A., Serra, J., Yu, D., 2010. Geochemical investigation of an offshore sewage sludge deposit, Barcelona, Catalonia, Spain. J. Anal. Appl. Pyrolysis 89, 204–217. https://doi.org/10.1016/j.jaap.2010.08.005

Long, E.R., Macdonald, D.D., Smith, S.L., Calder, F.D., 1995. Incidence of adverse biological effects within ranges of chemical concentrations in marine and estuarine sediments. Environ. Manage. 19, 81–97. https://doi.org/10.1007/BF02472006

Löwemark, L., Chen, H.-F., Yang, T.-N., Kylander, M., Yu, E.-F., Hsu, Y.-W., Lee, T.-Q., Song, S.-R., Jarvis, S., 2011. Normalizing XRF-scanner data: A cautionary note on the interpretation of high-resolution records from organic-rich lakes. J. Asian Earth Sci. 40, 1250–1256. https://doi.org/10.1016/j.jseaes.2010.06.002

Lyle, M., Backman, J., 2013. Data report: calibration of XRF-estimated CaCO3 along the Site U1338 splice, in: 320. p. 321. https://doi.org/10.2204/iodp.proc.320321.205.2013

MacLachlan, S.E., Hunt, J.E., Croudace, I.W., 2015. An empirical assessment of variable water content and grain-size on X-ray fluorescence core-scanning measurements of deep sea sediments, in: Micro-XRF Studies of Sediment Cores. Springer, pp. 173–185.

Manteca, J.I., Garcia, J.Á.L., Oyarzun, R., Carmona, C., 2014. The beach placer iron deposit of Portman Bay, Murcia, SE Spain: The result of 33 years of tailings disposal (1957-1990) to the Mediterranean seaside. Miner. Depos. 49, 777–783. https://doi.org/10.1007/s00126-014-0511-x

Martínez-Gómez, C., Fernández, B., Benedicto, J., Valdés, J., Campillo, J.A., León, V.M., Vethaak, A.D., 2012. Health status of red mullets from polluted areas of the Spanish Mediterranean coast, with special reference to Portmán (SE Spain). Mar. Environ. Res. 77, 50–59. https://doi.org/10.1016/j.marenvres.2012.02.002

Mejía-Piña, K.G., Huerta-Diaz, M.A., González-Yajimovich, O., 2016. Calibration of handheld X-ray fluorescence (XRF) equipment for optimum determination of elemental concentrations in sediment samples. Talanta 161, 359–367. https://doi.org/10.1016/j.talanta.2016.08.066

Morillo, J., Usero, J., Gracia, I., 2004. Heavy metal distribution in marine sediments from the southwest coast of Spain. Chemosphere 55, 431–442. https://doi.

org/10.1016/j.chemosphere.2003.10.047

Oyarzun, R., Manteca Martínez, J.I., López García, J.A., Carmona, C., 2013. An account of the events that led to full bay infilling with sulfide tailings at Portman (Spain), and the search for "black swans" in a potential land reclamation scenario. Sci. Total Environ. 454–455, 245–9. https://doi.org/10.1016/j.scitotenv.2013.03.030

Palanques, A., Lopez, L., Guillén, J., Puig, P., Masqué, P., 2017. Decline of trace metal pollution in the bottom sediments of the Barcelona City continental shelf (NW Mediterranean). Sci. Total Environ. 579, 755–767. https://doi.org/10.1016/j.scitotenv.2016.11.031

Palanques, A., Masqué, P., Puig, P., Sanchez-Cabeza, J.A., Frignani, M., Alvisi, F., 2008. Anthropogenic trace metals in the sedimentary record of the Llobregat continental shelf and adjacent Foix Submarine Canyon (northwestern Mediterranean). Mar. Geol. 248, 213–227. https://doi.org/10.1016/j.margeo.2007.11.001

Palanques, A., Sanchez-Cabeza, J.A., Masqué, P., León, L., 1998. Historical record of heavy metals in a highly contaminated Mediterranean deposit: The Besos prodelta. Mar. Chem. 61, 209–217. https://doi.org/10.1016/S0304-4203(98)00020-6

Pan, K., Wang, W.X., 2012. Trace metal contamination in estuarine and coastal environments in China. Sci. Total Environ. 421, 3–16. https://doi.org/10.1016/j.scitotenv.2011.03.013

Persaud, D., Jaagumagi, R., Hayton, A., 1993. Guidelines for the protection and management of aquatic sediment quality in Ontario.

Piippanen, T., Rautiainen, J., Tummavuori, J., 1997. Determination of copper, iron, molybdenum and silicon in hydrometallurgically roasted molybdenite concentrate solution by inductively coupled plasma atomic emission spectrometry. Anal. Chim. Acta 349, 327–331. https://doi.org/10.1016/S0003-2670(97)00190-6

Pourabadehei, M., Mulligan, C.N., 2016. Selection of an appropriate management strategy for contaminated sediment: A case study at a shallow contaminated harbour in Quebec, Canada. Environ. Pollut. 219, 846–857. https://doi.org/10.1016/j.envpol.2016.08.012

Ramsey, M.H., Potts, P.J., Webb, P.C., Watkins, P., Watson, J.S., Coles, B.J., 1995. An objective assessment of analytical method precision: comparison of ICP-AES and XRF for the analysis of silicate rocks. Chem. Geol. 124, 1–19. https://

doi.org/10.1016/0009-2541(95)00020-M

Richter, T.O., van der Gaast, S., Koster, B., Vaars, A., Gieles, R., de Stigter, H.C., De Haas, H., van Weering, T.C.E., 2006. The Avaatech XRF Core Scanner: technical description and applications to NE Atlantic sediments. Geol. Soc. London, Spec. Publ. 267, 39–50. https://doi.org/10.1144/GSL.SP.2006.267.01.03

Rodríguez-Germade, I., Rubio, B., Rey, D., Borrego, J., 2015a. Detection and Monitoring of REEs and Related Trace Elements with an ItraxTM Core Scanner in the Ría de Huelva (SW Spain). Water, Air, Soil Pollut. 226, 137. https://doi.org/10.1007/s11270-015-2389-3

Rodríguez-Germade, Isabel, Rubio, B., Rey, D., Vilas, F., López-Rodríguez, C.F., Comas, M.C., Martínez-Ruiz, F., 2015b. Optimization of Itrax core scanner measurement conditions for sediments from submarine mud volcanoes, in: Micro-XRF Studies of Sediment Cores. Springer, pp. 103–126.

Rollinson, H.R., 1993. Using geochemical data: evaluation. Present. Interpret. Singapore. Ongman.

Rothwell, R.G., Croudace, I. w., 2015. Twenty Years of XRF Core Scanning Marine Sediments: What Do Geochemical Proxies Tell Us? pp. 25–102. https://doi.org/10.1007/978-94-017-9849-5_2

Rothwell, R.G., Rack, F.R., 2006. New techniques in sediment core analysis: an introduction. Geol. Soc. London, Spec. Publ. 267, 1–29. https://doi.org/10.1144/GSL.SP.2006.267.01.01

Rubio, B., Álvarez-Iglesias, P., Vilas, F., 2010. Diagenesis and anthropogenesis of metals in the recent Holocene sedimentary record of the Ría de Vigo (NW Spain). Mar. Pollut. Bull. 60, 1122–1129. https://doi.org/10.1016/j.marpolbul.2010.04.014

Saylor, R.D., Edgerton, E.S., Hartsell, B.E., 2006. Linear regression techniques for use in the EC tracer method of secondary organic aerosol estimation. Atmos. Environ. 40, 7546–7556. https://doi.org/10.1016/j.atmosenv.2006.07.018

Scholze, F., Longoni, A., Fiorini, C., Strüder, L., Meidinger, N., Hartmann, R., Kawahara, N., Shoji, T., 2006. X-Ray Detectors and XRF Detection Channels, in: Handbook of Practical X-Ray Fluorescence Analysis. Springer, pp. 199–308.

Spofforth, D.J.A., Pälike, H., Green, D., 2008. Paleogene record of elemental concentrations in sediments from the Arctic Ocean obtained by XRF analyses. Paleoceanography 23. https://doi.org/10.1029/2007PA001489

Sprovieri, M., Feo, M.L., Prevedello, L., Manta, D.S., Sammartino, S., Tamburrino,

S., Marsella, E., 2007. Heavy metals, polycyclic aromatic hydrocarbons and polychlorinated biphenyls in surface sediments of the Naples harbour (southern Italy). Chemosphere 67, 998–1009. https://doi.org/10.1016/j.chemosphere.2006.10.055

Taylor, B.N., Kuyatt, C.E., 1994. Guidelines for evaluating and expressing the uncertainty of NIST measurement results. US Department of Commerce, Technology Administration, National Institute of Standards and Technology Gaithersburg, MD.

Tjallingii, Rik, Röhl, U., Kölling, M., Bickert, T., 2007. Influence of the water content on X-ray fluorescence core-scanning measurements in soft marine sediments. Geochemistry, Geophys. Geosystems 8. https://doi.org/10.1029/2006GC001393

U.S. Environmental Protection Agency, 2005. Contaminated sediment remediation guidance for hazardous waste sites, Office of Solid Waste and Emergency Response.

Webster, I.T., Hancock, G.J., Murray, A.S., 1995. Modelling the effect of salinity on radium desorption from sediments. Geochim. Cosmochim. Acta 59, 2469–2476. https://doi.org/10.1016/0016-7037(95)00141-7

Weltje, G.J., Tjallingii, R., 2008. Calibration of XRF core scanners for quantitative geochemical logging of sediment cores: Theory and application. Earth Planet. Sci. Lett. 274, 423–438. https://doi.org/10.1016/j.epsl.2008.07.054

York, D., Evensen, N.M., Martínez, M.L., De Basabe Delgado, J., 2004. Unified equations for the slope, intercept, and standard errors of the best straight line. Am. J. Phys. 72, 367–375. https://doi.org/10.1119/1.1632486

2.3 Physical and geochemical characterization of a submarine sulfide mine tailings deposit, Portmán Bay, SE Spain

Marc Cerdà-Domènech[a], Jaime Frigola[a], Anna Sanchez-Vidal[a], Nil Rodés[a], Maarten Van Daele[b], Marijn Boone[c], Andrea Baza[a], David Amblas[a], Emma Soldevilla[a], Jordi Garcia-Orellana[d,e], Miquel Canals[a] and Josep Roqué[f]

[(a)] GRC Geociències Marines, Departament de Dinàmica de la Terra i de l'Oceà, Facultat de Ciències de la Terra, Universitat de Barcelona, Barcelona, Spain
[(b)] Renard Centre of Marine Geology, Ghent University, Gent, Belgium.
[(c)] Centre for X-ray Tomography (UGCT), Department of Physics and Astronomy, Ghent University, Ghent, Belgium
[(d)] Institut de Ciència i Tecnologia Ambientals (ICTA), Universitat Autònoma de Barcelona, 08193 Bellaterra, Spain.
[(e)] Departament de Física, Universitat Autònoma de Barcelona, 08193 Bellaterra, Spain.
[(f)] Departament de Mineralogia, Petrologia i Geologia Ambiental, Facultat de Ciències de la Terra, Universitat de Barcelona, Barcelona, Spain.

Keywords: mine tailings, metals, contaminated sediment, XRF core scanner, metal(loid)

Abstract Disposal of mine wastes from sulfide ores in the coastal environment has been recognized as a critical source of metals and metalloids (metal(loid)s) into the water column and seabed sediments, also leading to benthic habitat loss and ecotoxicological impacts. Portmán Bay, SE of Spain, represents one of the most severe cases of mine-derived coastal impact all over the world. During thirty-three years (1957-1990), 57 million of tons of artificial soils rich in metal(loid)s (Fe, Mn, Zn, Pb and As) were directly discharged at the shoreline. Such massive dumping of mine waste resulted in the complete infill of the original Portmán Bay, with the tailings deposit also spreading out on the inner continental shelf. Here, we present the first physical and geochemical characterization of the top layers of the submarine extension of the mine tailings deposit of Portmán Bay together with that of the sediments pre-dating and post-dating such deposit. Fifty-two short sediment cores were analyzed within a multi-proxy approach using non-destructive, high resolution and continuous measuring techniques for determining the physical properties and elemental composition of the materials, to which radiometric dating methods were also applied.

Our results show that metal(loid)s concentrations in the tailings deposit are significantly higher than in other regions of the Mediterranean Basin. Post-dumping sediments present lower metal(loid)s concentrations than the mine tailings themselves, but still are noticeably higher than background concentrations previous to anthropogenic loads. Mean enrichment

factors (EFs) in the topmost sediment layer (0 − 1 cm) are 8 for Mn, 56 for Fe, 22 for Zn, 9 for As and 5 for Pb, respectively. We estimate in the upper sedimentary layer (0 − 14 cm) all over the study area, roughly representing the post-dumping period, a total mass of Mn, Fe, Zn, As and Pb of 6,700, $2.6 \cdot 10^5$, 7,700, 670 and 3,170 t, respectively. These large values evidence a persistent flux of metal(loid)s into the most recent shelf floor sediments some decades after the stopping of mine waste disposal. The dispersion patterns of metal(loid)s during the post-dumping time period is a key component to take into account in view of the potential impact of the remobilization of those materials in the partly started environmental remediation project of Portmán Bay.

2.3.1 Introduction

Mine tailings are the main waste product resulting from the separation of minerals from metal ores during mining operations (Lottermoser, 2010). Ores are generally concentrated by milling and froth flotation processes, which generate a fine-grained waste slurry fraction (Fuerstenau et al., 2007). Tailings resulting from sulfide ores consist of both solid and liquid phases, often with considerable amounts of metals and metalloids (e.g. Mn, Fe, Zn, As, Pb, Co, Cd or Hg), hereafter metal(loid)s, together with chemical products used during the ore concentration process (e.g. flotation reagents, pH regulators, oils, flocculants and coagulants)(Lottermoser, 2010).

The mineralogical composition of the mine tailings is dominated by silicates, carbonates and sulfides that are thermodynamically unstable in the presence of oxygen and water (Lindsay et al., 2015). Factors such as oxygen concentration, pore-water pH and the presence of S-oxidizing control the chemical oxidation processes occurring within mine tailing deposits (Andersen et al., 2001; Descostes et al., 2004; Root et al., 2015). Different combinations of these factors regulate adsorption-desorption, reduction-oxidation and precipitation-dissolution reactions, which in turn influence pore water pH and the mobility of metal(loid)s. It has been demonstrated that the geochemical composition of the mine tailings largely determines the ecotoxicological impacts of metal(loid)s from such deposits (Castilla and Nealler, 1978; Odhiambo et al., 1996; Lancellotti and Stotz, 2004; Sternal et al., 2017).

Mine tailings discharge into the sea is a rather common practice that has been developed as an alternative to land disposal in the last decades (Koski, 2012; Ramirez-Llodra et al., 2015). A variety of water depths and distance to shore schemas have been considered for such dumping, e.g. in very shallow waters close to the shoreline

(Lancellotti and Stotz, 2004; Franks et al., 2011), in deeper waters less than 100 m deep (Ellis and Ellis, 1994) and also at sites far from shore and deeper than 100 m and even 1,000 m (Franks et al., 2011; Hughes et al., 2015). Impacts on ecosystems are depth-related as habitats also are depth-related. Such impacts may be highly relevant in coastal shallow water habitats, which are characterized by high biodiversity and as providers of critical ecosystem services (Gattuso et al., 2018). Those impacts include seabed physical loss by waste placement, physical alteration of e bottom habitats and sediments with the smothering of benthic organisms, release of metal(loid)s within the seawater and sediment, and their bioaccumulation in marine organisms (Ankley, 1996; Mestre et al., 2017).

Some pioneering research have addressed the impacts of mine waste disposal over coastal environments in terms of metal(loid)s speciation and bioavailability together with their impact on benthic biodiversity (Ramirez et al., 2005; Pereira et al., 2008). Mine tailings deposits in coastal settings have been also identified as sources of metal(loid)s to coastal waters (Olsgard and Hasle, 1993; Josefson et al., 2008; Vogt, 2012).

Portmán Bay, in the southeastern coast of Spain, in the Mediterranean Sea, is one of the most striking examples of the impacts of mine waste disposal in coastal settings worldwide (Koski, 2012). From 1957 to 1990, an estimated volume of 57 million tons of sulfide mine tailings rich in Fe, Zn and Pb, but also other metal(loid)s such as As, Cu, Co and Cd, were pumped directly into the sea. Due to the action of waves and coastal currents, the tailings were transported into the bay resulting in its complete infill (Oyarzun et al., 2013) and spread on the inner continental shelf (Cerdà-Domènech et al., 2020).

Previous studies conducted in the emerged part of the tailing deposits of Portmán Bay have reported high contents of Fe, Zn, Pb, As, Cu and Cd, as well as beach black sands mostly made of magnetite (Peña et al., 2013; Manteca et al., 2014). Recent works have detected large metal(loid)s concentrations in pore waters of the emerged tailing deposit resulting for oxidative weathering. Indeed, Alorda-Kleinglass et al. (2019) have shown that part of the dissolved metal(loid)s are remobilized and transferred from the mine tailings to the coastal sea by submarine groundwater discharge (SGD) and pore water exchange (PEX).

The physicochemical properties and the distribution of metal(loid)s in the bulk of the

submarine extension of the mine tailings deposit are barely known even though it contains ~78% of the deposit, i.e. ~45 Mt (Manteca et al., 2014). A couple of studies have shown that the sediment lying on the seafloor present metal(loid)s concentrations that are very close to those observed in the emerged part of the tailings deposit (Martínez-Sánchez et al., 2008; Cerdà-Domènech et al., 2019). Some authors have also reported the presence of metal(loid)s in mussels and sea breams from the area nearby Portmán Bay (Martínez-Sánchez et al., 2008; Llull et al., 2017; Mestre et al., 2017).

The objective of this study is to provide the first physical and geochemical characterization of the uppermost layers of the submarine mine tailing deposit off Portmán Bay (SE, Spain), and to characterize the post-dumping sediments that have accumulated during the almost 30 years after the cessation of mine waste disposal. We equally aim at investigating the dispersal patterns and total mass accumulations of metal(loid)s in post-dumping sediments. Our findings might be of interest in the framework of environmental remediation project of the bay (BOE, 2011; Sánchez and Sirvent, 2013).

2.3.2 Geological context and mine tailing disposal

Portmán Bay is located in the province of Murcia, SE of Spain, where it forms the maritime façade of Sierra de Cartagena-La Unión, or Sierra Minera, which is one of the most important historical mining districts of Spain, where rich Pb-Zn sulfide ores have been exploited since pre-Roman times (Figure 2.12)(García-Lorenzo et al., 2014).

The coastal block of Sierra de Cartagena consists of two basement complexes named Nevado-Filábride (of Paleozoic to Triassic age) and Alpujárride (of Permian to Triassic age) which emerge as overlapping thrust sheets of Alpine age, where the main Pb and Zn ores were found. The mineral association in the Alpujárride sheet (or first "manto") is made of chlorite, sulfides, siderite and silica (paragenesis 1), whereas in the Nevado Filábride (or second "manto") it is composed by greenalite, magnetite, sulfides, siderite and silica (paragenesis 2) (Manteca, 1992).

The most intensive exploitation of the ores took place during the 19th and 20th centuries to obtain Pb, Zn, Ag and Fe. Within the 20th century the exploitation peak occurred during the 1957-1990 period when the company Sociedad Minero

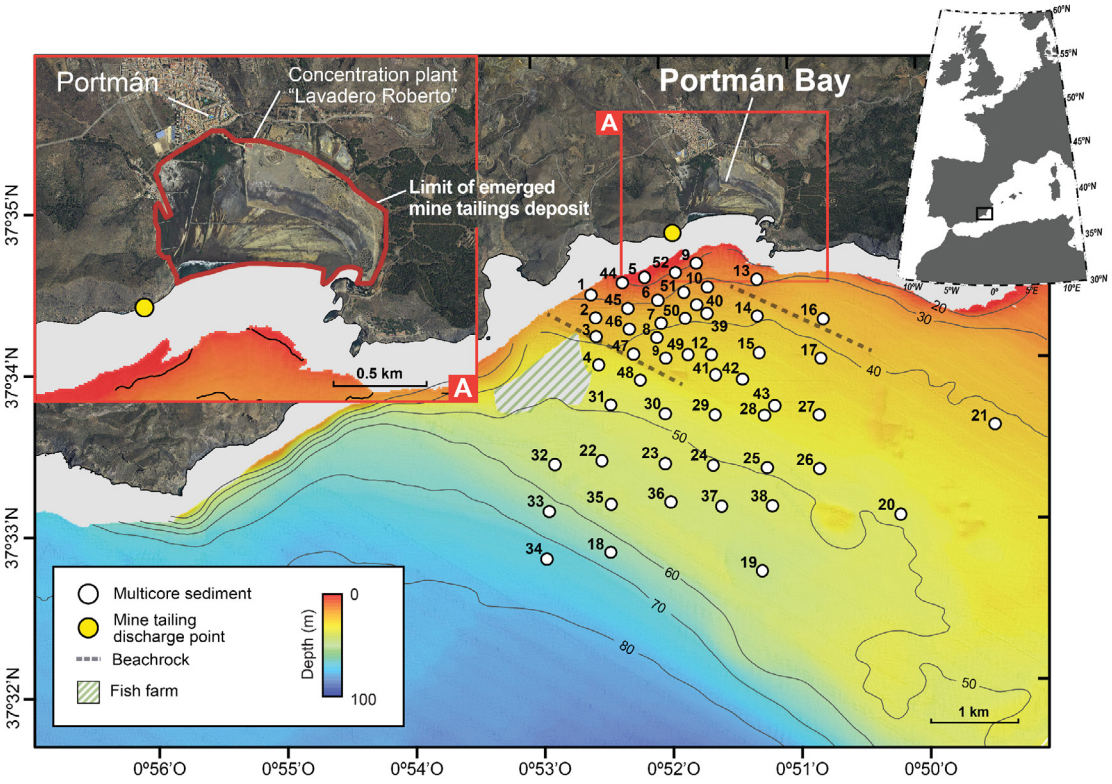

Figura 2.12 Bathymetric map of the inner continental shelf off Portmán Bay showing the location of the sampling stations (white dots) where the sediment cores analyzed in this study were collected, the mine tailing discharge point (yellow dot). Contours every 10 m. (A) Zoom of Portmán Bay in 2010 infilled with mine waste.

Metalúrgica Peñarroya España developed large-scale open-pit mining (Manteca, 1992). During this 33 years long period, large volumes of ores were milled until a grain-size of d80<180 μm and selectively separated and concentrated in a processing plant known as "Lavadero Roberto" (Figure 2.12.A). There, target minerals as galena, sphalerite and pyrite were separated from bulk ore by differential froth flotation to physically sort particles according to their hydrophilic behavior (Kawatra, 2011). Froth flotation depends on the ability of air burbles to adhere to specific mineral surfaces in a slurry. Those bubbles adhere to more hydrophobic particles that are subsequently carried to the surface of the liquid and solid mixture, where they concentrate and can be easily removed. Contrarily, hydrophilic particles remain in the liquid matrix and are incorporated to the mining residues or tailings. Additionally, part of the pyrite was removed from the primary tailings in a subsequent flotation step to produce sulfuric acid. From 1959 to 1967, magnetite was also recovered (Oyarzun et al., 2013).

From 1957 to 1990 the concentration plant processed 59,655,000 t of sulfide ores, of which 3,418,000 t were sulfide concentrates for Zn and Pb recovery, and 56,237,000 t were pumped into the sea as metal-rich hazardous tailings by means of a pipeline opening on the shoreline at short distance from the western edge of Portmán Bay (Manteca et al., 2014) (Figure 2.12). The tailings were made of clay, silt and sand grain sizes and were composed of carbonates (35.9 %), phyllosilicates (25.7 %), silica (20.0 %), Fe oxides (15.6 %) and sulfides (mainly pyrite). Recently, Cerdà-Domènech et al. (2020) have further evidenced the high concentrations of metal(loid)s in the tailings, with 1600 to 3400 ppm of Ti, 200 to 7000 ppm of Mn,1 to 26 % of Fe, 50 to 7300 ppm of Zn, 20 to 800 ppm of As and 40 to 5400 ppm of Pb.

From the discharge point the tailings spread into the bay and over the nearby inner continental shelf where they form nowadays a >10 m thick deposit in some places (unpublished data). The progressive accumulation of waste led to the complete infill of the original bay, subsequently causing a 500 − 600 m seaward shift of the shoreline (Manteca et al., 2014). In an early study, Pauc and Thibault (1976) concluded that wave action and associated coastal currents controlled the tailings sedimentation patterns and grain size distribution in Portmán Bay, with the bay's infill proceeding in roughly parallel fringes from west − where the discharge point was − to east. The coarser ferromagnetic grains mostly accumulated along a prograding foreshore and the inner nearshore, as shown by Peña et al. (2013), whereas fine-grained particles likely increase with water depth.

2.3.3 Materials and methods

2.3.3.1 Sample collection

Fifty-two short sediment cores (up to 50 cm long) from the submerged mine tailing deposit were collected with a multicorer system in August 2014 and March 2015 in the framework of EC and Spanish funded research projects MIDAS and NUREIEV, respectively (Figure 2.12). The multicorer system allowed recovering 6 tubs of sediments maximum 60 cm length, with very good preservation of the water-sediment interface. Once onboard, for each station, a sediment core was described and sliced at 1 cm intervals for grain-size analyses, and a second undisturbed sediment core was stored in a PVC tube for the non-destructive analyses.

2.3.3.2 Analytical procedures

2.3.3.2.1 High-resolution 3D imagery of sediment cores

High-resolution 3D volume reconstruction of the sediment cores was performed by means of a micro-X-ray Computed Tomography system (micro-CT, MultiTom Core from X-Ray Engineering) at the CORELAB Laboratory of the University of Barcelona. This equipment allows to quantify the X-ray attenuation produced by the analyzed object in multiple projections around 360° orientation, providing a 3D volume reconstruction of the inner density changes of the object scaled in grey levels, where darker and lighter zones represents lower and higher X-ray attenuation (Frigola et al., 2015). The scan was performed at 120 kV, 80W, exposure time of 120 second, and 1001 projections, resulting in a "voxel" resolution (volumetric pixel or cubic unit representing a 3D object; Duliu, 1999) of 0.125 x 0.125 x 0.125 mm. The micro-CT analysis of the whole set of cores resulted in ~$1.4 \cdot 10^5$ images (Tiff format), with a total weight of 1.30 Tb and more than 1.01 x 10^{12} bytes of data. Acquisition and reconstruction of 3D raw data were carried out with Acquila and RECON software packages (X ray Engineering) and finally processed using the Avizo (ThermoFisher Scientific) scientific data visualization and analysis software as well as the open source software ImageJ.

2.3.2.2.2 Elemental composition

The elemental chemical characterization of the materials was determined using an Avaatech XRF core scanner (XRF-CS) at the CORELAB laboratory of the University of Barcelona, which provides rapid, non-destructive, continuous and high-resolution scanning sediment cores (Jansen et al., 1998; Rothwell and Rack, 2006; Croudace and Rothwell, 2015). The XRF-CS was equipped with an Oxford Rhodium X-ray source (4 − 50 kV) and a Canberra X - Pips 1500 − 1.5 detector with a 125-μm beryllium window and a multichannel analyzer Canberra DSA 1000 (MCA). This configuration allows detecting a wide range of emission spectrum for elements with the atomic weight from Al to U.

Prior to scanning, the split cores were left for 16h at room temperature to reduce water content and the subsequent radiation absorption, thus increasing the intensity signal measured (Böning et al., 2007; Tjallingii et al., 2008). Then, cores were covered with an Ultralene X-ray transmission foil (4 μm width) to avoid desiccation and potential contamination, and finally scanned at 2 mm resolution. The excitation configuration

parameters used were 10 kV, 1.2 mA and 10 s without filter for elements with atomic weights between Al and Fe, and 30 kV, 1.6 mA current 50 s, with a Pd-thick filter for elements with atomic weights between Ni and Pb. The integration of the elemental peaks and the estimation of their intensity areas, expressed as counts per seconds (cps), was performed by means of bAxil spectrum analysis software (BrightSpec). For most of the target elements the integration of the peaks was carried out on the Kα X-ray emission lines (e.g. Mn, Fe, Zn and As). However, we used Lβ emission line for Pb in order to reduce the effect overlap with the As X-ray emission (Cerdà-Domènech et al., 2020). Since it was already known from previous studies that the mine tailings were rich in sulfur minerals as galena and sphalerite and also Fe and Mn oxides (Manteca et al., 2014; Cerdà-Domènech et al., 2020), the target elements selected in our study are Mn, Fe, Zn, As and Pb.

The high-resolution elemental intensity records obtained by means of XRF-CS were calibrated to absolute elemental concentrations by analyzing a relative small set of samples. Thus, we used the linear function obtained by Weighted Least Square model (WLS) described by Cerdà-Domènech et al., (2020). This calibration considers both analytical and statistical errors on the regression model that allows improving the accuracy of the regressions with higher correlation coefficients (0.99, 0.98, 0.96, 0.97 and 0.95 Mn, Fe, Zn, As and Pb, respectively) significantly reducing the associated errors of predicted concentrations.

2.3.3.2.3 Physical properties

Wet-bulk density (or gamma density) and magnetic susceptibility of the materials were determined with a Geotek Multi-Sensor Core Logger (MSCLs) at the CORELAB laboratory of the University of Barcelona. The MSCL provides simultaneous, continuous, high-resolution and non-destructive measurements of the physical properties of the sediments in whole or split sediment cores (Schultheiss and Weaver, 1992; Frigola et al., 2015). After equilibration to ambient room temperature (~20°C), the measurements were carried out at half-centimeter intervals. Fractional porosity was also estimated using gamma ray attenuation and assuming a grain density of 2.65 g cm^{-3} (quartz) and a water density of 1.025 g cm^{-3}.

2.3.3.2.4 Grain-size distribution

Grain-size de-carbonate characterization of the sediment cores was determined using a Coulter LS230 laser particle size analyzer at the Sedimentological Laboratory of the

University of Barcelona. Before the analysis, sediment samples were treated with 50 mL of 10% hydrogen peroxide to oxidize the organic matter, while carbonates were removed by the addition of 35 mL of 2.7% acetic acid—0.34 M sodium acetate solution (pH = 4). Samples were suspended and disaggregated with sodium polyphosphate for 4 hours and introduced into the particle size analyzer, which measures the percentage volume of particles in 116 size classes between 0.04 μm and 2,000 μm.

2.3.3.2.5 Background metal and metalloids concentration and enrichment factors

Determining metal(loid)s background levels prior to mine tailings discharge is necessary to assess the resulting levels of metal(loid)s contamination. The most common approach is to analyzing metal(loid)s concentrations in sediment samples from subsurface depths large enough to be devoid from the influence of the shallower contaminated layers and from bioturbation mixing (Loring, 1991). In the current study, we have assume that pre-dumping background metal(loid)s concentrations are those measured on the bottom of the more distal sediment cores MC-20, MC-36 and MC-37, where the tailings and post-tailings layers are very thin (Figure 2.12).

Background levels for Mn, Fe, Zn, As and Pb were constrained by averaging the three lowest concentrations previously determined by Cerdà-Domènech et al. (2020) on those cores (Table 2.6).

	Depth core	**Mn**	**Fe**	**Zn**	**As**	**Pb**
	cm	mg kg^{-1}	%	mg kg^{-1}	mg kg^{-1}	mg kg^{-1}
MC-20	20	190.9	0.11	43.6	16.1	39.1
MC-36	41	260.1	0.15	158.4	40.8	205.5
MC-37	25	284.6	0.15	152.8	30.7	209.6
Average		245.2	0.14	118.3	29.2	151.4

Table 2.6 Background concentration values of Mn, Fe, Zn, As and Pb on sediment cores MC-20, 36 and 37 and average values (Cerdà-Domènech et al. 2020).

The values thus obtained have been used to determine EFs along the sedimentary column. The EF is an indicator to assess the degree of contamination of the sediment, which generally requires normalization by means of a reference element like Al, Fe, Mn or Pb and grain-size. However, given the significant physicochemical influence of the mine tailings on key properties (e.g. grain-size, density and Al and Fe concentrations) of the marine sediments of the study are, using those variables

could bias EF values. That is why to obtain a qualitative estimation of EFs we have used the following equation:

$$EF = \frac{C_n}{B_n} \quad (13)$$

where, C_n is the measured concentration of a given metal(loid) (n) and B_n represents the background concentration of the same metal(loid) after values from Table 2.6.

2.3.3.2.6 Radiometric analysis

Sediment core MC-36 (Figure 2.12) was analyzed for ^{210}Pb to determine the age model and sedimentation rates. Samples sliced previously into 0.5 cm (0 to 5 cm) and 1 cm (5 cm to core bottom) thick sections were frozen and lyophilized. Radiometric analyses were carried out at Laboratori de Radioactivitat Ambiental of Universitat Autònoma de Barcelona for total ^{210}Pb activities through the measurement of its alpha-emitter daughter nuclide ^{210}Po (Sanchez-Cabeza et al., 1998). 200 − 300 mg samples with ^{209}Po as internal tracer supplied by IAEA (0.7031 ± 0.050 Bq mL^{-1}) were totally digested in acid media using an analytical microwave oven and Po plated on silver discs in HCl 1N at 70 °C while stirring for 8 hours. ^{210}Po activities were determined with an γ-spectrometer equipped with low background silicon surface barrier (SSB) detectors (EG&G Ortec) for 1 − 4 x 10^5 s. Samples were sealed at least 3 weeks prior to counting to allow equilibrium between ^{226}Ra and its short-lived daughters. ^{226}Ra activity was determined from ^{214}Pb through its 351 keV gamma line emission by spectrometry in a coaxial high-purity Ge. Excess ^{210}Pb (^{210}Pb$_{xs}$) was determined by subtracting the ^{226}Ra activity (assumed to represent the supported ^{210}Pb activity) from the total ^{210}Pb activity. The quality of the measurements is assessed through the participation on IAEA proficiency tests and continuous analyses of certificate materials and replicates.

2.3.3.3 Statistical analysis and numerical models

Principal Component analysis (PCA) was performed on the metal(loid)s concentration data of Mn, Fe, Zn, As and Pb. Before applying PCA routine, is necessary to standardize all variables in order to maximize the variance of each component thus improving the visualization of PCA results. In addition, Pearson correlation of metal(loid)s elements was obtained to discuss their physic and chemical relationship.

Both statistical analyses, Pearson correlation and Principal Component Analysis, have been implemented in MATLAB® with 7,279 measurements of metal(loid)s concentrations.

The distribution maps of the metal(loid)s concentration, density and magnetic susceptibility on the uppermost submarine sediments (< 14 cm) were obtained by means scatter interpolating routine of MATLAB®. This procedure performs a 3D interpolation of scattered data set returning an interpolating function that can apply at a predefined grid. Bilinear method was used for interpolation and extrapolation processes, which performs a linear interpolation firstly in one direction and after in the other direction (Lamotte et al., 1997). The grid extension was adjusted at the coordinate boundaries of the sediment cores location with a resolution or voxel size of 10 m x 10 m x 0.002 m. The 3D matrix volume obtained was slightly smoothed with a filter for improving image quality, and finally masked taking in account the morphology of the inner continental shelf of Sierra de Cartagena − La Unión.

2.3.4 Results

2.3.4.1 Sedimentological characterization of sedimentary facies

Six sedimentary facies are identified according to the results obtained from micro-CT and HR photographic imagery, grain-size, gamma density and magnetic susceptibility the analyses on the sediment cores. Twelve cores distributed along one coast-parallel and one mostly coast-perpendicular transects illustrate this perfectly (Figure 2.13). In addition, a detail of the micro-CT image, the grain-size distribution within the de-carbonated fraction, gamma density and magnetic susceptibility for each facies are shown in Figure 2.14.

Facies 1 consists of massive, light yellowish brown to dark brown fine sand with a thickness ranging from ~15 to ~25 cm. The micro-CT images show a homogeneous facies with high amounts of biogenic carbonate structures (i.e. shell fragments) and abundant bioturbation marks (Figure 2.13). Gamma density and magnetic susceptibility records show relatively high values (~1.95 g cm^{-3} and ~1,450 SI 10^{-5}). This facies was only identified in the most distal cores (e.g. at the bottom of core MC-36 and forming the entire MC-20 core).

Facies 2 presents highly laminated sediments, alternating yellowish-brown silts with dark brown fine sands. Its thickness is ~10 − 20 cm, with 0.5 − 1.5 cm thick internal

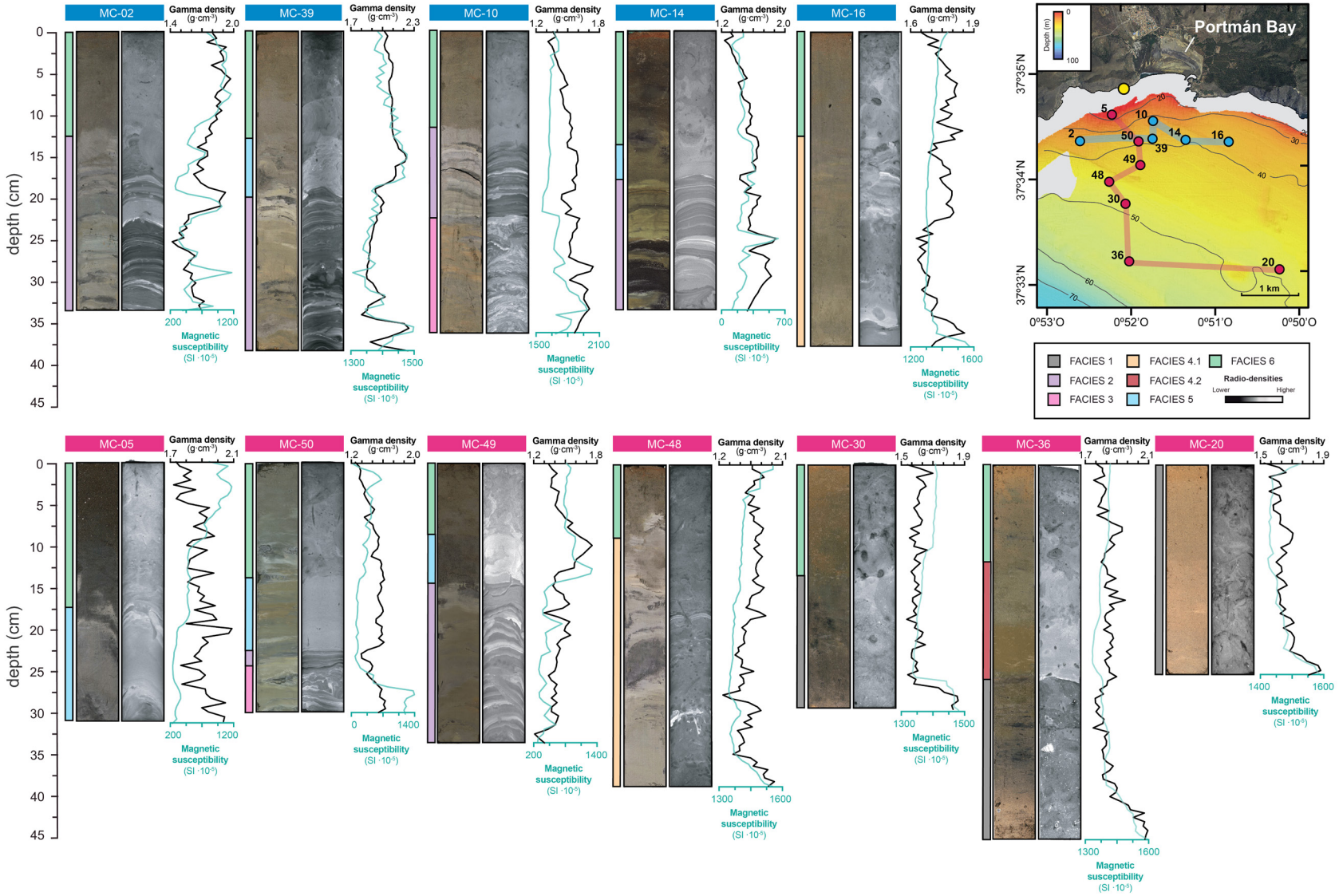

Figura 2.13 Micro-CT and photographic images, gamma density and magnetic susceptibility records from selected sediment cores representative of the mine tailings deposit and other deposits on the inner continental shelf of Portmán Bay. The facies described in the text are color-coded (see legend). The vertical scale is the same for all cores. The location of the cores is shown in the upper right inset map.

layering. It also shows cross-laminated structures, which is clearly visible in the micro-CT images of some cores (e.g. MC-49) where there is no bioturbation. Density values from this facies range from 1.8 to 2.1 g cm^{-3}, while magnetic susceptibility shows values similar to Facies 1 (~1,500 SI 10^{-5}). This facies is more frequent in sediment cores recovered close to the tailings discharge point and progressively disappears southwards and eastwards (Figure 2.13).

Facies 3 consists of highly deformed partly laminated materials made of light yellowish-brown silty materials, with thickness ranging from ~7 to 12 cm. This facies differs from other facies because of its chaotic structure with multiple successions of low and high-density materials (i.e. from 1.81 to 2.08 g cm^{-3}) and a rather high magnetic susceptibility (1,400 to 1,550 SI 10^{-5}). Facies 3 appears only in a few cores from the foot of the submerged slope of the tailings deposit (e.g. MC-10 and MC-50).

Facies 4 consists of light yellowish-brown silts. In micro-CT images it shows a sequence of disturbed and homogeneous layers with bioturbation marks increasing upwards. The structure and thickness of Facies 4 are highly variable, the later ranging from 10 to 40 cm. Also gamma density and magnetic susceptibility values are highly diverse. The later records allow dividing Facies 4 in two sub-facies. Sub-facies 4.1 is characterized by the lowest density values observed (1.65 − 1.75 g cm^{-3}) and by a wide range of magnetic susceptibility values (1,450 − 1,650 SI 10^{-5}). This facies occurs in cores located south of a submerged beachrock (e.g. MC-48) and in the most distal part of the study area to the east. Sub-facies 4.2 is characterized by relatively high densities (~1.9 g cm^{-3}) and lower magnetic susceptibility values (~1,400 SI 10^{-5}) than 4.1, and only appears at intermediate depths in cores MC-22 and MC-36.

Facies 5 is made of homogenous massive grayish brown fine sands. The lower boundary generally presents a smooth contact with lamination from formerly described Facies 2 (e.g. MC-05 and MC-50). This facies always appears between Facies 2 and Facies 6, with a thickness ranging from ~5 to ~25 cm. Bioturbation marks slightly altering the internal sediment structure are evident in some cores (e.g. MC-39). Density and magnetic susceptibility display especially high values from 1.8 to 2.1 g cm^{-3} and from 1,500 to 1,700 SI 10^{-5}, respectively. Facies 5 appears in four sediment cores located from the foot of the submerged slope of the tailings deposit (Figure 2.12).

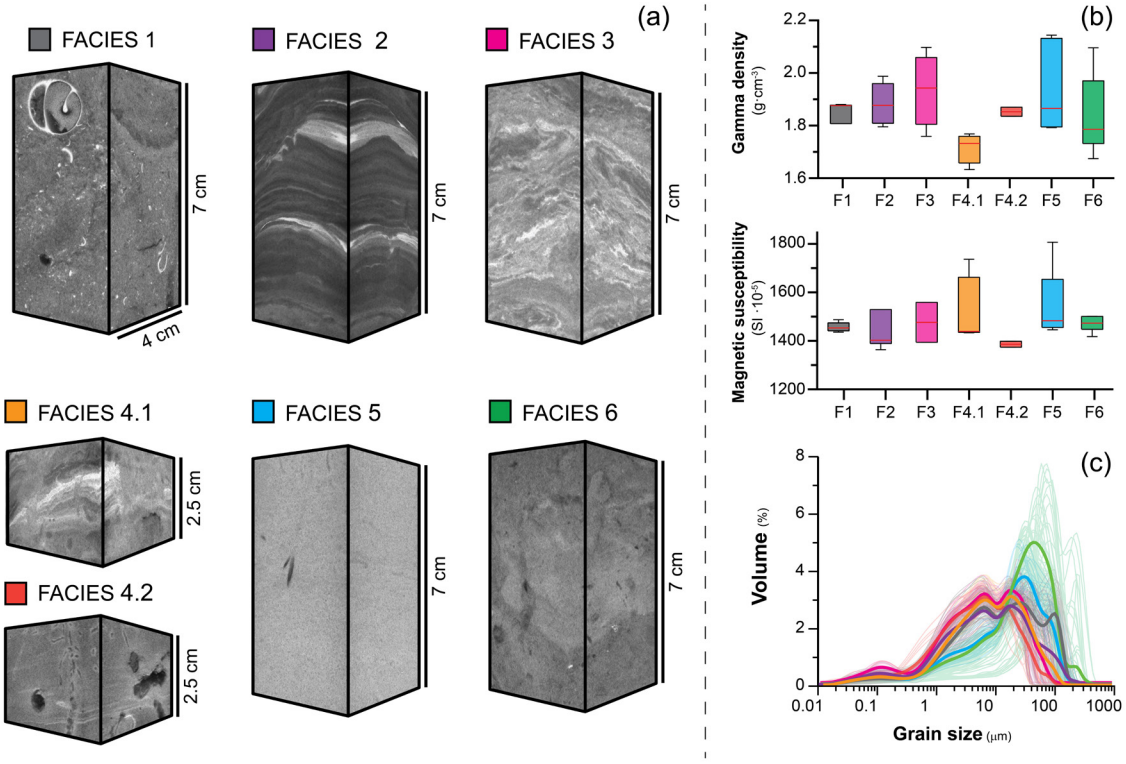

Figura 2.14 a) 3D tomography images of the sedimentary facies described in the main text. b) Gamma density and magnetic susceptibility ranges for each facies. c) Grain size distribution for each facies.

Facies 6 corresponds to the uppermost layer in proximal sediment cores. It consists of dark yellowish-brown silts and fine sands characterized by quite homogeneous and frequent bioturbation marks that increase toward the core top. Micro-CT images show that bioturbation marks at the bottom of this facies gradually fade into Facies 2 and Facies 5. It ranges between ~10 – 14 cm in thickness, being wider in sediments close to the coastline with relatively high density values, i.e. 1.70 – 1.95 g cm^{-3}. The mean magnetic susceptibility, ~1,500 SI 10^{-5}, increases significantly in the northern part of the inner continental shelf, close to shore (e.g. MC-05) (Figure 2.12).

2.3.4.2 Horizontal distribution of sedimentary facies

According to the spatial distribution of the associations of sedimentary facies described above, four main subareas can be distinguished in the study area (Figure 2.15). Subarea 1 extends from 20 to 43 m water depth, from the main body of the mine tailings deposit to the above-mentioned beachrock, which is rather close to the ancient discharge point. The facies association in Subarea 1 consists of the uppermost Facies 6, the laminated Facies 2 and occasionally the homogeneous Facies 5, as found

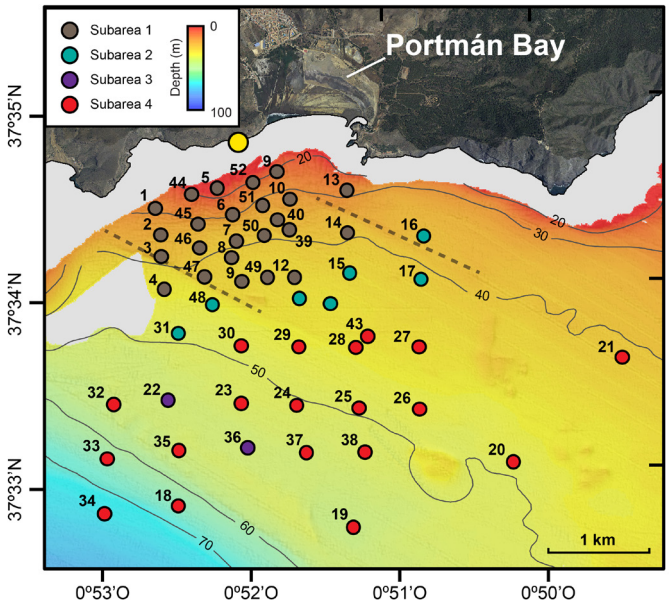

Figura 2.15 Distribution of the main associations of sedimentary facies in the study area, which allows identifying four distinct subareas (see figure legend).

in eighteen cores (Figure 2.15). Subarea 2 extends from the southern boundary of Subarea 1, across the beachrock and to the east. The facies association in Subarea 2 is made of Facies 6 and the highly deformed Sub-facies 4.1 (Figure 2.14). Subarea 3 appears in a small area southwest of Subarea 2, and is characterized by including Sub-facies 4.2 only in cores MC-22 and MC-36. Finally, Subarea 4 is defined by the presence of the biogenic carbonate-rich Facies 1. Subarea 2 has a transitional character between subareas 1 and 4.

2.3.4.3 Sediment geochemistry

The concentrations of Mn, Fe, Zn, As and Pb, and the relative XRF-CS abundances of S and Ca together with gamma density, magnetic susceptibility and grain-size are shown in Figure 2.16 for six representative sediment cores (MC-16, 36, 20, 14, 50 and 2). All metal(loid)s concentration records present a large variability, ranging from 110 to 10,370 mg kg^{-1} for Mn, 1 to 23 % for Fe, <7 to 13,340 mg kg^{-1} for Zn, <17 to 1,710 mg kg^{-1} for As, and 5 to 5,590 mg kg^{-1} for Pb (Table 2.6). Generally, metal(loid)s concentrations are higher close to the old mine tailings discharge point (subareas 1 and 2) to progressively lower in more distal locations (Subarea 4) (Figure 2.15). Even though As contents in core MC-20 are below the detection limit defined in the calibration procedure of XRF-CS by Cerdà-Domènech et al. (2020), they are still higher than those commonly found in Mediterranean Sea sediments (Buccolieri

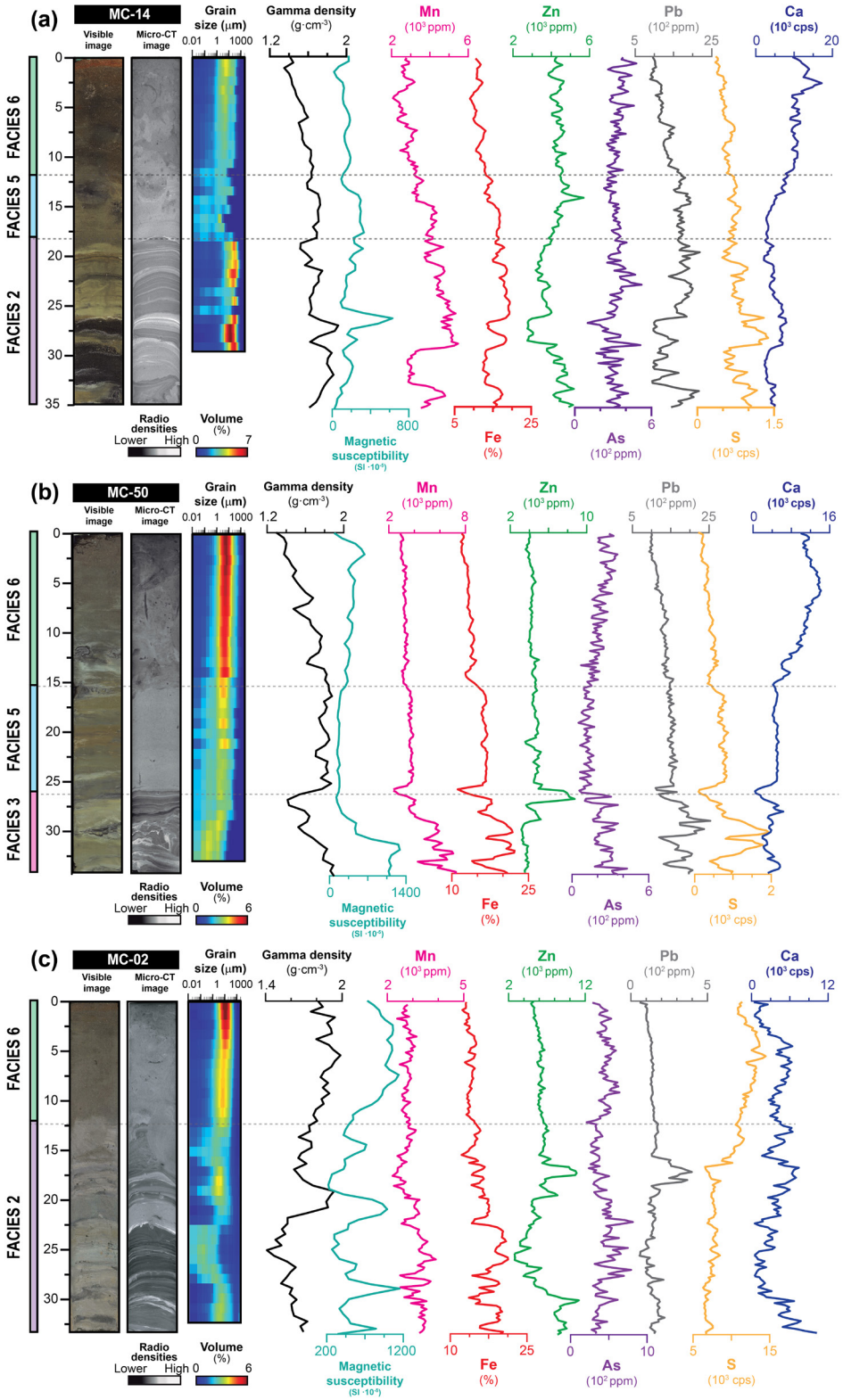

Figura 2.16 Physical and geochemical records of six sediment cores (see location in Figure 2.12). From left to right, sedimentary facies, optical and micro-CT images, heatmap of grain-size distribution, gamma density, magnetic susceptibility, metal(loid)s concentrations (Mn, Fe, Zn, As and Pb) and element intensities (S and Ca). As is not represented in core MC-20 because its contents are below the detection limit defined by Cerdà-Domènech et al. (2020).

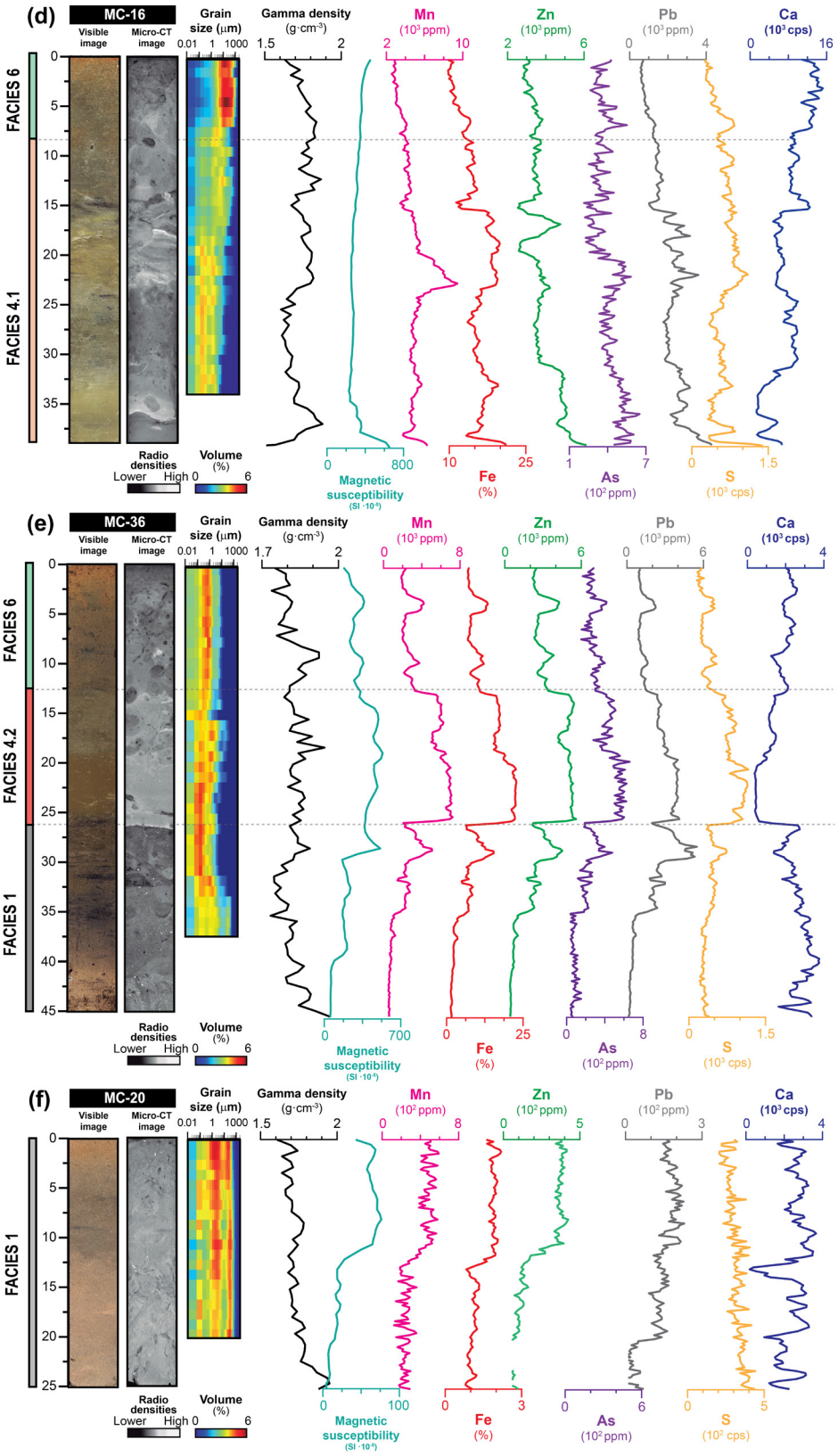
(d)
MC-16
Visible image
Micro-CT image
Grain size (µm)
0.01 1 1000
Gamma density (g·cm-3)
1.5 2
Mn (10³ ppm)
2 10
Zn (10³ ppm)
2 6
Pb (10³ ppm)
0 4
Ca (10³ cps)
0 16
FACIES 6
FACIES 4.1
0 5 10 15 20 25 30 35
Radio densities
Lower High
Volume (%)
0 6
0 800
Magnetic susceptibility (SI ·10⁻⁶)
10 25
Fe (%)
1 7
As (10² ppm)
0 1.5
S (10³ cps)
(e)
MC-36
Visible image
Micro-CT image
Grain size (µm)
0.01 1 1000
Gamma density (g·cm-3)
1.7 2
Mn (10³ ppm)
0 8
Zn (10³ ppm)
0 6
Pb (10³ ppm)
0 6
Ca (10³ cps)
0 4
FACIES 6
FACIES 4.2
FACIES 1
0 5 10 15 20 25 30 35 40 45
Radio densities
Lower High
Volume (%)
0 6
0 700
Magnetic susceptibility (SI ·10⁻⁶)
0 25
Fe (%)
0 8
As (10² ppm)
0 1.5
S (10³ cps)
(f)
MC-20
Visible image
Micro-CT image
Grain size (µm)
0.01 1 1000
Gamma density (g·cm-3)
1.5 2
Mn (10² ppm)
0 8
Zn (10² ppm)
0 5
Pb (10² ppm)
0 3
Ca (10³ cps)
0 4
FACIES 1
0 5 10 15 20 25
Radio densities
Lower High
Volume (%)
0 6
0 100
Magnetic susceptibility (SI ·10⁻⁶)
0 3
Fe (%)
0 6
As (10² ppm)
0 5
S (10² cps)

		Mn	Fe	Zn	As	Pb
		mg kg^{-1}	%	mg kg^{-1}	mg kg^{-1}	mg kg^{-1}
Facies 1	Min	110	1.0	<7	<17	<5
	Max	2,130	7.9	2,150	250	1,470
Facies 2	Min	1,570	8.4	1,260	110	860
	Max	9,920	21.6	13,340	1,710	5,590
Facies 3	Min	1,880	10.4	3,060	140	1,090
	Max	5,290	19.1	8,860	490	2,180
Facies 4,1	Min	1,660	8.2	3,100	210	1,180
	Max	6,890	21.7	11,250	520	4,470
Facies 4,2	Min	1,170	4.7	1,080	60	1,030
	Max	10,370	21.0	6,440	700	4,020
Facies 5	Min	2,460	11.6	2,850	190	1,350
	Max	7,280	23.0	5,330	610	4,190
Facies 6	Min	710	2.4	1,190	120	390
	Max	3,570	16.7	9,420	640	4,200

Table 2.7 Minimum and maximum metal(loid)s concentrations for the sedimentary facies identified in the submarine deposits off Portmán Bay expressed in mg kg^{-1} and % (m/m).

et al., 2006; Sprovieri et al., 2007; Palanques et al., 2008; Christophoridis et al., 2009; Martínez-Gómez et al., 2012), therefore evidencing the high metal enrichment in the submarine deposits off Portmán Bay (Oyarzun et al., 2013).

The identified sedimentary facies can be split in two groups according to metal(loid)s concentrations (Figure 2.16 and Table 2.7). Facies 1 presents the lowest concentrations for all targeted metal(loid)s, with Facies 6 showing slightly higher values. Concentrations of the investigated metal(loid)s are significantly higher in facies 2, 3, 4.1, 4.2, and 5, which are quite similar amongst them. Despite this variability, the more abundant metal(loid)s (i.e. Mn, Fe, Zn and Pb) display similar vertical profiles, with higher concentrations at core bottoms and an upwards-decreasing trend in all cores. The intensity profile of S shows a similar pattern likely due to the high content of sulfur minerals as galena (PbS) and sphalerite (ZnS) in the deposit. It is worth noting that in some sediment cores (e.g. MC-14 and 50), As concentrations slightly increase upwards (Figure 2.16.a,b). The elemental profile of Ca generally shows increasing values towards de top of the cores (e.g. MC-50 and MC-16), and especially high intensities in the bottom unit of MC-36 (Figure 2.16.e).

Pearson's correlation for Mn, Fe, Zn, Pb and As reveals a strong positive correlation ($r^2 > 0.7$), especially for the Mn-Fe-As-Pb cluster, with a statistical significance of

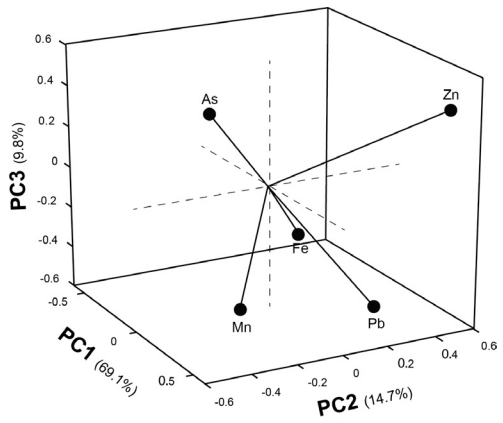

	PC1	PC2	PC3
Mn	0.472	-0.360	-0.383
Fe	0.516	-0.100	-0.013
Zn	0.377	0.738	0.430
As	0.414	-0.468	0.627
Pb	0.445	0.310	-0.525

Figure 2.17 Scatter plot and coefficient values of the three principal components obtained from Principal Component Analysis of Mn, Fe, Zn, As and Pb variability.

	Mn	Fe	Zn	As	Pb
Mn	1	0.885	0.372	0.639	0.673
Fe	0.885	1	0.625	0.718	0.711
Zn	0.372	0.625	1	0.390	0.596
As	0.639	0.718	0.390	1	0.444
Pb	0.673	0.711	0.596	0.444	1

Table 2.8 Pearson's correlation matrix for Mn, Fe, Zn, As and Pb in the fifty-two sediment cores.

$p<0.01$ (Table 2.8). The strongest correlations correspond to Mn-Fe, Fe-As and Fe-Pb pairs, with $r^2=0.885$, $r^2=0.718$ and $r^2=0.711$, respectively. Similar relations between elements are obtained from Principal Component Analysis (PCA). Three main principal components (PCs) are identified, accounting for 93.6% of the variation within the data set (69.1%, 14.7% and 9.8% for PC1, PC2 and PC3, respectively). PC1 is characterized by positive loadings for all elements, while positive loadings for PC2 are associated to Zn-Pb and negative loadings to Mn-Fe-As. Finally, high positive loadings on PC3 correspond to Zn and As, and negative loadings to Mn-Fe-Pb (Figure 2.17).

2.3.4.4 Age model and accumulation rates

Sediment core MC-36 is used as a reference core to illustrate $^{210}Pb_{xs}$ and Mn, Fe, Zn, As and Pb concentrations together with S and Ca element intensities (Figure 2.18). The $^{210}Pb_{xs}$ profile shows high values in the upper part with down core decreasing concentrations. From the core top to 4 cm core depth, $^{210}Pb_{xs}$ concentrations are essentially constant, which suggests a mixed interval likely due to bioturbation,

as shown by micro-CT imagery (Figure 2.18). From 4 to 13 cm, the concentration decrease markedly until the interval from 14 and 28 cm, where values are rather uniform despite some spikes, which may indicate a high sedimentation rate. Such pattern correlates with high contents of metal(loid)s and rare bioturbation marks (Facies 4.2, see Section 2.3.5.1). Below this interval, $^{210}Pb_{xs}$ concentrations decrease steadily again down to the core bottom until reaching the supported value (36 ± 2 Bq kg^{-1}).

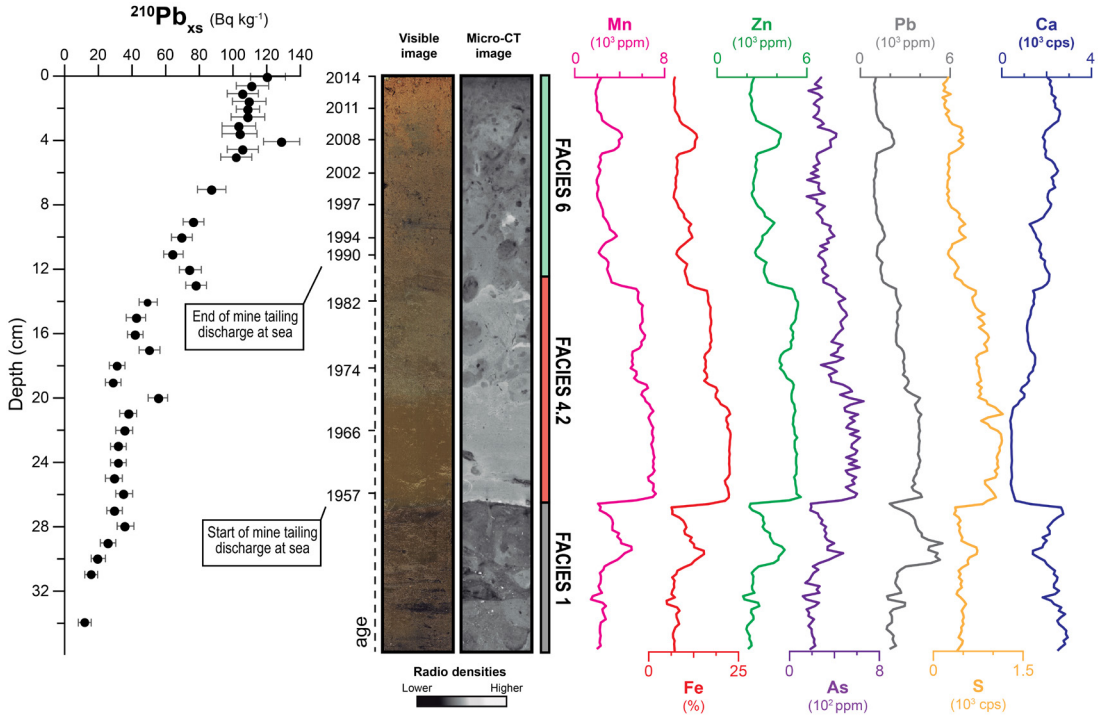

Figure 2.18 $^{210}Pb_{xs}$, Mn, Fe, Zn, As and Pb concentrations and S and Ca intensity profiles in sediment core MC-36, together with photographic and micro-CT images and indication of sedimentary facies. The age model is derived from the CF:CS model applied to the $^{210}Pb_{xs}$ concentration profile.

The mean accumulation rate (AR) can be obtained from the mean slope of the $^{210}Pb_{xs}$ concentration profile in the non-perturbed interval (i.e. from 6 to 16 cm) using the CF:CS model (Goldberg, 1963; Krishnaswamy et al., 1971). This allows deriving SRs for the different intervals. The AR for the uppermost interval (0 – 4 cm), representing the surficial mixing layer, is 0.147 ± 0.027 g cm^{-2} y^{-1}. The time interval attributed to this uppermost interval was quantified assuming the same AR of the 4 to 13 cm interval. The same AR was applied from 6 cm to the core bottom even though the AR during the mine tailings disposal likely was higher than in the post-dumping period. The age model shows that the end of the mine tailing discharge at sea, in

1990, corresponds approximately to 11 cm core depth, which is in agreement with the boundary of Facies 6 as described in Section 2.3.5.1. Furthermore, the lower boundary of Facies 4.2, from where metal(loid)s concentrations increase significantly up-core, corresponds to year 1957 located at 26 cm core depth coinciding with the start of mine tailings disposal at sea.

2.3.5 Discussion

2.3.5.1 Formation of the underwater extension of the mine tailings deposit

The multi-properties characterisation of the mine tailings deposit off Portmán Bay together with the distribution of the different sedimentary facies identified thanks to such characterisation and the age model are critical components to elucidate how the deposit grew and evolved since pre-dumping times to present. The patterns observed in vertical and horizontal variations of physical and geochemical records can be associated to the spreading and accommodation of the mine tailings from the discharge point through time. Therefore, integrating all those data should allow for a robust delineation of the deposit evolution and also to deciphering the main factors that governed the dispersal and burial of the tailings in the coastal marine environment. Even though the mine tailing facies identified in the present study correspond only to the uppermost part of the deposit. This weakness is minimised by the large number of sediment cores available and by their distribution all across the seabed area covered by the mine tailings.

The overall distribution of the above-described sedimentary facies is summarized in two N-S depth transects representing a conceptual depositional model (Figure 2.19). This model takes into account the physical and geochemical reality and the diversity of controlling factors involved in the deposit development, such as proximity to the discharge point, extremely high mine tailings supply and accumulation rates decreasing seaward, density segregation of the materials, availability of accommodation space, likely development of a seawards thinning sedimentary body, seabed features limiting the dispersion of the tailings, local signs of deformation of the tailings pile, and remobilization by high-energy hydrodynamic processes.

The low metal(loid)s concentrations and the predominant fine-sand grain size of the de-carbonated fraction of **Facies 1** indicates that it pre-dates mine tailings disposal. Such a view is further supported by the high amounts of Ca as measured by XRF,

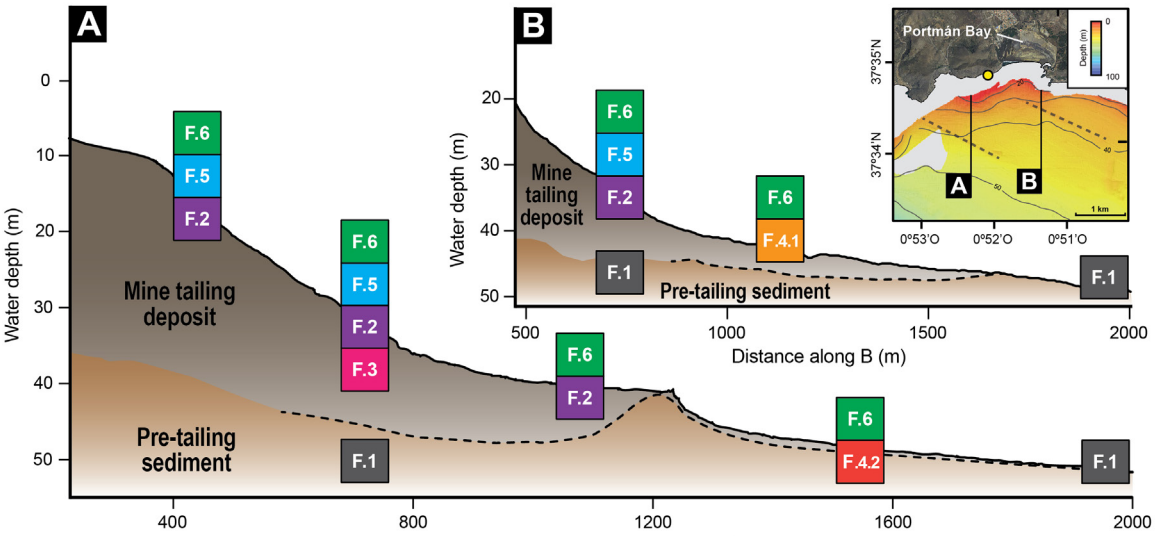

Figure 2.19 Conceptual depositional model of the mine tailings deposit off Portmán Bay along two N-S depth transects (A and B). Colour boxes illustrate the horizontal and vertical distribution of the sedimentary facies described in the main text. The lower boundary of the tailings deposit (dashed line) is indicative. Vertical exaggeration is 12.5x.

carbonate shells fragments and common bioturbation marks indicating an intense benthic biological activity at the time of deposition and afterwards. Carbonate-rich coarse-grained sediments are common in the inner continental shelf adjacent to the study area (Fernández Salas et al., 2016). All evidence indicates, therefore, that this basal facies corresponds to the natural sedimentation occurring in the area before the start of dumping of mine tailings. We have found it in two cores far from the discharge point (cores MC-20 and MC-36), where the tailings layer was thin enough to be crossed by our multicorer system. Consequently, we assume that this facies occurs below most or all the mine tailing deposit. Last but not least, radiometric dating of core MC-36 confirms that the boundary between Facies 1 and Facies 4.2 corresponds to year 1957, which coincides with the beginning of mine tailings discharge and the progressive burial of the natural shelf floor and its naturally occurring habitats (Figure 2.16).

Following the onset of dumping, tailings started to gradually cover Facies 1, first close to the discharge point on the coast. Grain size and density segregation allowed only minor fine supplies reaching more distal areas. The fast tailings discharge rates led subsequently to the complete infill of the original Portmán Bay in parallel with the development of a continuously growing tailings deposit advancing seaward. The very high accumulation rates in that period likely favoured deformation and

destabilisation at the front of the expanding tailings body. The resulting redeposition further favoured the spreading out of the tailings deposit at higher distances. All these processes left different signatures in the deposits being formed at that time, which we identify in facies 2, 3 and 4, including their spatial distribution. The elevated concentrations of metal(loid)s in those facies (e.g. Fe, Zn and Pb) clearly points to a mine waste origin and indeed these are mine tailings in *stricto sensu*. In the mining period, the pre-milling procedure of mineral ores resulted in fine grained mine tailings, with a mean grain-size less than 180 μm (Manteca, 2013), which fits perfectly with the dominance of silt and fine-sand fractions, especially in facies 2 and 3 within the proximal Subarea 1. Facies 4.1 and 4.2 are made of finer particles likely due to their greater distance to the discharge point. In any case, its high metal(loid)s contents clearly suggest they are made of mine tailings as well.

Facies 2 is observed mainly in the shoreline closest Subarea 1 (Figure 2.15). Its laminated character, with few cm layers, results from alternating black fine sands and yellowish silty materials. Such lamination, which is the main feature of the tailings deposit in the shallower Subarea 1 close to the coastline, likely results from continuous and extremely high tailings supply combined with the action of sedimentary processes leading to particle sorting, at least to some extent. The same layered pattern has been described in the emerged part of the mine tailings deposit, where it has been interpreted as a result of remobilization and reclassification processes in the near-shore environment (Manteca et al., 2014). Periods with calm sea conditions were prone to coarser particle settling and transport and deposition of finer particles, while more energetic periods, namely stormy periods, favoured transport of coarser particles and sorting of the overall particle population. High-energy events were also capable of triggering the remobilisation of discrete tailings volumes through gravity-driven processes likely including grain flows and mudflows.

We hypothesize that the dark layers within Facies 2 likely formed by accumulation of magnetite-rich black sands mainly coming from the beach in Portmán Bay and the shallowest parts of the deposit. We find now this layers interbedded with the yellowish silty layers representing the background tailings sedimentation. This view is well illustrated by the synchronized increase of magnetic susceptibility and grain size in the dark layers of core MC-14 at 22 − 23 cm and 27 − 28 cm, also coinciding with high values of Fe. Clearly, the spread of Facies 2, which is mostly found in Subarea 1, seems to be controlled by the proximity to the mine tailings discharge

point and, also, by the presence of a NW-SE oriented beachrock at about 40 m of water depth that likely acted as a barrier preventing a farther eastward expansion of the tailings (unpubl. results).

The physical and geochemical characteristics of **Facies 3** resemble those of Facies 2 except for its internal strong deformation. The same layers than in Facies 2 are found in Facies 3 but contorted and broken. This suggests that Facies 3 is in fact a deformation product of Facies 2. The contorted Facies 3 has been identified in few cores located at the foot of the submerged frontal slope of the tailings deposit (e.g. cores MC-10 and MC-50) (Figure 2.12). Thus, the most plausible explanation is that Facies 3 results from deformation of the tailings deposit likely by excess load where stress transfer because of elevated accumulation rates is highest. Of course, the cake-like structure of Facies 2, with alternating highly deformable (plastic) fine-grained layers and sandy layers, should have eased deformation and interpenetration leading to the development of Facies 3. This view is further supported by the stratigraphic relation between both facies, with Facies 3 located always below Facies 2, which points to Facies 3 as a basal deformation facies at the bottom of Facies 2.

Regarding **Facies 4**, its physical and geochemical values very similar to those of Facies 2, which suggests that they are genetically related and therefore, should have been deposited during the same broad time period. However, Facies 4 is found only at locations relatively far from shore. This, together with the fainter lamination and the more homogeneous layers that it presents, can be interpreted as a result of slow accumulation rates at some distance from the tailings discharge point. In other words, it represents fine-grained tailings spreading facies (sensu "étalement"). These reduced sedimentation rates likely favoured benthic biological activity, as shown by frequent bioturbation marks within this facies. The fading out of lamination in Facies 4 and its peripheral occurrence (with Subarea 2; (Figure 2.15) with respect to the presumed tailings depocentre suggests formation at the edges of the submarine mine tailings deposit.

The two sub-facies 4.1 and 4.2 differ noticeably in terms of magnetic susceptibility. The high magnetic susceptibility of **Sub-facies 4.1** (e.g. core MC-48), similar to those of Facies 2, points to active spreading of tailings beyond the shelf floor beachrock. In contrast, the low magnetic susceptibility and also the finer grain sizes from **Sub-facies 4.2** suggest the arrival of fines by near-bottom flows or perhaps from nepheloid layers (Figure 2.15) associated to reduced accumulation rates. The

^{210}Pb age model firmly supports this view as it demonstrates that Sub-facies 4.2 formed during the mine tailings disposal period (1957 – 1990).

Sediment cores collected close to shore in Subarea 1 also present the homogeneous **Facies 5**, which lays always on top of Facies 2 or Facies 4 (e.g. core MC-14, Figure 2.16). Its homogeneous character, together with high densities, fine grain sizes and rather low metal(loid)s concentrations illustrate that it differs from previously discussed mine tailings facies in strictu senso. The base of Facies 5 could be associated to the end of mine tailings disposal at sea, its materials being the result of subsequent reworking of the submerged top of the tailings deposit. Hydrodynamic forcing by coastal currents and wave action, especially during storms, likely led to resuspension, sorting and concentration of the tailings, which resulted in the development of a homogenised lag layer derived from the tailings. These hydrodynamic conditions would have favoured particle mixing in a new sedimentary setting with much reduced supplies compared to the previous dumping period.

The uppermost **Facies 6** is attributed to the re-establishment of natural sedimentation after the cessation of mine tailings disposal, as demonstrated by the significant reduction of metal(loid)s concentrations, the enhanced presence of bioturbation marks and its coarsening upward character (Figure 2.16.b). Facies 6 represents then the sedimentary product of the last twenty-five years, with an accumulation rate of 0.147 ± 0.027 g cm^{-2} y^{-1}, as shown by ^{210}Pb measurements in core MC-36. The absence of biogenic carbonates and higher metal concentration and magnetic susceptibility in Facies 6 than in the pre-tailings Facies 1 suggest a recent continuous flux of metal(loid)s, probably from the coastline, although other sources of dissolved metal(loid)s can also play a role (Alorda-Kleinglass, et al., 2019). The presence of few mine tailings particles, especially sulfides, and their oxidation products within marine sediments may lead to a decrease in pH, which would render problematic for benthic organisms with calcareous shells to thrive (Descostes et al., 2004). The high contents of Ca in the uppermost layers are mainly related to an increase of terrigenous carbonates, which are the dominating rock types in the nearby Sierra de Cartagena – La Unión (Manteca, 2013). Bioturbation marks observed in this post-tailings facies could indicate a progressive recovery of benthic activity after the cessation of mine waste disposal.

2.3.5.2 Geochemistry of metals and metalloids

The positive loadings of Mn, Fe, Pb, As and Zn on PC1 are indicative of the mineralogy of the mine tailings deposit, which is rich in galena (PbS), sphalerite (ZnS) and pyrite (FeS_2) sulfides. Moreover, the strong correlation between Fe and Mn (Pearson's correlation coefficient r^2=0.885) confirms the presence of the ferromanganese minerals, namely a mixture of iron and manganese oxides (MnO_2 and Fe_2O_3) that were also mined in Sierra de Cartagena − La Unión district. This high Fe-Mn correlation could result also from carbonates and manganese and iron halide salts like rhodochrosite or manganosiderite ($Fe,MnCO_3$) (Manteca, 2013). Besides Mn, As also shows a significant Pearson correlation with Fe (r^2=0.718), pointing to the presence of arsenopyrite (FeAsS), a mineral previously reported in sulfide ores from Sierra de Cartagena − La Unión mines (Oyarzun et al., 2013).

PC2 separates samples with significant positive loading of Zn and to a lesser extent Pb, and a negative loading of Mn, Fe and As. Besides the lower Pearson correlation of Zn and Pb with Mn, Fe and As, the results highlight the role of differentiation processes controlling the distribution and concentration patterns of metal(loid)s in the mine tailings deposit. As detailed in Section 2.3.5.3, the significant differences amongst the profiles of Zn and other metal(loid)s suggest that facies richer in those elements are likely related to direct accumulation of mine tailings (i.e facies 2, 3 and 5). This contrasting pattern may indicate different efficiencies between concentrating processes, as well as technical decisions and procedures in the flotation plant at the time of exploitation that could affect the composition of the tailings slurry finally released. It is well known that the froth flotation process generates two concentrates, first galena (PbS) and then sphalerite (ZnS), with a final step for pyrite (FeS_2) removal, which could also explain the distinct trend of Zn in our cores (Oyarzun et al., 2013).

2.3.5.3 Tracking of metals and metalloids dispersal

The metal(loid)s concentrations and EFs at three different depth levels down core are shown in figures 2.3.9 and 2.3.10. Geochemical records of all metal(loid)s here considered reveal strong similarities across the entire study area, with higher concentrations close to the mine tailings discharge point, which decrease south-eastwards. This is especially relevant in the 14 − 15 cm layer, which marks the transition between the mine tailings (Facies 2, 3, 4 and 5) and the post-tailings

materials (Facies 6) (Figure 2.20.a,b). In most cases metal(loid)s concentrations decrease upwards within the sediment cores from the level of year 1990 to present day. This implies that by the end of the tailings disposal period (i.e. the 14 – 15 cm level), the mean EFs are of 12 for Mn, 85 for Fe, 31 for Zn, 10 for As and 11 for Pb. In contrast, the topmost sediments (i.e. the 0 – 1 cm layer) displays EFs of 8 for Mn, 56 for Fe, 22 for Zn, 9 for As and 5 for Pb. Despite such a decrease of metal(loid) s enrichments towards the modern shelf floor, the concentrations found are still higher than those reported in other marine polluted areas, such as the continental shelf of Barcelona in Spain or Repparfjorden in northern Norway (Palanques et al., 2017; Sternal et al., 2017).

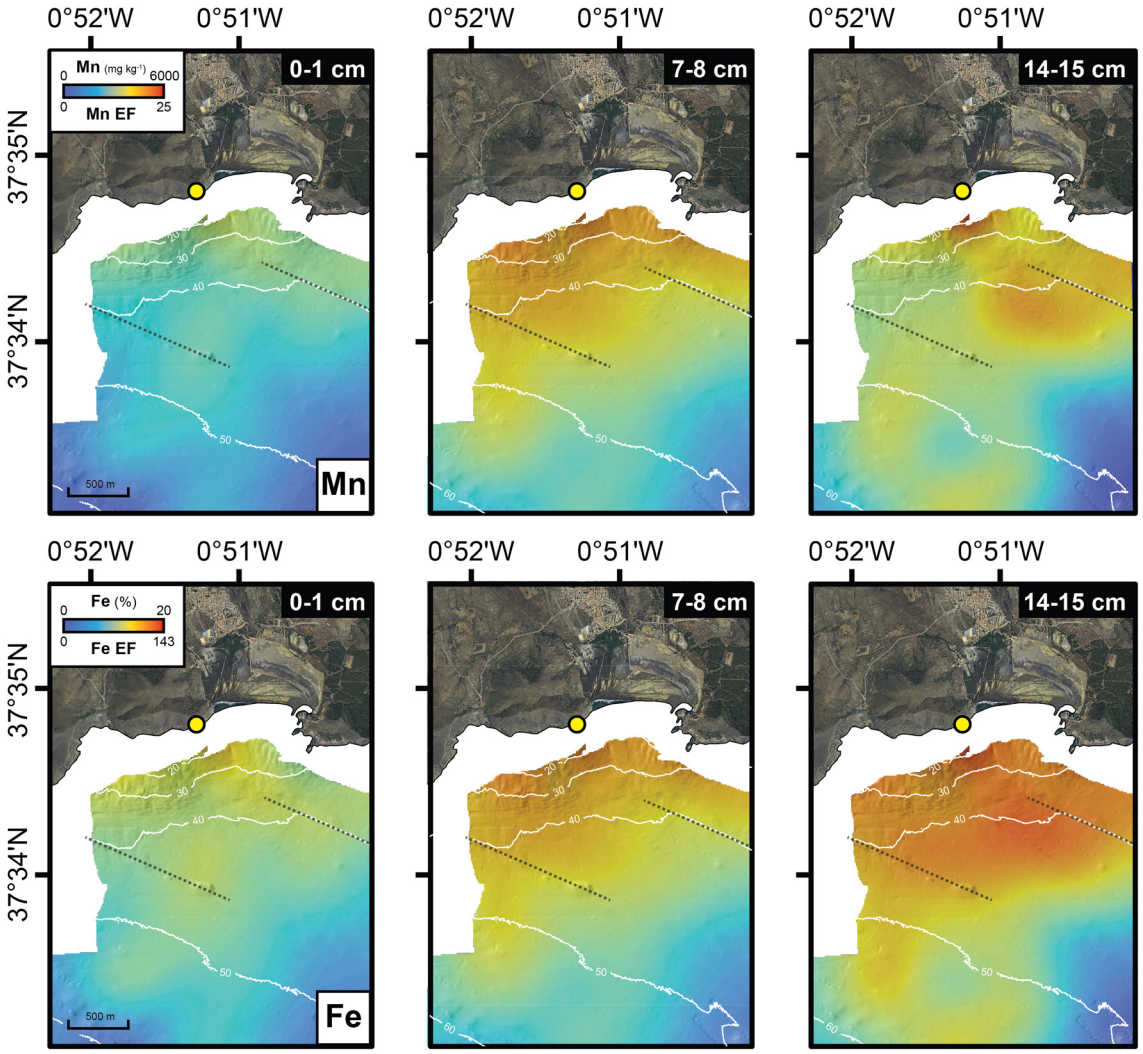

Figure 2.20 Interpolated distribution of Mn and Fe concentrations and enrichment factors (EF) in the deposits off Portmán Bay at three core depth levels: 0, 7 and 14 cm. The yellow point shows the location of the mine tailings discharge point and the dashed lines indicate the location of seabed beachrocks.

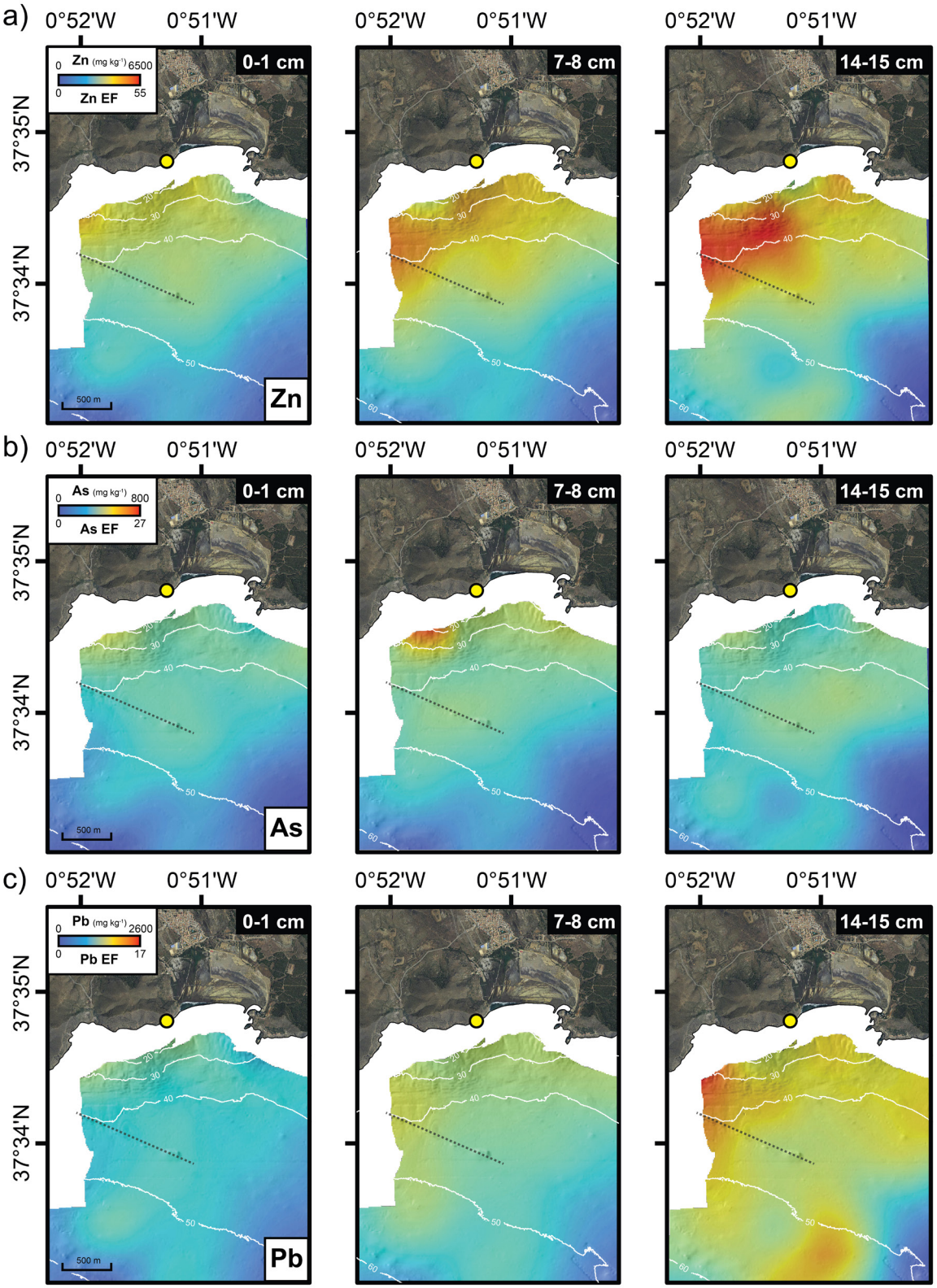

Figure 2.21 Interpolated distribution of Zn, As and Pb concentrations and enrichment factors (EF) in the deposits off Portmán Bay at three core depth levels: 0, 7 and 14 cm. The yellow point shows the location of the mine tailings discharge point and the dashed lines indicate the location of seabed beachrocks.

The distribution patterns of metal(loid)s and sedimentary facies (Figure 2.13, section 2.3.4.3) result not only from the location of the discharge point but also from hydrosedimentary dynamics in this part of the inner continental shelf of SE Spain, especially wave action. Mean wave direction data from "Puertos del Estado" off Portmán Bay for the 1990 – 2014 period is dominated by an easterly component and, to a lesser extent, a south-westerly one. The same dataset also shows a pronounced seasonal variability of wave direction. In summer, the south-westerly direction prevails while during winter wave direction is mostly from the east and south-east. These observations are in agreement with those made by Pauc and Thibault (1976) long time ago, which they used to depict the progressive infilling of the original Portmán Bay (Figure 2.12).

The combined effects of both easterly and south-westerly wave directions, together with the horseshoe shape of the bay (i.e. a potential natural trap of materials), provide the clues that explain the preferential north-westward transport and accumulation of the mine tailings during the dumping period from 1957 to 1990), together with the eastward decrease of metal(loid)s contents and laminated deposits over the inner shelf (Figure 2.19). The observed concentrations of metal(loid)s at the modern seafloor, i.e. within layers that formed after the stopping of mine tailings discharge, most likely result from erosion and seaward transport of minerals from the emerged part of the deposit and its beach front. A residual component from the underlying mine tailings may also add to the most recent sedimentary layers.

The presumed dominant particle transport by easterly waves leading to a preferential north-westwards accumulation of coarse grains, including magnetite-rich beach black sands, and to the seaward sorting and transport of finer particles is supported by the observed grain-size distribution in seafloor sediments (Facies 6). Cores from the western part of the study area show a sandy unimodal distribution (e.g. cores MC-02 and MC-50, Figure 2.16.b,c) whereas the cores from the eastern part display a fine sandy bimodal distribution (e.g. core MC-16, Figure 2.16.d). The topographic barrier effect of seabed beachrocks preventing farther spreading of the tailings is clearly visible in grain size patterns and, probably, on the thickness of the tailings deposit as well (Figure 2.20 and 2.21).

The interpolated distribution of metal(loid)s concentrations and EFs slice maps at 7 and 14 cm core depth evince a southerly flux, especially of Mn, Fe and Pb. That flux corresponds to Subarea 3 and sedimentary Facies 4.2, which is ~13 cm thick in core

MC-36 (Figure 2.16.e). That flux could result from the combination of two processes: (1) the infill of the main tailings depocentre probably by the end of the mining waste discharge period, and (2) the easterly predominant waves and associated coastal currents carrying finer particles westward and finally south-westward from this depocentre to more distal locations. The south-westward and also southward transport of the finer fraction with its metal(loid)s load could have been favoured by short wavelength sea storms that are common in the Western Mediterranean Sea. The main storms usually take place during autumn and spring and the transport associated to them could have led the finer particles to easily bypass the beachrock topographic barrier.

A remarkable feature visible on the interpolated metal(loid)s concentrations core depth slice maps is that Mn and Fe show a different pattern than Zn, As and Pb. Mn and Fe maximum concentrations and preferential deposition are eastward of the tailings discharge point, while maximum concentrations for Zn, As and Pb occur west of that point. Such distinct accumulation patterns suggest differential transport of mineral grains after entering the coastal sea. Fe and Mn are mainly associated to halide salts and oxides, which are much lighter than Zn, As and Pb minerals (i.e. sphalerite, arsenopyrite and galena). Because of this, it seems reasonable for Mn and Fe-rich particles to spread farther than heavier Zn, As and Pb-rich particles. This becomes also apparent from the density surface distribution at 14 cm core depth showing higher values for Zn and Pb close to the discharge point together with an eastward decreasing trend (Figure 2.21.a,b).

2.3.5.4 Contamination levels and total mass estimations

Sediment quality guidelines (SQGs) can be used to qualitatively assess pollution levels of sedimentary materials. SQGs are defined as the concentration range or limit for chemical compounds (e.g. metals, pesticides) that could lead to potential biological effects (Long et al., 1995). SQGs are based on empirical evidence and have been widely applied to evaluate ecotoxicological risks in diverse environments (Adamo et al., 2005; Buccolieri et al., 2006; Casado-Martínez et al., 2006; Palanques et al., 2008; Garcia-Orellana et al., 2011). The Spanish Harbour Authority (Comisión Nacional de Estrategias Marinas, 2015) identifies three Action Levels, A, B and C, while establishing the thresholds for identifying hazardous sediments in the management of dredged materials and its relocation in within the maritime-terrestrial public domain (Table 2.9).

	Action Level A	Action Level B	Action Level C	No dangerous sediment
Zn (mg kg^{-1})	205	410	70	<2,500
As (mg kg^{-1})	35	70	280	<1,000
Pb (mg kg^{-1})	80	218	600	<1,000

Table 2.9 Action Levels and threshold concentrations for dredged sediments to be considered as non dangerous developed by the Spanish Harbour Authority for Zn, As and Pb.

According to this classification, and using the metal(loid) concentration slice maps in Figure 2.21, 8.6 km^2 of surface sediments (0 − 1 cm) on the inner continental shelf off Portmán Bay have to be qualified as ecotoxicologically dangerous as they exceed the SQGs thresholds defined for Zn, As and Pb. Furthermore, 9.4 km^2 fall within Action Level C, which in case of dredging and relocation implies the need of containment for reducing the dispersion of metal(loid)s.

The interpolation of metal(loid)s concentrations as shown in the core depth slice maps in the deposits off Portmán Bay allows to quantitatively estimate the total accumulated mass of each metal in the layers formed after cessation of tailings discharge. Assuming that the top 14 cm of sediment correspond to the post-mining period (i.e. from 1990 to 2015, when the last research cruise was carried out), the total mass for each metal(loid)s can be expressed as follow:

$$T_{met} = \sum_{i=1}^{n} \left(Den_i \cdot C_{met,i} \cdot V_{voxel} \right) \quad (14)$$

where T_{met} is the total bulk mass of each metal(loid)s, Den_i is the density value of voxel i, $C_{met,i}$ is the concentration of metal(loid)s on voxel i and V_{voxel} is the voxel volume on the predefined grid (0.2 m^3, 10 m x 10 m x 0.002 m). Since both density and metal(loid)s concentrations have errors associated to analytical procedures and calibration of element concentrations (Cerdà-Domènech et al., 2020), the total bulk mass error must be constrained to assess the quality of the mass bulk model. Consequently, the errors of the total mass bulk of each metal(loid)s have been calculated according to the law of propagation of errors (Taylor and Kuyatt, 1994).

The estimated total mass of each element in the top 14 cm of the sedimentary record off Portmán Bay are 6,700 ± 1,400 t of Mn, $2.6 \cdot 10^5$ ± 3.9 10^3 t of Fe, 7,700 ± 1,600 t of Zn, 670 ± 140 t of As and 3,170 ± 650 t of Pb. These total masses would correspond to 0.012, 0.456, 0.013, 0.006 and 0.001%, respectively, of the total mass

of each element within the overall mass of tailings dumped during the discharge period in Portmán Bay (~57 Mt) according to Manteca et al. (2014).

2.3.5.5 Environmental considerations on metal(loid)s fluxes to seafloor sediments

The results above evidence a continuous flux of metal(loid)s to the seafloor about 25 years after the cessation of dumping. Since atmospheric deposition of metal(loid)s from the abandoned mines in Sierra de Cartagena − La Unión to the coastal sea can be considered negligible (Blondet et al., 2019), the main source of metal(loid)s to the coastal should be twofold: (i) from erosion and transport of mineral particles (e.g. galena, sphalerite, magnetite and pyrite) from the emerged part of the tailings deposits and the beach of Portmán Bay (Manteca et al., 2014), and (ii) from submarine groundwater fluxes carrying dissolved metal(loid)s from emerged part of the mine tailings deposit (Alorda-Kleinglass et al., 2019).

Indeed, Alorda-Kleinglass et al. (2019) determined that Submarine Groundwater Discharge (SGD) and Porewater Exchange (PEX) remobilize large amounts of dissolved metal(loid)s from the emerged part of the deposit into the marine environment. Dissolved metals can incorporate to the particulate phase through adsorption by particulate matter, thus being removed from the water column and accumulating in seafloor sediments (Bruland et al., 2013). The estimated total Pb and Zn fluxes calculated by Alorda-Kleinglass et al. (2019) are 3 ± 1 and 1670 ± 790 mol d^{-1} km^{-1}, respectively. Assuming a constant flux during the last 25 years and the current shoreline length of the beach front in Portmán Bay (~1 km), the total estimated fluxes are ~ 6 and ~ 900 t of dissolved Pb and Zn, respectively, which are less than the estimated mass of these metals being buried in the sedimentary record during the same period. Therefore, a significant contribution of erosion and transport of particulate metal(loid)s from the emerged section of the tailings deposit is needed to equal the overall budget. This interpretation is further supported by the decreasing trends in grain size and metal(loid)s concentrations in seafloor sediments in parallel with distance from the shoreline.

Also, during the 25 years post-dumping period, the finer fraction in the emerged surface layer seems to have been essentially removed by erosion and transport, and only fine black sands, essentially on Portmán's Bay beach, can still be remobilized. The resulting shift in the grain size of the remobilized materials through time can

be observed in Figure 2.16.a,c by a clear coarsening upwards trend in sediment cores, together with a decrease of metal(loid)s concentrations.

A significant process in the preservation of the tailings is the oxidation of minerals already at the time of ore processing itself, but also later on due to the action of waves and currents. The weathering of sulfide minerals has a direct influence on metal(loid) s speciation and partitioning and, consequently, on the release of those elements into the water column and the sediment pores (Nesbitt et al., 1995; Descostes et al., 2004; Hayes et al., 2014). Since speciation is also related to the mobility and bioavailability of metal(loid)s (Foster et al., 1998; Slowey et al., 2007), assessing their oxidation state is crucial for evaluating the ecotoxicological impacts they could have eventually (Mestre et al., 2017). Roqué et al. (2020) have demonstrated that As in the raw minerals (i.e. arsenopyrite) processed at Lavadero Roberto froth flotation plant was partially oxidized to As^{5+} during the processing of the ore mineral to subsequently re-precipitate as As^{3+} when discharged into the sea. This process pre-forms a scorodite-like coating on the surface of arsenopyrite grains, thus reducing As release to the water column . In any case, the decreasing trend of the metal(loid)s concentrations, the increase in magnetite content (a mineral resistant to oxidation; Lindsay et al., 2015) and the abundant bioturbation marks in the top layer (i.e. Facies 6) demonstrate a progressive re-establishment of the natural sedimentary conditions 25 years after the cessation of mine waste discharge at the coastal sea besides Portmán Bay.

2.3.6 Conclusions

The submerged extension of the mine tailings deposit off Portmán Bay still is nowadays, more than one quarter of century after the stopping of discharges, a significant source of metal(loid)s to the water column and seafloor sediments. Whereas the emerged part of the deposit is reasonably well described and characterized (Peña et al., 2013; Manteca et al., 2014) no detailed assessment of metal(loid)s concentrations and distribution in the submarine extension of the deposit was available to date. Also the development of the very same submerged extension on the adjacent shelf floor was unconstrained for the pre-, syn- and post-dumping time span.

This paper presents the first physical and geochemical characterization of sediments pre-dating the onset of tailings disposal (pre 1957, Facies 1), the uppermost part of the mine tailings deposit (1957 − 1990) and the sediments accumulated following the cessation of dumping (1990 − 2015). The analysis of 52 short cores has shown

that tailings facies (Facies 2, 3, 4 and 5) occur mainly in the innermost continental shelf, between the shoreline and a couple of seafloor beachrocks acting as partial topographic barriers to the spreading of tailings. The tailings deposit present metal(loid)s concentrations that are significantly higher than those found in other regions of the Mediterranean Sea. Differences amongst the tailings facies are attributed to the closeness to the discharge point on the coast, and also to oscillations in the tailings supply rate at different locations (proximal vs. distal with respect to the discharge point and the shoreline) and through time. Excess overload due to fast accumulation rates lead to deformation of cake-like layered facies made of interstratified plastic fine grained and sandy layers. Deformation Facies 3 is found in a few cores located at the foot of the submerged frontal slope of the tailings deposit. Coastal sea storms have eased the remobilization, sorting and dispersal of tailings, with coarser grain sizes tending to concentrate close to shore and fines exported farther seaward.

A post-dumping modern upper layer with a distinct facies (Facies 6) with still rather high metal(loid)s concentrations has been characterized and differentiated as well. Our results show mean EFs on the topmost sediment layer (0 − 1 cm depth) of 8 for Mn, 56 for Fe, 22 for Zn, 9 for As and 5 for Pb. These elevated metal(loid)s concentrations imply that approximately 8.6 km^2 of the inner continental shelf off Portmán Bay must be considered as dangerous sediment according to the SQGs the Spanish Harbour Authority (Comisión Nacional de Estrategias Marinas, 2015). A ^{210}Pb age in one of the sediment cores allows placing the exact level corresponding to the onset of tailings discharge in 1957 (26 cm core depth) and also the one corresponding to the end of the discharge period in 1990. Those limits fit perfectly with changes of sedimentary facies below and above. In the post-dumping (1990 − 2015) sediment layer capping the study area (i.e. the uppermost 14 cm of the sedimentary column), we estimate a total mass of 6,700, $2.6 \cdot 10^5$, 7,700, 670 and 3,170 t of Mn, Fe, Zn, As and Pb, respectively, which evidences a persistent flux of metal(loid)s to marine seafloor sediments along the 25 years following the cessation of mine tailings discharge.

The main limitation of the current study is the short length of the investigated sediment cores, which do not penetrate deep into the mine tailings deposit. Consequently, longer cores would be needed to fully characterize the distribution and concentrations of metal(loid)s, and the associated sedimentary facies, at intermediate and deep levels within the submarine mine tailing deposit so that the evolution and current state of this unique man-made coastal depositional body could be better constrained.

Acknowledgements: We would like to thank the crew of RV Ángeles Alvariño and all scientific and technical staff involved in the research cruises off Portmán Bay. This research has been funded by the research projects NUREIEV (CTM2013-44598-R) and NUREIEVA (ref. CTM2016-75953-C2-1-R). GRC Geociències Marines is funded by a Catalan Government Grups de Recerca Reconeguts grant (ref. 2017 SGR 315). M.C.-D. and A.B. acknowledge support from the Spanish Ministerio de Economía y Competitividad (MINECO) for PhD fellowships A-2014-9185 and BES-2017-080437 within NUREIEV and NUREIEVA projects respectively.

2.3.7 References

Adamo, P., Arienzo, M., Imperato, M., Naimo, D., Nardi, G., Stanzione, D., 2005. Distribution and partition of heavy metals in surface and sub-surface sediments of Naples city port. Chemosphere 61, 800–809. https://doi.org/10.1016/j.chemosphere.2005.04.001

Alorda-Kleinglass, A., Garcia-Orellana, J., Rodellas, V., Cerdà-Domènech, M., Tovar-Sánchez, A., Diego-Feliu, M., Trezzi, G., Sánchez-Quilez, D., Sanchez-Vidal, A., Canals, M., 2019. Remobilization of dissolved metals from a coastal mine tailing deposit driven by groundwater discharge and porewater exchange. Sci. Total Environ. 688, 1359–1372. https://doi.org/10.1016/j.scitotenv.2019.06.224

Andersen, M.S., Larsen, F., Postma, D., 2001. Pyrite oxidation in unsaturated aquifer sediments. Reaction stoichiometry and rate of oxidation. Environ. Sci. Technol. 35, 4074–4079. https://doi.org/10.1021/es0105919

Ankley, G.T., 1996. Evaluation of metal/acid-volatile sulfide relationships in the prediction of metal bioaccumulation by benthic macroinvertebrates. Environ. Toxicol. Chem. 15, 2138–2146. https://doi.org/10.1002/etc.5620151209

Blondet, I., Schreck, E., Viers, J., Casas, S., Jubany, I., Bahí, N., Zouiten, C., Dufréchou, G., Freydier, R., Galy-Lacaux, C., Martínez-Martínez, S., Faz, A., Soriano-Disla, M., Acosta, J.A., Darrozes, J., 2019. Atmospheric dust characterisation in the mining district of Cartagena-La Unión, Spain: Air quality and health risks assessment. Sci. Total Environ. 693, 133496. https://doi.org/10.1016/j.scitotenv.2019.07.302

Böning, P., Bard, E., Rose, J., 2007. Toward direct, micron-scale XRF elemental maps and quantitative profiles of wet marine sediments. Geochemistry, Geophys. Geosystems 8, 5. https://doi.org/10.1029/2006GC001480

Buccolieri, A., Buccolieri, G., Cardellicchio, N., Dell'Atti, A., Di Leo, A., Maci, A., 2006. Heavy metals in marine sediments of Taranto Gulf (Ionian Sea, Southern Italy). Mar. Chem. 99, 227–235. https://doi.org/10.1016/j.marchem.2005.09.009

Casado-Martínez, M.C., Buceta, J.L., Belzunce, M.J., DelValls, T.A., 2006. Using sediment quality guidelines for dredged material management in commercial ports from Spain. Environ. Int. 32, 388–396. https://doi.org/10.1016/j.envint.2005.09.003

Castilla, J.C., Nealler, E., 1978. Marine environmental impact due to mining activities of El Salvador copper mine, Chile. Mar. Pollut. Bull. 9, 67–70. https://doi.org/10.1016/0025-326X(78)90451-4

Cerdà-Domènech, M., Frigola, J., Sanchez-Vidal, A., Canals, M., 2020. Calibrating high resolution XRF core scanner data to obtain absolute metal concentrations in highly polluted marine deposits after two case studies off Portmán Bay and Barcelona, Spain. Sci. Total Environ. 717, 134778. https://doi.org/https://doi.org/10.1016/j.scitotenv.2019.134778

Comisión nacional de estrategias de Marinas, 2015. Directrices para la caracterización del material dragado y su reubicación en aguas del dominio público marítimo-terrestre. Minist. Agric. Aliment. y medio Ambient.

Croudace, I.W., Rothwell, R.G., 2015. Future developments and innovations in high-resolution core scanning, in: Micro-XRF Studies of Sediment Cores. Springer, pp. 627–647.

Boletín Oficial del Estado, 2011. Resolución de 10 de febrero de 2011, de la Secretaría de Estado de Cambio Climático, por la que se formula declaración de impacto ambiental del proyecto Regeneración y adecuación ambiental de la Bahía de Portmán, término municipal de La Unión, Murcia. BOE 45, 20530–20560.

Descostes, M., Vitorge, P., Beaucaire, C., 2004. Pyrite dissolution in acidic media. Geochim. Cosmochim. Acta 68, 4559–4569. https://doi.org/10.1016/j.gca.2004.04.012

Duliu, O.G., 1999. Computer axial tomography in geosciences: an overview. Earth-Science Rev. 48, 265–281. https://doi.org/10.1016/S0012-8252(99)00056-2

Ellis, D., Ellis, K., 1994. Very deep STD. Mar. Pollut. Bull. 28, 472–476. https://doi.

org/10.1016/0025-326X(94)90519-3

Fernández Salas, L.M., Durán, R., Mendes, I., Galparsoro, I., Lobo, F.J., Bárcenas, P., Rosa, F., Ribó, M., García-Gil, S., Ferrín, A., 2016. Shelves of the Iberian Peninsula and the Balearic Islands (I): Morphology and sediment types. Boletín Geológico y Minero, 2016, 126, 2-3, 327-376.

Foster, A.L., Brown, G.E., Tingle, T.N., Parks, G.A., 1998. Quantitative arsenic speciation in mine tailings using X-ray absorption spectroscopy. Am. Mineral. 83, 553–568. https://doi.org/10.2138/am-1998-5-616

Franks, D.M., Boger, D. V., Côte, C.M., Mulligan, D.R., 2011. Sustainable development principles for the disposal of mining and mineral processing wastes. Resour. Policy 36, 114–122. https://doi.org/10.1016/j.resourpol.2010.12.001

Frigola, J., Canals, M., Mata, P., 2015. Técnicas para el análisis no destructivo y en continuo de testigos de sedimento. Aplicación en el Margen Continental de Iberia. Bol. Geol. y Min. 126, 609–634.

Fuerstenau, M.C., Chander, S., Woods, R., 2007. Sulfide Mineral Flotation, in: SME (Ed.), Froth Flotation: A Century of Innovation.

García-Lorenzo, M.L., Martínez-Sánchez, M.J., Pérez-Sirvent, C., Agudo, I., Recio, C., 2014. Isotope geochemistry of waters affected by mining activities in Sierra Minera and Portman Bay (SE, Spain). Appl. Geochemistry 51, 139–147. https://doi.org/10.1016/j.apgeochem.2014.10.002.

Garcia-Orellana, J., Cañas, L., Masqué, P., Obrador, B., Olid, C., Pretus, J., 2011. Chronological reconstruction of metal contamination in the Port of Maó (Minorca, Spain). Mar. Pollut. Bull. 62, 1632–1640. https://doi.org/10.1016/j.marpolbul.2011.06.013.

Gattuso J.P., Magnan A.K., Bopp L., Cheung W., Duarte C.M., Hinkel J., Mcleod E., Micheli F., Oschlies A., Williamson P., Billé R., Chalastani V.I., Gates R.D., Irisson J.O., Middelburg J.J., Pörtner H.O., Rau G.H. (2018). Ocean Solutions to Address Climate Change and Its Effects on Marine Ecosystems. Front. Mar. Sci. 5, 337. http://doi.org/10.3389/fmars.2018.00337.

Goldberg, E.D., 1963. Geochronology with ^{210}Pb radioactive dating. Int. At. Energy Agency, Vienna 121, 130.

Hayes, S.M., Root, R.A., Perdrial, N., Maier, R.M., Chorover, J., 2014. Surficial weathering of iron sulfide mine tailings under semi-arid climate. Geochim. Cosmochim. Acta 141, 240–257. https://doi.org/10.1016/j.gca.2014.05.030

Hughes, D.J., Shimmield, T.M., Black, K.D., Howe, J.A., 2015. Ecological impacts of large-scale disposal of mining waste in the deep sea. Sci. Rep. 5, 9985. https://doi.org/10.1038/srep09985

Jansen, J.H., Van der Gaast, S. J., Koster, B., Vaars, A. J., 1998. CORTEX, a shipboard XRF-scanner for element analyses in split sediment cores. Mar. Geol. 151, 143–153. https://doi.org/10.1016/S0025-3227(98)00074-7

Josefson, A.B., Hansen, J.L.S., Asmund, G., Johansen, P., 2008. Threshold response of benthic macrofauna integrity to metal contamination in West Greenland. Mar. Pollut. Bull. 56, 1265–1274. https://doi.org/10.1016/j.marpolbul.2008.04.028

Kawatra, S.K., 2011. Froth Flotation – Fundamental Principles Flotation System. SME Min. Eng. Handb. 3rd Ed.

Koski, R.A. 2012. Metal dispersion resulting from mining activities in coastal environments: A pathways approach. Oceanography 25, 170–183. http://doi.org/10.5670/oceanog.2012.53.

Krishnaswamy, S., Lal, D., Martin, J.M., Meybeck, M., 1971. Geochronology of lake sediments. Earth Planet. Sci. Lett. 11, 407–414. https://doi.org/10.1016/0012-821X(71)90202-0

Lamotte, L.R., Rao, C.R., Toutenburg, H., 1997. Linear Models. J. Am. Stat. Assoc. https://doi.org/10.2307/2965595

Lancellotti, D.A., Stotz, W.B., 2004. Effects of shoreline discharge of iron mine tailings on a marine soft-bottom community in northern Chile. Mar. Pollut. Bull. 48, 303–12. https://doi.org/10.1016/j.marpolbul.2003.08.005

Lindsay, M.B.J.J., Moncur, M.C., Bain, J.G., Jambor, J.L., Ptacek, C.J., Blowes, D.W., 2015. Geochemical and mineralogical aspects of sulfide mine tailings. Appl. Geochemistry 57, 157–177. https://doi.org/10.1016/j.apgeochem.2015.01.009

Llull, R.M., Garí, M., Canals, M., Rey-Maquieira, T., Grimalt, J.O., 2017. Mercury concentrations in lean fish from the Western Mediterranean Sea: Dietary exposure and risk assessment in the population of the Balearic Islands. Environ.

Res. 158, 16–23. https://doi.org/10.1016/j.envres.2017.05.033

Long, E.R., Macdonald, D.D., Smith, S.L., Calder, F.D., 1995. Incidence of adverse biological effects within ranges of chemical concentrations in marine and estuarine sediments. Environ. Manage. 19, 81–97. https://doi.org/10.1007/BF02472006

Loring, D.H., 1991. Normalization of heavy-metal data from estuarine and coastal sediments. ICES J. Mar. Sci. 48, 101–115. https://doi.org/10.1093/icesjms/48.1.101

Lottermoser, B.G., 2010. Mine Wastes (third edition): Characterization, treatment and environmental impacts, Mine Wastes (Third Edition): Characterization, Treatment and Environmental Impacts. https://doi.org/10.1007/978-3-642-12419-8

Manteca Martínez, J.I., 1992. Los yacimientos Zn, Pb, Ag-Fe del distrito minero de la La Unión-Cartagena, Bética Oriental.

Manteca, J.I., 2013. Introducción a la geología y yacimientos minerales de Portmán, Portmán: de el Portus Magnus del Mediterráneo Occidental a la Bahía Aterrada. EDITUM, Murcia.

Manteca, J.I., García, J.Á.L., Oyarzun, R., Carmona, C., Garcia, J.Á.L., Oyarzun, R., Carmona, C., 2014. The beach placer iron deposit of Portman Bay, Murcia, SE Spain: The result of 33 years of tailings disposal (1957-1990) to the Mediterranean seaside. Miner. Depos. 49, 777–783. https://doi.org/10.1007/s00126-014-0511-x

Martínez-Sánchez, M.J., Navarro, M.C., Pérez-Sirvent, C., Marimón, J., Vidal, J., García-Lorenzo, M.L., Bech, J., 2008. Assessment of the mobility of metals in a mining-impacted coastal area (Spain, Western Mediterranean). J. Geochemical Explor. 96, 171–182. https://doi.org/10.1016/j.gexplo.2007.04.006

Mestre, N.C., Rocha, T.L., Canals, M., Cardoso, C., Danovaro, R., Dell'Anno, A., Gambi, C., Regoli, F., Sanchez-Vidal, A., Bebianno, M.J., 2017. Environmental hazard assessment of a marine mine tailings deposit site and potential implications for deep-sea mining. Environ. Pollut. 228, 169–178. https://doi.org/10.1016/j.envpol.2017.05.027

Nesbitt, H.W., Muir, I.J., Prarr, A.R., 1995. Oxidation of arsenopyrite by air and air-saturated, distilled water, and implications for mechanism of oxidation. Geochim. Cosmochim. Acta 59, 1773–1786. https://doi.org/10.1016/0016-7037(95)00081-A

Odhiambo, B.K., Macdonald, R.W., O'Brien, M.C., Harper, J.R., Yunker, M.B., 1996. Transport and fate of mine tailings in a coastal fjord of British Columbia as inferred from the sediment record. Sci. Total Environ. 191, 77–94. https://doi.org/10.1016/0048-9697(96)05250-3

Olsgard, F., Hasle, J.R., 1993. Impact of waste from titanium mining on benthic fauna. J. Exp. Mar. Bio. Ecol. 172, 185–213. https://doi.org/10.1016/0022-0981(93)90097-8

Oyarzun, R., Manteca Martínez, J.I., López García, J.A., Carmona, C., 2013. An account of the events that led to full bay infilling with sulfide tailings at Portman (Spain), and the search for "black swans" in a potential land reclamation scenario. Sci. Total Environ. 454–455, 245–9. https://doi.org/10.1016/j.scitotenv.2013.03.030

Palanques, A., Masqué, P., Puig, P., Sanchez-Cabeza, J.A., Frignani, M., Alvisi, F., 2008. Anthropogenic trace metals in the sedimentary record of the Llobregat continental shelf and adjacent Foix Submarine Canyon (northwestern Mediterranean). Mar. Geol. 248, 213–227. https://doi.org/10.1016/j.margeo.2007.11.001

Palanques, A., Lopez, L., Guillén, J., Puig, P., Masqué, P., 2017. Decline of trace metal pollution in the bottom sediments of the Barcelona City continental shelf (NW Mediterranean). Sci. Total Environ. 579, 755–767. https://doi.org/10.1016/j.scitotenv.2016.11.031

Pauc, H., Thibault, M., 1976. Lhydrodynamique et la dynamique des matériaux en suspension en baie de Portman (Province de Murcie, Espagne). Bull. BRGM 12th Ser. Sect. IV 3, 211–221.

Peña, J.A., Manteca, J.I., Martínez-Pagán, P., Teixidó, T., 2013. Magnetic gradient map of the mine tailings in Portman Bay (Murcia, Spain) and its contribution to the understanding of the bay infilling process. J. Appl. Geophys. 95, 115–120. https://doi.org/10.1016/j.jappgeo.2013.05.011

Pereira, A.A., Van Hattum, B., Brouwer, A., Van Bodegom, P.M., Rezende, C.E., Salomons, W., 2008. Effects of iron-ore mining and processing on metal bioavailability in a tropical coastal lagoon. J. Soils Sediments 8, 239–252. https://doi.org/10.1007/s11368-008-0017-1

Ramirez-Llodra, E., Trannum, H.C., Evenset, A., Levin, L.A., Andersson, M., Finne, T.E., Hilario, A., Flem, B., Christensen, G., Schaanning, M., Vanreusel, A., 2015. Submarine and deep-sea mine tailing placements: A review of current practices, environmental issues, natural analogs and knowledge gaps in Norway and internationally. Mar. Pollut. Bull. 97, 13–35. https://doi.org/10.1016/j.marpolbul.2015.05.062

Ramirez, M., Massolo, S., Frache, R., Correa, J.A., 2005. Metal speciation and environmental impact on sandy beaches due to El Salvador copper mine, Chile. Mar. Pollut. Bull. 50, 62–72. https://doi.org/10.1016/j.marpolbul.2004.08.010

Root, R.A., Hayes, S.M., Hammond, C.M., Maier, R.M., Chorover, J., 2015. Toxic metal(loid) speciation during weathering of iron sulfide mine tailings under semi-arid climate. Appl. Geochemistry 62, 131–149. https://doi.org/10.1016/j.apgeochem.2015.01.005

Roqué, J., Cerdà-Domènech, M., Sanchez-Vidal, A., Frigola, J., Amblàs, D., Cibin, G., Canals, M., 2020. Arsenic speciation in a submarine mine tailings deposit: combining synchrotron XAS and non-destructive analysis of sediment cores. (submitted).

Rothwell, R.G., Rack, F.R., 2006. New techniques in sediment core analysis: An introduction. Geol. Soc. Spec. Publ. 267(1), 1-29.

Sánchez, M.J., Sirvent, M. del C.P., 2013. Diagnóstico y recuperación de la contaminación del suelo en Portmán-Sierra Minera, in: Portmán: De El" Portus Magnus" Del Mediterráneo Occidental a La Bahía Aterrada. Servicio de Publicaciones, pp. 313–344.

Schultheiss, P.J., Weaver, P.P.E., 1992. Multi-sensor core logging for science and industry, in: OCEANS 1992 - Proceedings: Mastering the Oceans Through Technology.IEEE,pp.608–613.https://doi.org/10.1109/OCEANS.1992.607652

Slowey, A.J., Johnson, S.B., Newville, M., Brown, G.E., 2007. Speciation and colloid transport of arsenic from mine tailings. Appl. Geochemistry. 22(9), 1884-1898.

https://doi.org/10.1016/j.apgeochem.2007.03.053

Sternal, B., Junttila, J., Skirbekk, K., Forwick, M., Carroll, J.L., Pedersen, K.B., 2017. The impact of submarine copper mine tailing disposal from the 1970s on Repparfjorden, northern Norway. Mar. Pollut. Bull. 120, 136–153. https://doi.org/10.1016/j.marpolbul.2017.04.054

Taylor, B.N., Kuyatt, C.E., 1994. Guidelines for evaluating and expressing the uncertainty of NIST measurement results. US Department of Commerce, Technology Administration, National Institute of Standards and Technology Gaithersburg, MD.

Vogt, C., 2012. International Assessment of Marine and Riverine Disposal of Mine Tailings. Impact Assess. Soc. Econ. Dev. 34th Annu. Conf. Int. Assoc. I. 134.

2.4 Resum dels resultats

En la present Tesi, hom s'ha centrat en l'estudi de dos fluxos de metalls i metal·loides al medi marí: la descàrrega d'aigua subterrània i l'abocament de residus a la costa de Barcelona i Múrcia, ambdues a la costa mediterrània de la Península Ibèrica. Aquest estudi ha permès avançar en el desenvolupament de les metodologies emprades per a l'anàlisi i la quantificació dels fluxos de metalls i metal·loides d'origen antropogènic al medi marí, així com llur caracterització fisicoquímica i distribució en els sediments. A continuació es presenta un resum dels resultats obtinguts (per a una descripció més àmplia, consulteu els apartats 2.1, 2.2 i 2.3).

En l'estudi realitzat a l'aqüífer al·luvial de la Riera d'Argentona (subcapítol 2.1) s'ha monitoritzat la salinitat, el nivell piezomètric i la temperatura en dos piezòmetres durant dos anys. Els resultats mostren dos patrons temporals diferenciats en ambdós piezòmetres estudiats (PZ1 i PZ0): (1) valors estables de salinitat durant llargs períodes sense precipitació amb valors màxims d'entre 15 i 17 psu i (2) significants variacions de la salinitat durant períodes de precipitacions amb la corresponent reducció de la salinitat seguida d'un gradual increment (Figura 2.3.a,c). Tanmateix, en el piezòmetre més proper a la costa (PZ0), la reducció de la salinitat durant els períodes de precipitacions fou acompanyada d'un increment substancial de la salinitat que coincideix alhora amb l'increment de l'altura d'onada significativa (H_0)(Figura 2.4). L'anàlisi de les concentracions dels isòtops de Ra revela una variació molt significativa en el PZ1 d'entre 2 i 80 dpm 100 L^{-1} per al ^{223}Ra, 70 i 2.100 dpm 100 L^{-1} per al ^{224}Ra, 30 i 440 dpm 100 L^{-1} per al ^{226}Ra i 70 i 1.700 dpm100 L^{-1} per al ^{228}Ra. Alhora, les concentracions de Ra presenten una forta correlació positiva amb la salinitat (r^2= 0,91, 0,97, 0,87 i 0,95 pel ^{223}Ra, ^{224}Ra, ^{226}Ra i ^{228}Ra, respectivament; $p < 0.001$). Finalment, l'estudi detallat d'un episodi de precipitació suggereix que la concentració de Ra en l'aigua subterrània segueix el patró dels cicles de recàrrega d'aigua. Contràriament, la concentració de ^{222}Rn era constant durant tot el període d'estudi amb valors d'entre $40{\cdot}10^3$ a $120{\cdot}10^3$ dpm 100 L^{-1}.

L'estudi del subcapítol 2.2 s'ha enfocat essencialment en el desenvolupament d'un mètode de calibratge de les dades obtingudes mitjançant un escàner d'anàlisi de testimonis de sediment per fluorescència de raig X (*XRF core scanner*). Concretament, el mètode ha permès obtenir la concentració absoluta de cinc metalls (Ti, Mn, Fe, Zn i Pb) i un metal·loide (As) en testimonis de sediment corresponents a dues zones afectades per abocaments directes de residus de mineria (badia de Portmán) i

de llots de depuradora (desembocadura del riu Besòs)(Figura 2.7). Els resultats dels tres mètodes de regressió lineal emprats per correlacionar la intensitat elemental de l'equip XRF core scanner i la concentració total mostren coeficients de correlació superiors a r^2=0.94 per a tots els elements (Figura 2.8). Tanmateix, el mètode de regressió lineal weighted least-squares (WLS), el qual considera els errors analítics associats a ambdues variables, mostra una major correlació, un menor error associat i menor desviació del zero en la intersecció amb l'eix d'abscisses. Alhora, l'avaluació dels errors associats a les concentracions calibrades dels elements obtingudes a partir de la llei de propagació d'errors mostra que els errors obtinguts amb el mètode WLS són un factor 4,4, 4,2, 25,8, 14,0, 1,5 i 4,0 pel Ti, Mn, Fe, Zn, As i Pb inferior a la resta de mètodes analitzats (Figura 2.10). Així doncs, s'ha observat que per mitjà d'aquest calibratge (WLS) es pot avaluar el nivell de pol·lució del sediment seguint les estrictes guies de qualitat del sediment amb error inferior a 0,4 − 2% per al Fe, 1 − 7% per al Zn, 3 − 14% per al Pb i 5 − 16% per al Mn (Taula 2.4).

Finalment, en el subcapítol 2.3 es caracteritzà físicament i química el dipòsit submarí de residus miners a la badia de Portmán mitjançant un estudi integrat de múltiples variables obtingudes amb metodologies no destructives, d'alta resolució i en continu, incloent el mètode de calibratge desenvolupat en el subcapítol 2.2. Concretament, s'identificaren un total de sis fàcies sedimentàries en els cinquanta-dos testimonis de sediment analitzats (Figura 2.13 i 2.14). Concretament, quatre d'aquestes (fàcies 2, 3, 4 i 5) mostren una elevada concentració de metalls i metal·loides amb valors d'entre 1170 i 10.370 mg kg^{-1} per al Mn, 4,7 i 23 % per al Fe, 1.080 i 13.340 mg kg^{-1} per al Zn, 60 i 1.710 mg kg^{-1} per al As i d'entre 860 i 5.590 mg kg^{-1} per al Pb (Taula 2.7). En canvi, les dues fàcies restants 1 i 6 presentaven un contingut inferior amb valors de 110 i 2.130 mg kg^{-1} per al Mn, 1 i 16,7 % per al Fe, <7 i 9.420 mg kg^{-1} per al Zn, <17 i 650 mg kg^{-1} per al As i d'entre 5 i 4.200 mg kg^{-1} per al Pb (Taula 2.7). Alhora, les unitats amb major concentració de metalls i metal·loides presentaven una major densitat i susceptibilitat magnètica amb una mida de gra predominantment fina.

Atenint-nos a la caracterització sedimentològica realitzada anteriorment, els testimonis de sediment foren agrupats segons la distribució de les fàcies identificades (Figura 2.15). Els resultats mostren que els testimonis que contenen les fàcies 2, 3 i 5, agrupats en la subàrea 1, es localitzen al nord-oest de l'àrea d'estudi a prop del punt d'abocament dels residus miners. En canvi, els testimonis caracteritzats per la 4.1 i 4.2 corresponen a la subàrea 2 i 3 situades en el límit sud i sud-est de la subàrea 2.

Finalment, els testimonis més allunyats del punt d'abocament estaven caracteritzats principalment per la fàcies 1 (subàrea 4). Des d'una perspectiva geoquímica, els resultats mostren una diferenciació entre dos grups d'elements, per una banda el Mn, Fe, As i Pb, i per altra banda el Zn. Aquests resultats, que són corroborats per l'Anàlisi de Components Principals, el qual mostra una primera component principal (PC1) que explica el 69,1% de la variància mostral amb càrregues positives per Mn, Fe, Zn i As i una segona component principal (PC2) que explica el 14,7%, caracteritzada per una càrrega positiva de Zn, i en menor mesura del Pb (Figura 2.17, Taula 2.8).

Capítol 3

"Salpar de nou,
pensar-te en alta mar."
Aina Torres

Discussió

Fluxos de metalls i metal·loides per descàrregues d'aigües subterrànies: implicacions en llur quantificació mitjançant isòtops de Ra i ^{222}Rn.

Flux de metalls i metal·loides per abocament directe als sistemes costaners.

Metodologies de quantificació de les concentracions de metalls i metal·loides en sediments marins altament contaminats.

Caracterització sedimentològica i distribució de metalls i metal·loides en sediments marins altament contaminats de la badia de Portmán.

Models numèrics de distribució tridimensional de la concentració de metalls i metal·loides en el sediment marí: quantificació de la massa total elemental.

En aquest capítol es discuteixen conjuntament els resultats presentats als diferents apartats del capítol 2 amb la doble finalitat d'oferir una visió integradora i d'aprofundir en l'anàlisi crítica de les metodologies disponibles per a l'estudi dels fluxos de metalls i metal·loides d'origen antropogènic cap al medi marí. En aquesta Tesi s'han considerat dos tipus de fluxos: les descàrregues d'aigües subterrànies (DAS) i l'abocament directe de residus al mar costaner, prenent com a referència dues àrees de la costa mediterrània espanyola: Barcelona i Múrcia. Primer s'aborda la revisió de la metodologia de quantificació de les DAS mitjançant els isòtops del Ra, en tant que mecanisme de transport de metalls i metal·loides des del continent cap al mar costaner. En segon lloc, es profunditza en les metodologies de quantificació de la concentració i la distribució de metalls i metal·loides en els sediments marins a causa de l'abocament directe de residus al mar costaner.

3.1 Fluxos de metalls i metal·loides per descàrregues d'aigües subterrànies: implicacions en llur quantificació mitjançant isòtops de Ra i ^{222}Rn

En el primer article (subcapítol 2.1) es proposa una revisió de la metodologia de quantificació de les DAS per mitjà d'isòtops de Ra i ^{222}Rn, emprada per a determinar els fluxos associats de metalls i metal·loides cap al mar costaner (Rodellas et al., 2014; Trezzi et al., 2016). Per fer-ho, s'ha analitzat la variabilitat temporal de la posició de la interfase salina i de les concentracions dels isòtops de Ra i ^{222}Rn a l'aqüífer costaner de la riera d'Argentona.

La posició i la dinàmica de la interfase salina estan governades, en termes generals, pel gradient hidràulic entre l'aigua dolça de l'aqüífer i l'aigua salina a l'interior de l'aqüífer. És prou conegut que hi ha múltiples mecanismes oceanogràfics (p. ex. onades o el règim mareal) i terrestres (p. ex. precipitacions o extraccions d'aigua) que controlen el gradient hidràulic (Henderson et al., 2010; Santos et al., 2012; Li et al., 2008; Abarca et al., 2013). En ambients micromareals, com la mar Mediterrània, els mecanismes terrestres determinen el gradient hidràulic per sobre dels mecanismes oceanogràfics (Szymczycha et al., 2012; Gonneea i Charette, 2014). A l'aqüífer de la riera d'Argentona, el monitoratge realitzat durant dos anys confirma aquesta dominància del medi terrestre, i apunta al règim de precipitacions estacional com a principal mecanisme de control del gradient hidràulic i, per tant, de la posició de la interfase salina dins l'aqüífer (Figura 2.3.a,c).

Els resultats mostren que aquest règim, caracteritzat per llargs períodes secs, i períodes curts amb precipitacions intenses, té una forta influència sobre la posició de la interfase salina (Figura 2.3.a,d). En períodes de precipitacions, la recàrrega de l'aqüífer incrementa el gradient hidràulic entre ell i el mar, i força un desplaçament de la interfase salina en direcció al mar. Aquest procés es fa palès per la reducció de la salinitat a la part baixa del piezòmetre PZ1 durant els episodis de precipitacions. Un cop finalitza la recàrrega de l'aqüífer, el gradient hidràulic disminueix i la interfase es desplaça en direcció a terra, com reflecteix l'increment de la salinitat a la part baixa del PZ1 (Figura 2.3). Alhora, els resultats revelen que el desplaçament de la interfase salina és ràpid durant els episodis de pluja, d'hores a dies, mentre que la recuperació de llur posició inicial requereix setmanes o mesos. Aquest comportament l'il·lustra perfectament l'episodi de precipitacions analitzat (RFE-8) (Figura 2.3.d,e), amb una reducció de la salinitat en el piezòmetre PZ1-B de 13 a 0,3 en aproximadament 23 hores, mentre que la recuperació de la salinitat inicial fins arribar al valor de 13 − 15 requerí uns 6 mesos.

Anàlogament, el piezòmetre situat més a prop del mar (PZ0) mostra un patró similar a l'observat en el PZ1, tot i que també s'enregistraren increments significants de la salinitat, coincidents amb augments de l'onatge durant els temporals de llevant, molt característics de la Mediterrània occidental (Figura 2.4). L'increment de la freqüència i l'altura d'onada modifiquen l'equilibri del gradient hidràulic, tot desplaçant la interfase salina en direcció a terra i incrementant la salinitat a l'aqüífer més proper al mar (Moore i Wilson, 2005).

Puix que la desadsorció dels isòtops de Ra als aqüífers augmenta amb la salinitat (Figura 2.5.a) (Elsinger i Moore, 1980; Cho i Kim, 2016), els resultats assolits en aquesta Tesi demostren que la posició de la interfase salina exerceix una influència notable sobre el contingut de Ra a les aigües subterrànies. Les activitats de Ra obtingudes a aquestes aigües durant els dos anys de monitoratge mostren unes variacions significants d'un factor ~19, ~14, ~6 i ~11 pel ^{223}Ra, el ^{224}Ra, el ^{226}Ra i el ^{228}Ra, respectivament (Taula 2.1). Durant els episodis de precipitació, la reducció significativa de les concentracions de Ra es correlaciona, com és d'esperar, amb la reducció de la salinitat i, per tant, amb el desplaçament en direcció a mar de la interfase salina (Figura 2.3.e). Altrament, durant els períodes secs en que la posició de la interfase salina és estable, les concentracions de Ra són constants i més elevades. Les concentracions relativament estables del ^{222}Rn, amb variacions

mínimes d'un factor ~2 durant tot el període estudiat, indiquen una menor influència de la posició de la interfase salina. Això és degut al fet que el Rn és present a les aigües subterrànies en estat gasós, amb la seva producció controlada pel contingut de ^{226}Ra, pare radioactiu del ^{222}Rn, en estat dissolt o particulat a l'aigua de l'aqüífer (Dulaiova et al., 2008). La baixa influència de la salinitat en el comportament del ^{222}Rn corrobora aquest comportament (Figura 2.5).

L'elevada variabilitat de les concentracions de Ra a les aigües subterrànies esdevé la principal font d'incerteses a l'hora de quantificar les DAS emprant com a traçadors els isòtops del Ra (Elsinger i Moore, 1980; Cho i Kim, 2016). Aquesta quantificació es duu a terme mitjançant l'equació:

$$DAS = \frac{J_{Ra/Rn}}{Ra/Rn_{gw}} \quad (1)$$

on, $J_{Ra/Rn}$ és el flux dels isòtops de Ra i de ^{222}Rn cap al mar costaner en dpm d^{-1} i Ra/Rn_{gw} és la concentració de referència dels isòtops de Ra i del ^{222}Rn a les aigües subterrànies (en anglès, *end-member*, vegeu l'apartat 2.1). En el cas del Ra, el qual presenta més variabilitat, la magnitud de l'error potencial associat al seu end-member depèn de la representativitat d'aquest valor a l'àrea d'estudi. Per obtenir aquest valor, en estudis anteriors hom ha emprat diverses assumpcions: i) càlcul del valor mitjà de mesures realitzades a l'aqüífer, ii) selecció del valor de concentració més alt per obtenir la DAS mínima (estratègia conservadora), i iii) tria de la mostra més propera al punt de descàrrega al mar costaner. Michael et al. (2011) demostraren que els fluxos de DAS quantificats amb isòtops de Ra partint d'aquestes assumpcions diferien entre ells un factor de 10. Alhora, Cho i Kim (2016) han reportat que les activitats dels isòtops de Ra a l'aqüífer presenten una elevada variabilitat espacial i temporal com a resultat de canvis en la força iònica de la fase dissolta. En aquest sentit, els resultats presentats al subcapítol 2.1 aporten noves evidències sobre aquesta qüestió i desvelen una variabilitat temporal significativa de la concentració de Ra, d'aproximadament un ordre de magnitud, en aqüífers costaners micromareals. Aquesta variabilitat dificulta notablement la determinació d'un valor representatiu de Ra a l'aqüífer, i introdueix una incertesa potencial en la quantificació dels fluxos de les DAS i, consegüentment, en el fluxos de metalls i metal·loides associats. Del monitoratge dels paràmetres hidrogeològics descrit al subcapítol 2.1 es desprèn que l'elevada variabilitat d'aquests sistemes requereix un millor coneixement de la hidrodinàmica dels aqüífers costaners micromareals per poder quantificar les DAS

mitjançant isòtops de Ra. Alhora, puix que les descàrregues d'aigua subterrània i els fluxos de metalls i metal·loides associats augmenten durant els períodes de precipitacions, suggerim que l'avaluació de les DAS en aquests períodes hauria de ser una prioritat en futurs estudis d'aqüífers costaners micromareals, pel seu interès hidrogeològic i geoquímic.

L'anàlisi de les concentracions de Ra i un millor coneixement dels paràmetres hidrogeològics ha permès, per exemple, quantificar el flux de metalls i metal·loides per DAS i per difusió d'aigua intersticial (en anglès, *porewater exchange*, PEX) provinent del dipòsit emergit de residus miners de la badia de Portmán cap al mar costaner (Alorda et al., 2019). Això és especialment rellevant per bé que, a diferència de l'aqüífer de la riera d'Argentona, la posició de la interfase salina dins el dipòsit de residus miners de la badia de Portmán està controlada per l'onatge i, en menor mesura, pel règim mareal. Aquest mateix patró també s'ha observat al piezòmetre de l'aqüífer de la riera d'Argentona més proper al mar (PZ0) (Figura 2.4). Considerant el migrat règim de precipitacions a la badia de Portmán (<300 mm any^{-1}), el treball realitzat per Alorda et al. (2019) demostra que els fluxos de DAS estan fortament modulats pels típics temporals marítims de tardor propis de la Mediterrània Occidental. Alhora, el coneixement detallat de la hidrogeologia de la badia, amb la instal·lació de quatre piezòmetres instrumentats amb CTDs − metodologia similar a l'aplicada per l'estudi del subcapítol 2.1 − ha permès situar la zona preferent per a les DAS a l'oest de la badia. Contràriament, a l'est de la badia el principal mecanisme que modula el flux de metalls i metal·loides per PEX és el bombeig d'aigua per l'acció de les onades i, en menor mesura, les marees.

Els resultats revelen que el flux de metalls per DAS i PEX, quantificat mitjançant els isòtops de Ra, és de 2,7 ± 1.4 i 0,6 ± 0.3 mol d^{-1} km^{-1} per al Pb; 1600 ± 790 i 67 ± 34 mol d^{-1} km^{-1} per al Zn; i 145 ± 73 i 3200 ± 1800 mol d^{-1} km^{-1} per al Fe. Aquests fluxos són significativament més grans que els reportats per altres estudis (Windom et al., 2006; Rodellas et al., 2014; Tovar-Sánchez et al., 2014) i un ordre de magnitud superiors als quantificats per Trezzi et al. (2016) a la badia del Gorguel, adjacent a la badia de Portmán, i també afectada, tot i que en molta menor mesura, per l'abocament de residus miners. L'estudi realitzat per Alorda et al. (2019) és un exemple pràctic de l'aplicació de les conclusions obtingudes al subcapítol 2.1, que evidència la seva validesa per determinar el comportament temporal dels isòtops de Ra en aqüífers costaners, quan són emprats per quantificar els fluxos de DAS i de metalls i metal·loides associats.

3.2 Fluxos de metalls i metal·loides per abocament directe en sistemes costaners

3.2.1 Metodologies de quantificació de les concentracions de metalls i metal·loides en sediments marins altament contaminats

La determinació de les concentracions absolutes de metalls i metal·loides és indispensable per avaluar el grau de contaminació i pol·lució dels sediments marins (Ramirez et al., 2005; Palanques et al., 2008). Les tècniques utilitzades tradicionalment (p. ex. espectrometria de masses i d'emissió òptica de plasma acoblat inductivament, IPC-MS i ICP-OES, o fluorescència de raigs X) permeten una quantificació acurada, precisa i amb un baix error associat, tot i que el procediment químic suposa la destrucció de la mostra, alhora que són costoses i requereixen una elevada inversió de temps. Per aquest motiu, en el segon article (subcapítol 2.2) presentem un procediment que permet convertir les intensitats dels elements obtingudes mitjançant l'escàner de fluorescència de raigs X (*XRF core scanner*) en concentracions absolutes dels elements de manera precisa i amb un baix error associat (Figura 2.8). Aquest calibratge ha estat realitzat a partir de les mesures fetes en testimonis de sediments obtinguts en dos indrets, un impactat per abocaments de residus miners (badia de Portmán) i l'altre per abocament de fangs provinents d'una planta de tractament d'aigües residuals (davant la gola del riu Besòs, a Barcelona).

Els resultats obtinguts revelen que el coeficient de correlació (r^2) entre les variables intensitat (cps) i concentració absoluta dels metalls i metal·loides analitzats (Ti, Mn, Fe, Zn, As i Pb) és superior a 0.94 per a qualsevol dels tres mètodes de regressió lineal avaluats. Aquestes correlacions són superiors a les obtingudes en estudis anteriors (Figura 2.8) (Böning et al., 2007). Tot i això, un dels mètodes de regressió lineal, el mètode dels mínims quadrats ponderats (WLS), que considera els errors analítics d'ambdues variables, és el que presenta una menor desviació estàndard de l'estimador (S) i, alhora, una menor desviació del zero a l'eix de coordenades (Taula 2.3). Atès que qualsevol calibratge incorpora un seguit d'errors analítics i estadístics, determinar els errors associats a la concentració calibrada de cada metall i metal·loide és un procediment necessari per avaluar la qualitat i les limitacions del mètode aplicat. La distribució dels errors relatius obtinguts a partir de la propagació dels errors de la concentració calibrada (Figura 2.10) (Taylor i Kuyatt, 1994) demostra, com es podia esperar, que els errors augmenten significativament a concentracions baixes per a tots els mètodes de regressió, especialment quan ens apropem als

límits de detecció de l'equip (Ramsey et al., 1995). Tanmateix, el mètode WLS presenta uns errors associats significativament menors que els altres dos mètodes. Això s'explica per les diferències observades en la desviació estàndard del pendent entre els tres mètodes de regressió considerats (Taula 2.3). Concretament, aquesta desviació estàndard pel mètode OLS és superior a l'obtinguda pel mètode WLS en uns factors de 4,4, 4,2, 25,8, 14,0, 1,5 i 4,0 per al Ti, el Mn, el Fe, el Zn, el Al i el Pb, respectivament.

L'ús potencial d'aquesta metodologia en estudis de contaminació i pol·lució de sediments marins per metalls i metal·loides està condicionat per la capacitat de determinar llurs concentracions segons els estàndards de qualitat del sediment (en anglès, *sediment quality guidelines*, SQG). Servint-nos del principal estàndard de qualitat, del procediment desenvolupat a la secció 2.2 i del mètode de regressió lineal WLS, demostrem que les concentracions llindar de metalls i metal·loides establertes en aquestes guies es poden quantificar amb errors mínims, d'entre 0,4% i 2% per al Fe, 1% i 7% per al Zn, 3 i 14% per al Pb, i 5% i 16% per al Mn (Taula 2.4). Aquests resultats evidencien la robustesa metodològica del procediment de calibratge desenvolupat en aquesta Tesi, la qual cosa permet una quantificació acurada i precisa de les concentracions absolutes d'aquests metalls i metal·loides a partir de les mesures semi-quantitatives de l'*XRF core scanner*. Convé destacar que aquest és el primer estudi que incorpora i avalua els errors analítics i estadístics de la calibració de les mesures d'un equip d'*XRF core scanner* i, en conseqüència, evidencia la necessitat d'avaluar correctament els errors de les concentracions calibrades en futurs estudis.

3.2.2 Caracterització sedimentològica i distribució de metalls i metal·loides en els sediments marins altament contaminats de la badia de Portmán

Al subcapítol 2.3 presentem la primera caracterització física i química del dipòsit de residus miners submergits de la badia de Portmán. Això ha estat possible mitjançant la implementació d'un protocol que integra múltiples tècniques analítiques (Figura 1.16), entre les quals s'inclou l'anàlisi d'imatges 3D de tomografia computeritzada d'alta resolució, la determinació de paràmetres físics com la susceptibilitat magnètica i la densitat, la mesura de la composició química elemental i de la mida de gra, així com també la datació del sediment per ^{210}Pb. Així mateix, en aquest treball s'aplica per primera vegada el procediment de calibratge descrit a la secció 2.2, el qual ha

permès convertir ~14,000 mesures d'intensitats de metal·loides i metalls obtingudes *XRF core scanner* en concentracions absolutes dels elements identificats.

La integració d'aquestes tècniques ha permès diferenciar fàcies sedimentàries a partir de les característiques físiques i químiques dels materials. Així, dins el dipòsit de residus miners *stricto sensu* s'hi han identificat quatre fàcies diferenciades (fàcies 2, 3, 4 i 5), a les quals s'afegeixen les corresponent als sediments que predaten i postdaten els abocaments miners (fàcies 1 i 6, respectivament) (Figures 2.13 i 2.14). Això ha permès establir l'evolució sedimentària de la badia de Portmán al llarg de les darreres dècades amb l'accent en el període posterior al cessament de l'abocament de residus miners al mar i fins l'actualitat.

La Fàcies 1, formada per sorres fines a la fracció descarbonatada i amb unes concentracions de metalls i metal·loides relativament baixes (Figura 2.13) és present als testimonis més allunyats del punt d'abocament i de la costa en el seu conjunt. Aquesta fàcies presenta un contingut elevat de carbonats biogènics, marques de bioturbació i una alta intensitat de Ca, mesurada amb l'*XRF core scanner*. Els seus trets distintius indiquen que aquesta fàcies correspon als dipòsits sedimentaris característics de l'etapa prèvia a l'inici dels abocaments. Això ha estat confirmat per la datació amb ^{210}Pb del testimoni MC-36, que li atribueix una edat anterior a l'any 1957, quan començaren els abocaments (Figura 2.18). Als testimonis més distals, la Fàcies 1 es troba en superfície i està lleugerament influenciada pels residus miners.

Les fàcies, 2, 3, 4 i 5 se situen damunt la Fàcies 1. Estan formades per materials dipositats durant el període d'abocament de residus miners (Figura 2.19), en què el dipòsit resultant s'anà desenvolupant ràpidament en forma de cos progradant en direcció al mar. En paral·lel amb la progradació, part dels residus s'anaren estenent per la plataforma continental interna, sota la influència de l'onatge dominant de component est i sud-oest i els corrents litorals associats. Aquestes quatre fàcies presenten elevades concentracions de metalls i metal·loides (p. ex. Fe, Zn i Pb), com correspon a dipòsits resultants directament de l'abocament dels residus miners. Per tant, són fàcies pròpies de la pila de residus miners.

La Fàcies 2, localitzada al nord-oest de l'àrea d'estudi davant la badia de Portmán, al sector més proper al punt d'abocament (Figura 2.16.a,c), presenta una laminació nítida amb alternança de capes de sorres negres fines i nivells groguencs de gra més fi. Aquesta configuració seria el resultat d'un procés que combinaria taxes d'acumulació elevades amb la remobilització i la classificació per densitat de

les partícules minerals, probablement per l'acció constant de les onades i els corrents associats. Altrament, la Fàcies 3 presenta unes característiques físiques i geoquímiques similars a les de la Fàcies 2, però amb una forta deformació de la laminació (Figura 2.16.b). La localització d'aquesta unitat al talús que forma el foreset del cos de residus progradant suggereix que és el resultat de la deformació de l'estructura en capes alternants de la Fàcies 2, segurament per causa de l'elevada taxa d'acumulació i la sobrecàrrega provocada per sediments i la mateixa acumulació ràpida de materials sobreposats.

A mesura que augmenta la distància al punt de descàrrega a la costa, l'evident laminació observada a la Fàcies 2 s'esvaeix gradualment, tot i que les propietats geoquímiques són semblants a les de les fàcies més proximals. Aquests materials més allunyats de la costa constitueixen la Facies 4, la qual podria ser el resultat d'un procés d'acumulació de residus més lent. La reducció de les taxes de sedimentació amb la distància permeté certa activitat bentònica, clarament observable per l'increment de marques de bioturbació, absents a les fàcies 2 i 3 (Figura 2.16.a,b). Diferències significatives en la susceptibilitat magnètica permeten subdividir la Fàcies 4 en dues subfàcies, 4.1 i 4.2, cadascuna de les quals respon a processos de transport dels residus diferents. Els elevats valors de susceptibilitat magnètica de la Subfàcies 4.1, similars als de la Fàcies 2, podrien indicarien un procés de difusió dels residus més enllà dels límits de dos afloraments rocosos allargats o *beachrocks* al fons marí que feien de barrera natural parcial al seu escampall, situats l'un al sud i l'altre a l'est de l'àrea d'estudi (Figura 2.15). En canvi, la baixa susceptibilitat magnètica i l'abundància de fins de la Subfàcies 4.2 suggereixen l'acumulació per decantació de partícules fines remobilitzades provinents del mateix dipòsit submergit. La datació per ^{210}Pb del testimoni MC-36 confirma que la deposició de la Subfàcies 4.2 correspon encara al període comprès entre els anys 1957 i 1990, és a dir, dintre del període d'abocament de residus miners. Com la Fàcies 2, la Fàcies 5, formada per arenes fines homogènies i massives, només ha estat observada al talús que forma el foreset del cos de residus progradant, en relació amb els canals submarins normals a les isòbates que el solquen. Tot plegat, suggereix una formació tardana per efecte de corrents de densitat.

La clausura dels abocaments reduí significativament les taxes de sedimentació, i va deixar el sostre del dipòsit de residus exposat a l'acció directa de l'onatge i els corrents. S'inicià així un procés de triatge i concentració per densitats i mida de gra,

i de certa recuperació de les condicions de sedimentació prèvies als abocaments. Així, la Fàcies 6, la més superficial i recent, presenta una reducció significativa de les concentracions de metalls i metal·loides respecte als dipòsits infrajacents, un increment de la mida de gra i el retorn de les marques de bioturbació. La datació per ^{210}Pb indica que la base inferior de la Fàcies 6 correspon a l'any 1990, coincidint amb els cessament dels abocaments.

3.2.3 Models numèrics de distribució tridimensional de la concentració de metalls i metal·loides en sediments marins: quantificació de la massa elemental total

Per entendre la dispersió horitzontal de metalls i metal·loides als sediments marins superficials de la badia de Portmán, formats en acabar els abocaments, al subcapítol 2.3 hem modelitzat numèricament per interpolació tridimensional la distribució de les seves concentracions en els primers 14 cm de la seqüència sedimentària. Servint-nos dels algoritmes d'interpolació i adaptant-los a les especificitats del nostre model, hem integrat un total de 7.280 mesures tant de concentracions de metalls i metal·loides com de densitat i susceptibilitat magnètica en una malla amb una resolució de 10 x 10 x 0,002 m. Aquesta metodologia ens ha permès obtenir un volum de $2{,}2 \cdot 10^6$ m^3, que il·lustrem amb mapes de la distribució horitzontal dels elements investigats en els centímetres 0 − 1, 7 − 8 i 14 − 15 (Figures 2.20 i 2.21). Les matrius tridimensionals són una eina molt versàtil i fàcilment operable, que també ens ha permès quantificar la distribució dels factors d'enriquiment de cada metall i metal·loide.

A grans trets, els resultats mostren un increment de les concentracions de metalls i metal·loides cap al nord-oest de l'àrea d'estudi. Això és clarament visible al centímetre 14 de sediment, corresponent a la transició entre el sostre del dipòsit de residus miners i els sediments que el postdaten. Tot indica que la distribució observada és el resultat de la proximitat al punt d'abocament i de la dinàmica sedimentària a la plataforma interna, dominada per l'acció de les onades de component est i sud-oest i els corrents litorals associats. Els mapes de distribució de metalls i metal·loides confirmen l'existència d'un "punt calent" de concentració al nord-oest de l'àrea d'estudi, identificat a la secció 2.3.5.3, i d'una àrea perifèrica més allunyada de la badia *sensu strictu*, on les concentracions són significativament menors. La concentració de metalls i metal·loides en els centímetres superiors del

paquet sedimentari palesa una reducció respecte als dipòsits infrajacents formats directament a partir dels abocaments de residus miners. Tot i l'evident reducció de les concentracions de metalls i metal·loides, els factors d'enriquiment obtinguts en els sediments superficials post-abocament continuen essent molt més alts que els reportats en altres àrees costaneres igualment contaminades per metalls (p. ex. Palanques et al., 2017; Sternal et al., 2017).

Els resultats obtinguts en aigües de Portmán permeten, a més, dimensionar l'àrea de sediments superficials que cal considerar "perillosos" de 9,4 km^2 d'extensió. També s'ha pogut calcular la massa total de cadascun dels metalls i metal·loides investigats en els 14 cm superficials de sediment, tot combinant les matrius de concentracions i de densitat i el volum de cada vòxel del volum 3D. L'estimació de la massa total de cada metall en aquests primers 14 cm de sediment és de 6.700 ± 1.400 t per al Mn, $2{,}6 \cdot 10^5$ ± 3,9 10^3 t per al Fe, 7.700 ± 1.600 t per al Zn, 670 ± 140 t per al As i 3.170 ± 650 t per al Pb. Aquesta estimació, combinada amb l'anàlisi física i química dels sediments superficials, evidencia l'existència d'un flux persistent de metalls i metal·loides cap al fons de la plataforma continental interna vint-i-cinc anys després de la finalització de l'abocament de residus miners a la badia de Portmán.

Capítol 4

"Nosaltres cridarem amb veu nova les velles paraules."

Maria Àngels Anglada

Conclusions
i línies d'investigació futures

A la present Tesi doctoral hom revisa i desenvolupa un conjunt de metodologies per a l'anàlisi i la quantificació dels fluxos de metalls i metal·loides d'origen antropogènic cap a l'ambient marí costaner, i caracteritza dipòsits altament contaminats acumulats en aquest mateix ambient. Així, hem analitzat dos grups de processos determinants dels fluxos de metalls i metal·loides cap als sistemes costaners submergits: les descàrregues d'aigües subterrànies i l'abocament directe de residus. Sobre el terreny, l'estudi s'ha desenvolupat a les costes de Barcelona i de Múrcia, totes dues representatives de les costes mediterrànies altament antropitzades. El plantejament multidisciplinari d'aquesta Tesi ha permès un avenç significatiu, metodològic i de resultats, en l'estudi dels processos de contaminació per metalls i metal·loides en sistemes costaners.

L'anàlisi temporal dels isòtops de Ra de l'aqüífer costaner de la riera d'Argentona ens ha permès demostrar que llurs concentracions presenten una elevada variabilitat, principalment degut al desplaçament de la interfase salina en direcció al mar durant els períodes de recàrrega de l'aqüífer. Aquesta elevada variabilitat, de més d'un ordre de magnitud, dificulta l'estimació d'un valor representatiu de la concentració de Ra a l'aqüífer, paràmetre necessari per poder quantificar les descàrregues d'aigües subterrànies (DAS). Atenent al fet que els fluxos de metalls i metal·loides derivats de les DAS s'incrementen significativament durant els episodis de precipitacions, advoquem per la necessitat de seguir aprofundint en el coneixement hidrogeològic dels aqüífers costaners, així com del comportament dels isòtops de Ra, amb l'objectiu de reduir incerteses i quantificar aquests fluxos cap als sistemes costaners de manera més acurada.

S'ha desenvolupat satisfactòriament un procediment de calibratge per transformar grans quantitats de mesures semiquantitatives d'escàner de fluorescència de raigs X (*XRF core scanner*) en concentracions total de metalls i metal·loides. Els resultats revelen que el procediment analític i estadístic desenvolupat millora la qualitat de les regressions lineals en els tres mètodes emprats, de mínims quadrats ordinaris (OLS), de mínims quadrats ordinaris ponderats (WOLS) i de mínims quadrats ponderats (WLS). Aquest procediment també millora els coeficients de correlació i redueix la desviació del punt d'intersecció i les desviacions estàndards associades a les funcions obtingudes. Tanmateix, els resultats també demostren que l'aproximació mitjançant el mètode WLS, el qual té en compte els errors associats a ambdues variables, en aquest cas la intensitat elemental (cps) i la concentració absoluta (ppm o %), és més

avantatjosa, especialment quan es compara amb el mètode OLS. A més, debatem la idoneïtat de la metodologia de calibratge i la reducció dels errors associats per avaluar l'ecotoxicitat del sediment d'acord amb les estàndards de les corresponents guies de qualitat (en anglès, *sediment quality guidelines*, SQG). Els resultats demostren que el calibratge desenvolupat amb el mètode WLS permet quantificar els llindars de concentració establerts en diverses SQG amb un rang d'errors d'entre el 5% i el 16% per al Mn, 0,4% i el 2% per al Fe, l'1% i el 7% per al Zn, i el 3% i el 14% per al Pb.

L'aplicació d'aquesta metodologia a un extens estudi sobre els sediments altament contaminats per metalls i metal·loides a causa de l'abocament de residus miners a la badia de Portmán i a la plataforma interna adjacent també ha donat bons resultats. Per primer cop s'ha caracteritzat, físicament i química, la part més superficial del dipòsit de l'extensió submarina del dipòsit de residus miners de la badia de Portmán, i dels sediments acumulats en el període transcorregut des de la clausura de l'abocament l'any 1990. Per fer-ho possible, hem aplicat una metodologia que integra múltiples tècniques d'alta resolució, no destructives i de mesura continua, amb la qual hem analitzat cinquanta-dos testimonis curts de sediment (< 50 cm).

També hem aplicat tècniques de datació pel mètode del ^{210}Pb. El gruix de l'extensió submarina del dipòsit de residus, o si més no dels acumulats durant el període final dels abocaments, se situa principalment al nord-oest de l'àrea d'estudi, entre la línia de costa actual de la badia de Portmán i un beachrock aflorant localitzat a uns 45 m de profunditat, el qual produí un efecte barrera que limità l'expansió dels residus més mar endins. Les concentracions de metalls i metal·loides que mesurades en aquesta àrea (Fe, Zn, As, Pb) són més altes que les reportades en qualsevol altre indret de la mar Mediterrània.

La distribució de les concentracions de metalls i metal·loides a l'àrea d'estudi s'ha realitzat mitjançant modelització numèrica per interpolació tridimensional del conjunt de testimonis per diferents nivells de profunditat dins el dipòsit. Hem pogut demostrar així que els factors d'enriquiment en els sediments post-abocament, tot i haver-se reduït significativament respecte als del dipòsit infrajacent de residus miners *sensu strictu*, són notablement elevats; i també a la capa més superficial (0 − 1 cm), que presenta concentracions de metalls i metal·loides superiors a les mesurades en altres ambients marins costaners fortament contaminats. S'evidencia així un flux persistent de metalls i metal·loides cap al fons marí, un quart de segle després de la clausura dels abocaments al mar. Aquest mateix model també ens ha permès quantificar la massa

total de cada element en els primers 14 centímetres de sediment, corresponents al període posterior al cessament dels abocaments, és a dir entre 1990 i 2015, any en què s'efectuà la segona campanya d'obtenció de testimonis.

Els resultats d'aquesta Tesi provenen de l'aplicació d'un ampli ventall de tècniques analítiques avançades, i també de tècniques, numèriques, amb la finalitat d'identificar i quantificar els fluxos, la distribució i les concentracions de metalls i metal·loides en ambients costaners. L'aplicació i la integració de les dades proporcionades per aquest ventall de tècniques és clau per a poder analitzar en detall casos de contaminació com els tractats en aquesta Tesi. Tot plegat entenem que representa una contribució significativa a la millora dels coneixements sobre la contaminació antropogènica en els ambients marins costaners, susceptible de ser aplicada a altres indrets d'arreu del món amb problemàtiques similars.

Línies d'investigació futures

Arran dels treballs realitzats en el marc d'aquesta Tesi han sorgit, com és natural, noves preguntes i qüestions que poden esdevenir línies futures d'investigació. Algunes poden ser abordades amb dades ja disponibles actualment, i que ja s'han començat a treballar, mentre que altres requeririen la realització de noves recerques a mar i al laboratori. A continuació presentem, de forma esquemàtica, algunes línies d'investigació de futur que ens semblen especialment prometedores:

1) Aprofundiment en les metodologies de calibratge de mesures d'escàner de fluorescència de raigs X

El procediment de calibratge que presentem al subcapítol 2.2 permet la conversió de les intensitats obtingudes amb l'escàner de fluorescència de raigs X a concentracions absolutes emprant un nombre reduït de mostres. Aquest procediment és intencionadament poc complex amb l'objectiu d'esdevenir una eina pràctica a l'hora d'abordar la conversió d'un volum elevat de mesures. Tanmateix, presenta certes limitacions producte de l'efecte que canvis en la matriu dels sediments, en el contingut d'aigua i/o en la mida de gra de les partícules poden tenir en les mesures de la intensitat elemental. Amb l'objectiu de superar aquestes limitacions i obtenir una calibració universal per a qualsevol mesura mitjançant equips d'escàner de fluorescència de raigs X seria altament interessant ampliar les capacitats del procediment mitjançant l'adaptació dels

models log-ratio desenvolupats per Weltje i Tjallingii (2008), els quals deriven de la teoria de la fluorescència de raigs X, els principis de l'anàlisi computacional i l'evidència empírica.

2) Identificació i quantificació de l'activitat bentònica en el sediment superficial mitjançant l'estudi de marques de bioturbació a través d'imatges 3D de tomografia computeritzada

Les evidències que hem exposat en el subcapítol 2.3 assenyalen un increment de l'activitat d'organismes bentònics en el sediment superficial de la plataforma continental adjacent a la badia de Portmán (0 − 14 m de profunditat), segons mostren les marques de bioturbació observades a les imatges de micro-CT. Atenent a l'absència d'aquesta mena de marques al dipòsit de residus miners, la identificació de les espècies responsables i llur abundància per mitjà de l'anàlisi de les imatges 3D de micro-CT podria ajudar a entendre el restabliment, ni que sigui parcial, de les comunitats bentòniques un cop finalitzà l'abocament de residus, i també en comparació amb les comunitats i espècies observades en els sediments de sota els dipòsits de residus i en indrets propers lliures de residus d'aquest tipus.

3) Especiació de metalls i metal·loides i llur biodisponibilitat a l'extensió submarina del dipòsit de residus miners de la badia de Portmán

La determinació de l'estat d'oxidació dels metalls i metal·loides en el sediment marí acumulat després de cessar els abocaments a Portmán, així com en el dipòsit submergit de residus miners, té implicacions ecotoxicològiques evidents. Diversos treballs realitzats mitjançant espectrometria d'absorció de raigs X als sincrotrons Diamond Light Source (Anglaterra) i ALBA (Catalunya) han permès començar a entendre l'especiació d'elements com el Fe, el Al o el Pb en aquests ambients tan especials, de fet ambients extrems. En aquesta línia, convé destacar un treball en procés de revisió (Roqué et al., 2020) en el qual s'evidencia el procés de transformació química del As des del processament del mineral fins al seu abocament i enterrament en ambient marí. Els resultats d'aquests estudis poden ser rellevants, pensant també en el desenvolupament futur de la mineria oceànica profunda, i en el l'impacte de les activitats associades sobre organismes i ecosistemes marins.

4) Aplicació de models de distribució de metalls i metal·loides en el sediment marí superficial a escala regional

Tal com es deriva del subcapítol 2.3, els mapes de distribució de metalls i metal·loides en el sediment marí són una eina molt potent per avaluar llur dispersió i tendències. Atenent a l'increment dels fluxos de metalls i metal·loides d'origen antropogènic cap als sistemes costaners a les darreres dècades, la integració de dades de concentració i paràmetres físics del sediment mitjançant models d'interpolació tridimensional permetria aprofundir en el coneixement de les seves concentracions i distribucions. Aquesta línia d'investigació seria d'un interès notable en casos paradigmàtics com el Mar Menor o el Mar Adriàtic, especialment impactats per abocaments de residus de diversos tipus. En l'ampliació de l'aplicabilitat d'aquesta metodologia seria convenient refinar el models d'interpolació, reduint els errors associats i millorant la qualitat de les estimacions obtingudes. També seria altament interessant integrar aquests models de distribució amb dades d'onatge i atmosfèriques, per millorar la comprensió de la interacció entre els fluxos de metalls i metal·loides i les condicions oceanogràfiques.

Capítol 5

"Hi haurà amor engrunat al fons de les butxaques."
Maria Mercè Marçal

Bibliografia

Abarca, E., Karam, H., Hemond, H.F., Harvey, C.F., 2013. Transient groundwater dynamics in a coastal aquifer: The effects of tides, the lunar cycle, and the beach profile. Water Resour. Res. 49, 2473–2488. https://doi.org/10.1002/wrcr.20075

Abril, G.A., Wannaz, E.D., Mateos, A.C., Invernizzi, R., Plá, R.R., Pignata, M.L., 2014. Characterization of atmospheric emission sources of heavy metals and trace elements through a local-scale monitoring network using T. capillaris. Ecol. Indic. 40, 153–161. https://doi.org/10.1016/j.ecolind.2014.01.008

Acosta, J., Fontán, A., Muñoz, A., Muñoz-Martín, A., Rivera, J., Uchupi, E., 2013. The morpho-tectonic setting of the Southeast margin of Iberia and the adjacent oceanic Algero-Balearic Basin. Mar. Pet. Geol. 45, 17–41. https://doi.org/10.1016/j.marpetgeo.2013.04.005

Adachi, K., Tainosho, Y., 2004. Characterization of heavy metal particles embedded in tire dust. Environ. Int. 30, 1009–1017. https://doi.org/10.1016/j.envint.2004.04.004

Adamo, P., Arienzo, M., Imperato, M., Naimo, D., Nardi, G., Stanzione, D., 2005. Distribution and partition of heavy metals in surface and sub-surface sediments of Naples city port. Chemosphere 61, 800–809. https://doi.org/10.1016/j.chemosphere.2005.04.001

Alloway, B.J., 1990. Heavy metals in soils. Springer. https://doi.org/10.1016/s0165-9936(96)90032-1

Alorda-Kleinglass, A., Garcia-Orellana, J., Rodellas, V., Cerdà-Domènech, M., Tovar-Sánchez, A., Diego-Feliu, M., Trezzi, G., Sánchez-Quilez, D., Sanchez-Vidal, A., Canals, M., 2019. Remobilization of dissolved metals from a coastal mine tailing deposit driven by groundwater discharge and porewater exchange. Sci. Total Environ. 688, 1359–1372. https://doi.org/10.1016/j.scitotenv.2019.06.224

Andersen, M.S., Larsen, F., Postma, D., 2001. Pyrite oxidation in unsaturated aquifer sediments. Reaction stoichiometry and rate of oxidation. Environ. Sci. Technol. 35, 4074–4079. https://doi.org/10.1021/es0105919

Ankley, G.T., 1996. Evaluation of metal/acid-volatile sulfide relationships in the prediction of metal bioaccumulation by benthic macroinvertebrates. Environ.

Toxicol. Chem. 15, 2138–2146. https://doi.org/10.1002/etc.5620151209

Atkins, P., Jones, L., 1997. Chemistry - Molecules, Matter and Change, 3rd ed. WH Freeman New York.

Banos-González, I., Páez, P.B., 2013. Portmán: de el Portus Magnus del Mediterráneo occidental a la Bahía Aterrada. EDITUM.

Bastami, K.D., Neyestani, M.R., Shemirani, F., Soltani, F., Haghparast, S., Akbari, A., 2015. Heavy metal pollution assessment in relation to sediment properties in the coastal sediments of the southern Caspian Sea. Mar. Pollut. Bull. 92, 237–243. https://doi.org/10.1016/j.marpolbul.2014.12.035

Baucells, M., Lacort, G., Roura, M., de Gyves, J., 1988. Rapid determination of arsenic in the presence of lead in a zinc sulphide matrix by X-ray fluorescence spectrometry. Analyst 113, 1325−1328.

Bay, S.M., Zeng, E.Y., Lorenson, T.D., Tran, K., Alexander, C., 2003. Temporal and spatial distributions of contaminants in sediments of Santa Monica Bay, California. Mar. Environ. Res. 56, 255–276. https://doi.org/10.1016/S0141-1136(02)00334-3

Beck, A.J., Rapaglia, J.P., Cochran, J.K., Bokuniewicz, H.J., 2007. Radium mass-balance in Jamaica Bay, NY: Evidence for a substantial flux of submarine groundwater. Mar. Chem. 106, 419–441. https://doi.org/10.1016/j.marchem.2007.03.008

Beck, A.J., Cochran, J.K., Sañudo-Wilhelmy, S.A., 2009. Temporal trends of dissolved trace metals in Jamaica Bay, NY: Importance of wastewater input and submarine groundwater discharge in an urban estuary. Estuaries and Coasts 32, 535–550. https://doi.org/10.1007/s12237-009-9140-5

Beck, A.J., Cochran, M.A., 2013. Controls on solid-solution partitioning of radium in saturated marine sands. Mar. Chem. 156, 38−48. https://doi.org/10.1016/j.marchem.2013.01.008

Bergquist, B.A., Boyle, E.A., 2006. Iron isotopes in the Amazon River system: Weathering and transport signatures. Earth Planet. Sci. Lett. 248, 54–58. https://doi.org/10.1016/j.epsl.2006.05.004

Béthoux, J.P., Morin, P., Chaumery, C., Connan, O., Gentili, B., Ruiz-Pino,

D., 1998. Nutrients in the Mediterranean Sea, mass balance and statistical analysis of concentrations with respect to environmental change. Mar. Chem. 63, 155–168. https://doi.org/10.1016/S0304-4203(98)00059-0

Birch, G.F., 2018. A review of chemical-based sediment quality assessment methodologies for the marine environment. Mar. Pollut. Bull. 133, 218–232. https://doi.org/10.1016/j.marpolbul.2018.05.039

Blondet, I., Schreck, E., Viers, J., Casas, S., Jubany, I., Bahí, N., Zouiten, C., Dufréchou, G., Freydier, R., Galy-Lacaux, C., Martínez-Martínez, S., Faz, A., Soriano-Disla, M., Acosta, J.A., Darrozes, J., 2019. Atmospheric dust characterisation in the mining district of Cartagena-La Unión, Spain: Air quality and health risks assessment. Sci. Total Environ. 693, 133496. https://doi.org/10.1016/j.scitotenv.2019.07.302

Blum, P., 1997. Physical Properties Handbook: A Guide to the Shipboard Measurement of Physical Properties of Deep-Sea Cores. https://doi.org/10.2973/odp.tn.26.1997

Bokuniewicz, H., Cochran, J.K.K., Garcia-Orellana, J., Rodellas, V., Daniel, J.W.J.W., Heilbrun, C., 2015. Intertidal percolation through beach sands as a source of ^{224,223}Ra to Long Island Sound, New York, and Connecticut, United States. J. Mar. Res. 73, 123–140. https://doi.org/10.1357/002224015816665570

Böning, P., Bard, E., Rose, J., 2007. Toward direct, micron-scale XRF elemental maps and quantitative profiles of wet marine sediments. Geochemistry, Geophys. Geosystems 8, 5. https://doi.org/10.1029/2006GC001480

Bolentín Oficial del Estado, 2011. Resolución de 10 de febrero de 2011, de la Secretaría de Estado de Cambio Climático, por la que se formula declaración de impacto ambiental del proyecto Regeneración y adecuación ambiental de la Bahía de Portmán, término municipal de La Unión, Murcia. BOE 45, 20530–20560.

Bonnet, S., Guieu, C., 2006. Atmospheric forcing on the annual iron cycle in the western Mediterranean Sea: A 1-year survey. J. Geophys. Res. Ocean. 11, C9. https://doi.org/10.1029/2005JC003213

Borg, H., Jonsson, P., 1996. Large-scale metal distribution in Baltic Sea sediments. Mar. Pollut. Bull. 32, 8–21. https://doi.org/10.1016/0025-326X(95)00103-T

Bosch, A.C., O'Neill, B., Sigge, G.O., Kerwath, S.E., Hoffman, L.C., 2016. Heavy metals in marine fish meat and consumer health: A review. J. Sci. Food Agric. 96, 32–48. https://doi.org/10.1002/jsfa.7360

Boyd, P.W., Ellwood, M.J., 2010. The biogeochemical cycle of iron in the ocean. Nat. Geosci. 3, 675–682. https://doi.org/10.1038/ngeo964

Boyd, P., LaRoche, J., Gall, M., Frew, R., McKay, R.M.L., 1999. Role of iron, light, and silicate in controlling algal biomass in subantarctic waters SE of New Zealand. J. Geophys. Res. Ocean. 104, 13395–13408. https://doi.org/10.1029/1999jc900009

Boyle, E.A., Lee, J.M., Echegoyen, Y., Noble, A., Moos, S., Carrasco, G., Zhao, N., Kayser, R., Zhang, J., Gamo, T., Obata, H., Norisuye, K., 2014. Anthropogenic lead emissions in the ocean: The evolving global experiment. Oceanography 27, 69–75. https://doi.org/10.5670/oceanog.2014.10

Breitzke, M., 2006. Physical properties of marine sediments, in: Marine Geochemistry. pp. 27–71. https://doi.org/10.1007/3-540-32144-6_2

Bruland, K.W., Donat, J.R., Hutchins, D.A., 1991. Interactive influences of bioactive trace metals on biological production in oceanic waters. Limnol. Oceanogr. 36, 1555–1577. https://doi.org/10.4319/lo.1991.36.8.1555

Bruland, K.W., Lohan, M.C., 2003. Controls of trace metals in seawater. Treatise on Geochemistry, in: The Oceans and Marine Geochemistry. pp. 23–47. https://doi.org/10.1016/B978-0-08-095975-7.00602-1

Buccolieri, A., Buccolieri, G., Cardellicchio, N., Dell'Atti, A., Di Leo, A., Maci, A., 2006. Heavy metals in marine sediments of Taranto Gulf (Ionian Sea, Southern Italy). Mar. Chem. 99, 227–235. https://doi.org/10.1016/j.marchem.2005.09.009

Burger, J., Gaines, K.F., Boring, C.S., Stephens, W.L., Snodgrass, J., Dixon, C., McMahon, M., Shukla, S., Shukla, T., Gochfeld, M., 2002. Metal levels in fish from the Savannah river: Potential hazards to fish and other receptors. Environ. Res. 89, 85–97. https://doi.org/10.1006/enrs.2002.4330

Burke, L., Kura, Y., Kassem, K., Revenga, C., Spalding, M., McAllister, D., 2001. Pilot Analysis of Global Ecosystems: Coastal Ecosystems, Pilot Analysis of

Global Ecosystems.

Burnett, W.C., Dulaiova, H., 2003. Estimating the dynamics of groundwater input into the coastal zone via continuous radon-222 measurements. J. Environ. Radioact. 69, 21–35. https://doi.org/10.1016/S0265-931X(03)00084-5

Burnett, W.C., Taniguchi, M., Oberdorfer, J., 2001. Measurement and significance of the direct discharge of groundwater into the coastal zone. J. Sea Res. 46, 109–116. https://doi.org/10.1016/S1385-1101(01)00075-2

Burnett, W.C., Bokuniewicz, H., Huettel, M., Moore, W., Taniguchi, M., 2003. Groundwater and pore water inpunts to the coastal zone. Biogeochemistry 66, 3–33. https://doi.org/10.1023/B:BIOG.0000006066.21240.53

Burnett, W.C., Aggarwal, P.K., Aureli, A., Bokuniewicz, H., Cable, J.E., Charette, M.A. a, Kontar, E., Krupa, S., Kulkarni, K.M., Loveless, A., Moore, W.S., Oberdorfer, J.A. a, Oliveira, J., Ozyurt, N., Povinec, P., Privitera, A.M.G., Rajar, R., Ramessur, R.T., Scholten, J., Stieglitz, T., Taniguchi, M., Turner, J.V., 2006. Quantifying submarine groundwater discharge in the coastal zone via multiple methods. Sci. Total Environ. 367, 498–543. https://doi.org/10.1016/j.scitotenv.2006.05.009

Burnett, W.C., Wattayakorn, G., Taniguchi, M., Dulaiova, H., Sojisuporn, P., Rungsupa, S., Ishitobi, T., 2007. Groundwater-derived nutrient inputs to the Upper Gulf of Thailand. Cont. Shelf Res. 27, 176–190. https://doi.org/10.1016/j.csr.2006.09.006

Burnett, W.C., Peterson, R., Moore, W.S., de Oliveira, J., 2008. Radon and radium isotopes as tracers of submarine groundwater discharge – Results from the Ubatuba, Brazil SGD assessment intercomparison. Estuar. Coast. Shelf Sci. 76, 501–511. https://doi.org/10.1016/j.ecss.2007.07.027

Burnett, W.C., Sola, P., Chanyotha, S., Bidorn, B., Kritsananuwat, R., Chinfak, N., 2019. Tracing underground sources of pollution to coastal waters off Map Ta Phut, Rayong, Thailand. Mar. Pollut. Bull. 148, 75–84. https://doi.org/10.1016/j.marpolbul.2019.07.071

Calafat, A., 1986. Morfosedimentología de las costas del Maresme, Tesi de Llicenciatura.

Calvert, S.E., Pedersen, T.F., 2007. Chapter Fourteen Elemental Proxies for

Palaeoclimatic and Palaeoceanographic Variability in Marine Sediments: Interpretation and Application. Dev. Mar. Geol. 1, 567–644. https://doi.org/10.1016/S1572-5480(07)01019-6

Canals, M., Party, S., 2015. The two-vessel cruise to Portman Bay, SE Spain: a breakthrough experience. MIDAS Newsl. 3, 1–6.

Capello, M., Cutroneo, L., Consani, S., Dinelli, E., Vagge, G., Carbone, C., 2016. Marine sediment contamination and dynamics at the mouth of a contaminated torrent: The case of the Gromolo Torrent (Sestri Levante, north-western Italy). Mar. Pollut. Bull. 109, 128–141. https://doi.org/10.1016/j.marpolbul.2016.06.010

Carrera, J., Hidalgo, J.J., Slooten, L.J., Vazquez-Sune, E., 2010. Computational and conceptual issues in the calibration of seawater intrusion models. Hydrogeol. J. 18, 131–145. https://doi.org/10.1007/s10040-009-0524-1

Casado-Martínez, M.C., Buceta, J.L., Belzunce, M.J., DelValls, T.A., 2006. Using sediment quality guidelines for dredged material management in commercial ports from Spain. Environ. Int. 32, 388–396. https://doi.org/10.1016/j.envint.2005.09.003

Castilla, J.C., Nealler, E., 1978. Marine environmental impact due to mining activities of El Salvador copper mine, Chile. Mar. Pollut. Bull. 9, 67–70. https://doi.org/10.1016/0025-326X(78)90451-4

Catalan Water Agency, 2010. Model numèric de l'aqüífer al·luvial de la riera d'argentona.

Cearreta, A., Irabien, M.J., Leorri, E., Yusta, I., Croudace, I.W., Cundy, A.B., 2000. Recent anthropogenic impacts on the Bilbao Estuary, northern Spain: Geochemical and microfaunal evidence. Estuar. Coast. Shelf Sci. 50, 571–592. https://doi.org/10.1006/ecss.1999.0582

Cerdà-Domènech, M., Sanchez-Vidal, A., Frigola, J., Baraza, T., Andrade, L., Amblas, D., Canals, M., 2016. Multi-proxy characterization of the mine tailings deposit of Portmán Bay, SE Spain, in: Comission, M.S., Commission Internationale pour l'Exploration Scientifique de la mer Méditerranée (Eds.).

Cerdà-Domènech, M., Rodellas, V., Folch, A., Garcia-Orellana, J., 2017.

Constraining the temporal variations of Ra isotopes and Rn in the groundwater end-member: Implications for derived SGD estimates. Sci. Total Environ. 595, 849–857. https://doi.org/10.1016/j.scitotenv.2017.03.005

Cerdà-Domènech, M., Frigola, J., Sanchez-Vidal, A., Canals, M., 2020. Calibrating high resolution XRF core scanner data to obtain absolute metal concentrations in highly polluted marine deposits after two case studies off Portmán Bay and Barcelona, Spain. Sci. Total Environ. 717, 134778. https://doi.org/https://doi.org/10.1016/j.scitotenv.2019.134778

Cervantes-Guerra, Y.M., Pierra-Conde, A., Mai, J., Jürgen-Gursky, H., Van-Caneghem, J., Vandecasteele, C., 2019. The deep sea tailings placement (DSTP) as alternative for the residuals management in the mining industry. Minería y Geol. Rev. ciencias la tierra 35, 31–48.

Charette, M. a., Buesseler, K.O., Andrews, J.E., 2001. Utility of radium isotopes for evaluating the input and transport of groundwater-derived nitrogen to a Cape Cod estuary. Limnol. Oceanogr. 46, 465–470. https://doi.org/10.4319/lo.2001.46.2.0465

Charette, M.A., 2007. Hydrologic forcing of submarine groundwater discharge: Insight from a seasonal study of radium isotopes in a groundwater-dominated salt marsh estuary. Limnol. Oceanogr. 52, 230–239. https://doi.org/10.4319/lo.2007.52.1.0230

Charette, M.A., Dulaiova, H., Gonneea, M.E., Henderson, P.B., Moore, W.S., Scholten, J.C., Pham, M.K., 2012. GEOTRACES radium isotopes interlaboratory comparison experiment. Limnol. Oceanogr. Methods 10, 451–463. https://doi.org/10.4319/lom.2012.10.451

Chen, Q., Kissel, C., Govin, A., Liu, Z., Xie, X., 2016. Correction of interstitial water changes in calibration methods applied to XRF core-scanning major elements in long sediment cores: Case study from the South China Sea. Geochemistry, Geophys. Geosystems 17, 1925–1934. https://doi.org/10.1002/2016GC006320

Cho, H.M., Kim, G., 2016. Determining groundwater Ra end-member values for the estimation of the magnitude of submarine groundwater discharge using Ra isotope tracers. Geophys. Res. Lett. 43, 3865–3871. https://doi.

org/10.1002/2016GL068805

Christophoridis, C., Dedepsidis, D., Fytianos, K., 2009. Occurrence and distribution of selected heavy metals in the surface sediments of Thermaikos Gulf, N. Greece. Assessment using pollution indicators. J. Hazard. Mater. 168, 1082–1091. https://doi.org/10.1016/j.jhazmat.2009.02.154

Clark, R.B., 1992. Marine pollution. Oxford: Clarendon Press.

Cnudde, V., Masschaele, B., Dierick, M., Vlassenbroeck, J., Hoorebeke, L. Van, Jacobs, P., 2006. Recent progress in X-ray CT as a geosciences tool. Appl. Geochemistry 21, 826–832. https://doi.org/10.1016/j.apgeochem.2006.02.010

Comisión nacional de estrategias de Marinas, 2015. Directrices para la caracterización del material dragado y su reubicación en aguas del dominio público marítimo-terrestre, Ministerio de agricultura, alimentación y medio ambiente.

Crossland, C.J., Kremer, H.H., Lindeboom, H., Crossland, J.I.M., Le Tissier, M.D.A., 2005. Coastal fluxes in the Anthropocene: the land-ocean interactions in the coastal zone project of the International Geosphere-Biosphere Programme. Springer Science & Business Media.

Croudace, I.W., Warwick, P.E., Morris, J.E., 2012. Evidence for the preservation of technogenic tritiated organic compounds in an estuarine sedimentary environment. Environ. Sci. Technol. 46, 5704–5712. https://doi.org/10.1021/es204247f

Croudace, I.W., Rothwell, R.G., 2015. Future developments and innovations in high-resolution core scanning, in: Micro-XRF Studies of Sediment Cores. Springer, pp. 627–647.

Croudace, I.W., Teasdale, P.A., Cundy, A.B., 2019. 200-year industrial archaeological record preserved in an Isle of Man saltmarsh sediment sequence: Geochemical and radiochronological evidence. Quat. Int. 514, 195–203. https://doi.org/10.1016/j.quaint.2018.09.045

Davis, A.P., Shokouhian, M., Ni, S., 2001. Loading estimates of lead, copper, cadmium, and zinc in urban runoff from specific sources. Chemosphere 44, 997–1009. https://doi.org/10.1016/S0045-6535(00)00561-0

Dausman, A., Langevin, C.D., 2005. Movement of the saltwater interface in

the surficial aquifer system in response to hydrologic stresses and water-management practices, Broward County, Florida. US Department of the Interior, US Geological Survey.

De Boever, W., Diaz, A., Derluyn, H., De Kock, T., Van Stappen, J., Dewanckele, J., Bultreys, T., Boone, M., De Schryver, T., Skjønsfjell, E.T.B.B., Holler, M., Breiby, D.W., Cnudde, V., 2015. Characterization of composition and structure of clay minerals in sandstone with ptychographic X-ray nanotomography. Appl. Clay Sci. 118, 258–264. https://doi.org/10.1016/j.clay.2015.09.020

Dore, A.J., Hallsworth, S., McDonald, A.G., Werner, M., Kryza, M., Abbot, J., Nemitz, E., Dore, C.J., Malcolm, H., Vieno, M., Reis, S., Fowler, D., 2014. Quantifying missing annual emission sources of heavy metals in the United Kingdom with an atmospheric transport model. Sci. Total Environ. 479, 171–180. https://doi.org/10.1016/j.scitotenv.2014.02.001

Deming, W.E., 1943. Statistical adjustment of data., Dover Publications. Wiley.

Descostes, M., Vitorge, P., Beaucaire, C., 2004. Pyrite dissolution in acidic media. Geochim. Cosmochim. Acta 68, 4559–4569. https://doi.org/10.1016/j.gca.2004.04.012

Di Leonardo, R., Bellanca, A., Angelone, M., Leonardi, M., Neri, R., 2008. Impact of human activities on the central Mediterranean offshore: Evidence from Hg distribution in box-core sediments from the Ionian Sea. Appl. Geochemistry 23, 3756–3766. https://doi.org/10.1016/j.apgeochem.2008.09.010

Dierick, M., Van Loo, D., Masschaele, B., Van den Bulcke, J., Van Acker, J., Cnudde, V., Van Hoorebeke, L., 2014. Recent micro-CT scanner developments at UGCT. Nucl. Instruments Methods Phys. Res. Sect. B Beam Interact. with Mater. Atoms 324, 35–40. https://doi.org/10.1016/j.nimb.2013.10.051

Din, Z.B., 1992. Use of aluminium to normalize heavy-metal data from estuarine and coastal sediments of Straits of Melaka. Mar. Pollut. Bull. 24, 484–491. https://doi.org/10.1016/0025-326X(92)90472-I

Directive, E.U.W., 1991. Council Directive of 21. May 1991 concerning urban waste water treatment (91/271/EEC). J. Eur. Commun 34, 40.

Duffus, J.H., 2002. “heavy metals” - A meaningless term? (IUPAC technical report). Pure Appl. Chem. https://doi.org/10.1351/pac200274050793

Dulaiova, H., Burnett, W.C., 2008. Evaluation of the flushing rates of Apalachicola Bay, Florida via natural geochemical tracers. Mar. Chem. 109, 395–408. https://doi.org/10.1016/j.marchem.2007.09.001

Dulaiova, H., Gonneea, M.E., Henderson, P.B., Charette, M. a., 2008. Geochemical and physical sources of radon variation in a subterranean estuary - Implications for groundwater radon activities in submarine groundwater discharge studies. Mar. Chem. 110, 120–127. https://doi.org/10.1016/j.marchem.2008.02.011

Dulaquais, G., Boye, M., Middag, R., Owens, S., Puigcorbe, V., Buesseler, K., Masqué, P., De Baar, H.J.W., Carton, X., 2014. Contrasting biogeochemical cycles of cobalt in the surface western Atlantic Ocean. Global Biogeochem. Cycles 28, 1387–1412. https://doi.org/10.1002/2014GB004903

Duliu, O.G., 1999. Computer axial tomography in geosciences: an overview. Earth-Science Rev. 48, 265–281. https://doi.org/10.1016/S0012-8252(99)00056-2

Durán, R., Canals, M., Sanz, J.L., Lastras, G., Amblas, D., Micallef, A., 2014. Morphology and sediment dynamics of the northern Catalan continental shelf, northwestern Mediterranean Sea. Geomorphology 204, 1–20. https://doi.org/10.1016/j.geomorph.2012.10.004

Ellis, D., Ellis, K., 1994. Very deep STD. Mar. Pollut. Bull. 28, 472–476. https://doi.org/10.1016/0025-326X(94)90519-3

Ellis, D. V., Pedersen, T.F., Poling, G.W., Pelletier, C., Horne, I., 1995. Review of 23 years of std: Island copper mine, Canada. Mar. Georesources Geotechnol. 13, 59–99. https://doi.org/10.1080/10641199509388279

Elsinger, R.J., Moore, W.S., 1980. ^{226}Ra behavior in the Pee Dee River-Winyah Bay estuary. Earth Planet. Sci. Lett. 48, 239–249. https://doi.org/10.1016/0012-821X(80)90187-9

European Environment Agency, 2018. The European Pollutant Release and Transfer Register (E-PRTR), Member States reporting under Article 7 of Regulation (EC) No 166/2006’.

Falkowski, P.G., Barber, R.T., Smetacek, V., 1998. Biogeochemical controls and

feedbacks on ocean primary production. Science. 281, 200–206. https://doi.org/10.1126/science.281.5374.200

Fatoki, O.S., Mathabatha, S., 2001. An assessment of heavy metal pollution in the East London and Port Elizabeth harbours. Water SA 27, 233–240. https://doi.org/10.4314/wsa.v27i2.4997

Fernández Salas, L.M., Durán, R., Mendes, I., Galparsoro, I., Lobo, F.J., Bárcenas, P., Rosa, F., Ribó, M., García-Gil, S., Ferrín, A., 2016. Shelves of the Iberian Peninsula and the Balearic Islands (I): Morphology and sediment types. Boletín Geológico y Min. 126, 327–376.

Finlayson-Pitts, B.J., Pitts Jr, J.N., 1986. Atmospheric chemistry. Fundamentals and experimental techniques. John Wiley and Sons, New York, NY.

Folch, R., 1993. Mediterrànies. Biosfera. Enciclopèdia Catalana.

Fortin, D., Francus, P., Gebhardt, A.C., Hahn, A., Kliem, P., Lisé-Pronovost, A., Roychowdhury, R., Labrie, J., St-Onge, G., 2013. Destructive and non-destructive density determination: method comparison and evaluation from the Laguna Potrok Aike sedimentary record. Quat. Sci. Rev. 71, 147–153. https://doi.org/10.1016/j.quascirev.2012.08.024

Foster, A.L., Brown, G.E., Tingle, T.N., Parks, G.A., 1998. Quantitative arsenic speciation in mine tailings using X-ray absorption spectroscopy. Am. Mineral. 83, 553–568. https://doi.org/10.2138/am-1998-5-616

Franks, D.M., Boger, D. V., Côte, C.M., Mulligan, D.R., 2011. Sustainable development principles for the disposal of mining and mineral processing wastes. Resour. Policy 36, 114–122. https://doi.org/10.1016/j.resourpol.2010.12.001

Frigola, J., Canals, M., Mata, P., 2015. Técnicas para el análisis no destructivo y en continuo de testigos de sedimento. Aplicación en el Margen Continental de Iberia. Bol. Geol. y Min. 126, 609–634.

Fuerstenau, M.C., Chander, S., Woods, R., 2007. Sulfide Mineral Flotation, in: Froth Flotation: A Century of Innovation. Society for Mining, Metallurgy, and Exploration, Inc.(SME), Littleton, Colorado, pp. 425–464.

Fukushima, K., Saino, T., Kodama, Y., 1992. Trace metal contamination in Tokyo Bay, Japan. Sci. Total Environ. 125, 373–389. https://doi.org/10.1016/0048-

9697(92)90402-E

Garcia-Castellanos, D., Estrada, F., Jiménez-Munt, I., Gorini, C., Fernández, M., Vergés, J., De Vicente, R., 2009. Catastrophic flood of the Mediterranean after the Messinian salinity crisis. Nature 462, 778–781. https://doi.org/10.1038/nature08555

García-Lorenzo, M.L., Martínez-Sánchez, M.J., Pérez-Sirvent, C., Agudo, I., Recio, C., 2014. Isotope geochemistry of waters affected by mining activities in Sierra Minera and Portman Bay (SE, Spain). Appl. Geochemistry 51, 139–147. https://doi.org/10.1016/j.apgeochem.2014.10.002

Garcia-Orellana, J., Cochran, J.K., Bokuniewicz, H., Yang, S., Beck, a J., 2010. Time-series sampling of ^{223}Ra and ^{224}Ra at the inlet to Great South Bay (New York): A strategy for characterizing the dominant terms in the Ra budget of the bay. J. Environ. Radioact. 101, 582–588. https://doi.org/10.1016/j.jenvrad.2009.12.005

Garcia-Orellana, J., Cañas, L., Masqué, P., Obrador, B., Olid, C., Pretus, J., 2011. Chronological reconstruction of metal contamination in the Port of Maó (Minorca, Spain). Mar. Pollut. Bull. 62, 1632–1640. https://doi.org/10.1016/j.marpolbul.2011.06.013

Garcia-Solsona, E., Garcia-Orellana, J., Masqué, P., Dulaiova, H., 2008. Uncertainties associated with ^{223}Ra and ^{224}Ra measurements in water via a Delayed Coincidence Counter (RaDeCC). Mar. Chem. 109, 198–219. https://doi.org/10.1016/j.marchem.2007.11.006

Garcia-Solsona, E., Garcia-Orellana, J., Masqué, P., Garcés, E., Radakovitch, O., Mayer, A., Estradé, S., Basterretxea, G., 2010. An assessment of karstic submarine groundwater and associated nutrient discharge to a Mediterranean coastal area (Balearic Islands, Spain) using radium isotopes. Biogeochemistry 97, 211–229. https://doi.org/10.1007/s10533-009-9368-y

Gattuso J.P., Magnan A.K., Bopp L., Cheung W., Duarte C.M., Hinkel J., Mcleod E., Micheli F., Oschlies A., Williamson P., Billé R., Chalastani V.I., Gates R.D., Irisson J.O., Middelburg J.J., Pörtner H.O., Rau G.H. (2018). Ocean Solutions to Address Climate Change and Its Effects on Marine Ecosystems. Front. Mar. Sci. 5, 337. http://doi.org/10.3389/fmars.2018.00337.

Gasith, A., Resh, V.H., 1999. STREAMS IN MEDITERRANEAN CLIMATE REGIONS: Abiotic Influences and Biotic Responses to Predictable Seasonal Events. Annu. Rev. Ecol. Syst. 30, 51–81. https://doi.org/10.1146/annurev.ecolsys.30.1.51

Gerber, T.P., Amblas, D., Wolinsky, M.A., Pratson, L.F., Canals, M., 2009. A model for the long-profile shape of submarine canyons. J. Geophys. Res. Earth Surf. 114. https://doi.org/10.1029/2008JF001190

GESAMP, 2007. Estimates of Oil Entering the Marine Environment from Sea-based Activities. GESAMP Reports Stud.

GESAMP, 2016. Proceedings of the GESAMP International Workshop on the Impacts of Mine Tailings in the Marine Environment.(IMO/FAO/UNESCO-IOC/UNIDO/WMO/IAEA/UN/UNEP/UNDP Joint Group of Experts on the Scientific Aspects of Marine Environmental Protection). Rep. Stud. 94, 84.

Giddings, J.C., 1973. Chemistry, man, and environmental change. Canfield Press

Goldberg, E.D., 1963. Geochronology with ^{210}Pb radioactive dating. Int. At. Energy Agency, Vienna 121, 130.

Gómez-García, C., Martin-Hernandez, F., López García, J.Á., Martínez-Pagón, P., Manteca, J.I., Carmona, C., 2015. Rock magnetic characterization of the mine tailings in Portman Bay (Murcia, Spain) and its contribution to the understanding of the bay infilling process. J. Appl. Geophys. 120, 48–59. https://doi.org/10.1016/j.jappgeo.2015.06.008

Gonneea, M.E., Morris, P.J., Dulaiova, H., Charette, M. a., 2008. New perspectives on radium behavior within a subterranean estuary. Mar. Chem. 109, 250–267. https://doi.org/10.1016/j.marchem.2007.12.002

Gonneea, M.E., Mulligan, A.E., Charette, M.A., 2013. Seasonal cycles in radium and barium within a subterranean estuary: Implications for groundwater derived chemical fluxes to surface waters. Geochim. Cosmochim. Acta 119, 164–177. https://doi.org/10.1016/j.gca.2013.05.034

Gonneea, M.E., Charette, M.A., 2014. Hydrologic controls on nutrient cycling in an unconfined coastal aquifer. Environ. Sci. Technol. 48, 14178–14185.

https://doi.org/10.1021/es503313t

Gonneea, M.E., Charette, M.A., Liu, Q., Herrera-Silveira, J.A., Morales-Ojeda, S.M., 2014. Trace element geochemistry of groundwater in a karst subterranean estuary (Yucatan Peninsula, Mexico). Geochim. Cosmochim. Acta 132, 31–49. https://doi.org/10.1016/j.gca.2014.01.037 Grifoll, M., Aretxabaleta, A.L., Espino, M., Warner, J.C., 2012. Along-shelf current variability on the Catalan inner-shelf (NW Mediterranean). J. Geophys. Res. Ocean. 117, C9. https://doi.org/10.1029/2012JC008182

Guo, Y., Yang, S., 2016. Heavy metal enrichments in the Changjiang (Yangtze River) catchment and on the inner shelf of the East China Sea over the last 150years. Sci. Total Environ. 543, 105–115. https://doi.org/10.1016/j.scitotenv.2015.11.012

Hanebuth, T.J.J., King, M.L., Mendes, I., Lebreiro, S., Lobo, F.J., Oberle, F.K., Antón, L., Ferreira, P.A., Reguera, M.I., 2018. Hazard potential of widespread but hidden historic offshore heavy metal (Pb, Zn) contamination (Gulf of Cadiz, Spain). Sci. Total Environ. 637–638, 561–576. https://doi.org/10.1016/j.scitotenv.2018.04.352

Hatje, V., Andrade, R.L.B., Jesus, R.M., Masqué, P., Albergaria-Barbosa, A.C.R., de Andrade, J.B., Santos, A.C.S.S., 2019. Historical records of mercury deposition in dated sediment cores reveal the impacts of the legacy and present-day human activities in Todos os Santos Bay, Northeast Brazil. Mar. Pollut. Bull. 145, 396–406. https://doi.org/10.1016/j.marpolbul.2019.06.041

Hayes, S.M., Root, R.A., Perdrial, N., Maier, R.M., Chorover, J., 2014. Surficial weathering of iron sulfide mine tailings under semi-arid climate. Geochim. Cosmochim. Acta 141, 240–257. https://doi.org/10.1016/j.gca.2014.05.030

Hedge, L.H., Knott, N.A., Johnston, E.L., 2009. Dredging related metal bioaccumulation in oysters. Mar. Pollut. Bull. 58, 832–840. https://doi.org/10.1016/j.marpolbul.2009.01.020

Heiss, J.W., Michael, H.A., 2014. Saltwater-freshwater mixing dynamics in a sandy beach aquifer over tidal, spring-neap, and seasonal cycles. Water Resour. Res. 50, 6747-6766. https://doi.org/10.1002/2014WR015574

Henderson, R.D., Day-Lewis, F.D., Abarca, E., Harvey, C.F., Karam, H.N., Liu,

L., Lane, J.W.J., 2010. Marine electrical resistivity imaging of submarine groundwater discharge: sensitivity analysis and application in Waquoit Bay, Massachusetts, USA. Hydrogeol. J. 18, 173–185. https://doi.org/10.1007/s10040-009-0498-z

Hennekam, R., de Lange, G., De Rick, G., 2012. X-ray fluorescence core scanning of wet marine sediments: Methods to improve quality and reproducibility of highresolution paleoenvironmental records. Limnol. Oceanogr. Methods 10, 991–1003. https://doi.org/10.4319/lom.2012.10.991

Hennekam, R., Sweere, T., Tjallingii, R., de Lange, G.J., Reichart, G.J., 2018. Trace metal analysis of sediment cores using a novel X-ray fluorescence core scanning method. Quat. Int. 514, 55–67. https://doi.org/10.1016/j.quaint.2018.10.018

Herlng, J.G., Morel, F.M.M., 1990. Kinetics of Trace Metal Complexation: Ligand-Exchange Reactions. Environ. Sci. Technol. 24, 242–252. https://doi.org/10.1021/es00072a014

Hernández, C.V., 1978. Toponimia romana y de romanización en Murcia. Murgetana 53.

Herut, B., Krom, M.D., Pan, G., Mortimer, R., 1999. Atmospheric input of nitrogen and phosphorus to the Southeast Mediterranean: Sources, fluxes, and possible impact. Limnol. Oceanogr. 44, 1683–1692. https://doi.org/10.4319/lo.1999.44.7.1683

Honeyman, B.D., Santschi, P.H., 1988. Metals in aquatic systems. Environ. Sci. Technol. 22, 862–871. https://doi.org/10.1021/es00173a002

Hornberger, M.I., Luoma, S.N., Van Geen, A., Fuller, C., Anima, R., 1999. Historical trends of metals in the sediments of San Francisco Bay, California. Mar. Chem. 64, 39–55. https://doi.org/10.1016/S0304-4203(98)80083-2

Hughes, D.J., Shimmield, T.M., Black, K.D., Howe, J.A., 2015. Ecological impacts of large-scale disposal of mining waste in the deep sea. Sci. Rep. 5, 9985. https://doi.org/10.1038/srep09985

Hunt, J.E., Croudace, I.W., Maclachlan, S.E., 2015. Use of Calibrated Itrax-XRF data in determining turbidite Geochemistry and provenance in Agadir Basin, Northwest African Passive Margin, in: Micro-XRF Studies of Sediment

Cores: Applications of a Non-Destructive Tool for Environmental Sciences. pp. 127–146. https://doi.org/10.1007/978

Iglesias, O., Lastras, G., Canals, M., Olabarrieta, M., González, M., Aniel-Quiroga, Í., Otero, L., Durán, R., Amblas, D., Casamor, J.L., Tahchi, E., Tinti, S., de Mol, B., 2012. The BIG'95 submarine landslide-generated tsunami: A numerical Simulation. J. Geol. 120, 31–48. https://doi.org/10.1086/662718

Jansen, J.H., Van der Gaast, S. J., Koster, B., Vaars, A. J., 1998. CORTEX, a shipboard XRF-scanner for element analyses in split sediment cores. Mar. Geol. 151, 143–153. https://doi.org/10.1016/S0025-3227(98)00074-7

Johannes, R., 1980. The Ecological Significance of the Submarine Discharge of Groundwater. Mar. Ecol. Prog. Ser. 3, 365–373. https://doi.org/10.3354/meps003365

Johnson, A.C., Jin, X., Nakada, N., Sumpter, J.P., 2020. Learning from the past and considering the future of chemicals in the environment. Science, 367, 384–387. https://doi.org/10.1126/science.aay6637

Johnson, A.G., Glenn, C.R., Burnett, W.C., Peterson, R.N., Lucey, P.G., 2008. Aerial infrared imaging reveals large nutrient-rich groundwater inputs to the ocean. Geophys. Res. Lett. 35, L15606. https://doi.org/10.1029/2008GL034574

Jones, A.M., Pham, A.N., Collins, R.N., Waite, T.D., 2009. Dissociation kinetics of Fe(III)– and Al(III)–natural organic matter complexes at pH 6.0 and 8.0 and 25°C. Geochim. Cosmochim. Acta 73, 2875–2887. https://doi.org/https://doi.org/10.1016/j.gca.2009.02.022

Jordi, A., Basterretxea, G., Tovar-Sánchez, A., Alastuey, A., Querol, X., 2012. Copper aerosols inhibit phytoplankton growth in the Mediterranean Sea. Proc. Natl. Acad. Sci. U. S. A. 109, 21246–21249. https://doi.org/10.1073/pnas.1207567110

Josefson, A.B., Hansen, J.L.S., Asmund, G., Johansen, P., 2008. Threshold response of benthic macrofauna integrity to metal contamination in West Greenland. Mar. Pollut. Bull. 56, 1265–1274. https://doi.org/10.1016/j.marpolbul.2008.04.028

Junqué, E., Garí, M., Llull, R.M., Grimalt, J.O., 2018. Drivers of the accumulation of

mercury and organochlorine pollutants in Mediterranean lean fish and dietary significance. Sci. Total Environ. 634, 170–180. https://doi.org/10.1016/j.scitotenv.2018.03.335

Kak, Slaney, 1988. Principles of Tomographic Imaging, Institute for Electrical and Electronic Engineers. https://doi.org/10.1118/1.1455742

Kawatra, S.K., 2011. Froth Flotation – Fundamental Principles. Michigan Technical University.

Kelloway, S.J., Ward, C.R., Marjo, C.E., Wainwright, I.E., Cohen, D.R., 2014. Quantitative chemical profiling of coal using core-scanning X-ray fluorescence techniques. Int. J. Coal Geol. 128, 55–67. https://doi.org/10.1016/j.coal.2014.04.006

Keuken, M.P., Moerman, M., Voogt, M., Blom, M., Weijers, E.P., Röckmann, T., Dusek, U., 2013. Source contributions to PM2.5 and PM10 at an urban background and a street location. Atmos. Environ. 71, 26–35. https://doi.org/10.1016/j.atmosenv.2013.01.032

Kido, Y., Koshikawa, T., Tada, R., 2006. Rapid and quantitative major element analysis method for wet fine-grained sediments using an XRF microscanner. Mar. Geol. 229, 209–225. https://doi.org/10.1016/j.margeo.2006.03.002

Kim, G., Hwang, D.W., 2002. Tidal pumping of groundwater into the coastal ocean revealed from submarine ^{222}Rn and CH_4 monitoring. Geophys. Res. Lett. 29, 23-1-23–4. https://doi.org/10.1029/2002GL015093

Kim, G., Lee, K., Park, K.S., Hwang, D.W., Yang, Han-Soeb, Y., 2003. Large submarine groundwater discharge (SGD) from a volcanic island. Geophys. Res. Lett. 30, 2098. https://doi.org/10.1029/2003GL018378

Kim, G., Yun, S.T., Yang, H.S., Ryu, J.W., Burnett, W.C., Dulaiova, H., Sholkovitz, E., Moore, W.S., Charette, M. A., Bokuniewicz, H.J., Chanton, J.P., Yun, S.T., Yang, H.S., Ryu, J.W., 2005. Submarine groundwater discharge (SGD) into the Yellow Sea revealed by ^{228}Ra and ^{226}Ra isotopes: Implications for global silicate fluxes. Earth Planet. Sci. Lett. 237, 156–166. https://doi.org/10.1016/j.epsl.2005.06.011

Kress, N., Shoham-Frider, E., Galil, B.S., 2016. Twenty two years of sewage sludge

marine disposal monitoring in the Eastern Mediterranean Sea: Impact on sediment quality and infauna and the response to load reduction. Mar. Pollut. Bull. 110, 99–111. https://doi.org/10.1016/j.marpolbul.2016.06.076

Krishnaswamy, S., Lal, D., Martin, J.M., Meybeck, M., 1971. Geochronology of lake sediments. Earth Planet. Sci. Lett. 11, 407–414. https://doi.org/10.1016/0012-821X(71)90202-0

Kruge, M.A., Permanyer, A., Serra, J., Yu, D., 2010. Geochemical investigation of an offshore sewage sludge deposit, Barcelona, Catalonia, Spain. J. Anal. Appl. Pyrolysis 89, 204–217. https://doi.org/10.1016/j.jaap.2010.08.005

Koski, R., 2012. Metal Dispersion Resulting from Mining Activities in Coastal Environments: A Pathways Approach. Oceanography 25, 170–183. https://doi.org/10.5670/oceanog.2012.53

Lamotte, L.R., Rao, C.R., Toutenburg, H., 1997. Linear Models. J. Am. Stat. Assoc. https://doi.org/10.2307/2965595

Lancellotti, D.A., Stotz, W.B., 2004. Effects of shoreline discharge of iron mine tailings on a marine soft-bottom community in northern Chile. Mar. Pollut. Bull. 48, 303–12. https://doi.org/10.1016/j.marpolbul.2003.08.005

Lao, Q., Su, Q., Liu, G., Shen, Y., Chen, F., Lei, X., Qing, S., Wei, C., Zhang, C., Gao, J., 2019. Spatial distribution of and historical changes in heavy metals in the surface seawater and sediments of the Beibu Gulf, China. Mar. Pollut. Bull. 146, 427–434. https://doi.org/10.1016/j.marpolbul.2019.06.080

Lee, C.M., Jiao, J.J., Luo, X., Moore, W.S., 2012. Estimation of submarine groundwater discharge and associated nutrient fluxes in Tolo Harbour, Hong Kong. Sci. Total Environ. 433, 427–433. https://doi.org/10.1016/j.scitotenv.2012.06.073

Lee, G., Bigham, J.M., Faure, G., 2002. Removal of trace metals by coprecipitation with Fe, Al and Mn from natural waters contaminated with acid mine drainage in the Ducktown Mining District, Tennessee. Appl. Geochemistry 17, 569–581. https://doi.org/10.1016/S0883-2927(01)00125-1

Li, C., Song, C., Yin, Y., Sun, M., Tao, P., Shao, M., 2015. Spatial distribution and risk assessment of heavy metals in sediments of Shuangtaizi estuary, China. Mar.

Pollut. Bull. 98, 358–364. https://doi.org/10.1016/j.marpolbul.2015.05.051

Li, H., Boufadel, M.C., Weaver, J.W., 2008. Tide-induced seawater-groundwater circulation in shallow beach aquifers. J. Hydrol. 352, 211–224. https://doi.org/10.1016/j.jhydrol.2008.01.013

Li, R., Li, J., Cui, L., Wu, Y., Fu, H., Chen, J., Chen, M., 2017. Atmospheric emissions of Cu and Zn from coal combustion in China: Spatio-temporal distribution, human health effects, and short-term prediction. Environ. Pollut. 229, 724–734. https://doi.org/10.1016/j.envpol.2017.05.068

Lindsay, M.B., Moncur, M.C., Bain, J.G., Jambor, J.L., Ptacek, C.J., Blowes, D.W., 2015. Geochemical and mineralogical aspects of sulfide mine tailings. Appl. Geochemistry 57, 157–177. https://doi.org/10.1016/j.apgeochem.2015.01.009

Liquete, C., Canals, M., Lastras, G., Amblas, D., Urgeles, R., De Mol, B., De Batist, M., Hughes-Clarke, J.E., 2007. Long-term development and current status of the Barcelona continental shelf: A source-to-sink approach. Cont. Shelf Res. 27, 1779–1800. https://doi.org/10.1016/j.csr.2007.02.007

Liquete, C., Canals, M., De Mol, B., De Batist, M., Trincardi, F., 2008. Quaternary stratal architecture of the Barcelona prodeltaic continental shelf (NW Mediterranean). Mar. Geol. 250, 234–250. https://doi.org/10.1016/j.margeo.2008.01.014

Llull, R.M., Garí, M., Canals, M., Rey-Maquieira, T., Grimalt, J.O., 2017. Mercury concentrations in lean fish from the Western Mediterranean Sea: Dietary exposure and risk assessment in the population of the Balearic Islands. Environ. Res. 158, 16–23. https://doi.org/10.1016/j.envres.2017.05.033

Long, E.R., Macdonald, D.D., Smith, S.L., Calder, F.D., 1995. Incidence of adverse biological effects within ranges of chemical concentrations in marine and estuarine sediments. Environ. Manage. 19, 81–97. https://doi.org/10.1007/BF02472006

Lopes-Rocha, M., Langone, L., Miserocchi, S., Giordano, P., Guerra, R., 2017. Detecting long-term temporal trends in sediment-bound metals in the western Adriatic (Mediterranean Sea). Mar. Pollut. Bull. 124, 270–285. https://doi.org/10.1016/j.marpolbul.2017.07.026

Loring, D.H., 1991. Normalization of heavy-metal data from estuarine and coastal sediments. ICES J. Mar. Sci. 48, 101–115. https://doi.org/10.1093/icesjms/48.1.101

Lottermoser, B.G., 2010. Mine Wastes Characterization, treatment and environmental impacts. Springer. https://doi.org/10.1007/978-3-642-12419-8

Löwemark, L., Chen, H.-F., Yang, T.-N., Kylander, M., Yu, E.-F., Hsu, Y.-W., Lee, T.-Q., Song, S.-R., Jarvis, S., 2011. Normalizing XRF-scanner data: A cautionary note on the interpretation of high-resolution records from organic-rich lakes. J. Asian Earth Sci. 40, 1250–1256. https://doi.org/10.1016/j.jseaes.2010.06.002

Ludwig, W., Dumont, E., Meybeck, M., Heussner, S., 2009. River discharges of water and nutrients to the Mediterranean and Black Sea: Major drivers for ecosystem changes during past and future decades? Prog. Oceanogr. 80, 199–217. https://doi.org/10.1016/j.pocean.2009.02.001

Lyle, M., Backman, J., 2013. Data report: calibration of XRF-estimated $CaCO_3$ along the Site U1338 splice, in: 320. p. 321. https://doi.org/10.2204/iodp.proc.320321.205.2013

MacLachlan, S.E., Hunt, J.E., Croudace, I.W., 2015. An empirical assessment of variable water content and grain-size on X-ray fluorescence core-scanning measurements of deep sea sediments, in: Micro-XRF Studies of Sediment Cores. Springer, pp. 173–185.

Maher, B.A., Prospero, J.M., Mackie, D., Gaiero, D., Hesse, P.P., Balkanski, Y., 2010. Global connections between aeolian dust, climate and ocean biogeochemistry at the present day and at the last glacial maximum. Earth-Science Rev. 99, 61–97. https://doi.org/10.1016/j.earscirev.2009.12.001

Mahowald, N.M., Baker, A.R., Bergametti, G., Brooks, N., Duce, R.A., Jickells, T.D., Kubilay, N., Prospero, J.M., Tegen, I., 2005. Atmospheric global dust cycle and iron inputs to the ocean. Global Biogeochem. Cycles 19. https://doi.org/10.1029/2004GB002402

Manteca, J.I., 1992. Los yacimientos Zn, Pb, Ag-Fe del distrito minero de la La Unión-Cartagena, Bética Oriental. 134.

Manteca, J.I., 2013. Introducción a la geología y yacimientos minerales de Portmán, in: Páez, I.B.-G.P.B. (Ed.), Portmán: De El Portus Magnus Del Mediterráneo Occidental a La Bahía Aterrada. EDITUM, Murcia, p. 51.

Manteca, J.I., Garcia, J.Á.L., Oyarzun, R., Carmona, C., 2014. The beach placer iron deposit of Portman Bay, Murcia, SE Spain: The result of 33 years of tailings disposal (1957-1990) to the Mediterranean seaside. Miner. Depos. 49, 777–783. https://doi.org/10.1007/s00126-014-0511-x

Martínez-Gómez, C., Fernández, B., Benedicto, J., Valdés, J., Campillo, J.A., León, V.M., Vethaak, A.D., 2012. Health status of red mullets from polluted areas of the Spanish Mediterranean coast, with special reference to Portmán (SE Spain). Mar. Environ. Res. 77, 50–59. https://doi.org/10.1016/j.marenvres.2012.02.002

Martínez-Sánchez, M.J., Navarro, M.C., Pérez-Sirvent, C., Marimón, J., Vidal, J., García-Lorenzo, M.L., Bech, J., 2008. Assessment of the mobility of metals in a mining-impacted coastal area (Spain, Western Mediterranean). J. Geochemical Explor. 96, 171–182. https://doi.org/10.1016/j.gexplo.2007.04.006

Martínez-Soto, M.C.M.C., Tovar-Sánchez, A., Sánchez-Quiles, D., Rodellas, V., Garcia-Orellana, J., Basterretxea, G., 2016. Seasonal variation and sources of dissolved trace metals in Maó Harbour, Minorca Island. Sci. Total Environ. 565, 191–199. https://doi.org/10.1016/j.scitotenv.2016.03.244

Mason, R.P., Sheu, G.-R., 2002. Role of the ocean in the global mercury cycle. Global Biogeochem. Cycles 16, 1093. https://doi.org/10.1029/2001gb001440

Mason, R.P., 2013. Trace Metals in Aquatic Systems, Trace Metals in Aquatic Systems. John Wiley & Sons. https://doi.org/10.1002/9781118274576

Mathew, J., Gopinath, A., 2019. Spatial and Temporal Variations of Arsenic Distribution in a Tropical Estuary Along the West Coast of India. Mar. Pollut. Bull. 149, 110567. https://doi.org/10.1016/j.marpolbul.2019.110567

Mejía-Piña, K.G., Huerta-Diaz, M.A., González-Yajimovich, O., 2016. Calibration of handheld X-ray fluorescence (XRF) equipment for optimum determination of elemental concentrations in sediment samples. Talanta 161, 359–367. https://doi.org/10.1016/j.talanta.2016.08.066

Mestre, N.C., Rocha, T.L., Canals, M., Cardoso, C., Danovaro, R., Dell'Anno, A., Gambi, C., Regoli, F., Sanchez-Vidal, A., Bebianno, M.J., 2017. Environmental hazard assessment of a marine mine tailings deposit site and potential implications for deep-sea mining. Environ. Pollut. 228, 169–178. https://doi.org/10.1016/j.envpol.2017.05.027

Michael, H.A., Lubetsky, J.S., Harvey, C.F., 2003. Characterizing submarine groundwater discharge: A seepage meter study in Waquoit Bay, Massachusetts. Geophys. Res. Lett. 30. https://doi.org/10.1029/2002GL016000

Michael, H.A., Charette, M.A., Harvey, C.F., 2011. Patterns and variability of groundwater flow and radium activity at the coast: A case study from Waquoit Bay, Massachusetts. Mar. Chem. 127, 100–114. https://doi.org/10.1016/j.marchem.2011.08.001

Millot, C., 1999. Circulation in the Western Mediterranean Sea. J. Mar. Syst. 20, 423–442. https://doi.org/10.1016/S0924-7963(98)00078-5

Montoto, M., 1967. Estudio petrológico y petrogenético de las rocas graníticas de la Cadena Litoral Catalana. Univ. Barcelona. Secret. Public. Intercamb. Científico y extensión Univ. 800.

Moore, W.S., Reid, D.F., 1973. Extraction of radium from natural waters using manganese-impregnated acrylic fibers. J. Geophys. Res. 78, 8880. https://doi.org/10.1029/JC078i036p08880

Moore, W.S., 1996a. Using the radium quartet for evaluating groundwater input and water exchange in salt marshes. Geochim. Cosmochim. Acta 60, 4645–4652. https://doi.org/10.1016/S0016-7037(96)00289-X

Moore, W.S., 1996b. Large groundwater inputs to coastal waters revealed by 226Ra enrichments. Nature 380, 612–614. https://doi.org/10.1038/380612a0

Moore, W.S., 1999. The subterranean estuary: a reaction zone of ground water and sea water. Mar. Chem. 65, 111–125. https://doi.org/10.1016/S0304-4203(99)00014-6

Moore, W.S., 2003. Sources and fluxes of submarine groundwater discharge delineated by radium isotopes. Biogeochemistry 66, 75–93. https://doi.org/10.1023/B:BIOG.0000006065.77764.a0

Moore, W.S., Wilson, A.M., 2005. Advective flow through the upper continental shelf driven by storms, buoyancy, and submarine groundwater discharge. Earth Planet. Sci. Lett. 235, 564–576. https://doi.org/10.1016/j.epsl.2005.04.043

Moore, W.S., 2008. Fifteen years experience in measuring ^{224}Ra and ^{223}Ra by delayed-coincidence counting. Mar. Chem. 109, 188–197. https://doi.org/10.1016/j.marchem.2007.06.015

Moore, W.S., 2010. The effect of submarine groundwater discharge on the ocean. Ann. Rev. Mar. Sci. 2, 59–88. https://doi.org/10.1146/annurev-marine-120308-081019

Moore, W.S., Arnold, R., 1996. Measurement of ^{223}Ra and ^{224}Ra in coastal waters using a delayed coincidence counter. J. Geophys. Res. 101, 1321–1329. https://doi.org/10.1029/95jc03139

Morel, F.M.M., Price, N.M., 2003. The biogeochemical cycles of trace metals in the oceans. Science. 300, 944–947. https://doi.org/10.1126/science.1083545

Morillo, J., Usero, J., Gracia, I., 2004. Heavy metal distribution in marine sediments from the southwest coast of Spain. Chemosphere 55, 431–442. https://doi.org/10.1016/j.chemosphere.2003.10.047

Navarro, A., Carbonell, M., 2007. Evaluation of groundwater contamination beneath an urban environment: The Besòs river basin (Barcelona, Spain). J. Environ. Manage. 85, 259–269. https://doi.org/10.1016/j.jenvman.2006.08.021

Nesbitt, H.W., Muir, I.J., Prarr, A.R., 1995. Oxidation of arsenopyrite by air and air-saturated, distilled water, and implications for mechanism of oxidation. Geochim. Cosmochim. Acta 59, 1773–1786. https://doi.org/10.1016/0016-7037(95)00081-A

Odhiambo, B.K., Macdonald, R.W., O'Brien, M.C., Harper, J.R., Yunker, M.B., 1996. Transport and fate of mine tailings in a coastal fjord of British Columbia as inferred from the sediment record. Sci. Total Environ. 191, 77–94. https://doi.org/10.1016/0048-9697(96)05250-3

Ollivier, P., Claude, C., Radakovitch, O., Hamelin, B., 2007. TIMS measurements of ^{226}Ra and ^{228}Ra in the Gulf of Lion, an attempt to quantify submarine groundwater discharge. Mar. Chem. 109, 337–354. https://doi.org/10.1016/j.

marchem.2007.08.006

Olsgard, F., Hasle, J.R., 1993. Impact of waste from titanium mining on benthic fauna. J. Exp. Mar. Bio. Ecol. 172, 185–213. https://doi.org/10.1016/0022-0981(93)90097-8

Otero, X.L., Fernández, S., de Pablo Hernandez, M.A., Nizoli, E.C., Quesada, A., 2013. Plant communities as a key factor in biogeochemical processes involving micronutrients (Fe, Mn, Co, and Cu) in Antarctic soils (Byers Peninsula, maritime Antarctica). Geoderma 195, 145–154. https://doi.org/10.1016/j.geoderma.2012.11.018

Oyarzun, R., Manteca Martínez, J.I., López García, J.A., Carmona, C., 2013. An account of the events that led to full bay infilling with sulfide tailings at Portman (Spain), and the search for "black swans" in a potential land reclamation scenario. Sci. Total Environ. 454–455, 245–9. https://doi.org/10.1016/j.scitotenv.2013.03.030

Palanques, A., Diaz, J.I., Maldonado, A., 1991. Impact of the sewage sludge discharged in the Barcelona continental shelf. Oceanol. acta 14, 329–329.

Palanques, A., Sanchez-Cabeza, J.A., Masqué, P., León, L., 1998. Historical record of heavy metals in a highly contaminated Mediterranean deposit: The Besos prodelta. Mar. Chem. 61, 209–217. https://doi.org/10.1016/S0304-4203(98)00020-6

Palanques, A., Masqué, P., Puig, P., Sanchez-Cabeza, J.A., Frignani, M., Alvisi, F., 2008. Anthropogenic trace metals in the sedimentary record of the Llobregat continental shelf and adjacent Foix Submarine Canyon (northwestern Mediterranean). Mar. Geol. 248, 213–227. https://doi.org/10.1016/j.margeo.2007.11.001

Palanques, A., Lopez, L., Guillén, J., Puig, P., Masqué, P., 2017. Decline of trace metal pollution in the bottom sediments of the Barcelona City continental shelf (NW Mediterranean). Sci. Total Environ. 579, 755–767. https://doi.org/10.1016/j.scitotenv.2016.11.031

Pan, K., Wang, W.X., 2012. Trace metal contamination in estuarine and coastal environments in China. Sci. Total Environ. 421, 3–16. https://doi.org/10.1016/j.scitotenv.2011.03.013

Panzeca, C., Beck, A.J., Leblanc, K., Taylor, G.T., Hutchins, D.A., Sañudo-Wilhelmy, S.A., 2008. Potential cobalt limitation of vitamin B12 synthesis in the North Atlantic Ocean. Global Biogeochem. Cycles 22. https://doi.org/10.1029/2007GB003124

Patterson, C.C., 1965. Contaminated and natural lead environments of man. Arch. Environ. Health 11(3), 344–360. https://doi.org/10.1080/00039896.1965.10664229

Pauc, H., Thibault, M., 1976. Lhydrodynamique et la dynamique des matériaux en suspension en baie de Portman (Province de Murcie, Espagne). Bull. BRGM 3, 211–221.

Pavlidou, A., Papadopoulos, V.P., Hatzianestis, I., Simboura, N., Patiris, D., Tsabaris, C., 2014. Chemical inputs from a karstic submarine groundwater discharge (SGD) into an oligotrophic Mediterranean coastal area. Sci. Total Environ. 488, 1–13. https://doi.org/10.1016/j.scitotenv.2014.04.056

Paytan, A., Mackey, K.R.M., Chen, Y., Lima, I.D., Doney, S.C., Mahowald, N., Labiosa, R., Post, A.F., 2009. Toxicity of atmospheric aerosols on marine phytoplankton. Proc. Natl. Acad. Sci. U. S. A. 106(12), 4601–4605. https://doi.org/10.1073/pnas.0811486106

Peers, G., Price, N.M., 2006. Copper-containing plastocyanin used for electron transport by an oceanic diatom. Nature 441(7091), 341–344. https://doi.org/10.1038/nature04630

Peña, J.A., Manteca, J.I., Martínez-Pagán, P., Teixidó, T., 2013. Magnetic gradient map of the mine tailings in Portman Bay (Murcia, Spain) and its contribution to the understanding of the bay infilling process. J. Appl. Geophys. 95, 115–120. https://doi.org/10.1016/j.jappgeo.2013.05.011

Pereira, A.A., Van Hattum, B., Brouwer, A., Van Bodegom, P.M., Rezende, C.E., Salomons, W., 2008. Effects of iron-ore mining and processing on metal bioavailability in a tropical coastal lagoon. J. Soils Sediments 8, 239–252. https://doi.org/10.1007/s11368-008-0017-1

Persaud, D., Jaagumagi, R., Hayton, A., 1993. Guidelines for the protection and management of aquatic sediment quality in Ontario.

Picotti, V., Negri, A., Capaccioni, B., 2014. The geological origins and paleoceanographic history of the Mediterranean Region: Tethys to present, in: The Mediterranean Sea: Its History and Present Challenges. pp. 3–10. https://doi.org/10.1007/978-94-007-6704-1_1

Piippanen, T., Rautiainen, J., Tummavuori, J., 1997. Determination of copper, iron, molybdenum and silicon in hydrometallurgically roasted molybdenite concentrate solution by inductively coupled plasma atomic emission spectrometry. Anal. Chim. Acta 349, 327–331. https://doi.org/10.1016/S0003-2670(97)00190-6

Pourabadehei, M., Mulligan, C.N., 2016. Selection of an appropriate management strategy for contaminated sediment: A case study at a shallow contaminated harbour in Quebec, Canada. Environ. Pollut. 219, 846–857. https://doi.org/10.1016/j.envpol.2016.08.012

Programe, U.N.E., 2017. 2017 Mediterranean Quality Status Report.

Protano, C., Zinnà, L., Giampaoli, S., Spica, V.R., Chiavarini, S., Vitali, M., 2014. Heavy metal pollution and potential ecological risks in rivers: A case study from Southern Italy. Bull. Environ. Contam. Toxicol. 92(1), 75–80. https://doi.org/10.1007/s00128-013-1150-0

Puig, P., Palanques, A, Sanchez-Cabeza, J., Masque, P., 1999. Heavy metals in particulate matter and sediments in the southern Barcelona sedimentation system - (North-western Mediterranean). Mar. Chem. 63, 311–329. https://doi.org/Doi 10.1016/S0304-4203(98)00069-3

Querol, X., Viana, M., Alastuey, A., Amato, F., Moreno, T., Castillo, S., Pey, J., de la Rosa, J., Sánchez de la Campa, A., Artíñano, B., Salvador, P., García Dos Santos, S., Fernández-Patier, R., Moreno-Grau, S., Negral, L., Minguillón, M.C., Monfort, E., Gil, J.I., Inza, A., Ortega, L.A., Santamaría, J.M., Zabalza, J., 2007. Source origin of trace elements in PM from regional background, urban and industrial sites of Spain. Atmos. Environ. 41, 7219–7231. https://doi.org/10.1016/j.atmosenv.2007.05.022

Rahman, M.M., Dong, Z., Naidu, R., 2015. Concentrations of arsenic and other elements in groundwater of Bangladesh and West Bengal, India: Potential cancer risk. Chemosphere 139, 54–64. https://doi.org/10.1016/j.

chemosphere.2015.05.051

Ramirez, M., Massolo, S., Frache, R., Correa, J.A., 2005. Metal speciation and environmental impact on sandy beaches due to El Salvador copper mine, Chile. Mar. Pollut. Bull. 50, 62–72. https://doi.org/10.1016/j.marpolbul.2004.08.010

Ramirez-Llodra, E., Trannum, H.C., Evenset, A., Levin, L.A., Andersson, M., Finne, T.E., Hilario, A., Flem, B., Christensen, G., Schaanning, M., Vanreusel, A., 2015. Submarine and deep-sea mine tailing placements: A review of current practices, environmental issues, natural analogs and knowledge gaps in Norway and internationally. Mar. Pollut. Bull. 97, 13–35. https://doi.org/10.1016/j.marpolbul.2015.05.062

Ramsey, M.H., Potts, P.J., Webb, P.C., Watkins, P., Watson, J.S., Coles, B.J., 1995. An objective assessment of analytical method precision: comparison of ICP-AES and XRF for the analysis of silicate rocks. Chem. Geol. 124, 1–19. https://doi.org/10.1016/0009-2541(95)00020-M

Rapaglia, J., Koukoulas, S., Zaggia, L., Lichter, M., Manfé, G., Vafeidis, A.T., 2012. Quantification of submarine groundwater discharge and optimal radium sampling distribution in the Lesina Lagoon, Italy. J. Mar. Syst. 91, 11–19. https://doi.org/10.1016/j.jmarsys.2011.09.003

Ribeiro, A.P., Figueiredo, A.M.G., Santos, J.O. dos, Dantas, E., Cotrim, M.E.B., Cesar Lopes Figueira, R., V. Silva Filho, E., Cesar Wasserman, J., 2013. Combined SEM/AVS and attenuation of concentration models for the assessment of bioavailability and mobility of metals in sediments of Sepetiba Bay (SE Brazil). Mar. Pollut. Bull. 68(1–2), 55–63. https://doi.org/10.1016/j.marpolbul.2012.12.023

Richter, T.O., van der Gaast, S., Koster, B., Vaars, A., Gieles, R., de Stigter, H.C., De Haas, H., van Weering, T.C.E., 2006. The Avaatech XRF Core Scanner: technical description and applications to NE Atlantic sediments. Geol. Soc. London, Spec. Publ. 267, 39–50. https://doi.org/10.1144/GSL.SP.2006.267.01.03

Ridgway, J., Shimmield, G., 2002. Estuaries as Repositories of Historical Contamination and their Impact on Shelf Seas. Estuar. Coast. Shelf Sci. 55, 903–928. https://doi.org/10.1006/ecss.2002.1035

Rijkenberg, M.J.A., Middag, R., Laan, P., Gerringa, L.J.A., Van Aken, H.M., Schoemann, V., De Jong, J.T.M., De Baar, H.J.W., 2014. The distribution of dissolved iron in the West Atlantic Ocean. PLoS One 9. https://doi.org/10.1371/journal.pone.0101323

Rodellas, V., Garcia-Orellana, J., Tovar-Sánchez, A., Basterretxea, G., López-Garcia, J.M.J.M., Sánchez-Quiles, D., Garcia-Solsona, E., Masqué, P., 2014. Submarine groundwater discharge as a source of nutrients and trace metals in a Mediterranean bay (Palma Beach, Balearic Islands). Mar. Chem. 160, 56–66. https://doi.org/10.1016/j.marchem.2014.01.007

Rodellas, V., Garcia-Orellana, J., Masqué, P., Feldman, M., Weinstein, Y., Boyle, E.A.E.A., 2015a. Submarine groundwater discharge as a major source of nutrients to the Mediterranean Sea. Proc. Natl. Acad. Sci. 112, 201419049. https://doi.org/10.1073/pnas.1419049112

Rodellas, V., Garcia-Orellana, J., Masqué, P., Font-Muñoz, J.S.J.S., 2015b. The influence of sediment sources on radium-derived estimates of Submarine Groundwater Discharge. Mar. Chem. 171, 107–117. https://doi.org/10.1016/j.marchem.2015.02.010

Rodellas, V., Garcia-Orellana, J., Trezzi, G., Masqué, P., Stieglitz, T.C., Bokuniewicz, H., Cochran, J.K., Berdalet, E., 2017. Using the radium quartet to quantify submarine groundwater discharge and porewater exchange. Geochim. Cosmochim. Acta 196, 58–73. https://doi.org/http://dx.doi.org/10.1016/j.gca.2016.09.016

Rodríguez-Germade, I., Rubio, B., Rey, D., Borrego, J., 2015a. Detection and Monitoring of REEs and Related Trace Elements with an ItraxTM Core Scanner in the Ría de Huelva (SW Spain). Water, Air, Soil Pollut. 226, 137. https://doi.org/10.1007/s11270-015-2389-3

Rodríguez-Germade, I., Rubio, B., Rey, D., Vilas, F., López-Rodríguez, C.F., Comas, M.C., Martínez-Ruiz, F., 2015b. Optimization of Itrax core scanner measurement conditions for sediments from submarine mud volcanoes, in: Micro-XRF Studies of Sediment Cores. Springer, pp. 103–126.

Rollinson, H.R., 1993. Using geochemical data: evaluation. Present. Interpret. Singapore. Ongman.

Root, R.A., Hayes, S.M., Hammond, C.M., Maier, R.M., Chorover, J., 2015. Toxic metal(loid) speciation during weathering of iron sulfide mine tailings under semi-arid climate. Appl. Geochemistry 62, 131–149. https://doi.org/10.1016/j.apgeochem.2015.01.005

Roqué, J., Cerdà-Domènech, M., Sanchez-Vidal, A., Frigola, J., Amblàs, D., Cibin, G., Canals, M., 2020. Arsenic speciation in a submarine mine tailings deposit: combining synchrotron XAS and non-destructive analysis of sediment cores. (submitted).

Rothwell, R.G., Croudace, I., 2015. Twenty Years of XRF Core Scanning Marine Sediments: What Do Geochemical Proxies Tell Us? pp. 25–102. https://doi.org/10.1007/978-94-017-9849-5_2

Rothwell, R.G., Rack, F.R., 2006. New techniques in sediment core analysis: an introduction. Geol. Soc. Spec. Publ. 267, 1–29. https://doi.org/10.1144/GSL.SP.2006.267.01.01

Rubio, B., Álvarez-Iglesias, P., Vilas, F., 2010. Diagenesis and anthropogenesis of metals in the recent Holocene sedimentary record of the Ría de Vigo (NW Spain). Mar. Pollut. Bull. 60, 1122–1129. https://doi.org/10.1016/j.marpolbul.2010.04.014

Rumín-Caparrós, A., Sanchez-Vidal, A., González-Pola, C., Lastras, G., Calafat, A., Canals, M., 2016. Particle fluxes and their drivers in the Avilés submarine canyon and adjacent slope, central Cantabrian margin, Bay of Biscay. Prog. Oceanogr. 144, 39–61. https://doi.org/10.1016/j.pocean.2016.03.004

Rushton, K.R., 1980. Differing positions of saline interfaces in aquifers and observation boreholes. J. Hydrol. 48, 185–189. https://doi.org/10.1016/0022-1694(80)90074-8

Sadat-Noori, M., Santos, I.R., Tait, D.R., Maher, D.T., 2016. Fresh meteoric versus recirculated saline groundwater nutrient inputs into a subtropical estuary. Sci. Total Environ. 566, 1440–1453. https://doi.org/10.1016/j.scitotenv.2016.06.008

Sallas Campmany, M., 2011. TERMCAT: centre de terminologia. Omnis Cell. https://doi.org/10.2436/oc.v0i5.43936

Sánchez, M.J., Sirvent, M. del C.P., 2013. Diagnóstico y recuperación de la contaminación del suelo en Portmán-Sierra Minera, in: Portmán: De El" Portus Magnus" Del Mediterráneo Occidental a La Bahía Aterrada. Servicio de Publicaciones, pp. 313–344.

Sanchez-Cabeza, J.A., Masqué, P., Ani-Ragolta, I., 1998. 210Pb and210Po analysis in sediments and soils by microwave acid digestion. J. Radioanal. Nucl. Chem. 227, 19–22. https://doi.org/10.1007/BF02386425

Santos, I.R., Eyre, B.D., Huettel, M., 2012. The driving forces of porewater and groundwater flow in permeable coastal sediments: A review. Estuar. Coast. Shelf Sci. 98, 1–15. https://doi.org/10.1016/j.ecss.2011.10.024

Sanz de Galdeano, C., 1990. Geologic evolution of the Betic Cordilleras in the Western Mediterranean, Miocene to the present. Tectonophysics 172, 107–119.

Saylor, R.D., Edgerton, E.S., Hartsell, B.E., 2006. Linear regression techniques for use in the EC tracer method of secondary organic aerosol estimation. Atmos. Environ. 40, 7546–7556. https://doi.org/10.1016/j.atmosenv.2006.07.018

Schauer, J.J., Lough, G.C., Shafer, M.M., Christensen, W.F., Arndt, M.F., DeMinter, J.T., Park, J.S., 2006. Characterization of metals emitted from motor vehicles. Res. Rep. Health. Eff. Inst.

Schlosser, C., Karstensen, J., Woodward, E.M.S., 2019. Distribution of dissolved and leachable particulate Pb in the water column along the GEOTRACES section GA10 in the South Atlantic. Deep. Res. Part I Oceanogr. Res. Pap. 148, 132–142. https://doi.org/10.1016/j.dsr.2019.05.001

Scholze, F., Longoni, A., Fiorini, C., Strüder, L., Meidinger, N., Hartmann, R., Kawahara, N., Shoji, T., 2006. X-Ray Detectors and XRF Detection Channels, in: Handbook of Practical X-Ray Fluorescence Analysis. Springer, pp. 199–308.

Schultheiss, P.J., Weaver, P.P.E., 1992. Multi-sensor core logging for science and industry, in: OCEANS 1992 - Proceedings: Mastering the Oceans Through Technology. IEEE, pp. 608–613. https://doi.org/10.1109/OCEANS.1992.607652

Selin, N.E., Javob, D.J., Park, R.J., Yantosca, R.M., Strode, S., Jaeglé, L., Jaffe, D., 2007. Chemical cycling and deposition of atmospheric mercury: Global constraints from observations. J. Geophys. Res. Atmos. 112, D02308. https://doi.org/10.1029/2006JD007450

Serra, J., Sorribas, J., 1995. Característiques dinàmiques de la costa del Maresme. Atzavara 6, 4–10.

Shalev, E., Lazar, A., Wollman, S., Kington, S., Yechieli, Y., Gvirtzman, H., 2009. Biased monitoring of fresh water-salt water mixing zone in coastal aquifers. Ground Water 47, 49–56. https://doi.org/10.1111/j.1745-6584.2008.00502.x

Simonsen, A.M.T., Pedersen, K.B., Jensen, P.E., Elberling, B., Bach, L., 2019. Lability of toxic elements in Submarine Tailings Disposal: The relationship between metal fractionation and metal uptake by sandworms (Alitta virens). Sci. Total Environ. 696, 133903. https://doi.org/10.1016/j.scitotenv.2019.133903

Slowey, A.J., Johnson, S.B., Newville, M., Brown, G.E., 2007. Speciation and colloid transport of arsenic from mine tailings. Appl. Geochemistry. 22.9, 1884-1898. https://doi.org/10.1016/j.apgeochem.2007.03.053

Smith, K., Huyck, H., 1999. An overview of the abundance, relative mobility, bioavailability, and human toxicity of metals. Environ. geochemistry Miner. Depos. 6, 29–70. https://doi.org/10.5382/Rev.06.02

Smoak, J.M., Sanders, C.J., Patchineelam, S.R., Moore, W.S., 2012. Radium mass balance and submarine groundwater discharge in Sepetiba Bay, Rio de Janeiro State, Brazil. J. South Am. Earth Sci. 39, 44–51. https://doi.org/10.1016/j.jsames.2012.07.004

Spofforth, D.J.A., Pälike, H., Green, D., 2008. Paleogene record of elemental concentrations in sediments from the Arctic Ocean obtained by XRF analyses. Paleoceanography 23. https://doi.org/10.1029/2007PA001489

Sprovieri, M., Feo, M.L., Prevedello, L., Manta, D.S., Sammartino, S., Tamburrino, S., Marsella, E., 2007. Heavy metals, polycyclic aromatic hydrocarbons and polychlorinated biphenyls in surface sediments of the Naples harbour (southern Italy). Chemosphere 67, 998–1009. https://doi.org/10.1016/j.chemosphere.2006.10.055

Sternal, B., Junttila, J., Skirbekk, K., Forwick, M., Carroll, J.L., Pedersen, K.B., 2017. The impact of submarine copper mine tailing disposal from the 1970s on Repparfjorden, northern Norway. Mar. Pollut. Bull. 120, 136–153. https://doi.org/10.1016/j.marpolbul.2017.04.054

Sun, Y., Torgersen, T., 1998. The effects of water content and Mn-fiber surface conditions on ^{224}Ra measurement by ^{220}Rn emanation. Mar. Chem. 62, 299–306. https://doi.org/10.1016/S0304-4203(98)00019-X

Sunda, W.G., 2012. Feedback interactions between trace metal nutrients and phytoplankton in the ocean. Front. Microbiol. 3, 204. https://doi.org/10.3389/fmicb.2012.00204

Swarzenski, P.W., 2007. U/Th Series Radionuclides as Coastal Groundwater Tracers. Chem. Rev. 107, 663−674. https://doi.org/10.1021/cr0503761

Syvitski, J.P.M., 2003. Supply and flux of sediment along hydrological pathways: Research for the 21st century. Glob. Planet. Change 39, 1–11. https://doi.org/10.1016/S0921-8181(03)00008-0

Szymczycha, B., Vogler, S., Pempkowiak, J., 2012. Nutrient fluxes via submarine groundwater discharge to the Bay of Puck, southern Baltic Sea. Sci. Total Environ. 438, 86−93. https://doi.org/10.1016/j.scitotenv.2012.08.058

Taylor, B.N., Kuyatt, C.E., 1994. Guidelines for evaluating and expressing the uncertainty of NIST measurement results. US Department of Commerce, Technology Administration, National Institute of Standards and Technology Gaithersburg, MD.

Tellam, J.H., Lloyd, J.W., Walters, M., 1986. The morphology of a saline groundwater body: Its investigation, description and possible explanation. J. Hydrol. 83, 1−21. https://doi.org/10.1016/0022-1694(86)90179-4

Tjallingii, R., Röhl, U., Kölling, M., Bickert, T., 2007. Influence of the water content on X-ray fluorescence corescanning measurements in soft marine sediments. Geochemistry, Geophys. Geosystems 8. https://doi.org/10.1029/2006GC001393

Tjallingii, R., Claussen, M., Stuut, J.-B.W., Fohlmeister, J., Jahn, A., Bickert, T., Lamy, F., Röhl, U., 2008. Coherent high- and low-latitude control of the

northwest African hydrological balance. Nat. Geosci. 1, 670–675. https://doi.org/10.1038/ngeo289

Tomczak, M., Godfrey, J.S., 2013. Regional oceanography: an introduction. Elsevier.

Tovar-Sánchez, A., Basterretxea, G., Rodellas, V., Sánchez-Quiles, D., García-Orellana, J., Masqué, P., Jordi, A., López, J.M.J.M., Garcia-Solsona, E., 2014. Contribution of Groundwater Discharge to the Coastal Dissolved Nutrients and Trace Metal Concentrations in Majorca Island: Karstic vs Detrital Systems. Environ. Sci. Technol. 48, 11819–11827. https://doi.org/10.1021/es502958t

Tovar-Sánchez, A., González-Ortegón, E., Duarte, C.M., 2019. Trace metal partitioning in the top meter of the ocean. Sci. Total Environ. 652, 907–914. https://doi.org/10.1016/j.scitotenv.2018.10.315

Trezzi, G., Garcia-Orellana, J., Rodellas, V., Santos-Echeandia, J., Tovar-Sánchez, A., Garcia-Solsona, E., Masqué, P., 2016a. Submarine groundwater discharge: A significant source of dissolved trace metals to the North Western Mediterranean Sea. Mar. Chem. 186, 90–100. https://doi.org/10.1016/j.marchem.2016.08.004

Trezzi, G., Garcia-Orellana, J., Santos-Echeandia, J., Rodellas, V., Garcia-Solsona, E., Garcia-Fernandez, G., Masqué, P., 2016b. The influence of a metal-enriched mining waste deposit on submarine groundwater discharge to the coastal sea. Mar. Chem. 178, 35–45. https://doi.org/10.1016/j.marchem.2015.12.004

Trezzi, G., Garcia-Orellana, J., Rodellas, V., Masqué, P., Garcia-Solsona, E., Andersson, P.S., 2017. Assessing the role of submarine groundwater discharge as a source of Sr to the Mediterranean Sea. Geochim. Cosmochim. Acta 200, 42–54. https://doi.org/10.1016/j.gca.2016.12.005

Tueros, I., Rodríguez, J.G., Borja, A., Solaun, O., Valencia, V., Millán, E., 2008. Dissolved metal background levels in marine waters, for the assessment of the physico-chemical status, within the European Water Framework Directive. Sci. Total Environ. 407, 40–52. https://doi.org/10.1016/j.scitotenv.2008.08.026

Twining, B.S., Baines, S.B., 2013. The Trace Metal Composition of Marine Phytoplankton. Ann. Rev. Mar. Sci. 5, 191–215. https://doi.org/10.1146/annurev-marine-121211-172322

Ussher, S.J., Achterberg, E.P., Powell, C., Baker, A.R., Jickells, T.D., Torres, R., Worsfold, P.J., 2013. Impact of atmospheric deposition on the contrasting iron biogeochemistry of the North and South Atlantic Ocean. Global Biogeochem. Cycles 27, 1094–1107. https://doi.org/10.1002/gbc.20056

U.S. Environmental Protection Agency, 2005. Contaminated sediment remediation guidance for hazardous waste sites, Office of Solid Waste and Emergency Response.

Van Daele, M., Bertrand, S., Meyer, I., Moernaut, J., Vandoorne, W., Siani, G., Tanghe, N., Ghazoui, Z., Pino, M., Urrutia, R., De Batist, M., 2016. Late Quaternary evolution of Lago Castor (Chile, 45.6°S): Timing of the deglaciation in northern Patagonia and evolution of the southern westerlies during the last 17 kyr. Quat. Sci. Rev. 133, 130–146. https://doi.org/10.1016/j.quascirev.2015.12.021

Vance, D., Archer, C., Bermin, J., Perkins, J., Statham, P.J., Lohan, M.C., Ellwood, M.J., Mills, R.A., 2008. The copper isotope geochemistry of rivers and the oceans. Earth Planet. Sci. Lett. 274, 204–213. https://doi.org/10.1016/j.epsl.2008.07.026

Vogt, C., 2012. International Assessment of Marine and Riverine Disposal of Mine Tailings. Impact Assess. Soc. Econ. Dev. - 34th Annu. Conf. Int. Assoc. I 134.

Wagner, M., Hendy, I.L., 2017. Trace metal evidence for a poorly ventilated glacial Southern Ocean. Quat. Sci. Rev. 170, 109–120. https://doi.org/10.1016/j.quascirev.2017.06.014

Wang, Q., Li, H., Zhang, Y., Wang, X., Zhang, C., Xiao, K., Qu, W., 2019. Evaluations of submarine groundwater discharge and associated heavy metal fluxes in Bohai Bay, China. Sci. Total Environ. 696, 133873. https://doi.org/10.1016/j.scitotenv.2019.133873

Walling, D.E., 2009. The Impact of Global Change on Erosion and Sediment Transport by Rivers: Current Progress and Future ChallengesThe Impact of Global Change publications series. United Nations World Water Assess. Program.

Webster, I.T., Hancock, G.J., Murray, A.S., 1995. Modelling the effect of salinity on radium desorption from sediments. Geochim. Cosmochim. Acta 59,

2469–2476. https://doi.org/10.1016/0016-7037(95)00141-7

Weltje, G.J., Tjallingii, R., 2008. Calibration of XRF core scanners for quantitative geochemical logging of sediment cores: Theory and application. Earth Planet. Sci. Lett. 274, 423–438. https://doi.org/10.1016/j.epsl.2008.07.054

Wenning, R.J., 2005. Use of Sediment Quality Guidelines and Related Tools for the Assessment of Contaminated Sediments, Use of Sediment Quality Guidelines and Related Tools for the Assessment of Contaminated Sediments. SETAC.

Windom, H.L., Moore, W.S., Niencheski, L.F.H., Jahnke, R.A., 2006. Submarine groundwater discharge: A large, previously unrecognized source of dissolved iron to the South Atlantic Ocean. Mar. Chem. 102, 252–266. https://doi.org/10.1016/j.marchem.2006.06.016

Wu, L., Kravchinsky, V.A., Potter, D.K., 2015. PMTec: A new MATLAB toolbox for absolute plate motion reconstructions from paleomagnetism. Comput. Geosci. 82, 139–151. https://doi.org/10.1016/j.cageo.2015.06.009

Yeats, P.A., Bewers, J.M., 1982. Discharge of metals from the St. Lawrence River. Can. J. Earth Sci. 19, 982–992. https://doi.org/10.1139/e82-082

York, D., Evensen, N.M., Martínez, M.L., De Basabe Delgado, J., 2004. Unified equations for the slope, intercept, and standard errors of the best straight line. Am. J. Phys. 72, 367–375. https://doi.org/10.1119/1.1632486

Zekollari, H., 2017. TopoZeko: A MATLAB function for 3-D and 4-D topographical visualization in geosciences. SoftwareX 6, 285–292. https://doi.org/10.1016/j.softx.2017.10.004

Zhang, H., Walker, T.R., Davis, E., Ma, G., 2019. Spatiotemporal characterization of metals in small craft harbour sediments in Nova Scotia, Canada. Mar. Pollut. Bull. 140, 493–502. https://doi.org/10.1016/j.marpolbul.2019.02.004

Zhao, H., Shao, Y., Yin, C., Jiang, Y., Li, X., 2016. An index for estimating the potential metal pollution contribution to atmospheric particulate matter from road dust in Beijing. Sci. Total Environ. 550, 167–175. https://doi.org/10.1016/j.scitotenv.2016.01.110

Annex

Science of the Total Environment 595 (2017) 849–857

Contents lists available at ScienceDirect

Science of the Total Environment

journal homepage: www.elsevier.com/locate/scitotenv

Constraining the temporal variations of Ra isotopes and Rn in the groundwater end-member: Implications for derived SGD estimates

Marc Cerdà-Domènech [a,*], Valentí Rodellas [b,c], Albert Folch [d,e], Jordi Garcia-Orellana [b,f]

[a] GRC Geociències Marines, Dep. de Dinàmica de la Terra i de l'Oceà, Universitat de Barcelona, 08028 Barcelona, Spain
[b] Institut de Ciència i Tecnologia Ambientals (ICTA), Universitat Autònoma de Barcelona, 08193 Bellaterra, Spain
[c] Centre de Recherche et d'Enseignement de Géosciences de l'Environment (CEREGE), Aix-Marseille Université, 13545 Aix-en-Provence, France
[d] Department of Civil and Environmental Engineering, Universitat Politècnica de Catalunya (UPC), 08034 Barcelona, Spain
[e] Associated Unit: Hydrogeology (UPC-CSIC), Spain.
[f] Departament de Física, Universitat Autònoma de Barcelona, 08193 Bellaterra, Spain

HIGHLIGHTS

- Ra isotopes and ^{222}Rn were measured for nearly two years in a coastal piezometer.
- High Ra variability was registered, especially during intense rainfall events.
- ^{222}Rn displayed minor variations due to the no influence of groundwater salinity on radon emanation.
- The hydrodynamics of coastal aquifers must be considered as essential to understand SGD fluxes.

GRAPHICAL ABSTRACT

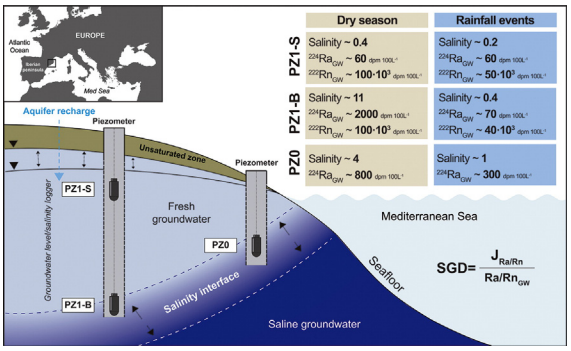

ARTICLE INFO

Article history:
Received 25 January 2017
Received in revised form 28 February 2017
Accepted 1 March 2017
Available online xxxx

Editor: D. Barcelo

Keywords:
Submarine groundwater discharge
Radium
Radon
Salinity interface
End-member

ABSTRACT

Submarine groundwater discharge (SGD) has been recognized as an important supplier of chemical compounds to the ocean that may influence coastal geochemical cycles. Radium isotopes (^{223}Ra, ^{224}Ra, ^{226}Ra, ^{228}Ra) and radon (^{222}Rn) have been widely applied as tracers of SGD. Their application requires the appropriate characterization of both the concentrations of tracers in the discharging groundwater and their distribution in the coastal water column. This study evaluates the temporal evolution of Ra isotopes and ^{222}Rn concentrations in a dynamic subterranean estuary of a microtidal Mediterranean coastal aquifer that experiences large displacements of the fresh-saltwater interface as a necessary initial step in evaluating the influence of SGD in coastal waters. We show that changes in groundwater salinities due to the seaward displacement of the fresh-saltwater interface produced large variations in Ra activities in groundwater (by a factor of ~19, ~14, ~6, and ~11 for ^{223}Ra, ^{224}Ra, ^{226}Ra and ^{228}Ra, respectively), most importantly during rainfall events. In contrast, the ^{222}Rn activities in groundwater oscillated only by a factor of 3 during these rainy periods. The large temporal variability in Ra activities hampers the characterization of the SGD end-member when using Ra isotopes as tracers, and thus presents a challenge for obtaining accurate SGD estimates. This study emphasizes the need to understand the hydrodynamics of coastal aquifers to appropriately constrain the Ra isotopes and ^{222}Rn concentrations in groundwater and when applying both tracers in dynamic microtidal coastal systems.

© 2017 Elsevier B.V. All rights reserved.

* Corresponding author at: GRC Geociències Marines, Departament de Dinàmica de la Terra i de l'Oceà, Facultat de Ciències de la Terra, Universitat de Barcelona, c/Martí Franquès s/n, 08028 Barcelona, Spain.
E-mail address: cerda.domenech@ub.edu (M. Cerdà-Domènech).

http://dx.doi.org/10.1016/j.scitotenv.2017.03.005
0048-9697/© 2017 Elsevier B.V. All rights reserved.

1. Introduction

Submarine Groundwater Discharge (SGD) includes both meteoric fresh groundwater flowing into the sea and seawater recirculation through coastal aquifers (Burnett et al., 2003). Both flows mix in coastal aquifers, so-called subterranean estuaries (STEs), where biogeochemical reactions occur as a consequence of interactions between terrestrially derived groundwater, recirculated seawater and the geological matrix (Moore, 1999). This dynamic mixing zone influences the transfer of several chemical constituents to the coastal ocean (Tovar-Sánchez et al., 2014; Sadat-Noori et al., 2016). SGD is now recognized as a relevant source of nutrients, trace metals and other compounds and contaminants to the coastal sea (Kim et al., 2003; Johnson et al., 2008; Gonneea et al., 2014; Pavlidou et al., 2014; Rodellas et al., 2015b; Trezzi et al., 2016).

Radium (Ra) isotopes (^{223}Ra, ^{224}Ra, ^{226}Ra, ^{228}Ra) and radon (^{222}Rn) have been widely used as tracers to quantify SGD (e.g., Charette et al., 2001; Moore, 2003; Burnett et al., 2006; Burnett et al., 2008; Lee et al., 2012). Ra isotopes and ^{222}Rn, which are continuously produced in geological materials by the decay of their uranium and thorium parents, are appropriate SGD tracers, mainly because they behave conservatively once released to the sea and because they are significantly enriched in SGD fluids relative to seawater (Burnett et al., 2006). The approach used to estimate SGD flows using Ra isotopes or ^{222}Rn is based on characterizing the flux of Ra/Rn supplied by SGD (J_{Ra} or J_{Rn}) using the Ra/Rn distribution in coastal waters and the Ra/Rn concentration in groundwater inflowing to the sea, the so-called SGD end-member (Ra_{GW} or Rn_{GW}) (Burnett and Dulaiova, 2003; Moore, 1996a).

Most SGD studies have been devoted primarily to estimating the fluxes of Ra and Rn (J_{Ra} or J_{Rn}) (e.g., Kim et al., 2005; Beck et al., 2008; Smoak et al., 2012), whereas the Ra and Rn concentrations in the groundwater end-member have been largely overlooked, even though they are a critical component of the tracer-derived estimates (Cho and Kim, 2016; Burnett et al., 2007; Gonneea et al., 2008, 2013). Ra activities in subterranean estuaries can vary significantly (one or two orders of magnitude) over space and time at a given study site (Ollivier et al., 2007; Beck et al., 2008). Thus, the lack of constraint on this term remains a significant source of uncertainty in Ra-derived SGD estimates (Charette, 2007; Gonneea et al., 2013).

Several factors influence Ra activities in SGD, including the presence of Mn-Fe oxides (Gonneea et al., 2008), the pH of the subterranean estuary (Beck and Cochran, 2013), the ionic strength (Elsinger and Moore, 1980; Webster et al., 1995), the properties of the geological matrix (Swarzenski, 2007) and the residence time within the STE (Rodellas et al., 2017). Among them, the ionic strength of the solution (i.e., its salinity) has long been recognized as the main factor influencing the Ra activities in the SGD end-member, and Ra desorption increases significantly with salinity (Cho and Kim, 2016; Elsinger and Moore, 1980; Webster et al., 1995). As a consequence, Ra activities in SGD may vary substantially depending on the position of the freshwater-saltwater interface within the subterranean estuary. The position of this interface may oscillate, due to variations in the hydraulic gradient of the fresh groundwater (caused by, e.g., recharge and abstraction) and marine driving forces (e.g., tides, wave and storms) (Gonneea et al., 2013; Heiss and Michael, 2014). These temporal oscillations of Ra activity in STEs, along with the spatial heterogeneity of coastal aquifers, make it difficult to characterize the Ra_{GW} end-member, which is needed to provide accurate estimates of SGD (Michael et al., 2011).

Unlike Ra, Rn is an inert gas. Thus, its chemical behavior is not influenced by the physicochemical characteristics of the coastal aquifer (e.g., groundwater salinity, temperature or redox conditions). Radon activities in coastal aquifers are thus primarily controlled by the content of ^{226}Ra in the aquifer solids and dissolved in groundwater (Dulaiova et al., 2008). However, the physical and geochemical processes occurring in coastal aquifers (e.g., manganese cycling or ionic exchange) can affect the ^{226}Ra distribution, thus driving changes in the ^{222}Rn concentration of groundwater (Dulaiova et al., 2008).

In contrast to many coastal areas of the world, the Mediterranean Sea is characterized by a microtidal regime, with tidal amplitudes commonly lower than 0.2 m. Therefore, these coastal aquifers are not significantly influenced by tidal pumping. As a consequence, the location and movement of the salinity interface in subterranean estuaries in the Mediterranean region, as well as in other microtidal sea regions (e.g., the Caribbean Sea or the Baltic Sea), are mainly regulated by hydrogeological factors, such as aquifer properties and the aquifer water budget. Thus, understanding the hydrogeological characteristics (i.e. recharge, discharge, etc.) of coastal aquifers in microtidal regions and their impacts on the Ra and Rn concentrations in groundwater is particularly important for improving tracer-derived estimates of SGD.

This study evaluates the temporal evolution of Ra isotopes and ^{222}Rn concentrations in a Mediterranean microtidal coastal aquifer (Argentona, Catalonia, Eastern Iberian Peninsula) over almost 2 years. During this period, two piezometers (PZ) were continuously monitored to measure variations in groundwater levels, salinity and the Ra and ^{222}Rn concentrations in the groundwater. The aim of this study is to assess hydrogeological dynamics affecting the variability in the concentrations of Ra isotopes and ^{222}Rn in groundwater from this coastal microtidal aquifer. This variability may have critical implications for the quantification of Ra/Rn-derived SGD fluxes and therefore their implications for coastal biogeochemical cycles.

2. Study area and methods

2.1. Study area: the Argentona alluvial aquifer and the oceanographic setting

The Argentona alluvial aquifer is located between the Catalan Littoral Mountain Range and the Mediterranean Sea (Barcelona, NW Mediterranean) and extends in the SW-NE direction (Fig. 1). It has an area of approximately 35 km^2 that is mainly devoted to agricultural uses. The climatology of this region is characterized by Western Mediterranean conditions, and the region experiences high temperatures in summer (mean ~23 °C) and mild temperatures in winter (mean ~10 °C). The annual precipitation of the area ranges from 500 to 800 mm, and

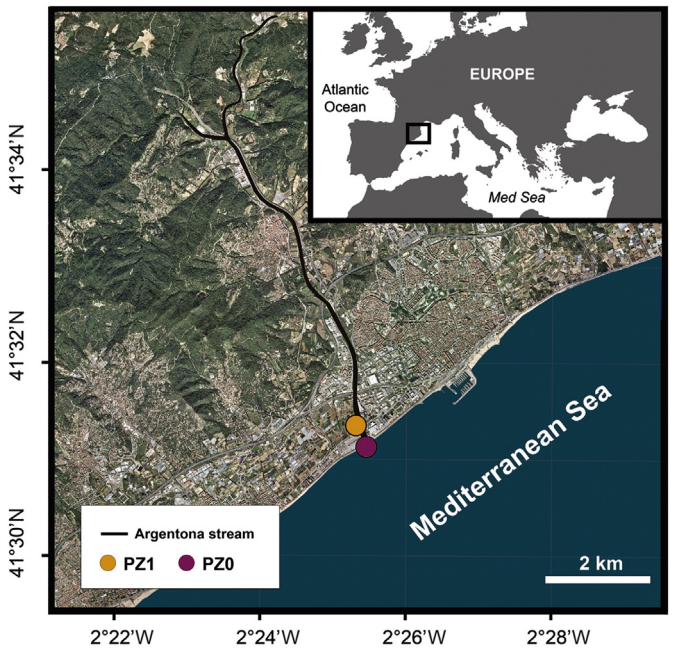

Fig. 1. Location of the Argentona stream in the NW Mediterranean Sea, including the location of the two monitored piezometers (PZ).

is mainly related to intense and short storms during the fall and spring season. Surface water flows in the Argentona main stream are restricted to the rainy seasons, particularly during major rainfall events (e.g., >50 mm in a few hours).

The Argentona aquifer is associated with a tectonic fault and sinking blocks where stream valleys have developed. The geology of the alluvial aquifer, which is unconfined, is dominated by detrital Quaternary sediments that are the product of chemical weathering of the granitic basement along fissures (Montoto, 1967). These sediments constitute layers of unconsolidated sands, gravels and clays deposited in an alluvial fan system during basin formation. In the nearshore area, the aquifer is mainly composed of marine sands (Catalan Water Agency, 2010).

A water budget for the aquifer conducted by the Catalan Water Agency (ACA), which used a numerical flow model of the aquifer system and covered the period 2006–2009, estimated an aquifer recharge rate between $3.6 \cdot 10^6$ to $5.4 \cdot 10^6$ m^3 y^{-1}. Major outputs from the aquifer include urban, agricultural and industrial extraction ($(1.4–1.9) \cdot 10^6$ m^3 y^{-1}) and fresh groundwater discharge to the sea ($(1.2–2.4) \cdot 10^6$ m^3 y^{-1}).

2.2. Groundwater monitoring and sample collection

During a period of 2 years (from January 2013 to December 2014), hydrogeological conditions (groundwater level and salinity), Ra isotopes and ^{222}Rn activities were monitored in the Argentona coastal aquifer using two entirely screened piezometers. The first piezometer, PZ1, was drilled to a depth of 35 m by the Catalan Water Agency in 2007. It is located 380 m from the shoreline and has a groundwater level approximately 6–7 m below the ground surface. The second piezometer, PZ0, which was only monitored for 7 months (May 2014 to December 2014), was drilled approximately 8 m from the shoreline to a depth of 2 m. Three CTD-Diver® data loggers were installed in the piezometers to measure temporal salinity, temperature and groundwater table variations. The first instrument was installed in PZ1 10 m below the ground surface (3–4 m below the water level) to evaluate the freshwater conditions (hereinafter referred to as PZ1-S). The second instrument was installed in PZ1 at a depth of 34 m to monitor variations in the mixing zone between the freshwater and saltwater (hereinafter referred to as PZ1-B) (Fig. 1). (3) The third instrument was installed in PZ0 at a depth of 1.8 m below the ground surface to evaluate conditions in the groundwater close to the coastal seepage face. Variations in air pressure were compensated for using air pressure measurements that were made simultaneously using a Baro-Diver® that was also installed at the top of the PZ1 piezometer.

Groundwater samples were collected at the same depths where the CTDs were installed, samples from PZ1-S ($n = 15$) were collected 10 m below the ground surface, samples from PZ1-B ($n = 15$) were collected 34 m below the ground surface, and samples from PZ0 ($n = 8$) were collected 1.5 m below the ground surface. A submersible pump was used to collect samples with volumes of 60 L (PZ1-S), 25 L (PZ1-B) and 10 L (PZ0) for Ra isotopes. Samples with volumes of 250-mL were collected for ^{222}Rn analyses from PZ1-S and PZ1-B. Radon-222 was not analyzed in PZ0 due to the low water level (<20 cm), which increased the exchange of ^{222}Rn with the air and did not permit us to obtain a representative sample. During each sampling survey, salinity and temperature were measured in situ using a YSI-556 handheld probe.

Water samples for Ra isotopes were filtered through MnO_2-impregnated acrylic fibers (hereinafter referred to as Mn fibers) at flow rates <1 L min^{-1} to quantitatively sorb Ra onto the Mn fibers (Moore and Reid, 1973). For the ^{222}Rn samples, groundwater was pumped directly through a tube that reached to the bottom of each 250-mL bottle. The groundwater was allowed to overflow for several volumes of the sample bottle to reduce Rn losses to the atmosphere.

2.3. Analytical methods

Once in the laboratory, the Mn fibers containing the Ra isotopes were rinsed with Ra-free water (Sun and Torgersen, 1998), partially dried and placed in a Radium Delayed Coincidence Counter (RaDeCC) to quantify the short-lived Ra isotopes, ^{223}Ra and ^{224}Ra (Garcia-Solsona et al., 2008; Moore and Arnold, 1996). After these measurements, the Mn fibers were ashed (820 °C, 16 h), ground and aged for 3 weeks in counting vials to allow ^{222}Rn to come into secular equilibrium with ^{226}Ra. Samples were measured using a well-type HPGe gamma detector. ^{226}Ra and ^{228}Ra were measured via ^{214}Pb at the 351.9 keV photopeak and ^{228}Ac at the 911 keV photopeak, respectively. ^{222}Rn activities in groundwater samples were determined using a portable ^{222}Rn-in-air alpha spectrometer RAD7 (Durridge Inc.) coupled with a RAD—H_2O attachment that allows the direct determination of ^{222}Rn from 250-mL bottles (Burnett et al., 2001).

3. Results

3.1. Hydrogeological features and dynamics

Results of the continuous monitoring of the groundwater table and salinity at PZ1 are shown in Fig. 2. The fresh groundwater part of the coastal aquifer (PZ1-S) showed relatively constant salinities (~0.4) with minimum values of 0.05 occurring during some rainfall events (Fig. 2b). In contrast, salinities at the bottom level (PZ1-B) varied significantly during the studied period and ranged from 0.3 to 17 (Fig. 2c). Two general patterns in salinity can be identified at the bottom. (1) Salinities were stable during dry periods (sometimes showing minor and constant salinity increases due to reductions in recharge), with maximum values of 15–17 (e.g., January–February 2013 and July–September 2013). On the other hand, (2) large fluctuations occur during rainfall events, and sudden decreases in groundwater salinity were followed by gradual increases after rain/recharge episodes. This behavior is exemplified by a particular rainfall event (RFE-8; Fig. 2d, e). After the precipitation fell, the groundwater table increased by 60 cm and the salinity at the bottom of PZ1 decreased sharply (over 23 h) from 13 to 0.2. This fast piezometric response to precipitation can be attributed to the hydrogeological features of the alluvial aquifer, which has a high hydraulic conductivity and a small non-saturated zone in the lower part of the basin (Catalan Water Agency, 2010), but it is also accentuated due to the use of a fully screened piezometer (Shalev et al., 2009). Under stable conditions, an equilibrium exists between the aquifer, which is governed by the laws of groundwater motion, and the entire screened piezometer, which is governed by the hydrostatic law (Rushton, 1980). However, under changing conditions, this equilibrium is broken, and the position of the salinity interface in the piezometer may not correspond to its actual position in the aquifer (Rushton, 1980; Tellam et al., 1986; Carrera et al., 2010). For instance, during heavy rainfall events, the higher hydraulic level of fresh groundwater occurring in the upper part of the entirely screened piezometer pushes the saltwater downward faster than it occurs in the aquifer. As a result, after these episodes, salinity decreased faster in the piezometer than in the aquifer itself.

Rainfall-derived aquifer recharge produced an increase in the hydraulic gradient between the coastal aquifer and the sea, leading to seaward displacement of the salinity interface and a significant decrease in groundwater salinity in the bottom section of the piezometer (Fig. 2c, e). Once the infiltration of rainfall water had finished, the hydraulic gradient decreased gradually, resulting in landward displacement of the salinity interface and a consequent increase in groundwater salinity in the bottom section of the piezometer (Fig. 2c, e). While the seaward displacement of the salinity interface occurred shortly (a few hours to days) after the precipitation episode, several weeks or even months were needed to recover the salinity values observed prior to the rain event(s). For instance, salinity at PZ1-B decreased from 13 to 0.3 in

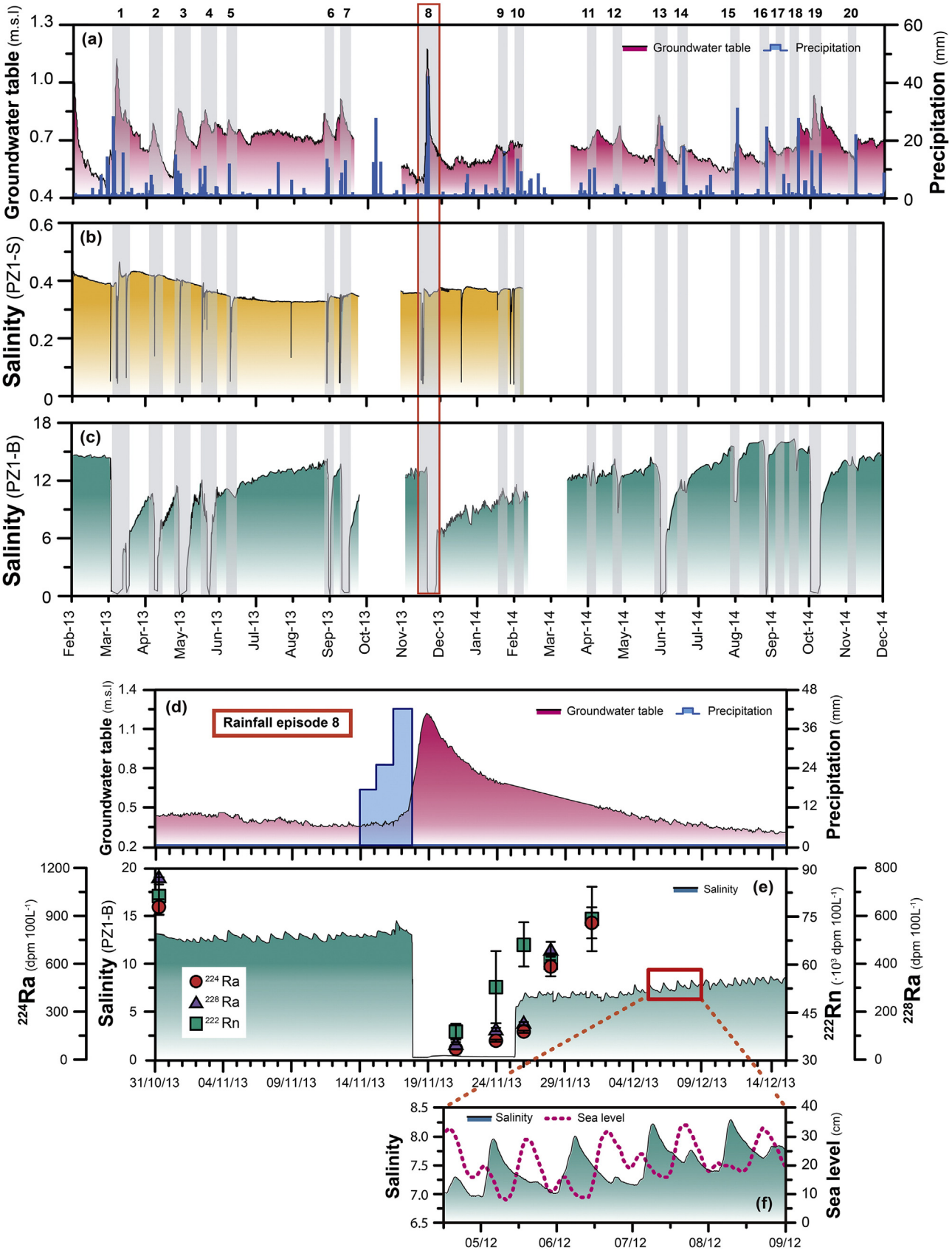

Fig. 2. Temporal evolution of the hydrogeological conditions and the Ra and Rn activities in the coastal aquifer: (a) daily cumulative precipitation in the area and measured groundwater table elevations in the coastal aquifer; (b) and (c) groundwater salinities in the shallow (PZ1-S) and bottom (PZ1-B) parts, respectively, of piezometer PZ1; (d) groundwater table elevation and precipitation records from rainfall episode 8 (RFE-8); (e) variations in Rn and Ra activities and salinity in PZ1-B during RFE-8; (f) sea level and salinity oscillations in PZ1-B. Vertical gray lines indicate rainfall events (RFEs) that significantly affected groundwater table elevation.

less than a day (~23 h) associated with RFE-8, whereas several months (~6 months) were needed to recover the initial salinity of 13–15 (Fig. 2e).

Unlike aquifers dominated by tidal cycles, the impact of microtides on the hydraulic gradient, and consequently the position of the salinity interface, can be negligible in PZ1. As shown in Fig. 2f, the tidal range in the area was on the order of ~20 cm (data compiled from the Barcelona mareograph and obtained from the State Ports Authority; www.puertos.es), a pattern commonly observed in the NW Mediterranean Sea. These small tidal oscillations induced only small variations in the groundwater table and in the groundwater salinities at the bottom of the piezometer (tidally derived groundwater salinity variations of ~1).

Regarding PZ0, the piezometer closest to the shoreline but located in the same aquifer unit, the recorded data on groundwater table and salinity followed a similar pattern as those observed in PZ1 (Fig. 3). Namely, stable salinities were observed during dry periods, with maximum values of 3 (e.g., May 2014 and August–November 2014), and fluctuations of salinity were observed during rainfall events, with salinity decreasing to reach minimum values of 0.1. Although the piezometers, PZ1 and PZ0, are located 380 and 8 m from the shoreline, respectively, CTDs installed in both piezometers registered almost the same variations in the groundwater table and salinity (e.g., RFE-12, 13, 14 and 16), indicating similar responses to recharge/rain events, as expected. However, various significant increases in groundwater salinities in PZ0 (up to salinities higher than 18 which is the maximum salinity that can be measured with the CTD diver installed at PZ0) that did not correspond with the fluctuations recorded in PZ1 were also observed. These salinity increases in PZ0 coincided with increases in the significant wave height (H_0) in the coastal sea, mainly related to the eastern storms characteristic of the spring and autumn seasons in the northwestern Mediterranean Sea. The increase in the frequency and height of waves at the shoreline modifies the equilibrium of the hydraulic gradient, moving the salinity interface landward and increasing the salinity in PZ0 (Moore and Wilson, 2005). The influence of these storms on PZ0 lasted for short periods (<6 days), and PZ0 rapidly recovered the groundwater salinities observed before storm events, due to the contrary effect of the downward groundwater flow of the aquifer. Given the limited influence of these kinds of storm events, the groundwater recharge-discharge cycle appears to be the main driver controlling the position of the salinity interface in the studied NW Mediterranean coastal aquifer.

3.2. Ra isotopes and ^{222}Rn characterization in groundwater

The activities of Ra isotopes and ^{222}Rn measured in groundwater samples from PZ1-S, PZ1-B and PZ0, together with their corresponding salinities, are presented in Table 1. The activities of Ra isotopes in shallow groundwater (PZ1-S) samples showed relatively constant values that ranged from 0.4 to 3.8 dpm 100 L^{-1} for ^{223}Ra, 40 to 90 dpm 100 L^{-1} for ^{224}Ra, 9 to 20 dpm 100 L^{-1} for ^{226}Ra and 60 to 90 dpm 100 L^{-1} for ^{228}Ra. The activity of Ra in PZ1-B presented a larger variability, and these values ranged from 2 to 80 dpm 100 L^{-1} for ^{223}Ra, 70 to 2100 dpm 100 L^{-1} for ^{224}Ra, 30 to 440 dpm 100 L^{-1} for ^{226}Ra and 70 to 1700 dpm 100 L^{-1} for ^{228}Ra. The activities of Ra isotopes were particularly low during rainfall events, when groundwater salinities in the piezometer were minimal, whereas the largest activities were measured during dry periods that corresponded to the highest groundwater salinities. On the other hand, Ra activities in PZ0 showed a similar variability as those seen in PZ1-B, and they ranged from 3 to 10 dpm 100 L^{-1} for ^{223}Ra, 260 to 830 dpm 100 L^{-1} for ^{224}Ra, 40 to 70 dpm 100 L^{-1} for ^{226}Ra and from 200 to 760 dpm 100 L^{-1} for ^{228}Ra. Ra activities in groundwater samples were higher than values commonly found in NW Mediterranean coastal aquifers (e.g., Rodellas et al., 2015a), most likely due to the high radium content of the granitic basement (which are rich in ^{232}Th decay chain radionuclides) and the relatively high salinities of the groundwater in the aquifer that favor radium desorption. The activities of Ra isotopes measured in the two piezometers showed strong positive correlations with salinity (R^2 = 0.91, 0.97, 0.87 and 0.95 for ^{223}Ra, ^{224}Ra, ^{226}Ra and ^{228}Ra, respectively; $p < 0.001$),

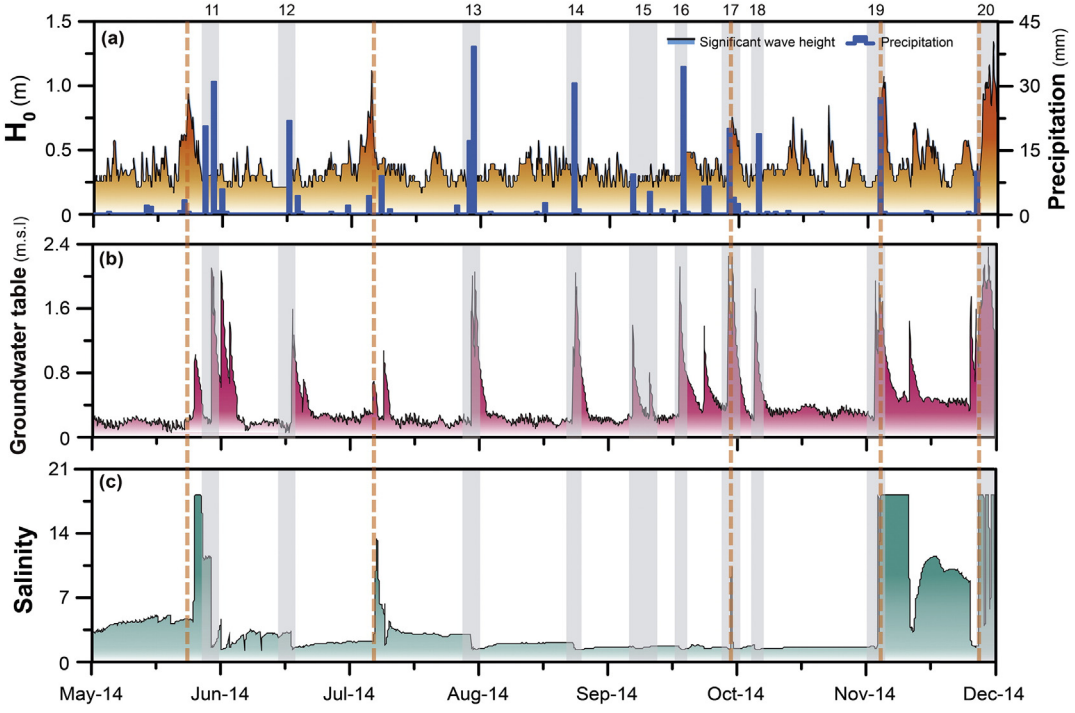

Fig. 3. Temporal evolution of hydrogeological conditions in PZ0: (a) significant wave heights of coastal seawater (H_0) derived from the SIMAR dataset (2115138) oceanographic model (State Ports Authority; www.puertos.es); (b) daily cumulative precipitation in the area and measured groundwater table elevations in the coastal aquifer; (c) groundwater salinities in PZ0, notice that the maximum salinity measurable with the CTD-diver is 18. Vertical gray lines and orange dotted lines indicate the major rainfall events (RFEs) and eastern storm events respectively, that significantly affected groundwater table elevation or salinity in PZ0.

suggesting that the groundwater sampled in PZ0, which is near the discharge area, has similar characteristics as the groundwater in PZ1 (Fig. 4a). Unlike Ra isotopes activities, the activities of ^{222}Rn in groundwater samples reflected relatively constant concentrations in the water samples from PZ1-S and PZ1-B throughout the studied period, with values ranged from $40 \cdot 10^3$ to $120 \cdot 10^3$ dpm 100 L^{-1} (Fig. 4b).

A detailed analysis of the rainfall event RFE-8 suggested that Ra activities in groundwater from PZ1-B followed a pattern linked to groundwater recharge cycles (Fig. 2; Table 1). Thus, just after the precipitation event, Ra activities diminished by a factor of ~19, ~14, ~6, and ~11 for ^{223}Ra, ^{224}Ra, ^{226}Ra and ^{228}Ra, respectively, in a short period of time (Table 1). A few days after the event, and coupled with an increase of groundwater salinity, Ra activities gradually increased toward the activities measured before the rainfall event. The activity of ^{222}Rn followed a similar pattern to those of the Ra isotopes, although it only decreased by a factor of ~2 (from $81 \cdot 10^3$ to $39 \cdot 10^3$ dpm 100 L^{-1}) after the precipitation event.

4. Discussion

4.1. Variability in the activity of ^{222}Rn and the activities of Ra isotopes

The activities of Ra isotopes measured in groundwater from PZ1 and PZ0 spanned a wide range. In particular, ^{224}Ra in PZ1-B varied by a factor of 31 during the 2 monitored years, whereas ^{222}Rn activities were relatively constant throughout the sampling period and varied by less than a factor of 3. This contrasting pattern between Ra isotopes and ^{222}Rn is likely a consequence of differences in their geochemical behavior in the subterranean estuary. Radium desorption is an exchange process that is highly dependent on the ionic strength (salinity) of the solution; it commonly represents the main factor determining the activities of Ra isotopes dissolved in groundwater (Cho and Kim, 2016; Gonneea et al., 2008). Consequently, the activities of Ra isotopes in fresh groundwater from the shallow depths of the subterranean estuary are considerably lower than those in brackish groundwater from greater depths. Ra activities at the salinity interface are likely explained by binary mixing between low-Ra, low-salinity groundwater and high-Ra, high-salinity groundwater. Indeed, this behavior explains the strong linear correlations between the concentrations of Ra isotopes and groundwater salinities observed over the entire period of the study (Fig. 4a). Unlike Ra isotopes, groundwater salinity has little influence on the behavior of ^{222}Rn in the aquifer because it is a noble gas. Moreover, ^{222}Rn supported by ^{226}Ra dissolved in groundwater usually represents a minor fraction of the total ^{222}Rn activity in groundwater. Therefore, similar ^{222}Rn activities are expected in fresh, brackish and salty groundwater, thus explaining the lack of significant correlations between ^{222}Rn activities and salinity in groundwater from the studied site (Fig. 4b). However, it should be noted that, after rainfall events, ^{222}Rn activities decreased

Table 1
Salinity, Ra isotopes and ^{222}Rn activities and Activity Ratios (ARs) in the shallow and bottom parts of piezometer PZ1 (n.a: not analyzed).

	Date	Sal	^{222}Rn (10^3 dpm 100 L^{-1})	^{223}Ra	^{224}Ra (dpm 100 L^{-1})	^{226}Ra	^{228}Ra	^{224}Ra/^{228}Ra AR	^{226}Ra/^{228}Ra AR
PZ1-S (shallow)									
ARG3-PZ1-S	20/12/12	0.51	90 ± 5	2.0 ± 0.3	85 ± 5	18 ± 1	85 ± 4	43 ± 7	0.21 ± 0.01
ARG4-PZ1-S	29/1/13	0.42	101 ± 7	0.8 ± 0.2	53 ± 3	9 ± 1	70 ± 3	70 ± 20	0.13 ± 0.02
ARG6-PZ1-S	24/4/13	0.39	86 ± 8	0.8 ± 0.2	56 ± 4	14 ± 1	65 ± 4	37 ± 20	0.22 ± 0.02
ARG7-PZ1-S	28/5/13	0.36	90 ± 8	0.9 ± 0.1	50 ± 3	10 ± 1	56 ± 1	474 ± 300	0.18 ± 0.02
ARG8-PZ1-S	28/6/13	0.35	85 ± 3	0.4 ± 0.2	44 ± 3	n.a	n.a	222 ± 112	n.a
ARG10-PZ1-S	23/9/13	0.39	80 ± 9	1.5 ± 0.2	66 ± 3	n.a	n.a	47 ± 7	n.a
ARG11-PZ1-S	30/10/13	0.40	76 ± 12	1.2 ± 0.2	68 ± 3	13 ± 1	65 ± 5	56 ± 8	0.20 ± 0.02
ARG12-PZ1-S	21/11/13	0.37	45 ± 3	0.8 ± 0.2	59 ± 3	12 ± 1	62 ± 5	74 ± 20	0.19 ± 0.02
ARG13-PZ1-S	24/11/13	0.37	57 ± 6	0.9 ± 0.2	56 ± 3	n.a	n.a	63 ± 13	n.a
ARG15-PZ1-S	26/11/13	0.39	62 ± 3	0.6 ± 0.2	61 ± 3	n.a	n.a	3 ± 1	n.a
ARG16-PZ1-S	28/11/13	0.39	57 ± 8	0.5 ± 0.2	60 ± 3	13 ± 1	68 ± 5	114 ± 40	n.a
ARG17-PZ1-S	1/12/13	0.39	52 ± 4	0.8 ± 0.2	59 ± 3	n.a	n.a	73 ± 20	0.19 ± 0.02
ARG18-PZ1-S	9/12/13	0.38	n.a	0.4 ± 0.2	56 ± 3	n.a	n.a	139 ± 70	n.a
ARG19-PZ1-S	9/2/14	0.36	n.a	0.5 ± 0.2	43 ± 2	n.a	n.a	85 ± 30	n.a
ARG20-PZ1-S	13/4/14	0.39	n.a	3.8 ± 0.5	62 ± 3	12 ± 1	60 ± 5	16 ± 2	0.20 ± 0.02
PZ1-B (bottom)									
ARG3-PZ1-B	20/12/12	8.68	94 ± 12	42 ± 5	1704 ± 123	193 ± 11	1108 ± 50	1.54 ± 0.13	0.17 ± 0.01
ARG4-PZ1-B	29/1/13	6.43	103 ± 5	21 ± 2	1179 ± 90	106 ± 8	658 ± 47	1.79 ± 0.18	0.16 ± 0.02
ARG6-PZ1-B	24/4/13	11.14	95 ± 13	55 ± 4	2074 ± 108	251 ± 11	1596 ± 68	1.30 ± 0.09	0.16 ± 0.01
ARG7-PZ1-B	28/5/13	3.47	81 ± 14	20 ± 2	737 ± 40	26 ± 2	574 ± 27	1.28 ± 0.09	0.05 ± 0.01
ARG8-PZ1-B	28/6/13	5.46	92 ± 4	22 ± 1	1102 ± 50	161 ± 7	762 ± 30	1.45 ± 0.09	0.21 ± 0.01
ARG10-PZ1-B	23/9/13	4.32	83 ± 5	33 ± 2	917 ± 50	n.a	n.a	n.a	n.a
ARG11-PZ1-B	30/10/13	4.55	81 ± 6	30 ± 2	956 ± 50	178 ± 8	764 ± 30	1.25 ± 0.08	0.23 ± 0.01
ARG12-PZ1-B	21/11/13	0.39	39 ± 2	1.6 ± 0.5	67 ± 4	29 ± 6	68 ± 5	0.99 ± 0.08	0.42 ± 0.09
ARG13-PZ1-B	24/11/13	0.74	53 ± 11	3.6 ± 0.5	118 ± 7	34 ± 2	125 ± 7	0.94 ± 0.08	0.28 ± 0.02
ARG15-PZ1-B	26/11/13	0.98	66 ± 7	3 ± 1	160 ± 8	33 ± 2	139 ± 7	1.15 ± 0.08	0.24 ± 0.02
ARG16-PZ1-B	28/11/13	3.57	61 ± 2	17 ± 2	582 ± 40	79 ± 6	461 ± 30	1.26 ± 0.12	0.17 ± 0.02
ARG17-PZ1-B	1/12/13	5.60	74 ± 10	33 ± 4	856 ± 100	n.a	n.a	n.a	n.a
ARG18-PZ1-B	9/12/13	8.00	82 ± 5	61 ± 7	1516 ± 80	244 ± 30	1344 ± 137	1.14 ± 0.13	0.18 ± 0.03
ARG19-PZ1-B	9/2/14	10.36	n.a	23 ± 2	1513 ± 70	n.a	n.a	n.a	n.a
ARG20-PZ1-B	13/4/14	11.42	n.a	82 ± 6	1834 ± 121	440 ± 18	1715 ± 70	1.07 ± 0.08	0.22 ± 0.01
PZ0									
ARG21-PZ0	24/4/14	0.75	n.a	5 ± 0.4	257 ± 11	47 ± 4	222 ± 12	1.16 ± 0.08	0.21 ± 0.02
ARG22-PZ0	30/4/14	2.99	n.a	9 ± 2	762 ± 33	62 ± 7	755 ± 95	1.01 ± 0.13	0.08 ± 0.01
ARG23-PZ0	13/5/14	3.85	n.a	9 ± 2	828 ± 35	40 ± 7	741 ± 117	1.12 ± 0.18	0.05 ± 0.01
ARG24-PZ0	16/5/14	3.51	n.a	12 ± 2	802 ± 37	67 ± 4	480 ± 67	1.67 ± 0.25	0.14 ± 0.02
ARG25-PZ0	3/6/14	1.20	n.a	3 ± 1	313 ± 15	n.a	n.a	n.a	n.a
ARG26-PZ0	7/6/14	1.70	n.a	4 ± 1	392 ± 19	38 ± 6	232 ± 34	1.69 ± 0.26	0.16 ± 0.04
ARG27-PZ0	11/6/14	1.70	n.a	4 ± 1	357 ± 16	55 ± 11	343 ± 51	1.04 ± 0.16	0.15 ± 0.04
ARG28-PZ0	26/6/14	2.30	n.a	8 ± 2	517 ± 23	67 ± 12	200 ± 44	2.59 ± 0.58	0.34 ± 0.10

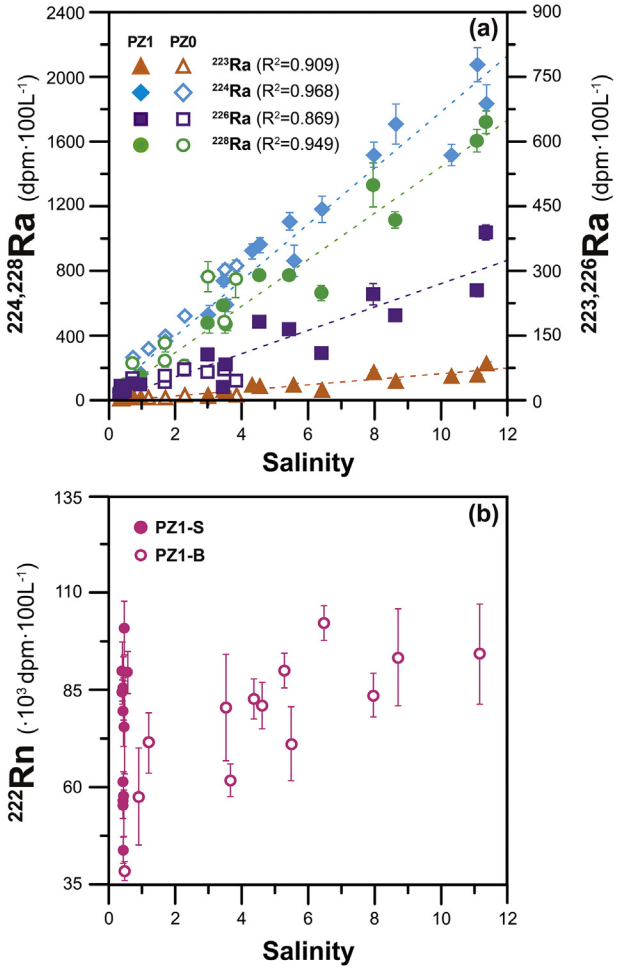

Fig. 4. Ra isotopes (a) and ^{222}Rn activities (b) vs salinity in groundwater from the Argentona aquifer (PZ1-S, PZ1-B and PZ0). Dashed lines represent the best linear fits to the data.

considerably, together with salinity. This coupled ^{222}Rn-salinity decrease is attributed to dilution that is due to the vertical infiltration of rainwater into the highly permeable coastal aquifer, since rainwater has a salinity close to 0 and contains negligible amounts of ^{222}Rn. After the rainwater had interacted with the geological matrix, the activity of ^{222}Rn in the meteoric fresh water started to increase, due to its production within the aquifer solids. Concentrations in equilibrium with the aquifer matrix were achieved within 15–20 days after rainwater infiltration into the aquifer.

4.2. Temporal variability of the salinity interface: Implications for Ra- and Rn-derived SGD estimates

The position and dynamics of the salinity interface are influenced to a large degree by multiple forcing mechanisms, which include marine (e.g., wave setup and swash infiltration, as well as tidal pumping) and terrestrial drivers (e.g., recharge patterns) (Li et al., 2008; Henderson et al., 2010; Santos et al., 2012; Abarca et al., 2013). Whereas tides are physical forces that are relevant for determining freshwater-seawater mixing in most coastal areas (Kim and Hwang, 2002; Michael et al., 2003; Charette, 2007; Bokuniewicz et al., 2015), they play a minor role in microtidal environments such as the Mediterranean Sea, the Baltic Sea and the Caribbean Sea (Szymczycha et al., 2012; Gonneea et al., 2014; Rodellas et al., 2014;). In such systems, the dynamics of the salinity interface are mainly governed by the inland hydraulic gradient, which mainly reflects the terrestrial groundwater recharge rate (Dausman and Langevin, 2005). Microtidal coastal aquifers are thus highly influenced by precipitation regimes, and they become highly dynamic systems when precipitation events are temporally variable. This pattern is commonly observed in the Mediterranean basin, where 4–6 short (lasting hours to a few days) and intense (a maximum precipitation rate of 40 mm day^{-1} occurred during the studied period, but it can be much higher) rainfall events represent >70% of the annual precipitation (e.g., RFE-1, 8, 13 and 15, Fig. 2) (Gasith and Resh, 1999). According to the change in hydraulic gradient observed in PZ0 (the closest to the sea) over a period of nearly 8 months, it can be estimated that 50% of the discharge is produced during and/or within a few days after rain events. Thus, short and intense rainfall events are likely to produce the highest rates of fresh SGD to the coastal sea, which would account for a significant proportion of the freshwater that seeps into the sea yearly. For the rest of the year, fresh SGD flows are expected to be significantly lower and more constant. Thus, estimating SGD fluxes in microtidal systems during periods of intense precipitation are particularly relevant from both a hydrogeological and a biogeochemical perspective.

The quantification of SGD flows to the coastal sea using Ra isotopes and ^{222}Rn requires accurately characterizing their activities in groundwater discharging to the coastal sea (i.e., the SGD end-member). Indeed, Ra- and ^{222}Rn-derived SGD fluxes can only be resolved at the level that the tracer concentration in the end-member can be constrained. Thus, the selection of an appropriate end-member is commonly the main source of uncertainty in final SGD estimates (Cho and Kim, 2016; Burnett et al., 2007; Dulaiova et al., 2008; Garcia-Orellana et al., 2010; Gonneea et al., 2013). Given that Ra isotopes are highly influenced by the ionic strength of the dissolved phase, freshwater-seawater mixing dynamics are key processes in understanding the distribution of Ra in a coastal aquifer and in constraining the Ra concentration in the SGD end-member (Charette et al., 2001; Gonneea et al., 2013; Michael et al., 2011). Indeed, several studies have reported that the activities of Ra isotopes in the SGD end-member vary over a wide range (up to orders of magnitude) both in space and time, and are often linked to changes in the ionic strength of the dissolved phase (Cho and Kim, 2016). Thus, accurately evaluating the complex and dynamic mixing of fresh groundwater with seawater (i.e., the position of the salinity interface) becomes critical for obtaining reliable Ra-derived SGD estimates.

In highly dynamic microtidal systems, achieving an appropriate understanding of the hydrodynamics of coastal aquifers requires significant monitoring and characterization efforts that are often unavailable when SGD studies are conducted. To overcome this limited hydrogeological understanding, studies that use Ra isotopes to quantify SGD commonly rely on collecting a relatively large number of samples, as well as using different approaches to characterize the SGD end-member (potential approaches include, e.g., averaging the Ra activities from all the samples collected (Gonneea et al., 2014)), taking the maximum measured Ra activities to obtain conservative estimates (Moore, 1996b), or using ranges of Ra activities covering the samples collected (Kim et al., 2005). Whereas these approaches may work in many of the tidal systems studied, using them in coastal aquifers characterized by highly dynamic freshwater-seawater mixing zones (with large salinity and thus large Ra variations) may introduce large uncertainties into the final SGD quantification. Constraining Ra activities in the SGD end-member during (or just after) intense rainfall events may be particularly challenging, given the large temporal variations in salinity and Ra in coastal groundwater, making it difficult to obtain reliable SGD estimates. As detailed above, it should be noted that inputs of fresh groundwater to coastal seas are expected to be much higher during these rainfall periods, and thus, the SGD evaluations during these periods have a major hydrological and biogeochemical interest. Conversely, Ra activities in the SGD end-member can be more easily constrained during dry periods because they are associated with reduced variability in coastal groundwater, thus allowing appropriate estimates of Ra-derived SGD fluxes to be made for the rest of the year.

Unlike Ra isotopes, the activity of ^{222}Rn in coastal groundwater appears to be relatively constant throughout the year due to the relatively small influence of groundwater salinity on ^{222}Rn behavior, even during intense rainy events (^{222}Rn activities only varied by a factor 2 during these events). These small variations allow us to better constraint the activity of ^{222}Rn in the SGD end-member and, thus, better estimate SGD flows during rainy periods. This observed pattern suggests that ^{222}Rn may be a more appropriate SGD tracer than Ra isotopes in systems with highly dynamic salinity interfaces, particularly during the wet season, when groundwater salinities (and thus Ra activities) may change significantly over short temporal scales. However, whereas the Rn end-member can be relatively well constrained, Rn-derived SGD estimates are highly sensitive to Rn mixing losses and especially the loss of Rn to the atmosphere by degassing. These two loss terms are difficult to determine, particularly under conditions with strong winds and high waves, which often occur concurrently with eastern storm events.

5. Conclusions

Understanding the behavior of tracers used to determine submarine groundwater discharge (SGD) fluxes is crucial for accurately quantifying groundwater- and chemical- driven fluxes to the ocean in order to better understand coastal biogeochemical cycles. The results obtained in this work reveal that activities of Ra isotopes, which are commonly used tracers to quantify SGD, show a large variability in microtidal coastal groundwater systems throughout the year and particularly during intense rainfall events (e.g., activity changes by a factor of ~19, ~14, ~6, and ~11 for ^{223}Ra, ^{224}Ra, ^{226}Ra and ^{228}Ra during a particular rainfall event, RFE-8). This large variability, which is linked to the displacement of the salinity interface seawards, complicates the accurate estimation of the Ra-SGD end-member, resulting in Ra-derived SGD estimates with large uncertainties. In contrast, ^{222}Rn activities present only minor variations (by a factor of 3), as a consequence of the relatively small influence of groundwater salinity on ^{222}Rn activities. In microtidal systems, high SGD-driven fluxes to the sea of both freshwater and dissolved chemical compounds are expected to occur during the rainy season and/or intense rainfall events. Thus, scientific efforts should be particularly directed toward understanding SGD fluxes during this season, when the influence of SGD on hydrological budgets is expected to be significant. The observed differences between the rainy season and the dry period indicate that appropriate SGD quantification over longer (monthly or yearly) time scales cannot be carried out properly without considering the temporal variability in Ra activities.

In addition to the difficulties in estimating SGD flows during rainfall events (which are mainly due to the difficulty of characterizing the SGD end-member), the extreme variability in the concentrations of chemical compounds (e.g., nutrients, trace metals, contaminants, and other species) in the groundwater poses an additional challenge in constraining a representative groundwater end-member. The fluxes of dissolved compounds transported by SGD have usually been calculated by multiplying the SGD flux derived using Ra isotopes or Rn by the concentration of the chemical compounds in the inflowing SGD. As in the case of the Ra end-member, it is particularly critical to identify a representative concentration of the studied dissolved chemical compound in the discharging groundwater during intense rainfall events. A poor understanding of the behavior of dissolved chemicals in the coastal aquifer during rainfall events may lead to large uncertainties in SGD-driven chemical fluxes. Since the SGD-driven fluxes during the wet periods may account for a significant fraction of the chemical fluxes to the coastal areas, it is expected that the impact of SGD on coastal biogeochemical cycles is particularly relevant during these events. Characterizing the behavior of Ra/Rn and dissolved chemical compounds within subterranean estuaries during rainfall events in microtidal systems remains a challenge, which must be considered in future studies of SGD-driven nutrient fluxes to coastal areas in order to understand the relative impact of SGD on coastal biogeochemical cycles.

Acknowledgments

This work was funded by projects CGL2013-48869-C2-1 and CGL2013-48869-C2-2-R of the Spanish Government. M.C.D acknowledges financial support from the Ministerio de Economía y Competitividad (PhD fellowship, A-2014-9185) through the NUREIEV project (CTM2013-44598-R) coordinated by GRC Geociències Marines of the Departament de Dinàmica de la Terra i de l'Oceà (Universitat de Barcelona). The authors wish to thank the Generalitat de Catalunya for its support of MERS (2014 SGR-1356) and Agència Catalana de l'Aigua (ACA). V.R. also acknowledges financial support from the European Union's FP7 program (Marie Curie Actions PCOFUND-GA-2013-609102) through the PRESTIGE program coordinated by Campus France. This study is a contribution to the ANR @RAction chair (ANR-14-ACHN-0007-01) and Labex OT-Med (ANR-11-LABEX-0061), which was funded by the "Investissements d'Avenir" program through the A*MIDEX project (ANR-11-IDEX-0001-02) of the French National Research Agency (ANR).

References

Abarca, E., Karam, H., Hemond, H.F., Harvey, C.F., 2013. Transient groundwater dynamics in a coastal aquifer: the effects of tides, the lunar cycle, and the beach profile. Water Resour. Res. 49:2473–2488. http://dx.doi.org/10.1002/wrcr.20075.

Beck, A.J., Cochran, M.A., 2013. Controls on solid-solution partitioning of radium in saturated marine sands. Mar. Chem. 156:38–48. http://dx.doi.org/10.1016/j.marchem.2013.01.008.

Beck, A.J., Rapaglia, J.P., Cochran, J.K., Bokuniewicz, H.J., Yang, S., 2008. Submarine groundwater discharge to Great South Bay, NY, estimated using Ra isotopes. Mar. Chem. 109: 279–291. http://dx.doi.org/10.1016/j.marchem.2007.07.011.

Bokuniewicz, H., Cochran, J.K., Garcia-Orellana, J., Rodellas, V., Daniel, J.W., Heilbrun, C., 2015. Intertidal percolation through beach sands as a source of 224,223 Ra to Long Island Sound, New York, and Connecticut, United States. J. Mar. Res. 73, 123–140.

Burnett, W.C.C., Aggarwal, P.K.K., Aureli, A., Bokuniewicz, H., Cable, J.E.E., Charette, M.A., Kontar, E., Krupa, S., Kulkarni, K.M., Loveless, A., Moore, W.S., Oberdorfer, J.A., Oliveira, J., Ozyurt, N., Povinec, P., Privitera, A.M., Rajar, R., Ramessur, R.T., Scholten, J., Stieglitz, T., Taniguchi, M., Turner, J.V., 2006. Quantifying submarine groundwater discharge in the coastal zone via multiple methods. Sci. Total Environ. 367: 498–543. http://dx.doi.org/10.1016/j.scitotenv.2006.05.009.

Burnett, W.C., Bokuniewicz, H., Huettel, M., Moore, W., Taniguchi, M., 2003. Groundwater and pore water inputs to the coastal zone. Biogeochemistry 66, 3–33.

Burnett, W.C., Dulaiova, H., 2003. Estimating the dynamics of groundwater input into the coastal zone via continuous radon-222 measurements. J. Environ. Radioact. 69:21–35. http://dx.doi.org/10.1016/S0265-931X(03)00084-5.

Burnett, W.C., Peterson, R., Moore, W.S., de Oliveira, J., 2008. Radon and radium isotopes as tracers of submarine groundwater discharge – results from the Ubatuba, Brazil SGD assessment intercomparison. Estuar. Coast. Shelf Sci. 76:501–511. http://dx.doi.org/10.1016/j.ecss.2007.07.027.

Burnett, W.C., Taniguchi, M., Oberdorfer, J., 2001. Measurement and significance of the direct discharge of groundwater into the coastal zone. J. Sea Res. 46:109–116. http://dx.doi.org/10.1016/S1385-1101(01)00075-2.

Burnett, W.C., Wattayakorn, G., Taniguchi, M., Dulaiova, H., Sojisuporn, P., Rungsupa, S., Ishitobi, T., 2007. Groundwater-derived nutrient inputs to the Upper Gulf of Thailand. Cont. Shelf Res. 27:176–190. http://dx.doi.org/10.1016/j.csr.2006.09.006.

Carrera, J., Hidalgo, J.J., Slooten, L.J., Vazquez-Sune, E., 2010. Computational and conceptual issues in the calibration of seawater intrusion models. Hydrogeol. J. 18:131–145. http://dx.doi.org/10.1007/s10040-009-0524-1.

Catalan Water Agency, 2010. Model numèric de l'aqüífer al·luvial de la riera d'argentona.

Charette, M.A., 2007. Hydrologic forcing of submarine groundwater discharge: insight from a seasonal study of radium isotopes in a groundwater-dominated salt marsh estuary. Limnol. Oceanogr. 52:230–239. http://dx.doi.org/10.4319/lo.2007.52.1.0230.

Charette, M.a., Buesseler, K.O., Andrews, J.E., 2001. Utility of radium isotopes for evaluating the input and transport of groundwater-derived nitrogen to a Cape Cod estuary. Limnol. Oceanogr. 46:465–470. http://dx.doi.org/10.4319/lo.2001.46.2.0465.

Cho, H.-M., Kim, G., 2016. Determining groundwater Ra end-member values for the estimation of the magnitude of submarine groundwater discharge using Ra isotope tracers. Geophys. Res. Lett. 43:3865–3871. http://dx.doi.org/10.1002/2016GL068805.

Dausman, A., Langevin, C.D., 2005. Movement of the Saltwater Interface in the Surficial Aquifer System in Response to Hydrologic Stresses and Water-management Practices, Broward County, Florida.

Dulaiova, H., Gonneea, M.E., Henderson, P.B., Charette, M.a., 2008. Geochemical and physical sources of radon variation in a subterranean estuary - implications for groundwater radon activities in submarine groundwater discharge studies. Mar. Chem. 110: 120–127. http://dx.doi.org/10.1016/j.marchem.2008.02.011.

Elsinger, R.J., Moore, W.S., 1980. 226Ra behavior in the pee Dee River-Winyah Bay estuary. Earth Planet. Sci. Lett. 48:239–249. http://dx.doi.org/10.1016/0012-821X(80)90187-9.

Garcia-Orellana, J., Cochran, J.K., Bokuniewicz, H., Yang, S., Beck, A.J., 2010. Time-series sampling of 223Ra and 224Ra at the inlet to Great South Bay (New York): a strategy for characterizing the dominant terms in the Ra budget of the bay. J. Environ. Radioact. 101:582–588. http://dx.doi.org/10.1016/j.jenvrad.2009.12.005.

Garcia-Solsona, E., Garcia-Orellana, J., Masqué, P., Dulaiova, H., 2008. Uncertainties associated with 223Ra and 224Ra measurements in water via a Delayed Coincidence Counter (RaDeCC). Mar. Chem. 109:198–219. http://dx.doi.org/10.1016/j.marchem.2007.11.006.

Gasith, A., Resh, V.H., 1999. Streams in Mediterranean climate regions: abiotic influences and biotic responses to predictable seasonal events. Annu. Rev. Ecol. Syst. 30:51–81. http://dx.doi.org/10.1146/annurev.ecolsys.30.1.51.

Gonneea, M.E., Charette, M.A., Liu, Q., Herrera-Silveira, J.A., Morales-Ojeda, S.M., 2014. Trace element geochemistry of groundwater in a karst subterranean estuary (Yucatan Peninsula, Mexico). Geochim. Cosmochim. Acta 132:31–49. http://dx.doi.org/10.1016/j.gca.2014.01.037.

Gonneea, M.E., Morris, P.J., Dulaiova, H., Charette, M.a., 2008. New perspectives on radium behavior within a subterranean estuary. Mar. Chem. 109:250–267. http://dx.doi.org/10.1016/j.marchem.2007.12.002.

Gonneea, M.E., Mulligan, A.E., Charette, M.A., 2013. Seasonal cycles in radium and barium within a subterranean estuary: implications for groundwater derived chemical fluxes to surface waters. Geochim. Cosmochim. Acta 119:164–177. http://dx.doi.org/10.1016/j.gca.2013.05.034.

Heiss, J.W., Michael, H.A., 2014. Saltwater-freshwater mixing dynamics in a sandy beach aquifer over tidal, spring-neap, and seasonal cycles. Water Resour. Res. 50. http://dx.doi.org/10.1002/2014WR015574.

Henderson, R.D., Day-Lewis, F.D., Abarca, E., Harvey, C.F., Karam, H.N., Liu, L., Lane, J.W.J., 2010. Marine electrical resistivity imaging of submarine groundwater discharge: sensitivity analysis and application in Waquoit Bay, Massachusetts, USA. Hydrogeol. J. 18:173–185. http://dx.doi.org/10.1007/s10040-009-0498-z.

Johnson, A.G., Glenn, C.R., Burnett, W.C., Peterson, R.N., Lucey, P.G., 2008. Aerial infrared imaging reveals large nutrient-rich groundwater inputs to the ocean. Geophys. Res. Lett. 35, L15606. http://dx.doi.org/10.1029/2008GL034574.

Kim, G., Hwang, D.-W., 2002. Tidal pumping of groundwater into the coastal ocean revealed from submarine 222 Rn and CH 4 monitoring. Geophys. Res. Lett. 29. http://dx.doi.org/10.1029/2002GL015093 23-1-23–4.

Kim, G., Lee, K.-K., Park, K.-S., Hwang, D.-W., Yang, Han-Soeb, 2003. Large submarine groundwater discharge (SGD) from a volcanic island. Geophys. Res. Lett. 30:2098. http://dx.doi.org/10.1029/2003GL018378.

Kim, G., Yun, S.-T., Yang, H.-S., Ryu, J.-W., Burnett, W.C., Dulaiova, H., Sholkovitz, E., Moore, W.S., Charette, M.a., Bokuniewicz, H.J., Chanton, J.P., Yun, S.-T., Yang, H.-S., Ryu, J.-W., 2005. Submarine groundwater discharge (SGD) into the Yellow Sea revealed by 228Ra and 226Ra isotopes: implications for global silicate fluxes. Earth Planet. Sci. Lett. 237:156–166. http://dx.doi.org/10.1016/j.epsl.2005.06.011.

Lee, C.M., Jiao, J.J., Luo, X., Moore, W.S., 2012. Estimation of submarine groundwater discharge and associated nutrient fluxes in Tolo Harbour, Hong Kong. Sci. Total Environ. 433:427–433. http://dx.doi.org/10.1016/j.scitotenv.2012.06.073.

Li, H., Boufadel, M.C., Weaver, J.W., 2008. Tide-induced seawater-groundwater circulation in shallow beach aquifers. J. Hydrol. 352:211–224. http://dx.doi.org/10.1016/j.jhydrol.2008.01.013.

Michael, H.A., Charette, M.A., Harvey, C.F., 2011. Patterns and variability of groundwater flow and radium activity at the coast: a case study from Waquoit Bay, Massachusetts. Mar. Chem. 127:100–114. http://dx.doi.org/10.1016/j.marchem.2011.08.001.

Michael, H.A., Lubetsky, J.S., Harvey, C.F., 2003. Characterizing submarine groundwater discharge: a seepage meter study in Waquoit Bay, Massachusetts. Geophys. Res. Lett. 30. http://dx.doi.org/10.1029/2002GL016000.

Montoto, M., 1967. Estudio petrológico y petrogenético de las rocas graníticas de la Cadena Litoral Catalana. p. 800.

Moore, W.S., 1996a. Using the radium quartet for evaluating groundwater input and water exchange in salt marshes. Geochim. Cosmochim. Acta 60:4645–4652. http://dx.doi.org/10.1016/S0016-7037(96)00289-X.

Moore, W.S., 1996b. Large groundwater inputs to coastal waters revealed by 226Ra enrichments. Nature 380:612–614. http://dx.doi.org/10.1038/380612a0.

Moore, W.S., 1999. The subterranean estuary: a reaction zone of ground water and sea water. Mar. Chem. 65, 111–125.

Moore, W.S., 2003. Sources and fluxes of submarine groundwater discharge delineated by radium isotopes. Biogeochemistry 66:75–93. http://dx.doi.org/10.1023/B:BIOG.0000006065.77764.a0.

Moore, W.S., Arnold, R., 1996. Measurement of 223Ra and 224Ra in coastal waters using a delayed coincidence counter. J. Geophys. Res. 101:1321–1329. http://dx.doi.org/10.1029/95jc03139.

Moore, W.S., Reid, D.F., 1973. Extraction of radium from natural waters using manganese-impregnated acrylic fibers. J. Geophys. Res. 78:8880. http://dx.doi.org/10.1029/JC078i036p08880.

Moore, W.S., Wilson, A.M., 2005. Advective flow through the upper continental shelf driven by storms, buoyancy, and submarine groundwater discharge. Earth Planet. Sci. Lett. 235:564–576. http://dx.doi.org/10.1016/j.epsl.2005.04.043.

Ollivier, P., Claude, C., Radakovitch, O., Hamelin, B., 2007. TIMS measurements of 226Ra and 228Ra in the Gulf of Lion, an attempt to quantify submarine groundwater discharge. Mar. Chem. 109:337–354. http://dx.doi.org/10.1016/j.marchem.2007.08.006.

Pavlidou, A., Papadopoulos, V.P., Hatzianestis, I., Simboura, N., Patiris, D., Tsabaris, C., 2014. Chemical inputs from a karstic submarine groundwater discharge (SGD) into an oligotrophic Mediterranean coastal area. Sci. Total Environ. 488:1–13. http://dx.doi.org/10.1016/j.scitotenv.2014.04.056.

Rodellas, V., Garcia-Orellana, J., Masqué, P., Feldman, M., Weinstein, Y., 2015a. Submarine groundwater discharge as a major source of nutrients to the Mediterranean Sea. Proc. Natl. Acad. Sci. 112:201419049. http://dx.doi.org/10.1073/pnas.1419049112.

Rodellas, V., Garcia-Orellana, J., Masqué, P., Font-Muñoz, J.S., 2015b. The influence of sediment sources on radium-derived estimates of Submarine Groundwater Discharge. Mar. Chem. 171:107–117. http://dx.doi.org/10.1016/j.marchem.2015.02.010.

Rodellas, V., Garcia-Orellana, J., Tovar-Sánchez, A., Basterretxea, G., López-Garcia, J.M., Sánchez-Quiles, D., Garcia-Solsona, E., Masqué, P., 2014. Submarine groundwater discharge as a source of nutrients and trace metals in a Mediterranean bay (Palma Beach, Balearic Islands). Mar. Chem. 160:56–66. http://dx.doi.org/10.1016/j.marchem.2014.01.007.

Rodellas, V., Garcia-Orellana, J., Trezzi, G., Masqué, P., Stieglitz, T.C., Bokuniewicz, H., Cochran, J.K., Berdalet, E., 2017. Using the radium quartet to quantify submarine groundwater discharge and porewater exchange. Geochim. Cosmochim. Acta 196:58–73. http://dx.doi.org/10.1016/j.gca.2016.09.016.

Rushton, K.R., 1980. Differing positions of saline interfaces in aquifers and observation boreholes. J. Hydrol. 48:185–189. http://dx.doi.org/10.1016/0022-1694(80)90074-8.

Sadat-Noori, M., Santos, I.R., Tait, D.R., Maher, D.T., 2016. Fresh meteoric versus recirculated saline groundwater nutrient inputs into a subtropical estuary. Sci. Total Environ. 566:1440–1453. http://dx.doi.org/10.1016/j.scitotenv.2016.06.008.

Santos, I.R., Eyre, B.D., Huettel, M., 2012. The driving forces of porewater and groundwater flow in permeable coastal sediments: a review. Estuar. Coast. Shelf Sci. 98:1–15. http://dx.doi.org/10.1016/j.ecss.2011.10.024.

Shalev, E., Lazar, A., Wollman, S., Kington, S., Yechieli, Y., Gvirtzman, H., 2009. Biased monitoring of fresh water-salt water mixing zone in coastal aquifers. Ground Water 47:49–56. http://dx.doi.org/10.1111/j.1745-6584.2008.00502.x.

Smoak, J.M., Sanders, C.J., Patchineelam, S.R., Moore, W.S., 2012. Radium mass balance and submarine groundwater discharge in Sepetiba Bay, Rio de Janeiro State, Brazil. J. S. Am. Earth Sci. 39:44–51. http://dx.doi.org/10.1016/j.jsames.2012.07.004.

Sun, Y., Torgersen, T., 1998. The effects of water content and Mn-fiber surface conditions on 224Ra measurement by 220Rn emanation. Mar. Chem. 62:299–306. http://dx.doi.org/10.1016/S0304-4203(98)00019-X.

Swarzenski, P.W., 2007. U/Th series radionuclides as coastal groundwater tracers. Chem. Rev. 107:663–674. http://dx.doi.org/10.1021/cr0503761.

Szymczycha, B., Vogler, S., Pempkowiak, J., 2012. Nutrient fluxes via submarine groundwater discharge to the Bay of Puck, southern Baltic Sea. Sci. Total Environ. 438:86–93. http://dx.doi.org/10.1016/j.scitotenv.2012.08.058.

Tellam, J.H., Lloyd, J.W., Walters, M., 1986. The morphology of a saline groundwater body: its investigation, description and possible explanation. J. Hydrol. 83:1–21. http://dx.doi.org/10.1016/0022-1694(86)90179-4.

Tovar-Sánchez, A., Basterretxea, G., Rodellas, V., Sánchez-Quiles, D., García-Orellana, J., Masqué, P., Jordi, A., López, J.M., Garcia-Solsona, E., 2014. Contribution of groundwater discharge to the coastal dissolved nutrients and trace metal concentrations in Majorca Island: Karstic vs detrital systems. Environ. Sci. Technol. 48:11819–11827. http://dx.doi.org/10.1021/es502958t.

Trezzi, G., Garcia-Orellana, J., Rodellas, V., Santos-Echeandia, J., Tovar-Sánchez, A., Garcia-Solsona, E., Masqué, P., 2016. Submarine groundwater discharge: a significant source of dissolved trace metals to the North Western Mediterranean Sea. Mar. Chem. 186:90–100. http://dx.doi.org/10.1016/j.marchem.2016.08.004.

Webster, I.T., Hancock, G.J., Murray, A.S., 1995. Modelling the effect of salinity on radium desorption from sediments. Geochim. Cosmochim. Acta 59:2469–2476. http://dx.doi.org/10.1016/0016-7037(95)00141-7.

Science of the Total Environment 717 (2020) 134778

Contents lists available at ScienceDirect

Science of the Total Environment

journal homepage: www.elsevier.com/locate/scitotenv

Calibrating high resolution XRF core scanner data to obtain absolute metal concentrations in highly polluted marine deposits after two case studies off Portmán Bay and Barcelona, Spain

M. Cerdà-Domènech, J. Frigola *, A. Sanchez-Vidal, M. Canals

GRC Geociències Marines, Departament de Dinàmica de la Terra i de l'Oceà, Facultat de Ciències de la Terra, Universitat de Barcelona, Barcelona, Spain

HIGHLIGHTS

- High-resolution XRF-CS data were calibrated to obtain quantitative concentration.
- Calibration method increases the correlation coefficient and reduces the data deviation.
- WLS regression method reduced significantly the errors of calibrated element concentration.
- Low errors allow assessing metal pollution levels according to sediment quality guidelines.
- Errors of the calibrated element concentration must be evaluated in future calibration studies.

GRAPHICAL ABSTRACT

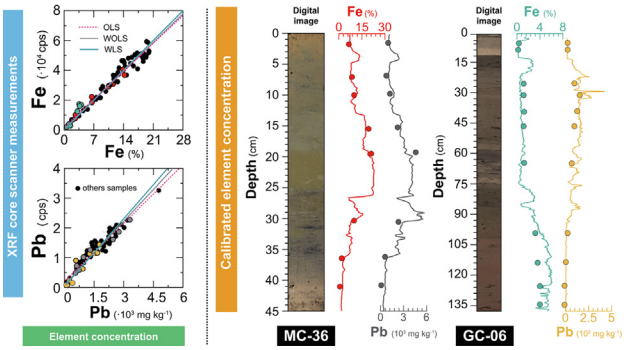

ARTICLE INFO

Article history:
Received 14 August 2019
Received in revised form 30 September 2019
Accepted 30 September 2019
Available online 5 November 2019

Editor; Damia Barcelo

Keywords:
XRF core scanner
Calibration
Trace metals
Contaminated sediment
Sediment quality guidelines

ABSTRACT

X-ray fluorescence core scanners (XRF-CS) allow rapid, non-destructive, continuous and high-resolution analyses of the elemental composition of sediment cores, providing large sets of semi-quantitative data. These data can be converted to quantitative data through the linear regression approach using a relatively small number of discrete samples analyzed by techniques providing absolute concentrations. However, a precise characterization of the errors associated with the linear function is required to evaluate the quality of the calibrated element concentrations. Here we present a calibration of high-resolution XRF-CS for six metals (Ti, Mn, Fe, Zn, Pb and As) measured in heavily contaminated marine deposits so that absolute concentrations are obtained. In order to determine the best linear function for conversion of XRF data, we have tested three regression methods: the ordinary least-squares (OLS), which does not consider the standard error in any variable (x and y), the weighted ordinary least-squares (WOLS), which considers the weighted standard error of the vertical variable (y), and the weighted least-squares (WLS), which incorporates the standard error in both x and y variables. We demonstrate that the calibration method presented in this study significantly increases the correlation coefficient, higher than $r^2 = 0.94$, and reduces both the data deviation and the errors of the linear function for the three regression methods. Nonetheless, the WLS appears as the best regression method to minimize errors in the calibrated element concentrations. Our results open the door to use calibrated XRF-CS data to evaluate marine sediment pollution according to the levels of the strictest sediment quality guidelines (SQG) with errors lower than

* Corresponding author at: GRC Geociències Marines, Departament de Dinàmica de la Terra i de l'Oceà, Facultat de Ciències de la Terra, Universitat de Barcelona, c/ Martí Franquès s/n, 08028 Barcelona, Spain.
E-mail address: jfrigola@ub.edu (J. Frigola).

https://doi.org/10.1016/j.scitotenv.2019.134778
0048-9697/© 2019 Elsevier B.V. All rights reserved.

0.4%–2% for Fe, 1%–7% for Zn, 3–14% for Pb and 5%–16% for Mn. They highlight the robustness of the calibration procedure here presented for accurate and precise quantification of element concentrations from XRF-CS semi-quantitative data.

© 2019 Elsevier B.V. All rights reserved.

1. Introduction

X-ray fluorescence core scanners (XRF-CS) allow rapid and non-destructive acquisition of high resolution, continuous elemental composition data from sediments on split cores. XRF-CS have been widely used in the last decades to estimate relative changes of the chemical composition of marine and lacustrine sediments in a variety of geosciences research topics (Rothwell and Rack, 2006) such as paleoclimatology and paleoceanography (Calvert and Pedersen, 2007), sedimentology (Croudace et al., 2012; Croudace and Rothwell, 2015), lithostratigraphy or diagenesis studies (Löwemark et al., 2011; Croudace et al., 2019). Furthermore, XRF-CS have further been used in the analysis of cores made of hard rock, loess, peat bogs, river deposits and polluted materials, and also on speleothems and wood samples for a variety of purposes (Rothwell and Croudace, 2015; Hanebuth et al., 2015; Guo and Yang, 2016).

Elemental intensities obtained by means of XRF-CS are expressed in counts (cts) or counts per second (cps), which depend on the excitation conditions and the X-ray exposure time in every analysis. Since XRF-CS analyses are performed in fresh untreated materials, changes in elemental intensities can be affected by pore water content (Böning et al., 2007), grain size variations (Richter et al., 2006), sediment roughness and matrix modifications (Hennekam et al., 2018; Hennekam and De Rick, 2012; Tjallingii et al., 2007; Weltje and Tjallingii, 2008). Because of these reasons, the records of the measured down-core elemental intensity cannot be considered quantitative, although they are assumed to reflect proportional changes in element concentrations. Normalization with a conservative element, e.g. Al (Din, 1992), is a common practice to overcome some of these problems, especially those affecting the dilution of heavier elements, i.e. the closed-sum effect (Rollinson, 1993; Löwemark et al., 2011), to finally achieve a better assessment of relative changes. Nonetheless, normalization with conservative elements can be problematic in coarse-grained industrial wastes such as mine tailings or foundry slags. For some studies it may be not necessary converting XRF-CS data into absolute concentrations, and both element intensities and ratios are frequently used for identifying relative changes in the intensity of the processes controlling the accumulation of each element. Using the logarithm of elemental ratios, i.e. log-ratios, has also become common practice to better represent changes in element concentrations, as log-ratios preserve a lineal relation between XRF-CS data and element concentrations, thus allowing sound statistical modelling of compositional data (Weltje and Tjallingii, 2008).

Determining absolute concentrations of elements is, however, crucial in many studies, such as those addressing environmental pollution issues. On the other side, performing large amounts of analyses to get absolute concentrations by means of conventional methods (e.g. Inductively Coupled Plasma-Mass or Emission Spectrometry, ICP-MS or ICP-OES, or off-line X-ray fluorescence, XRF) involving the treatment and final destruction of the samples is very time consuming and costly. Conversely, non-destructive XRF-CS analyses quickly and cheaply supply high-resolution, practically continuous along core data. But this implies one step further to get absolute concentration data from measured XRF-CS elemental intensities (Jansen et al., 1998; Kido et al., 2006; Spofforth et al., 2008; Lyle and Backman, 2013; MacLachlan et al., 2015; Hunt et al., 2015). Such conversion provides a powerful tool to determine pollution levels in sediments from contaminated areas at very high resolution, thus rendering unnecessary to perform chemical analyses of plenty of discrete samples along the whole core (Rodríguez-Germade et al., 2015a, 2015b). The benefits of such an approach in terms of cost and time saving are obvious. Despite this, errors associated with such conversion have not been addressed so often, thus leaving a lack of information regarding range errors in the transformation estimates, which can be of the utmost importance for evaluating contamination levels.

The most common practice for the conversion of the XRF-CS data to absolute concentrations is the ordinary least-squares (OLS) regression method for stablishing a linear function between pairs of values obtained by means of two different analytical techniques (Böning et al., 2007; Chen et al., 2016; Mejía-Piña et al., 2016; Tjallingii et al., 2007; Weltje and Tjallingii, 2008). This classic method, widely implemented in spreadsheet software, does not consider the standard error associated with both abscissas (x) and ordered (y) variables, i.e. element concentration and element intensity, respectively. Few solutions have been proposed for introducing x and y standard error in the least-squares procedure. One option is to include the weighting of the standard error only in the ordered axis (y), called weighted ordinary least-squares (WOLS). However, the most accepted method is the unified solution proposed by York et al. (2004) that incorporates standard error in both x and y, called weighted least-squares (WLS).

In this study, we present a novel calibration procedure to convert high-resolution XRF-CS from highly polluted submarine deposits collected offshore Portmán Bay and Barcelona, in Spain, into absolute concentrations for five metals, namely Ti, Mn, Fe, Zn, and Pb and one metalloid, namely As. The above-mentioned three linear least-squares methods, i.e. OLS, WOLS, and WLS, have been tested to assess the quality of the linear regressions thus obtained together with the influence of the standard deviation of both element concentration and element intensity measurements. Our results highlight that establishing a detailed calibration procedure is critical to obtain high quality records for calibrated concentrations derived from XRF-CS semi-quantitative measurements. In turn, we also demonstrate the potential of XRF-CS data calibration to precisely establish metal contents in highly polluted marine deposits according to sediment quality guidelines (SQGs).

2. Methods

2.1. Study area and sample collection

Core samples considered in this study were obtained from two heavily polluted inner continental shelves offshore Portmán Bay (Murcia, SW Spain) and Barcelona (Catalonia, NE Spain), in the western Mediterranean Sea. From 1957 to 1990 about 60 Mt of metal bearing mine tailings were dumped into Portmán Bay from a froth flotation plant on the coast (Oyarzun et al., 2013). Such sustained discharge resulted in a mean advance of the shoreline of 650 m and in the complete infill of the original horseshoe-shaped Portmán Bay (Manteca et al., 2014). The dumped tailings form today a prograding coastal prism with its thickest and more extensive lays submerged over the inner continental shelf (Canals and shipboard party, 2015). Our target metals (Mn and Fe), trace metals (Zn and Pb) and the metalloid (As) have been selected because of the compositional characteristics of the mine tailing deposit off

Portmán Bay, which is rich in galena (PbS), sphalerite (ZnS) and pyrite (FeS) derivatives, also containing significant amounts of Mn and As (Manteca et al., 2014; Gómez-García et al., 2015).

Up to 50 cm long high-quality sediment cores from the submerged mine tailings deposit were collected with a multicorer system in August 2014 and March 2015 within the framework of EC and Spanish funded research projects MIDAS and NUREIEV, respectively. Eleven of these cores distributed from the proximal to the distal part of the submarine deposit down to 55 m of water depth) were selected for detailed scanning with XRF-CS (Fig. 1a and Table 1). The cored materials consisted mostly of silts with abundant fine sands, especially at some levels. Visual inspection showed two distinct units in most cores: (i) a lower unit made of dark greenish grey materials, with no bioturbation and occasional highly laminated intervals, and (ii) a ~20 cm thick, quite homogeneous and dark top unit with abundant bioturbation. According to Cerdà-Domènech et al. 2016, this depositional change is most likely related with the end of the mine tailings dump into the sea and its re-accommodation in the posterior years until present together with the re-establishment of natural-like sedimentation conditions.

The second study area offshore Barcelona is in front of the Besòs River mouth where sewage sludge from a single primary treatment plant of wastewater accumulated for an unknown period of time. Sludge was discharged through a 3 km long pipe lying on the seafloor. Previous studies have shown that the resulting deposit is rich in metals (including those found in the mine tailings deposit off Portmán Bay) and organic matter (Palanques et al., 1998, 2017; Kruge et al., 2010). In the current study we analyzed a sediment core collected from this sludge deposit in February 2017 with a gravity corer (Fig. 1b and Table 1) during the UNIBARNA 2017 cruise organized by the University of Barcelona. The materials consisted mainly of organic matter-rich clays.

The above-mentioned background information on the nature of the pollution in both sites led to the selection of the previously referred five metals (Ti, Mn, Fe, Zn and Pb) and one metalloid (As) to carry out the calibration of XRF-CS data for obtaining fine-tuned absolute concentrations. These elements are thus con-

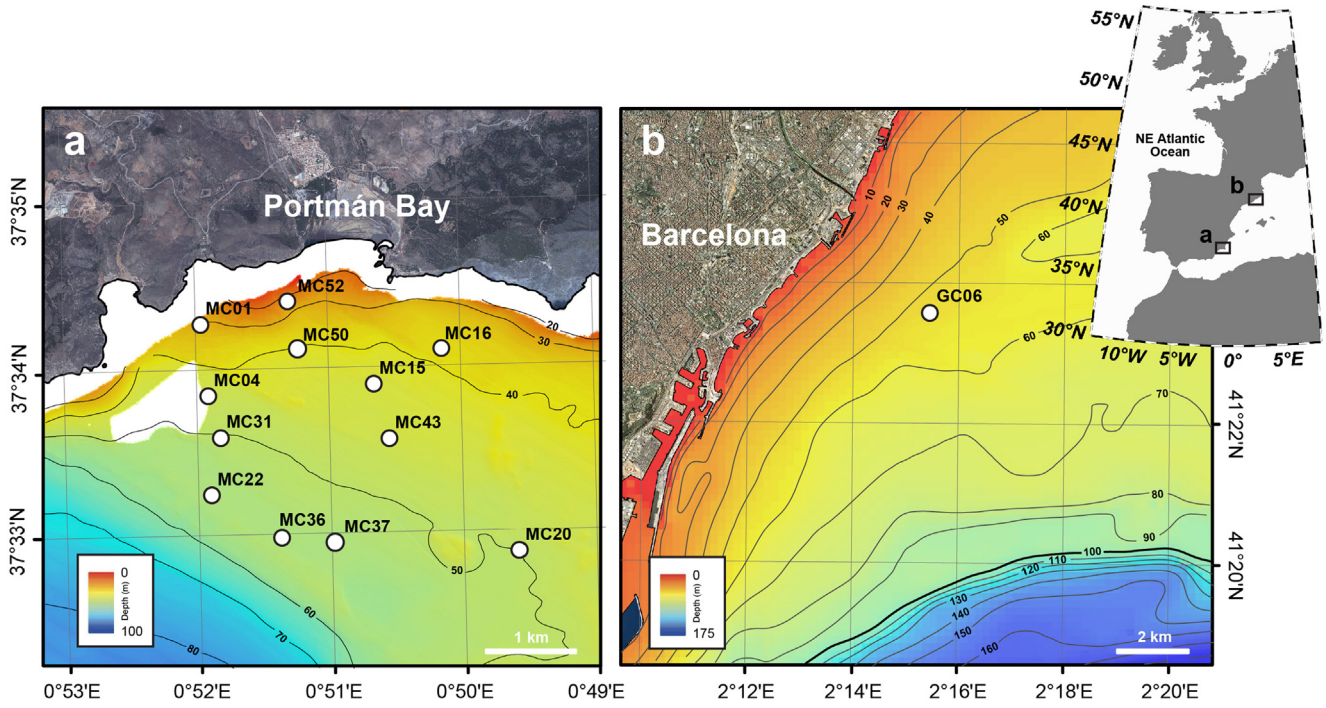

Fig. 1. General bathymetric maps of the inner continental shelf off (a) Portmán Bay and (b) Barcelona showing the location of the sediment cores analyzed in this study. Contours every 10 m.

Table 1
Sediment core depth, latitude, longitude, sampling device and length.

Station ID	Depth (m)	Latitude	Longitude	Device	Lenght (cm)
MC-01	29.7	37°34.449′N	0° 51.961′W	Multicorer	37.0
MC-04	46.0	37°34.016′N	0° 51.928′W	Multicorer	29.5
MC-15	43.4	37°34.070′N	0°50.659′W	Multicorer	40.0
MC-20	49.5	37°33.047′N	0°49.586′W	Multicorer	25.3
MC-22	53.9	37°33.420′N	0°51.902′W	Multicorer	55.5
MC-31	50.0	37°33.765′N	0°51.826′W	Multicorer	15.0
MC-36	53.7	37°33.155′N	0°51.377′W	Multicorer	45.3
MC-37	53.3	37°33.122′N	0°50.978′W	Multicorer	29.5
MC-43	44.9	37°33.740′N	0°50.548′W	Multicorer	24.6
MC-50	39.8	37°34.291′N	0°51.230′W	Multicorer	33.4
MC-52	23.1	37°34.577′N	0°51.298′W	Multicorer	28.0
GC-06	53.0	41°23.856′N	2°15.953′E	Gravity corer	137.0

sidered to be highly significant and have a diagnostic value for the studied reference deposits.

We are aware most studies on marine sediment pollution are focused on trace metals (and metalloids), especially As, Pb, Cd, Cu or Co (e.g. Buccolieri et al., 2006; Palanques et al., 2017). However, trace metals like Cd, Cu or Co appear in concentrations that according to the manufacturer are close to the detection limits of the Avaatech XRF core scanner, which may hinder highly accurate and precise calibrations for them. Also, for these reason Ti, Mn, Fe, Zn, As and Pb are the target elements selected in our study.

2.2. XRF core scanner analysis

All sediment cores have been scanned with an Avaatech XRF core scanner at the CORELAB facility of the University of Barcelona. The core scanner is equipped with an Oxford Rhodium X-ray source (4–50 kV) and a Canberra X-Pips 1500-1.5 Detector with a 125-μm beryllium window and a multichannel analyzer Canberra DSA 1000 (MCA). This configuration allows detecting a wide range of emission spectra for elements with atomic weight from Al to U.

Prior to scanning, the split cores were left for 16 h at room temperature to evaporate water, thus reducing the water effect on the radiation absorption and increasing the measured signal intensity (Böning et al., 2007; Tjallingii et al., 2007). Then, the cores were covered with Ultralene X-ray transmission foil (4 μm thick) to avoid desiccation and potential contamination and scanned at 2 mm resolution. The excitation configuration parameters were set at 10 kV and 1.2 mA during 10 s for elements with atomic weights between Al and Fe, and 30 kV and 1.6 mA during 50 s, with a Pd-thick filter, for elements with atomic weights between Ni and Pb. Each element presents various energy emissions in the X-ray spectrum that correspond to the different electron states of the atom. Ti, Mn, Fe, Zn and As intensities, expressed as counts (cts) were obtained by integration of their K_α X-ray emission line. Lead intensity was obtained by integration of the L_β emission line in order to reduce the effect on the integration produced by the overlap of Pb (L_α) and As (K_α). The bAxil spectrum analysis software (BrightSpec) was used to obtain the integration of the elemental peaks and the estimation of their intensity areas, expressed as counts per seconds (cps).

2.3. Geochemical analysis of discrete samples

77 subsamples from core tops were analyzed for quantitative metal concentrations by means of ICP-OES and ICP-MS. In order to obtain the best representative calibration function between XRF intensities and the absolute concentrations of each metal, subsamples were selected considering the widest range of intensities from all target elements. As XRF core scanner analyses were carried out at 2 mm resolution, subsamples were extracted from 1 cm-width intervals with essentially constant intensities to avoid interferences eventually coming out from layers with different responses. To further reduce eventual multi-layer interferences, subsamples were obtained from the area irradiated during XRF core scanning ($2 \times 12\ mm^2$) and from a maximum depth of 2 mm in the split sediment core, which corresponds approximately to the maximum penetration of X-rays in soft sediment. Obviously, the minimum mass of sample (~1 g dry) needed for ICP analyses was also taken into account while subsampling the split cores.

Each subsample was lyophilized, grounded and homogenized with an agate mortar, and placed in a Teflon reactor with 2.5 mL of HNO_3 (65%) at 100 °C for 18 h. The extract was poured into a polyethylene tube and centrifuged 3 min at 3000 rpm to separate the solid phase. The supernatant was decanted and diluted with HNO_3 at 1% until 50-mL ready to be analyzed were obtained. The residue was placed again into a Teflon reactor, leached with 1 mL HNO_3 (65%), 7 mL of HF and 1 mL H_2O_2, and heated for 18 h at 100C. Then, 2 mL $HClO_4$ were added to the Teflon reactor and heated in a sand bath at 270C until all acid volume evaporated. The hot residue was further treated with 2 mL $HClO_4$ and heated again in the sand bath at 270 °C until the acid evaporated. The resultant residue was leached with 2 mL HNO_3 (65%) and 2 mL H_2O_2, and decanted into a volumetric flask where it was diluted with HNO_3 at 1% until 50-mL.

Two solutions per sample were analyzed using a Perkin-Elmer Elan-6000 ICP-MS for metals in lower concentrations (Ti, Zn, As and Pb) and a Perkin Elmer Optima 8300 ICP-OES for metals in higher concentrations (Mn and Fe).

2.4. Standard deviation of XRF-CS and ICP-MS/OES measurements

The error associated with the XRF-CS and the ICP-MS/OES measurements, hereinafter referred to as standard deviation, has been examined to quantify its influence on the calibration function. The standard deviation of the XRF-CS measurements was obtained directly through the spectral analysis software (bAxil) that adjusts the regression function to the spectral emission of each element by a non-linear least-squares algorithm. This allows detecting the deviation of the spectral areas with regards to the regression model, which increases when the spectral peak is not well defined, as it is generally the case for low intensity peaks. The standard deviation of the ICP-MS/OES analysis has been calculated as the mean standard deviation of the three measurements performed on each sample.

2.5. Calibration of element intensities to absolute concentrations

Defining the best regression line between two experimental data sets is a significant tool to predict the theoretical value of one variable from the other variable (Webster et al., 1995; Piippanen et al., 1997; Saylor et al., 2006; Hennekam and De Rick, 2012). Generally, the linear relationship between n number of (x_i, y_i) data pairs (i = 0,. . .,n) can be described by the function:

$$y(x) = \beta_0 + \beta_1 bx \tag{1}$$

where $\beta_1$is the slope of the straight line and β_0 is the y-axis intersection.

The ordinary least-squares (OLS) method has been extensively used to provide a linear function between x (as the independent variable) and y (as the dependent variable). By definition, the OLS method minimizes the sum of the squares of the y residuals:

$$\sum_{i=1}^{n} (y_i - Y_p)^2 = \sum_{i=1}^{n} (y_i - \beta_0 + \beta_1 x_i)^2 \tag{2}$$

where Y_p is the y-prediction and y_i is each point lying on the regression.

Although OLS is a simple solution to obtain a linear function, if one or both variables have associated errors, the OLS regression can be biased. Considering only the effect of the y-errors in the regression, the x_i and y_{i1} data pairs can be weighted by a factor inversely proportional to the variance of the y-values:

$$\sum_{i=1}^{n} w_i (y_i - y_p)^2 = \sum_{i=1}^{n} w_i (y_i - \beta_0 + \beta_1 x_i)^2 \tag{3}$$

$$w_i = \frac{1}{\sigma_1^2}, \tag{4}$$

where w_i is the weight factor and σ_1^2 is the standard error of y-values.

This derivation of the OLS method, named weighted ordinary least-squares (WOLS), considers that the dependent variable, y, contains a random error of measurement, while the independent variable, x, is error-free. However, the measured analytical data generally includes instrumental errors in both directions, which vary from point to point with no fixed relation to each other. Deming (1943) proposed a solution with errors in both regressed variables that minimize the sum of squared residuals, as:

$$S = \sum \left[\omega(X_i)(x_i - X_i)^2 + \omega(Y_i)(y_i - Y_i)^2\right] \quad (5)$$

$$\omega(X_i) = \frac{1}{\sigma_{X_i}^2},\ \omega(Y_i) = \frac{1}{\sigma_{Y_i}^2} \quad (6)$$

where (x_i, y_i) are the observed points, (X_i, Y_i) are predicted values and $(\sigma_{X_i}, \sigma_{Y_i})$ correspond to the standard errors of each variable.

York et al. (2004) proposed a general solution to the sum of squared residuals (Eq. (5)) by unifying the problem of finding parameters β_1 and β_0 through an iterative numerical least-squares technique including the possibility of identifying a correlation factor between the errors of x and y. In this weighted least-squares (WLS) regression technique the unification of standard errors in both x and y observations is presented as:

$$W_i = \frac{w(X_i)w(Y_i)}{w(X_i) + b^2 w(X_i) - 3br_i\sqrt{w(X_i)w(Y_i)}.} \quad (7)$$

where $w(X_i)$ and $w(Y_i)$ are the weights of X_i and Y_i, b is the slope of the best line and r_i is the correlation coefficient between errors in X_i and Y_i.

In order to compare and assess the impact of the standard deviation of the element intensity and concentration in both directions of the linear function, the three regression methods (OLS, WOLS, and WLS) have been implemented in Matlab version 2016a or higher. The XRF-CS outputs expressed in cps have been defined as the dependent variable (y_i) and the metal concentrations expressed in % (weight/weight) and mg kg^{-1} have been set as the independent variable (x_i). The quality of the linear function has been determined by two goodness-of-fit measures: the correlation coefficient (r^2) and the standard deviation of the estimate (S). The correlation coefficient (r^2), described as the degree of association between two variables, has been widely used as a quality index for regression models and is defined as:

$$r^2 = \frac{cov\ (X,\ Y)}{\sqrt{var(X)var(Y)}} = \frac{\frac{1}{N}\sum_{i=1}^{n}(x_i - x^-)(y_i - y^-)}{\sqrt{\frac{1}{N}\sum_{i=1}^{n}(x_i - x^-)^2 \sum_{i=1}^{n}(y_i - y^-)^2}} \quad (8)$$

where y_i and $x_i$are the observational values, $\bar{y}$and $\bar{x}$ are the mean values of y_i and $x_i$values, and W_i is the weight value expressed in Eq. (4). In the case of WLS, York's (2004) solution differs from the mean value of y_i,as defined by:

$$\bar{y} = \frac{\sum W_i x_i}{\sum W_i} \quad (9)$$

Otherwise, the standard deviation of the estimate (S) is a measure of the accuracy of the predictions and provides the absolute measure of the data point distance from the linear function, which is expressed in the units of the dependent variable and is defined by:

$$S^2\ (OLS) = \sum_{i=1}^{n} \frac{(y_i - y_p)^2}{n-2} = \sum_{i=1}^{n} \frac{(y_i - \beta_0 + \beta_1 x_i)^2}{n-2} \quad (10)$$

$$S^2(WOLS/WLS) = \sum_{i=1}^{n} W_i \frac{(y_i - y_p)^2}{n-2} = \sum_{i=1}^{n} W_i \frac{(y_i - \beta_0 + \beta_1 x_i)^2}{n-2} \quad (11)$$

where y_p is the prediction value from the data point y_i, n the number of observations and W_i the weighted parameter defined in Eqs. (4) and (6) for WOLS and WLS methods, respectively.

3. Results and discussion

3.1. Linear function estimated by OLS, WOLS and WLS methods

Element intensities and concentrations in marine sediments off Portmán Bay and Barcelona, and the linear functions estimated by OLS, WOLS and WLS methods are presented in Fig. 2 and Table 2. The main parameters assessed to compare the three linear functions for each element are the statistical significance (P), the y-intercept value, the relative standard deviation of the slope (RSD) and the residual plot, as well as the goodness-of-fit measures: the correlation coefficient (r^2) and the standard deviation of the estimate (S). Contrary to previous researches (e.g. Mejía-Piña et al., 2016), the linear functions have not been adjusted to pass through the origin of coordinates, thus allowing to determine the influence of errors associated to the XRF-CS output in the linear function. Metal concentrations measured in Portmán's Bay samples show a larger variability, with values of 1600–3400 mg kg^{-1} for Ti, 200–7000 mg kg^{-1} for Mn, 1–26% for Fe, 50–7300 mg kg^{-1} for Zn, 20–800 mg kg^{-1} for As and 40–5400 mg kg^{-1} for Pb. These concentrations are noticeably higher than those reported from other sites in the Mediterranean Sea (e.g. Buccolieri et al., 2006; Sprovieri et al., 2007; Palanques et al., 2008; Christophoridis et al., 2009; Martínez-Gómez et al., 2012), thus evidencing metal enrichment in Portmán's mine tailings deposit (Oyarzun et al., 2013). Metal concentrations are significantly lower in sediments from the Barcelona inner continental shelf, ranging from 540 to 4440 mg kg^{-1} for Ti, 220–430 mg kg^{-1} for Mn, 0.4–4.0% for Fe, 110–1150 mg kg^{-1} for Zn, 5–200 mg kg^{-1} for As and 30–1730 mg kg^{-1} for Pb.

The three regression methods (OLS, WOLS, and WLS) show correlation coefficients better than $r^2 = 0.94$ for all elements (Table 2), which are higher than those obtained in previous studies (Böning et al., 2007; Tjallingii et al., 2007). However, the WLS method presents a significantly lower standard deviation of the estimate (S) compared to the OLS method, which shows the highest values. Since the correlation coefficient simply provides a relative quantification of the dependence variable variance that can be explained by the regression model, the standard deviation of the estimate is more adequate to quantitatively evaluate the precision of the linear function. Indeed, the standard deviation of the estimate decreases when the analytical standard deviations in both variables are weighted in the WOLS and WLS methods (Table 2).

Increasing the precision has a direct influence mainly on the relative standard deviation of the slope (RSD), which represents the main source of errors in the linear function. Accordingly, the results show that RSDs from OLS and WOLS methods are significantly higher than those obtained with the WLS method for all elements except As, which displays a relatively high RSD for the three methods (Table 2). The differences between OLS/WOLS and WLS regression methods are especially clear in the case of Ti, element which also presents a significant scattering. As high RSD for the three regression methods is likely related to the large standard deviation of the As intensity values (Supplementary Material, Table S1), which is in turn affected by the overlapping of the emission peaks of Pb and As given their close proximity (Pb Lα 10.551 KeV and As Kα 10.543 KeV, Fig. 3b). Indeed, the peak area of a characteristic XRF line could be partially overlapped by a contiguous peak, which may affect significantly the determination of the peak area (cts). Such overlapping has been noticed elsewhere in samples with high concentrations of sulfides (Baucells et al., 1988).

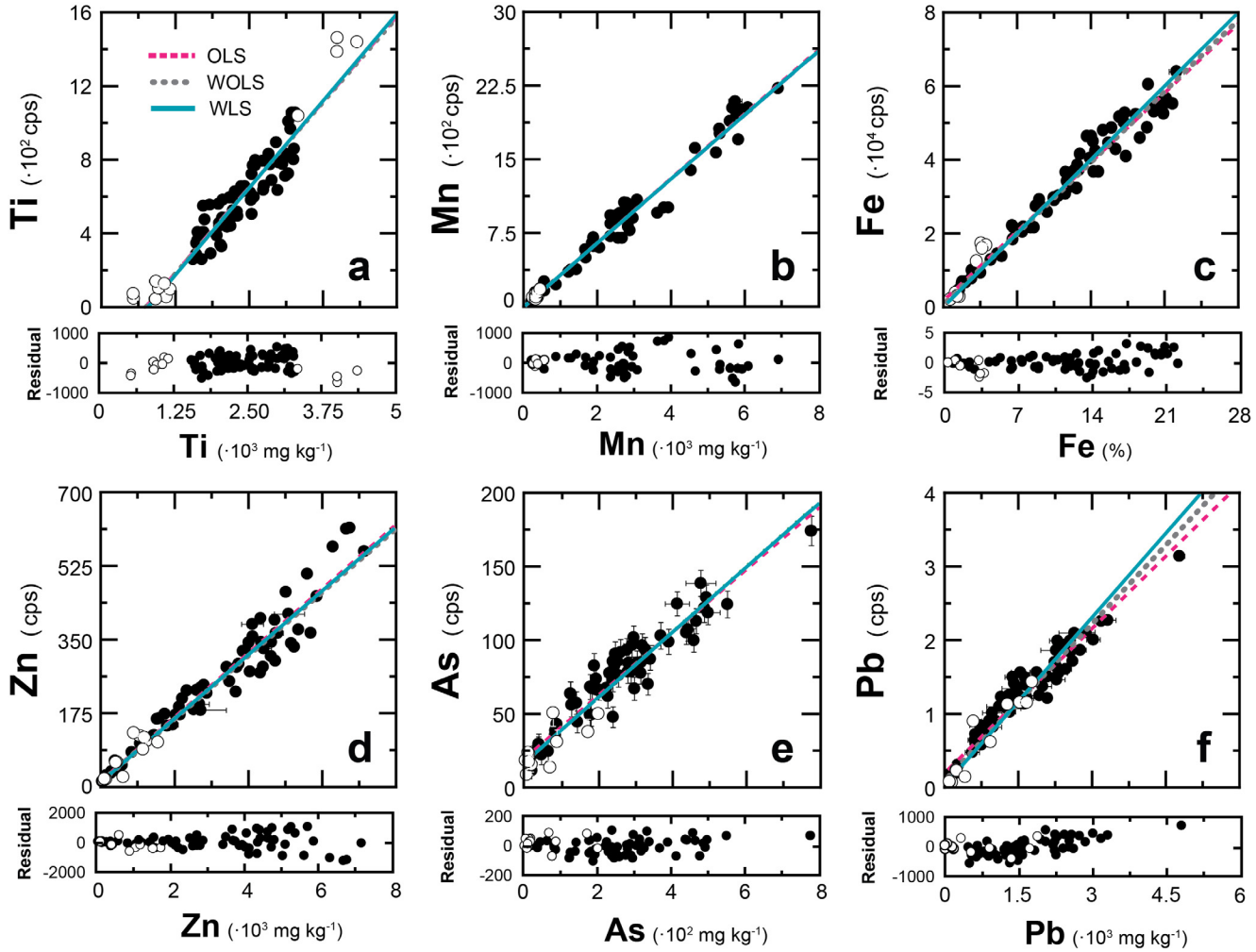

Fig. 2. Scatterplots of element intensities in counts per second (cps) and chemical concentration expressed in % and mg kg^{-1} for (a) Ti, (b) Mn, (c) Fe, (d) Zn, (e) As and (f) Pb from Portmán Bay (black dots) and Barcelona (white open dots) inner shelf sediment samples. Continuous blue and dashed dark grey and pink lines indicate the regression equation line for each statistical model, namely WLS, WOLS and OLS (see legend in plot a). Residual values in cps for the correlation of each data pair is shown in the smaller plots below each main plot.

Table 2
Statistical parameters of OLS, WOLS and WLS regression models for each analyzed metal including: intercept value, slope, relative standard deviation of the slope (RSD), statistical significance (P), correlation coefficient (r^2) and number of observations (n). Statistical significance (p) for all regressions was $p < 0.001$.

		Intercept		Slope		RSD	S	r^2	n
Ti	OLS	−276.07	34.74	0.3708	0.0142	3.82	95.8	0.949	77
	WOLS	−269.23	35.74	0.3678	0.0146	3.96	5.0	0.946	77
	WLS	−296.24	7.82	0.3776	0.0033	0.87	4.2	0.949	77
Mn	OLS	−1.51	19.58	0.3279	0.0064	1.96	101	0.988	66
	WOLS	2.20	19.07	0.3264	0.0063	1.92	4.8	0.988	66
	WLS	0.12	3.68	0.3262	0.0015	0.47	3.9	0.989	66
Fe	OLS	1367.7	633.3	2535.0	51.8	2.04	3096	0.985	77
	WOLS	439.4	420.8	2626.2	34.4	1.31	55.3	0.994	77
	WLS	−197.0	9.3	2695.8	2.2	0.08	23.3	0.993	77
Zn	OLS	9.31	7.29	0.0762	0.0021	2.77	37.0	0.972	77
	WOLS	7.56	3.57	0.0768	0.0010	1.35	16.6	0.993	77
	WLS	6.90	0.19	0.0758	0.0002	0.20	11.5	0.987	77
As	OLS	19.41	2.08	0.2133	0.0076	3.57	10.8	0.955	77
	WOLS	17.36	2.03	0.2226	0.0074	3.34	1.5	0.961	77
	WLS	16.71	1.27	0.2203	0.0055	2.48	1.4	0.958	77
Pb	OLS	21.56	3.26	0.0654	0.0020	3.01	16.3	0.967	77
	WOLS	11.98	2.82	0.0724	0.0017	2.35	8.6	0.980	77
	WLS	5.20	0.32	0.0761	0.0006	0.75	4.1	0.985	77

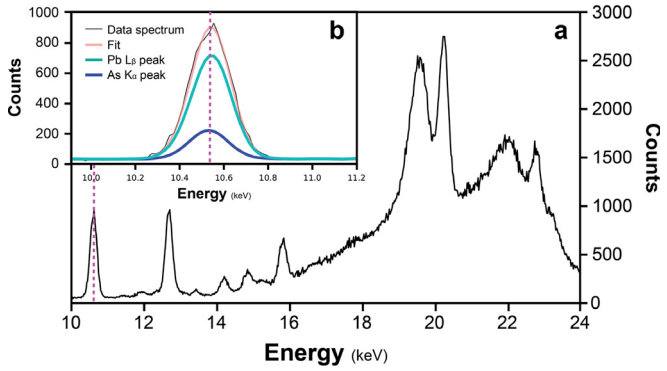

Fig. 3. a) Example of the X-ray spectrum plot of one sample measured at 30 kV and 1.6 mA during 50 s, with a Pd-thick filter. b) Detail of spectral overlap of As Kα and Pb L_β.

To overcome the above limitation the spectral analysis software determines the peak area (e.g. As K_α) by a mathematical adjust considering the emission probability from another peak (e.g. As K_β) that would increase the standard deviation of the element intensity (Scholze et al., 2006). The standard deviation can be slightly reduced by selecting a non-overlapping XRF peak for the element intensity estimation, like the secondary line emission of As K_β (11.726 KeV) and Pb L_β (12.614 KeV). However, while the Pb L_β peak that we have selected to determine the element intensity of Pb is relatively pronounced in our samples, the As K_β peak area is significantly lower than the K_α peak (Fig. 3b). This implies that its integration would generate again rather high standard deviations. For a more accurate analysis and to reduce the standard deviation of the integrated As intensities, it would be necessary to use a predefined standard calibration to quantify the interference factor between Pb Lα and As Kα peaks (Baucells et al., 1988).

As shown in Fig. 2, the y-intercept values for all models show minimum deviations from zero for Mn, Fe, Zn, As and Pb, which might be related to the wide concentration range and the high accuracy of the linear regression. In contrast, the elevated negative y-intercept for Ti (Fig. 2a) is likely related to a matrix effect and to indirect excitation that are both more common in transition elements like Ti. This occurs when part of the Ti-emitted fluorescence is scattered or absorbed by Ca, thus enhancing its measured intensity and, consequently, leading to a negative intercept (e.g. Böning et al., 2007). The deviation of the y-intercept from zero is particularly relevant in calibration studies for obtaining element concentrations at lower values, and is directly related to the detection limit of the regression method. Indeed, a comparison between the y-intercept values after the three regression methods shows that, with the exception of Ti and As, the WLS method presents a minor y-intercept deviation from zero than OLS and WOLS (Table 2). Moreover, all regressions show a robust statistical significance (P), with a P-value lower than 0.001, and the residual values plots evidence a constant distribution of data for all concentrations range (Fig. 2).

Overall, the regressions obtained for the six target metals show lower scattering and standard deviation of the slope, as well as higher correlation coefficients, than those from previous calibration studies (e.g. Böning et al., 2007; Tjallingii et al., 2007). These results can be attributed to the increased element intensities recorded due to the reduction of water content in the split core. Indeed, Tjallingii et al., 2007a found that the thin water film formed under the foil that covers the split core strongly reduces element intensities. Given that the analytical precision of the XRF core scanner varies with the element intensity (Ramsey et al., 1995), the drying step of 16 h before performing XRF analyses contributed to reduce the scatter of the regression. This leads to an enhanced accuracy of the linear function by decreasing the deviation of the observed value from the fitted value provided by the linear function, thus improving the correlation coefficient. Nonetheless, the high-resolution sediment subsampling carried out in the same irradiated area and the avoidance of interferences between different sediment layers likely contributed to minimize the scattering effect. Additionally, even though the element intensities measured by XRF-CS are largely influenced by lithology and other sediment characteristics (Rodríguez-Germade et al., 2015a, 2015b), our results present a very good overlay between intensity data from the two sampling locations (Fig. 2).

Our results evidence that the calibration method used in our study to convert XRF-CS output data into fully quantitative data improves significantly the quality of the linear regression for the three regression methods, as illustrated by high correlation coefficients, low errors and deviation to zero. Nevertheless, WLS appears to be the best method for highly accurate determinations of the linear function between element intensities and concentrations. This points out that analytical and statistical errors should be properly evaluated in calibration studies to convert XRF-CS output data into quantitative concentrations.

3.2. Errors of calibrated elemental concentrations

The most commonly applied approach to obtain quantitative elemental data from XRF-CS outputs is to replace the *y* variable of the linear functions by the element intensity value (Kelloway et al., 2014; Chen et al., 2016; Mejía-Piña et al., 2016). Given that these linear functions have errors associated to the slope and the intersect, and also to element intensities (Table 2), it is necessary to determine the errors of the calibrated element concentration in order to evaluate the quality and the limitations of the linear functions. Considering the three linear functions (OLS, WOLS and WLS) obtained for each element, 1850 element intensities have been converted into calibrated element concentrations. The errors of the calibrated element concentrations have been calculated according to the law of propagation of errors (Taylor and Kuyatt, 1994):

$$\Delta f = \Delta f(x_1, x_2, \cdots, x_n; \Delta x_1, \Delta x_2, \cdots, \Delta x_n) = \left[\sum_{i=1}^{n} \left(\frac{\partial f}{\partial x_i}\Delta x_i\right)^2\right]^{1/2} \quad (12)$$

where *f* is the given function, *n* is the number of uncorrelated variables (x_1, x_2, …, x_n) and their errors ($\Delta x_1, \Delta x_2, \cdots, \Delta x_n$). The relative errors calculated as the ratio of the errors to the calibrated element concentration for each linear regression (OLS, WOLS and WLS) has been regressed by the least-squares method to evaluate their distribution (Fig. 4 and Supplementary Material, Table S2).

As expected, the three regression methods are characterized by an exponential increase of the relative errors at low calibrated element concentrations. However, each element showed different trends. For Fe and Zn, errors of the calibrated concentrations by the WLS method were significantly lower than those obtained from OLS and WOLS, especially at low concentrations. Instead, Ti, Mn and Pb differences in errors after the three methods were minor. The contrasting patterns between the three regression methods (OLS, WOLS, and WLS) likely result from the differences in their slopes and intercept errors, which commonly represent the main error factor in the linear functions (cf. Section 3.1). Indeed, as shown in Table 2, relative standard deviations of the slope for the OLS method are higher than those from the WLS method by a factor ~4.4, ~4.2, ~25.8, ~14.0, ~1.5 and ~4.0 for Ti, Mn, Fe, Zn, As and Pb. In contrast, As shows the same trend independently of

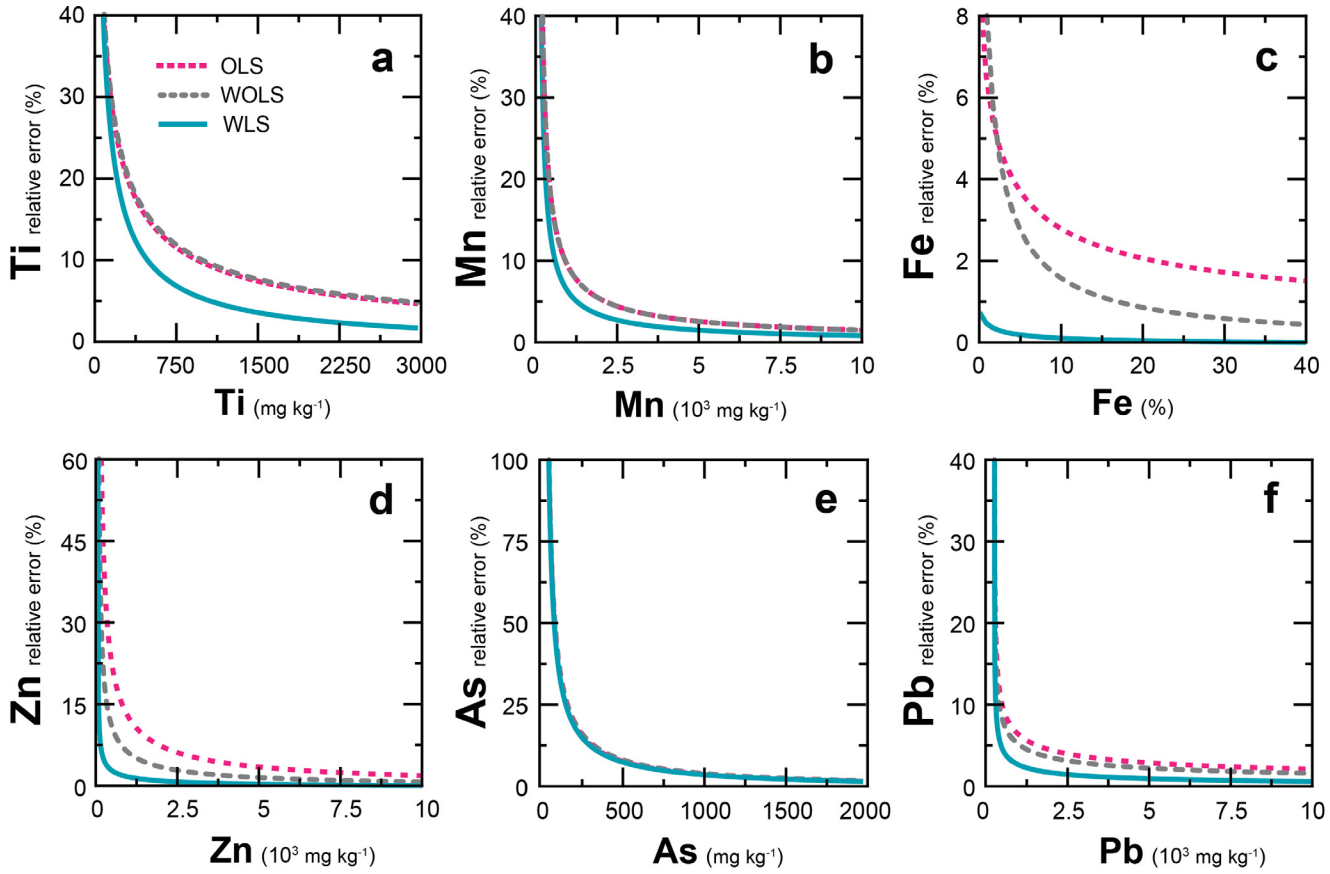

Fig. 4. Relative errors of the calibrated concentrations as a function of the calibrated concentrations in % for (a) Ti, (b) Mn, (c) Fe, (d) Zn, (e) As and (f) Pb as a function of concentration prediction expressed in % and mg kg^{-1} for each regression model (see legend in plot a).

the regression model and a minimal standard deviation from OLS to WLS, which relates to the high standard deviation in As intensities due to the spectral overlap between Pb L_β and As K_β peaks (Section 3.1, Fig. 3).

Nevertheless, obtaining the calibrated element concentrations requires an accurate methodology to avoid the influence of the effects of the physical properties so that the correlation coefficient is increased and the scattering is reduced (e.g. Tjallingii et al., 2007a). An accurate estimation of the errors is also required to evaluate the quality of the regression method and the representativeness of the results (Weltje and Tjallingii, 2008). Beyond the high correlation and lower scattering achieved from the three regression methods, likely due to the calibration methodology developed in this study, our results demonstrate that the regression method most commonly used (OLS) for XFR-CS calibrations is the one developing the highest errors for the calibrated element concentrations. This is mainly related to the non-weighted analytical errors. In contrast, the WLS method, which considers the analytical and statistical errors in the calibration of the XRF-CS output, provides more accurate calibrations, significantly reducing the errors of the calibrated element concentrations.

Our results also reveal that the exponential distribution of the errors observed in Fig. 4 is mainly explained by the influence of the standard deviation of the element intensity (Supplementary Material, Table S1). It is well known that the relative standard deviation of XRF-CS measurements increases exponentially as the concentration falls down to the detection limit (Ramsey et al., 1995). Depending on energy resolution and detection efficiency, the irregularities in the spectral signal are more significant at low peak areas (Scholze et al., 2006). Consequently, the nonlinear least-squares algorithm cannot adjust accurately the peak area, thus resulting in an increase of the standard deviation of the element intensity and hence in an increase of errors for the calibrated element at low concentrations. Some authors (e.g. Rodríguez-Germade et al., 2015a, 2015b; Hennekam et al., 2018) have demonstrated that increasing exposure time should reduce the standard deviation of the element intensity. However, the increase of exposure time also implies an augmentation of the time required for analysis and of associated costs, which should be taken into account too.

3.3. Sediment quality guideline levels and XRF-CS calibration

In the last century, anthropogenic fluxes of metals to the marine environment has grown as a result of accelerated industrial, urban, agricultural and mining developments (Di Leonardo et al., 2008; Palanques et al., 2008; Pan and Wang, 2012; Hanebuth et al., 2018). Commonly, the pollution degree of marine sediments assessed by using sediment quality guidelines (SQGs), which are defined as the concentration range or limit of the chemical compounds (e.g. trace metals, PCBs, pesticides or PAH) that could produce potential biological effects (Long et al., 1995). SQGs have been widely applied to evaluate ecotoxicological risks and biological effects in harbors (Fatoki and Mathabatha, 2001; Adamo et al., 2005; Casado-Martínez et al., 2006; Garcia-Orellana et al., 2011; Pourabadehei and Mulligan, 2016) and also in estuarine and coastal environments (Fukushima et al., 1992; Morillo et al., 2004; Buccolieri et al., 2006; Palanques et al., 2008; Rubio et al., 2010). Classically, performing pollution studies of marine sedi-

ments relied on conventional analytical methods requiring discrete samples from whole sediment cores, involving significant laboratory effort and time, together with high costs, which generally led to a reduction in the total number of samples finally analyzed (Rodríguez-Germade et al., 2015a, 2015b). The calibration of the XRF-CS output data appears as a major step forward to overcome these limitations, as it advantageously provides high-resolution metal concentration data in a fast, continuous and repeatable way (Fig. 5). However, for a meaningful use of XRF-CS calibrated data it is mandatory to quantify and minimize the errors of the calibrated element concentrations. This becomes even more necessary to assess pollution levels through SQGs at low element concentrations.

We have considered the concentration limits defined in three widely used SQGs (see further down) to estimate the relative errors of the calibrated element concentration for such limits using the WLS method developed in this study for XRF-CS data calibration. Those SQGs address various potential biological effects of the chemicals, which are: (i) the lowest effect level and severe effect level developed by the Ontario Ministry of the Environment (Persaud et al., 1993): (ii) moderately polluted and heavily polluted levels developed by the Environmental Protection Agency (U.S. Environmental Protection Agency, 2005); and (iii) action level B and action level C developed by the Spanish Harbor Authority "Puertos del Estado" on the basis of the "Guidelines for the characterization of dredged material and its relocation in waters of the maritime-terrestrial public domain" (Comisión nacional de estrategias marinas, 2015). A summary of metal concentration limits and associated relative errors for each of the above SQGs, expressed in percentage, is shown in Table 3.

It is to be noted that SQGs are usually based on standardized analytical procedures, especially when results can constrain management actions. Also, as aptly pointed out by Böning et al. (2007), it is reasonable to expect some degree of data scattering rather than a perfect correlation between XRF and ICP data. In any case, these factors do not condition the calculated errors as assessing the errors of the regression functions by any method (OLS, WOLS and, WLS) as well as propagating the errors of the cal-

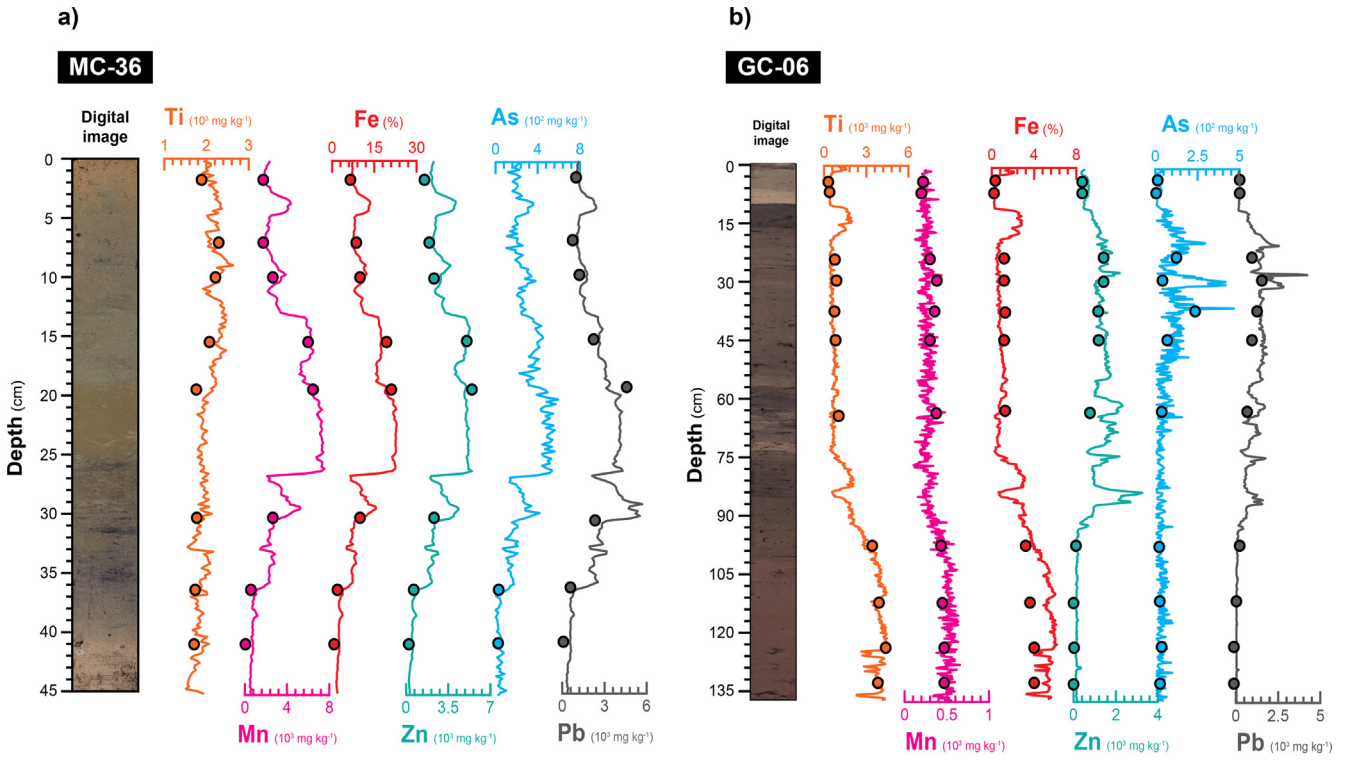

Fig. 5. Calibrated element concentration of sediment cores (a) MC-36 in Fig. 1a and (b) GC6 in Fig. 1b from the inner continental shelf offshore Portmán Bay and Barcelona, respectively. Points show the location of discrete subsamples on which that were analyzed by IPC-MS/OES for absolute metal concentrations, subsequently used for calibrations (Fig. 2). Note that core logs in the figure are at cm-scale whereas XRF scans were carried out at 2 mm resolution. Therefore, location of subsamples is merely indicative. All subsamples were extracted from 1 cm-width intervals with essentially constant intensities to avoid eventual multi-layer interferences (see main text for further explanation).

Table 3
Metal concentration limits and associated relative errors quantified after the WLS regression method for three widely used sediment quality guidelines (SQGs) in mg kg^{-1}.

	Spanish Harbor Authority				Ontario Ministry of the Environment				Environmental Protection Agency			
	Action level B		Action level C		Lowest level		Severe level		Mod. polluted		Heavily polluted	
	Limit	%Error	Limit	%Error	Limit	%Error	Limit	%Error	Limit	%Error	Limit	%Error
Mn (mg kg^{-1})	–	–	–	–	460	11	1100	5	300	16	500	11
Fe (%)	–	–	–	–	2	1	4	0.4	2	0.6	2.5	0.5
Zn (mg kg^{-1})	410	3	1640	1	120	6	820	2	90	7	200	4
As (mg kg^{-1})	70	>40	280	14	6	>40	33	>40	3	>40	8	>40
Pb (mg kg^{-1})	218	5	600	3	31	14	250	5	40	12	60	10

Table 4
Minimum, maximum and averaged minimum and maximum (lower row) metal concentrations in this research and coastal and harbour sediments worldwide.

Reference papers	Environment	Ti (mg kg^{-1})		Mn (mg kg^{-1})		Fe (%)		Zn (mg kg^{-1})		As (mg kg^{-1})		Pb (mg kg^{-1})	
		Min	Max	Min	Max	Min	Max	Min	Max	Min	Max	Min	Max
This research	Portmán Bay	1600	3400	200	7000	1	26	50	7300	20	800	40	5400
	Barcelona cont. shelf	540	4400	220	430	0.4	4	110	1150	2	200	30	1730
Coastal areas													
Palanques et al., 2017	Barcelona cont. shelf	–	–	–	–	–	–	100	990	–	–	50	760
Buccolieri et al., 2006	Gulf of Taranto	2340	3880	550	2830	0.3	0.4	90	130	–	–	50	80
Capello et al., 2016	Gromolo Torrent	–	–	299	1207	1.8	8.8	78.7	262.7	9	23	14	43
Fukushima et al., 1992	Tokio Bay	2520	3700	350	1540	3	4.1	106	405	–	–	25	58
Raj and Jayaprakash, 2007	Bay of Bengal	–	–	260	460	1.7	3.7	40	200	–	–	25	37
Morillo et al., 2004	Huelva Estuary	–	–	180	576	1.6	3.5	141	649	–	–	20	197
Rubio et al., 2010	Vigo Ria	–	–	263	306	5	7	85	135	–	–	36	84
Harbors													
Adamo et al., 2005	Port of Naples	240	480	100	420	–	–	40	1200	8	21	40	310
Guevara-Riba et al., 2004	Port of Barcelona	–	–	255	427	2.2	3	183	1133	–	–	86	589
Pourabadehei and Mulligan, 2016	Quebec harbor	–	–	–	–	–	–	66	563	4.6	18.4	11	212
Romano et al., 2008	Pozzouli Gulf	–	–	–	–	1.3	8.9	50	6300	10	837	21	2811
Casado-Martínez et al., 2006	Port of Cartagena	–	–	–	–	–	–	900	8660	62	101	487	1397
He and Morrison, 2001	Port Kemblar harbor	–	–	–	–	7.3	10	1209	2220	14	46	151	484
Fatoki and Mathabatha, 2001	Elizabeth harbor	–	–	103	499	0.4	1.5	19	126	–	–	9	62
Muller-Karulis et al., 2003	Ventspils harbor	–	–	162	1120	0.6	3.8	17	254	–	–	3	44
Metal concentration average		1450	3170	250	1400	2	7	190	1860	20	260	70	840

ibrated element concentrations allow constraining calibration procedure errors and evaluating the quality of the regression functions and the data themselves, thus significantly contributing to improve comparisons.

Even though the errors depend on each SQGs, the errors of the calibrated element concentration for each limit in the guidelines should be considered satisfactory for most metals under consideration (Mn, Fe, Zn and Pb) but As. Titanium is not included in the referred SQGs. Iron shows the lesser relative errors, from 0.4% to 2%, due to the high concentration limits considered in SQGs and also to the low errors of the linear function. For the rest of metals under consideration also included in SQGs, Zn ranges from 1% to 7%, Pb from 3 to 14%, and Mn from 5% to 16%. Errors for As are equal or higher than 14%, because of the large standard deviation of the linear function resulting from the Pb peak overlap effect (cf. Section 3.1). The range of metal concentration levels found in coastal and harbor sediments worldwide (Table 4) reinforces the potential applicability to many polluted settings of the calibration method presented in this paper.

4. Conclusions

Calibrating XRF-CS output data from polluted marine sediments is critical to obtain absolute concentrations at high resolution in a rapid, non-destructive and continuous way. Practical issues to take fully into account when converting XRF-CS semi-quantitative data into quantitative data are the physical properties of the sediment (e.g. pore water content, grain size, sediment irregularities and changes in matrix) and the selected excitation configuration parameters, as both have an influence on measurements. The resulting errors in the linear function of the calibration should be addressed so that the quality of the calibrated metal concentration data could be assessed. Our results, derived from the analysis of metal-polluted sediments from two locations off Portmán Bay and Barcelona, in the Mediterranean Sea off Spain, demonstrate that the applied calibration procedure improves the quality of the linear regression for any of the three most widely applied regression methods (OLS, WOLS, and WLS), thus increasing correlation coefficients and reducing the data deviation from the linear function. Of the three regression methods, WLS appears as the best suited as it provides accurate calibrated element concentrations from XRF-CS output data. The WLS method considers the standard deviation of the element intensity and of concentrations in the regression significantly reducing the errors of the calibrated element concentration, which is particularly advantageous when compared with the most commonly used regression method (OLS). Reducing the errors is critical when using XRF-CS calibrations to assess metal pollution levels according to SQGs. Indeed, our results evidence that a fine-tuned calibration of XRF-CS output data using the WLS regression method allows quantifying the Mn, Fe, Zn and Pb concentration limits according three widely used SQGs with low levels of errors, namely 0.4% to 2% for Fe, 1% to 7% for Zn, 3 to 14% for Pb and 5% to 16% for Mn. The only drawback, which is unrelated to the calibration method itself, results from the Pb and As peaks overlap which affects the quantification of As absolute concentrations. Beyond the regression methods assessed to obtain the linear functions (OLS, WOLS, and WLS), this is the first study in incorporating and evaluating the analytical and statistical errors of the calibration of the XRF-CS data, and in evidencing that the errors of the calibrated element concentration must be properly evaluated in future calibration studies.

Declaration of Competing Interest

The authors declare that they have no known competing financial interests or personal relationships that could have appeared to influence the work reported in this paper.

Acknowledgements

We would like to thank the crew of RV Ángeles Alvariño and all scientific and technical staff involved in the NUREIEV and NUREIVA research cruises. We thank Maite Romero, Francisco Menéndez, and Bárbara Baena from the Scientific and Technical Centres of the University of Barcelona for technical assistance with the ICP-OES and ICP-MS. This research has been funded by the research projects NUREIEV (CTM2013-44598-R) and NUREIEVA (ref. CTM2016-75953-C2-1-R), and a Catalan Government Grups de Recerca Consolidats grant to GRC Geociències Marines (ref. 2017 SGR 315). J.F. acknowledges financial support from the Generalitat

de Catalunya through a Serra Húnter Tenure-eligible Lecturer contract, and M.C.D from the Ministerio de Economía y Competitividad (PhD fellowship, A-2014-9185) through the NUREIEV project coordinated by GRC Geociències Marines of the Departament de Dinàmica de la Terra i de l'Oceà (Universitat de Barcelona).

Appendix A. Supplementary data

Supplementary data to this article can be found online at https://doi.org/10.1016/j.scitotenv.2019.134778.

References

Adamo, P., Arienzo, M., Imperato, M., Naimo, D., Nardi, G., Stanzione, D., 2005. Distribution and partition of heavy metals in surface and sub-surface sediments of Naples city port. Chemosphere 61, 800–809. https://doi.org/10.1016/j.chemosphere.2005.04.001.

Baucells, M., Lacort, G., Roura, M., de Gyves, J., 1988. Rapid determination of arsenic in the presence of lead in a zinc sulphide matrix by X-ray fluorescence spectrometry. Analyst 113, 1325–1328.

Böning, P., Bard, E., Rose, J., 2007. Toward direct, micron-scale XRF elemental maps and quantitative profiles of wet marine sediments. Geochem. Geophys. Geosyst. 8. https://doi.org/10.1029/2006GC001480. n/a-n/a.

Buccolieri, A., Buccolieri, G., Cardellicchio, N., Dell'Atti, A., Di Leo, A., Maci, A., 2006. Heavy metals in marine sediments of Taranto Gulf (Ionian Sea, Southern Italy). Mar. Chem. 99, 227–235. https://doi.org/10.1016/j.marchem.2005.09.009.

Calvert, S.E., Pedersen, T.F., 2007. Chapter fourteen elemental proxies for palaeoclimatic and palaeoceanographic variability in marine sediments: interpretation and application. Dev. Mar. Geol. 1, 567–644. https://doi.org/10.1016/S1572-5480(07)01019-6.

Canals, M., shipboard party, 2015. The two-vessel cruise to Portman Bay, SE Spain: a breakthrough experience. MIDAS Newsl. 3, 1–6.

Capello, M., Cutroneo, L., Consani, S., Dinelli, E., Vagge, G., Carbone, C., 2016. Marine sediment contamination and dynamics at the mouth of a contaminated torrent: the case of the Gromolo Torrent (Sestri Levante, north-western Italy). Mar. Pollut. Bull. 109, 128–141. https://doi.org/10.1016/j.marpolbul.2016.06.010.

Casado-Martínez, M.C., Buceta, J.L., Belzunce, M.J., DelValls, T.A., 2006. Using sediment quality guidelines for dredged material management in commercial ports from Spain. Environ. Int. 32, 388–396. https://doi.org/10.1016/j.envint.2005.09.003.

Cerdà-Domènech, M., Sanchez-Vidal, A., Frigola, J., Baraza, T., Andrade, L., Amblas, D., Canals, M., 2016. Multi-proxy characterization of the mine tailings deposit of Portmán Bay, SE Spain. In: Comission, M.S., Commission Internationale pour l'Exploration Scientifique de la mer Méditerranée (Eds.).

Chen, Q., Kissel, C., Govin, A., Liu, Z., Xie, X., 2016. Correction of interstitial water changes in calibration methods applied to XRF core-scanning major elements in long sediment cores: case study from the South China Sea. Geochem. Geophys. Geosyst. 17, 1925–1934. https://doi.org/10.1002/2016GC006320.

Christophoridis, C., Dedepsidis, D., Fytianos, K., 2009. Occurrence and distribution of selected heavy metals in the surface sediments of Thermaikos Gulf, N. Greece. Assessment using pollution indicators. J. Hazard. Mater. 168, 1082–1091. https://doi.org/10.1016/j.jhazmat.2009.02.154.

Comisión nacional de estrategias de Marinas, 2015. Directrices para la caracterización del material dragado y su reubicación en aguas del dominio público marítimo-terrestre, Ministerio de agricultura, alimentación y medio ambiente.

Croudace, I.W., Rothwell, R.G., 2015. Future developments and innovations in high-resolution core scanning. In: Micro-XRF Studies of Sediment Cores. Springer, pp. 627–647.

Croudace, I.W., Warwick, P.E., Morris, J.E., 2012. Evidence for the preservation of technogenic tritiated organic compounds in an estuarine sedimentary environment. Environ. Sci. Technol. 46, 5704–5712. https://doi.org/10.1021/es204247f.

Croudace, I.W., Teasdale, P.A., Cundy, A.B., 2019. 200-year industrial archaeological record preserved in an Isle of Man saltmarsh sediment sequence: geochemical and radiochronological evidence. Quat. Int. 514, 195–203. https://doi.org/10.1016/j.quaint.2018.09.045.

Deming, W.E., 1943. Statistical Adjustment of Data. John Wiley & Sons and Chapman & Hall, New York and London, p. 261.

Di Leonardo, R., Bellanca, A., Angelone, M., Leonardi, M., Neri, R., 2008. Impact of human activities on the central Mediterranean offshore: evidence from Hg distribution in box-core sediments from the Ionian Sea. Appl. Geochem. 23, 3756–3766. https://doi.org/10.1016/j.apgeochem.2008.09.010.

Din, Z.B., 1992. Use of aluminium to normalize heavy-metal data from estuarine and coastal sediments of Straits of Melaka. Mar. Pollut. Bull. https://doi.org/10.1016/0025-326X(92)90472-I.

Fatoki, O.S., Mathabatha, S., 2001. An assessment of heavy metal pollution in the East London and Port Elizabeth harbours. Water SA 27, 233–240. https://doi.org/10.4314/wsa.v27i2.4997.

Fukushima, K., Saino, T., Kodama, Y., 1992. Trace metal contamination in Tokyo Bay, Japan. Sci. Total Environ. 125, 373–389. https://doi.org/10.1016/0048-9697(92)90402-E.

Garcia-Orellana, J., Cañas, L., Masqué, P., Obrador, B., Olid, C., Pretus, J., 2011. Chronological reconstruction of metal contamination in the Port of Maó (Minorca, Spain). Mar. Pollut. Bull. 62, 1632–1640. https://doi.org/10.1016/j.marpolbul.2011.06.013.

Gómez-García, C., Martin-Hernandez, F., López García, J.Á., Martínez-Pagón, P., Manteca, J.I., Carmona, C., 2015. Rock magnetic characterization of the mine tailings in Portman Bay (Murcia, Spain) and its contribution to the understanding of the bay infilling process. J. Appl. Geophys. 120, 48–59. https://doi.org/10.1016/j.jappgeo.2015.06.008.

Guevara-Riba, A., Sahuquillo, A., Rubio, R., Rauret, G., 2004. Assessment of metal mobility in dredged harbour sediments from Barcelona, Spain. Sci. Total Environ. 321, 241–255. https://doi.org/10.1016/j.scitotenv.2003.08.021.

Guo, Y., Yang, S., 2016. Heavy metal enrichments in the Changjiang (Yangtze River) catchment and on the inner shelf of the East China Sea over the last 150 years. Sci. Total Environ. 543, 105–115. https://doi.org/10.1016/j.scitotenv.2015.11.012.

Hanebuth, T.J.J., Zhang, W., Hofmann, A.L., Löwemark, L.A., Schwenk, T., 2015. Oceanic density fronts steering bottom-current induced sedimentation deduced from a 50ka contourite-drift record and numerical modeling (off NW Spain). Quat. Sci. Rev. 112, 207–225. https://doi.org/10.1016/j.quascirev.2015.01.027.

Hanebuth, T.J.J., King, M.L., Mendes, I., Lebreiro, S., Lobo, F.J., Oberle, F.K., Antón, L., Ferreira, P.A., Reguera, M.I., 2018. Hazard potential of widespread but hidden historic offshore heavy metal (Pb, Zn) contamination (Gulf of Cadiz, Spain). Sci. Total Environ. 637–638, 561–576. https://doi.org/10.1016/j.scitotenv.2018.04.352.

He, Z., Morrison, R.J., 2001. Changes in the marine environment of Port Kembla Harbour, NSW, Australia, 1975–1995: a review. Mar. Pollut. Bull. 42, 193–201. https://doi.org/10.1016/S0025-326X(00)00142-9.

Hennekam, R., De Rick, G., 2012. X-ray fluorescence core scanning of wet marine sediments: Methods to improve quality and reproducibility of highresolution paleoenvironmental records. Limnol. Oceanogr. Methods 10. https://doi.org/10.4319/lom.2012.10.991.

Hennekam, R., Sweere, T., Tjallingii, R., de Lange, G.J., Reichart, G.J., 2018. Trace metal analysis of sediment cores using a novel X-ray fluorescence core scanning method. Quat. Int. 514, 55–67. https://doi.org/10.1016/j.quaint.2018.10.018.

Hunt, J.E., Croudace, I.W., Maclachlan, S.E., 2015. Use of Calibrated Itrax-XRF data in determining turbidite Geochemistry and provenance in Agadir Basin, Northwest African Passive Margin, in: Micro-XRF Studies of Sediment Cores: applications of a Non-Destructive Tool for. Environ. Sci., 127–146 10.1007/978.

Jansen, J.H.H.F., Van der Gaast, S.J., Koster, B., Vaars, A.J., 1998. CORTEX, a shipboard XRF-scanner for element analyses in split sediment cores. Mar. Geol. 151, 143–153. https://doi.org/10.1016/S0025-3227(98)00074-7.

Kelloway, S.J., Ward, C.R., Marjo, C.E., Wainwright, I.E., Cohen, D.R., 2014. Quantitative chemical profiling of coal using core-scanning X-ray fluorescence techniques. Int. J. Coal Geol. 128, 55–67. https://doi.org/10.1016/j.coal.2014.04.006.

Kido, Y., Koshikawa, T., Tada, R., 2006. Rapid and quantitative major element analysis method for wet fine-grained sediments using an XRF microscanner. Mar. Geol. 229, 209–225. https://doi.org/10.1016/j.margeo.2006.03.002.

Kruge, M.A., Permanyer, A., Serra, J., Yu, D., 2010. Geochemical investigation of an offshore sewage sludge deposit, Barcelona, Catalonia, Spain. J. Anal. Appl. Pyrolysis 89, 204–217. https://doi.org/10.1016/j.jaap.2010.08.005.

Long, E.R., Macdonald, D.D., Smith, S.L., Calder, F.D., 1995. Incidence of adverse biological effects within ranges of chemical concentrations in marine and estuarine sediments. Environ. Manage. 19, 81–97. https://doi.org/10.1007/BF02472006.

Löwemark, L., Chen, H.-F., Yang, T.-N., Kylander, M., Yu, E.-F., Hsu, Y.-W., Lee, T.-Q., Song, S.-R., Jarvis, S., 2011. Normalizing XRF-scanner data: a cautionary note on the interpretation of high-resolution records from organic-rich lakes. J. Asian Earth Sci. 40, 1250–1256. https://doi.org/10.1016/j.jseaes.2010.06.002.

Lyle, M., Backman, J., 2013. Data report: calibration of XRF-estimated CaCO3 along the Site U1338 splice. In: 320. p. 321. doi:10.2204/iodp.proc.320321.205.2013.

MacLachlan, S.E., Hunt, J.E., Croudace, I.W., 2015. An empirical assessment of variable water content and grain-size on X-ray fluorescence core-scanning measurements of deep sea sediments. In: Micro-XRF Studies of Sediment Cores. Springer, pp. 173–185.

Manteca, J.I., Garcia, J.Á.L., Oyarzun, R., Carmona, C., 2014. The beach placer iron deposit of Portman Bay, Murcia, SE Spain: The result of 33 years of tailings disposal (1957–1990) to the Mediterranean seaside. Miner. Depos. 49, 777–783. https://doi.org/10.1007/s00126-014-0511-x.

Martínez-Gómez, C., Fernández, B., Benedicto, J., Valdés, J., Campillo, J.A., León, V.M., Vethaak, A.D., 2012. Health status of red mullets from polluted areas of the Spanish Mediterranean coast, with special reference to Portmán (SE Spain). Mar. Environ. Res. 77, 50–59. https://doi.org/10.1016/j.marenvres.2012.02.002.

Mejía-Piña, K.G., Huerta-Diaz, M.A., González-Yajimovich, O., 2016. Calibration of handheld X-ray fluorescence (XRF) equipment for optimum determination of elemental concentrations in sediment samples. Talanta 161, 359–367. https://doi.org/10.1016/j.talanta.2016.08.066.

Morillo, J., Usero, J., Gracia, I., 2004. Heavy metal distribution in marine sediments from the southwest coast of Spain. Chemosphere 55, 431–442. https://doi.org/10.1016/j.chemosphere.2003.10.047.

Muller-Karulis, B., Poikane, R., Seglins, V., 2003. Heavy metals in the Ventspils Harbour: normalization based on a multi-parameter dataset. Environ. Geol. 43, 445–456. https://doi.org/10.1007/s002540100377.

Oyarzun, R., Manteca Martínez, J.I., López García, J.A., Carmona, C., 2013. An account of the events that led to full bay infilling with sulfide tailings at Portman (Spain), and the search for "black swans" in a potential land reclamation scenario. Sci. Total Environ. 454–455, 245–249. https://doi.org/10.1016/j.scitotenv.2013.03.030.

Palanques, A., Sanchez-Cabeza, J.A., Masqué, P., León, L., 1998. Historical record of heavy metals in a highly contaminated Mediterranean deposit: the Besos prodelta. Mar. Chem. 61, 209–217. https://doi.org/10.1016/S0304-4203(98)00020-6.

Palanques, A., Masqué, P., Puig, P., Sanchez-Cabeza, J.A., Frignani, M., Alvisi, F., 2008. Anthropogenic trace metals in the sedimentary record of the Llobregat continental shelf and adjacent Foix Submarine Canyon (northwestern Mediterranean). Mar. Geol. 248, 213–227. https://doi.org/10.1016/j.margeo.2007.11.001.

Palanques, A., Lopez, L., Guillén, J., Puig, P., Masqué, P., 2017. Decline of trace metal pollution in the bottom sediments of the Barcelona City continental shelf (NW Mediterranean). Sci. Total Environ. 579, 755–767. https://doi.org/10.1016/j.scitotenv.2016.11.031.

Pan, K., Wang, W.X., 2012. Trace metal contamination in estuarine and coastal environments in China. Sci. Total Environ. 421, 3–16. https://doi.org/10.1016/j.scitotenv.2011.03.013.

Persaud, D., Jaagumagi, R., Hayton, A., 1993. Guidelines for the protection and management of aquatic sediment quality in Ontario.

Piippanen, T., Rautiainen, J., Tummavuori, J., 1997. Determination of copper, iron, molybdenum and silicon in hydrometallurgically roasted molybdenite concentrate solution by inductively coupled plasma atomic emission spectrometry. Anal. Chim. Acta 349, 327–331. https://doi.org/10.1016/S0003-2670(97)00190-6.

Pourabadehei, M., Mulligan, C.N., 2016. Selection of an appropriate management strategy for contaminated sediment: a case study at a shallow contaminated harbour in Quebec. Canada. Environ. Pollut. 219, 846–857. https://doi.org/10.1016/j.envpol.2016.08.012.

Raj, S.M., Jayaprakash, M., 2007. Distribution and enrichment of trace metals in marine sediments of Bay of Bengal, off Ennore, south-east coast of India. Environ. Geol. 56, 207–217. https://doi.org/10.1007/s00254-007-1156-1.

Ramsey, M.H., Potts, P.J., Webb, P.C., Watkins, P., Watson, J.S., Coles, B.J., 1995. An objective assessment of analytical method precision: comparison of ICP-AES and XRF for the analysis of silicate rocks. Chem. Geol. 124, 1–19. https://doi.org/10.1016/0009-2541(95)00020-M.

Richter, T.O., van der Gaast, S., Koster, B., Vaars, A., Gieles, R., de Stigter, H.C., De Haas, H., van Weering, T.C.E., 2006. The Avaatech XRF Core Scanner: technical description and applications to NE Atlantic sediments. Geol. Soc. London, Spec. Publ. 267, pp. 39–50. doi:10.1144/GSL.SP.2006.267.01.03.

Rodríguez-Germade, I., Rubio, B., Rey, D., Borrego, J., 2015a. Detection and Monitoring of REEs and Related Trace Elements with an Itrax™ Core Scanner in the Ría de Huelva (SW Spain). Water Air Soil Pollut. 226, 137. https://doi.org/10.1007/s11270-015-2389-3.

Rodríguez-Germade, Isabel, Rubio, B., Rey, D., Vilas, F., López-Rodríguez, C.F., Comas, M.C., Martínez-Ruiz, F., 2015b. Optimization of Itrax core scanner measurement conditions for sediments from submarine mud volcanoes. In: Micro-XRF Studies of Sediment Cores. Springer, pp. 103–126.

Rollinson, H.R., 1993. Using geochemical data: evaluation. Present. Interpret. Singapore. Ongman.

Romano, E., Bergamin, L., Finoia, M.G., Carboni, M.G., Ausili, A., Gabellini, M., 2008. Industrial pollution at Bagnoli (Naples, Italy): Benthic foraminifera as a tool in integrated programs of environmental characterisation. Mar. Pollut. Bull. 56, 439–457. https://doi.org/10.1016/j.marpolbul.2007.11.003.

Rothwell, R.G., Croudace, I. W., 2015. Twenty Years of XRF Core Scanning Marine Sediments: What Do Geochemical Proxies Tell Us? pp. 25–102. doi:10.1007/978-94-017-9849-5_2.

Rothwell, R.G., Rack, F.R., 2006. New techniques in sediment core analysis: an introduction. Geol. Soc. London, Spec. Publ. 267, 1–29. doi:10.1144/GSL.SP.2006.267.01.01.

Rubio, B., Álvarez-Iglesias, P., Vilas, F., 2010. Diagenesis and anthropogenesis of metals in the recent Holocene sedimentary record of the Ría de Vigo (NW Spain). Mar. Pollut. Bull. 60, 1122–1129. https://doi.org/10.1016/j.marpolbul.2010.04.014.

Saylor, R.D., Edgerton, E.S., Hartsell, B.E., 2006. Linear regression techniques for use in the EC tracer method of secondary organic aerosol estimation. Atmos. Environ. 40, 7546–7556. https://doi.org/10.1016/j.atmosenv.2006.07.018.

Scholze, F., Longoni, A., Fiorini, C., Strüder, L., Meidinger, N., Hartmann, R., Kawahara, N., Shoji, T., 2006. X-ray detectors and XRF detection channels. In: Handbook of Practical X-Ray Fluorescence Analysis. Springer, pp. 199–308.

Spofforth, D.J.A., Pälike, H., Green, D., 2008. Paleogene record of elemental concentrations in sediments from the Arctic Ocean obtained by XRF analyses. Paleoceanography 23. https://doi.org/10.1029/2007PA001489.

Sprovieri, M., Feo, M.L., Prevedello, L., Manta, D.S., Sammartino, S., Tamburrino, S., Marsella, E., 2007. Heavy metals, polycyclic aromatic hydrocarbons and polychlorinated biphenyls in surface sediments of the Naples harbour (southern Italy). Chemosphere 67, 998–1009. https://doi.org/10.1016/j.chemosphere.2006.10.055.

Taylor, B.N., Kuyatt, C.E., 1994. Guidelines for evaluating and expressing the uncertainty of NIST measurement results. US Department of Commerce, Technology Administration, National Institute of Standards and Technology Gaithersburg, MD.

Tjallingii, Rik, Röhl, U., Kölling, M., Bickert, T., 2007a. Influence of the water content on X-ray fluorescence core-scanning measurements in soft marine sediments. Geochem. Geophys. Geosyst. 8. https://doi.org/10.1029/2006GC001393. n/a-n/a.

U.S. Environmental Protection Agency, 2005. Contaminated sediment remediation guidance for hazardous waste sites, Office of Solid Waste and Emergency Response. <https://doi.org/http://scholar.google.com/scholar?hl=en&btnG=Search&q=intitle:Contaminated+Sediment+Remediation+Guidance+for+Hazardous+Waste+Sites#1>.

Webster, I.T., Hancock, G.J., Murray, A.S., 1995. Modelling the effect of salinity on radium desorption from sediments. Geochim. Cosmochim. Acta 59, 2469–2476. https://doi.org/10.1016/0016-7037(95)00141-7.

Weltje, G.J., Tjallingii, R., 2008. Calibration of XRF core scanners for quantitative geochemical logging of sediment cores: Theory and application. Earth Planet. Sci. Lett. 274, 423–438. https://doi.org/10.1016/j.epsl.2008.07.054.

York, D., Evensen, N.M., Martínez, M.L., De Basabe Delgado, J., 2004. Unified equations for the slope, intercept, and standard errors of the best straight line. Am. J. Phys. 72, 367–375. https://doi.org/10.1119/1.1632486.

Índex, abreviatures, símbols i sigles

Índex terminològic

Abreviatures, símbols i sigles

AVS	*Acid Volatil Sulfurs*
CTD-Diver	*Conductivity, Temperaturature and Depth Diver*
DAS	*Descàrrega d'Aigua Subterrània*
e.g	*(exempli gratia, ll.) per exemple*
EF	*Enrichment Factor*
et al.	*(et alii, ll.) i altres*
GEBCO	*General Bathymetric Chart of the Oceans*
GRCGM	*Grup de Recerca Consolidat en Geociències Marines*
i.e.	*(id est, ll.) és a dir*
ICP-MS	*Inductively Coupled Plasma-Mass*
ICP-OES	*Inductively Coupled Plasma-Optical Emission Spectrometry*
MEDISTRAES	*Mezcla y dispersión en el transporte de energía y solutos*
micro-CT	*Micro Computed Tomography*
MIDAS	*Managing Impacts Of Deep Sea Resource Exploitation*
MSCL	*Multi-sensor Core Logger*
NUREIEV	*NUevos REtos en la investigación de cañones submarinos: Indicadores del Estado ambiental y Variabilidad espacio-temporal – El papel de los temporales*
NUREIEVA	*NUevos REtos de Investigación en el ambiente Extremo de los Vertidos mineros de la Bahía de Portmán: aplicación de tecnologías Avanzadas*
OLS	*Ordinary Least-Squares*
p.ex.	*per exemple*
PCA	*Principal Component Analysis*
PEX	*Porewater Exchange*
RaDeCC	*Radium Delayed Coincidence Counter*
ref.	*referència / reference*
RFE	*Rainfall Event*
RSD	*Relative Standard Deviation of the slope*
SGD	*Submarine Groundwater Discharge*
SQG	*Sediment Quality Guideline*
WLS	*Weighted Least-Squares*
WOLS	*Weighted Ordinary Least-Squares*
XRF-CS	*X-Ray Fluorescence Core Scanner*

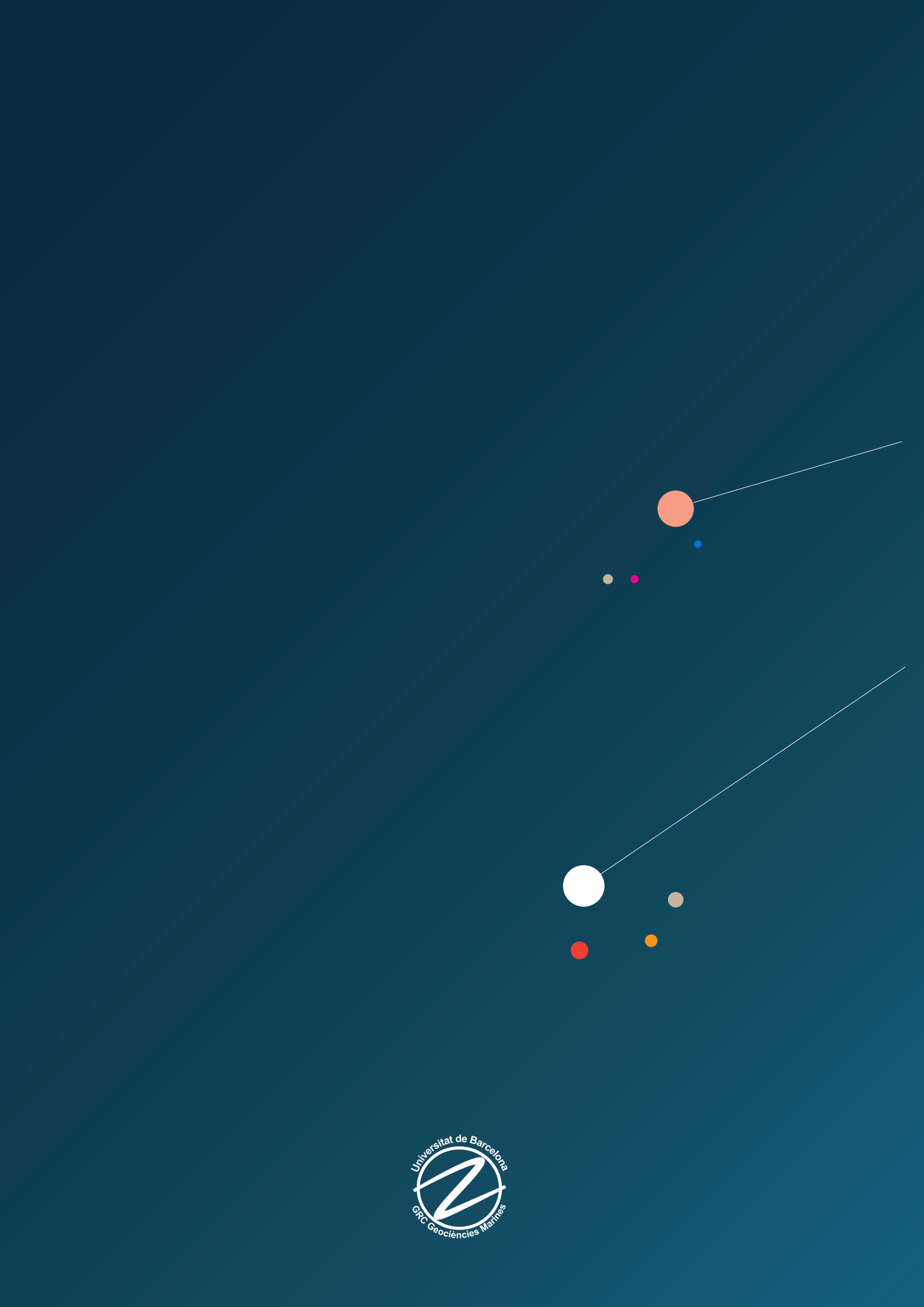
Universitat de Barcelona
GRC Geociències Marines